The Na^+-Activated K^+ Channel Slack Limits Kainic Acid-Induced Seizure Severity in Mice by Modulating the Survival, Excitability and Firing Properties of Hippocampal Neurons

Dissertation

der Mathematisch-Naturwissenschaftlichen Fakultät

der Eberhard Karls Universität Tübingen

zur Erlangung des Grades eines

Doktors der Naturwissenschaften

(Dr. rer. nat.)

Vorgelegt von

M. Sc. David Skrabak

aus Bonlanden jetzt Filderstadt

Tübingen

2023

Gedruckt mit Genehmigung der Mathematisch-Naturwissenschaftlichen Fakultät der Eberhard Karls Universität Tübingen

Tag der mündlichen Qualifikation:	07.03.2024
Dekan:	Prof. Dr. Thilo Stehle
1. Berichterstatter/-in:	Prof. Dr. Robert Lukowski
2. Berichterstatter/-in:	Prof. Dr. Dr. Achim Schmidtko

Table of Contents

List of Figures

List of Tables

Abbreviations

(AD)SHE	Autosomal Dominant Sleep-related Hypermotor Epilepsy
AC	Adenylate cyclase
AED	Anti-epileptic drug
aHP	After hyperpolarization
AIS	Axonal initial segment
AMPA	α-amino-3-hydroxy-5-methyl-4-isoxazolepropionate
AP	Action potential
BDNF	Brain derived neurotrophic factor
C. elegans	*Caenorhabditis elegans*
CA	Cornu ammonis region of the hippocampus
$[Ca^{2+}]_i$	Intracellular Ca^{2+} concentration
CFP	Cyan fluorescent protein
CHO cells	Chinese hamster ovary cells
CNS	Central nervous system
DAG	Diacylglycerol
DEE	Developmental and epileptic encephalopathy
DG	Dentate gyrus of the hippocampus
div	Days *in vitro*
DRG	Dorsal root ganglion
EEG	Electroencephalogram
EIMFS	Epilepsy of infancy with migration focal seizures
EPSP	Excitatory postsynaptic potential
ER	Endoplasmic reticulum
ES	Entorhinal cortex
FMRP	Fragile mental retardation protein
GABA	γ-amino-butyric-acid
$GABA_A$	Ionotropic GABA receptor
$GABA_B$	Metabotropic GABA receptor
GAR	$GABA_A$ receptor subunit
GluA	AMPA receptor subunit
GluK	Kainate receptor subunit
GluN	NMDA receptor subunit
GOF	Gain-of-function mutation
GPCR	G-protein coupled receptor
HP	Hyperpolarization
HPRT	Hypoxanthine-guanine phosphoribosyl transferase
HS	Hippocampal sclerosis
HSC	Hippocampal slice cultures
i.p.	intraperitonially
iGluR	Ionotropic glutamate receptor subunit
ILAE	International league against epilepsy
I_{NaP}	Persistent Na_V mediated Na^+ inward current
I_{NaT}	Transient Na_V mediated Na^+ inward current
iPSC	Induced pluripotent stem cell
IPSP	Inhibitory postsynaptic potential

KA	Kainic acid
KI	Knock-In
K_{Na}	Na^+ -activated K^+ current
KO	Knock-out
K_V	Voltage-gated potassium channel
LOF	Loss-of-function mutation
mAChR	Muscarinic acetylcholine receptor subunit
mGluR	Metabotropic glutamate receptor subunit
MOI	Multiplicity of infection
nAChR	Nicotinic acetylcholine receptor subunit
Na_V	Voltage-gated sodium channel
NFS interneurons	Non-fast-spiking interneurons
NMDA	N-methyl-D-Aspartate-receptor
P	postnatal day
PCR	Polymerase chain reaction
PDS	Paroxysmal depolarization shift
PDZ	Postsynaptic density 95/disc large/zona occludes
PHN	Primary hippocampal neurons
PI	Propidium iodide
Pilo	Pilocarpine
PIP_2	Phosphatidylinositol-4,5-bisphosphate
PiTX	Picrotoxin
PKA	Protein kinase A
PKC	Protein kinase C
PLC	Phospholipase C
PTZ	Pentylenetetrazol
PV^+	Parvalbumin positive interneurons
RCK	Regulator of conductance of K^+
REM	Rapid-eye-movement sleep phase
RMP	Resting membrane potential
ROI	Regions of interest
RT	Reverse transcriptase
RT-PCR	Real-time quantitative PCR
SE	Status epilepticus
Slack	Sequence like a calcium activated K^+ channel
Slick	Sequence like an intermediate conductance K^+ channel
SPF	Specific pathogen free
SRS	Spontaneous recurrent seizures
SSc	Seizure score
TCS	Tonic-clonic-seizures
TLE	Temporal lobe epilepsy
TMD	Transmembrane domain
TTX	Tetrodotoxin
VGCC	Voltage-gated Ca^{2+} channel
YFP	Yellow fluorescent protein

1. Abstract

The rare epilepsy disorders *Epilepsy of Infancy with Migrating Focal Seizures* (EIMFS) and *Autosomal Dominant Sleep-related Hypermotor Epilepsy* (AD)SHE are characterized by early onset of severe seizures. Both disorders are refractory to anti-epileptic drugs and associated with mutations in *KCNT1*, the gene encoding the sodium- (Na^+) activated potassium- (K^+) channel Slack. To date, approximately 60 pathogenic mutations associated with EIMFS or (AD)SHE had been identified in *KCNT1*, most of which cause a gain-of-function (GOF), resulting in increased Slack K^+ currents. While these GOF mutations result in overexcited nervous tissue, high network activity and disturbed electrical rhythms, also a loss-of-function Slack variant has been linked to epilepsies in one patient and increased neuronal vulnerability *in vivo* and *in vitro*.

As Slack crucially modulates neuronal excitability, we investigated its role during epileptic seizures using wildtype ($Slack^{+/+}$) and global Slack knock-out ($Slack^{-/-}$) mice in a Kainic acid (KA)-induced model of acute epilepsy. Compared to $Slack^{+/+}$, 4-week-old juvenile and 12-week-old adult $Slack^{-/-}$ mice displayed increased seizure scores and mortality after KA application, indicating a neuroprotective role of Slack during epileptic seizures *in vivo*. Strikingly, 24 hours after seizure onset, hippocampal GFAP, GluA and GluN mRNA levels are equal between KA-treated $Slack^{+/+}$ and $Slack^{-/-}$, suggesting a more prominent role for Slack during acute seizures. In addition to these findings *in vivo*, organotypic $Slack^{+/+}$ and $Slack^{-/-}$ hippocampal slice cultures were exposed to KA and cell death was quantified by propidium iodide uptake. Compared to $Slack^{+/+}$, sclerosis like neuronal cell loss was significantly increased in the CA regions of hippocampal slices derived from $Slack^{-/-}$ brains, confirming our *in vivo* results of KA-induced seizures in mice. To confirm these results independent of hippocampal circuitries, dissociated hippocampal neurons were treated with KA. Conformingly, compared to $Slack^{+/+}$, also individual $Slack^{-/-}$ neurons responded with increased cell death to KA treatment. To elucidate whether these differences in neuronal vulnerability are caused by a differential subcellular ion homeostasis, we next assessed intracellular Ca^{2+} and K^+ dynamics in dissociated primary hippocampal neurons derived from $Slack^{+/+}$ and $Slack^{-/-}$ mice in response to KA treatment. Interestingly, compared with $Slack^{+/+}$, $Slack^{-/-}$ hippocampal neurons showed increased intracellular Ca^{2+} dynamics in response to low but not high KA concentrations, which was not modulated by AMPA (NBQX) or NMDA receptor blockers (DL-AP5) or the “Slack activator” Loxapine. This suggests that the neuroprotective effect of Slack is mediated on the level of altered thresholds for neuronal activation patterns. Next, we employed a K^+-sensitive FRET-sensor to record intracellular K^+ dynamics in these primary

hippocampal neurons among KA-exposure. Unexpectedly, under these conditions, KA-induced K^+-efflux was significantly increased in Slack$^{-/-}$ compared to Slack$^{+/+}$ hippocampal neurons. Finally, patch-clamp recordings identified amplified TTX-sensitive transient and persistent inward currents in Slack$^{-/-}$ neurons compared to Slack$^{+/+}$. Fittingly, KA and current provoked AP firing was accelerated in current-clamped Slack$^{-/-}$ compared to Slack$^{-/-}$ neurons owing to faster accessibility of the AP threshold, increased AP rise slope and shortened after-hyperpolarization.

Based on these findings, we propose that loss of Slack leads to increased neuronal response to glutamatergic signals, ultimately causing detrimental epileptiform activity. It may additionally involve alterations of other K^+ channel activities that facilitate reactivation of, for instance, voltage-gated (TTX-sensitive) Na^+ channels to subsequently drive KA-induced overexcitability in Slack$^{-/-}$ neurons. We conclude that a careful modulation of Slack activity is necessary for otherwise untreatable epilepsy syndromes.

2. Zusammenfassung

Die seltenen Epilepsieerkrankungen *Epilepsy of Infancy with Migrating Focal Seizures* (EIMFS) und *Autosomal Dominant Sleep-related Hypermotor Epilepsy* (AD)SHE sind durch ein frühes Auftreten schwerer Anfälle gekennzeichnet. Beide Erkrankungen sind refraktär gegenüber Antiepileptika und gehen mit Mutationen in *KCNT1* einher, dem Gen, das für den Natrium (Na^+) -aktivierten Kalium- (K^+) Kanal Slack kodiert. Bisher wurden etwa 60 pathogene Mutationen in *KCNT1* identifiziert, die mit EIMFS oder (AD)SHE assoziiert sind. Die meisten davon führen zu einem Funktionsgewinn (*gain-of-function*, GOF), der zu erhöhten Slack-K^+-Strömen führt. Während diese GOF-Mutationen zu übererregtem Nervengewebe führen, wurde auch eine Slack-Variante mit Funktionsverlust (*loss-of-function*, LOF) mit Epilepsien bei Patienten und einer erhöhten neuronalen Anfälligkeit *in vivo* und *in vitro* in Verbindung gebracht.

Da Slack die neuronale Erregbarkeit entscheidend moduliert, wurde in diesem Projekt die Rolle von Slack während epileptischer Anfälle unter Verwendung von Wildtyp- ($Slack^{+/+}$) und globalen Slack-Knock-out-Mäusen ($Slack^{-/-}$) im Kainsäure (KA)-induzierten akuten Epilepsiemodell untersucht. Im Vergleich zu $Slack^{+/+}$ Mäusen wiesen 4 Wochen alte juvenile und 12 Wochen alte adulte $Slack^{-/-}$ Mäuse nach KA-Behandlung eine erhöhte Anfallsintensität -und Mortalität auf, was auf eine neuroprotektive Rolle von Slack bei epileptischen Anfällen *in vivo* hinweist. Auffallend ist, dass 24 Stunden nach Beginn der Anfälle die GFAP-, GluA- und GluN-mRNA Expressionslevel im Hippocampus zwischen KA-behandelten $Slack^{+/+}$ und $Slack^{-/-}$ Mäusen gleich sind, was darauf hindeutet, dass Genotyp-spezifische Unterschiede auf akute Anfälle beschränkt sind. Zusätzlich zu diesen *in vivo* Ergebnissen wurden organotypische Hippocampus-Schnittkulturen von $Slack^{+/+}$ und $Slack^{-/-}$ Mäusen mit KA behandelt und der Zelltod durch Propidiumiodid-Färbungen quantifiziert. Im Vergleich zu $Slack^{+/+}$ war der skleroseähnliche neuronale Zellverlust in den CA-Regionen von Hippocampus-Schnitten, die von $Slack^{-/-}$ Tieren stammten, signifikant erhöht, was die *in vivo* Ergebnisse von KA-induzierten Anfällen bei Mäusen bestätigt. Um diese Ergebnisse unabhängig von Hippocampus-Vernetzungen zu bestätigen, wurden dissoziierte Hippocampus-Neuronen mit KA behandelt. Da auch einzelne $Slack^{-/-}$ Neuronen, im Vergleich zu $Slack^{+/+}$ Neuronen, mit verstärktem Zelltod auf KA-Behandlungen reagierten, konnten die bisherigen Ergebnisse weiter bestätigt werden. Um zu klären, ob diese Unterschiede in der neuronalen Anfälligkeit durch eine unterschiedliche subzelluläre Ionenhomöostase verursacht werden, wurde als nächstes die intrazelluläre Ca^{2+}- und K^+-Dynamik in dissoziierten primären Hippocampus-Neuronen von $Slack^{+/+}$ und $Slack^{-/-}$ Mäusen als

Reaktion auf eine KA-Behandlung untersucht. Interessanterweise zeigten Slack$^{-/-}$ Hippocampus-Neurone im Vergleich zu Slack$^{+/+}$ eine erhöhte intrazelluläre Ca^{2+}-Dynamik in Folge niedriger, aber nicht hoher KA-Konzentrationen was durch AMPA- (NBQX) oder NMDA-Rezeptorblocker (DL-AP5) oder dem „Slack-Aktivator“ Loxapin nicht moduliert wurde. Dies deutet darauf hin, dass die neuroprotektive Wirkung von Slack auf Ebene veränderter Schwellwerte für neuronale Aktivierungsmuster beruht. Als nächstes wurde K^+-sensitive FRET-Sensor verwendet, um die intrazelluläre K^+-Dynamik während KA-Exposition in diesen primären Hippocampus-Neuronen aufzuzeichnen. Unerwarteterweise war unter diesen Bedingungen der KA-induzierte K^+-Efflux in Slack$^{-/-}$ im Vergleich zu Slack$^{+/+}$ Hippocampus-Neuronen deutlich erhöht. Schließlich wurden mittels Patch-Clamp-Verfahren verstärkte TTX-sensitive transiente und persistente Einwärtsströme in Slack$^{-/-}$-Neuronen im Vergleich zu Slack$^{+/+}$ festgestellt. Passend dazu war das KA- und stromprovozierte AP-Feuern in Slack$^{-/-}$ Neuronen im Vergleich zu Slack$^{+/+}$ Neuronen im Current-Clamp-Modus beschleunigt, was auf eine schnellere Erreichbarkeit der AP-Schwelle, eine erhöhte AP-Anstiegssteigung und eine verkürzte Nach-Hyperpolarisation zurückzuführen war.

Zusammengenommen deuten die Befunde darauf hin, dass der Verlust von Slack zu einer verstärkten neuronalen Reaktion auf glutamaterge Signale führt, die letztlich eine schädliche epileptiforme Aktivität verursacht. Möglicherweise kommt es zusätzlich zu Veränderungen anderer K^+-Kanalaktivitäten, die beispielsweise die Reaktivierung von spannungsabhängigen Na^+-Kanälen erleichtern, um anschließend die KA-induzierte Übererregbarkeit in Slack$^{-/-}$-Neuronen zu fördern. Dies kann zu dem Schluss führen, dass eine sorgfältige bzw. behutsame Modulation der Slack-Aktivität geboten ist, um ansonsten unbehandelbare Epilepsiesyndrome adäquat zu therapieren.

3. Introduction

3.1. Epileptic seizures and epilepsy

Epileptic seizures affect 10% of the worldwide population over lifetime, leading to epilepsy in up to 2% of all cases (Minghui et al., 2014). Clinically epileptic seizures are defined as transient abnormal synchronized and excessive activities of neuronal populations over whole brain regions, resulting in a variety of conditions such as convulsion or syncope, lasting usually less than 2 minutes (Fisher et al., 2005; Scharfman, 2007). Since epileptic seizures are diverse in their appearance, they were classified into four groups: (1) focal, (2) generalized, (3) unknown, and (4) unclassified. Focal epileptic seizures are locally restricted and generated by a local unilateral neuronal network, within bilateral networks or networks of unknown origin (Fisher et al., 2017; Oyrer et al., 2018). For focal seizures, a macroscopic structural alteration can frequently be determined as the cause, with mesial-temporal lobe sclerosis as the most common origin (Sontheimer, 2015). Generalized seizures arise from bilateral neuronal networks and activate both hemispheres at the onset of seizures (Falco-Walter, 2020). This type of seizure is usually genetically determined (genetically generalized epilepsies) with an onset in childhood, but also adolescence, and a characteristic electroencephalogram (EEG), including generalized spike-waves (Oyrer et al., 2018; Sontheimer, 2015). Beyond seizure classification in focal-, generalized-, and unknown-seizures, seizure manifestations are very heterogeneous as the affected brain regions determine their appearance. For example, when motor cortex is affected, repetitive (clonic) abnormal involuntary muscle contractions occur and are characterized as seizures with motor onset. Tonic-clonic-seizures (TCS) belong to the class of motor onset seizures. This type of seizures accounts for the majority of adult seizures and initiate with tonic muscle contractions in the first approximately 10 seconds that pass on to a clonic phase with repeated jerks and muscle contraction lasting for minutes, ultimately leading to a post-ictal suppression with a sudden silent phase in the EEG (Sontheimer, 2015). If this type of severe seizures persists for longer than 5 minutes, a so-called status epilepticus (SE) is reached that is not self-sustaining, making acute medical termination of urgent need (Sontheimer, 2015). It applies to all seizure types that following an initial seizure, the total risk to suffer from further seizures or epilepsy is approximately 50% (Beghi, 2020).

Epilepsy is a severe and chronic syndrome characterized by spontaneous recurrent seizures (SRS) resulting from hypersynchronous neuronal discharges (Scharfman, 2007). The incidence of epilepsy is 61.4 per 100,000 with a prevalence of 7.60 per 1,000

(Fiest et al., 2017) with two peaks – in first years of live (86 in 100,000) and between 30 and 59 years of life (23 to 31 in 100,000) (Hauser et al., 1993; Ottman, 2005). Seizure disorders carry a signature of EEG signals with interictal spikes or sharp waves that corelate directly with the clinical appearance. One important feature is a paroxysmal depolarization shift (PDS) on a cellular level and hence a high voltage (10 to 15 mV higher compared to resting membrane potential) and long lasting depolarization (100 to 200 ms) that contains bursts of action potentials (Holmes, 1995). The interictal PDS, representing the epileptic focus, is followed by a large hyperpolarization that limits the duration of interictal paroxysms, topographically surrounding the epileptic focus (Holmes, 1995). Like the classification of seizures, also epilepsies are structured primary by seizure type and secondary by etiology. According to the international league against epilepsy (ILAE), epilepsies can be focal, generalized, combined generalized and focal, or unknown (Scheffer et al., 2017). The most common group of epilepsy is focal with unknown etiology with 17.5 / 100,000 affected persons in the US (Scheffer et al., 2017). Etiologies of epilepsies are various, including either genetic determinants or structural disorders of the brain (Baulac et al., 1998; Ho et al., 1998; Lehericy et al., 1995; Oyrer et al., 2018). Still, etiology is unknown in 50% of the patients (Neligan et al., 2012). To date 50 different epilepsy syndromes can be distinguished into genetic / idiopathic disorders with spontaneous onset and no link to external cause or symptomatic / acquired with known or suspected cause. The distribution pattern of etiology differs especially for genetic epilepsies between children and adults. While in both, children and adults, metabolic, immune, and infectious epilepsies can be found in ≤5%, unknown in 40% and structural epilepsy between 25 and 27% of cases, genetic epilepsies are more frequent in children with 32%, compared to adults with 26% (Falco-Walter, 2020). Interestingly, among genetic epilepsies, 17% are linked to variants of voltage-gated-ion channels and 10% to ligand-gated ion-channels (Oyrer et al., 2018), most frequently including mutations of these genes that are either acquired spontaneously / *de novo* or inherited autosomal dominant (Sontheimer, 2015), suggesting ion channels to play an integral role in epilepsy pathogenesis. Those epilepsy causing mutations in ligand -and voltage-gated ion channels are summarized and termed channelopathies (Oyrer et al., 2018) and further introduced in section 3.3.4., 3.4 and 3.5. 20% of epilepsy patients have a poor prognosis with recurrent seizures despite intensive treatment, for example progressive neurological disorders and idiopathic partial epilepsies (Beghi, 2020; Oyrer et al., 2018). This refractory, however, probably reflects the various mechanisms for seizure generation in a given patient, rather than a single genetic variant which mediates epilepsies (Scharfman, 2007).

Based on the heterogeny of clinical manifestation, it is not surprising that processes that convert a normal brain to an epileptic one - epileptogenesis - are spatiotemporally complex, maybe including various neuronal circuitries or networks, cell types and neurotransmitters (Scharfman, 2007). Epileptogenesis was also characterized as sub-threshold circuitry dysfunction, provoking synchroneity and imbalance in neuronal inhibition and excitation starting from single pace maker cells, structures, or functionalities (Goldberg & Coulter, 2013). Hence, the term “epileptogenesis” accounts frequently for the most fundamental aspects and functions of the central nervous system (CNS) such as the cellular transmembrane potential, action potentials, neurotransmission and wiring (Scharfman, 2007). To date, numerous functionalities, structures, circuitries, cells, and proteins were found to directly provoke seizures and epilepsies. Among possible factors, circuitry dysfunctions and the function of neurotransmitters including glutamate (see section 1.3.4.), acetylcholine or γ-amino-butyric-acid (GABA) (see section 1.5), but also ion channel function (see section 1.4) are especially frequent and important. Dysregulation in neuronal activities lead especially within the hippocampus to histopathologic alterations. Hence, the hippocampus is a brain structure especially vulnerable to epilepsy, stroke and ischemia (Knierim, 2015).

3.2. The hippocampus

The hippocampus is a subcortical formation of three layers – stratum oriens, stratum pyramidal and stratum molecular – that can be functionally differentiated into cornu ammonis (CA) 1, CA2 and CA3 region along the septotemporal axis. The distal end of the hippocampal CA region ends in the polymorph layer or hilus, which is part of the dentate gyrus (DG). The DG is composed of the granular layer containing the granular cells and molecular layer with a ventral and dorsal leaflet (Trepel, 2015). The hippocampal circuitries are well studied especially to unravel the memory function and its molecular deposit, the long term potentiation, together with spatiotemporal framework for contextual and spatial learning and behaviour that are mediated by so called grid cells, place cells and circuit functions (Knierim, 2015). Furthermore, physiological conditions are directly linked to hippocampal activity with approximately 8 Hz (θ, theta) oscillation during locomotion, exploring behaviour or rapid-eye-movement (REM)-sleep phase, or large-irregular activity with intermitted bursts during eating, grooming and slow-wave-sleep (Knierim, 2015). The principal input to the hippocampus are afferences from the entorhinal cortex (EC) that in turn receive input from cortical areas such as the prefrontal cortex, important for higher order brain functions. This EC afferences enter the classic tri-synaptic hippocampal pathway: The EC projections, called performant path,

project to granular cells located in the DG. The granular cells project their mossy fibres to the pyramidal neurons of the CA3 region which subsequently project by Schaffer collaterals to the CA1 region that finally projects to distal regions as the subiculum and EC (see Fig. 1) (Moser & Moser, 1998). The description of this simplified circuitry can be completed by a multitude of further wirings.

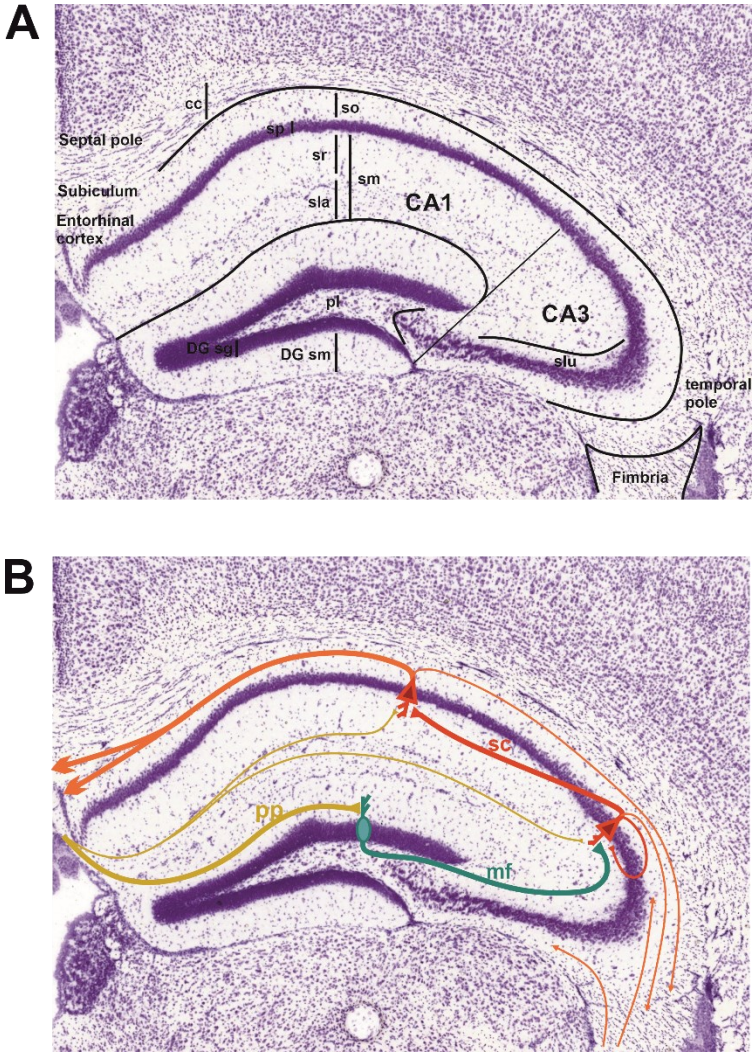

Figure 1: Coronal section of the mouse hippocampal formation.

(A) Nissl-stained coronal section of the mouse hippocampus with principal regions, cells, and orientation. The pyramidal cells (pc) containing stratum pyramidale (sp) with dorsal located stratum orients (so) and ventral located stratum molecular (sm), that is divided in stratum radiatum (sr) and stratum lacunosum (sl), are separated in cornu ammonis (CA) 1 to CA3 regions from the septal to the temporal pole. The CA3 region leads to the hilus or polymorph layer (pl) of the dentate gyrus (DG) with the granular cells (gc) containing granular layer (gl) and molecular layer (ml). **(B)** Principal connections of the mouse hippocampus. Afferent projections especially from the entorhinal cortex (EC) reach the hippocampus predominantly via the performant path (pp, yellow line) to dendrites of gc. Via mossy fibre (mf, green line) gc project to pc of the CA3 region which projects via Schaffer collaterals (sc, red line) to the CA1 region (Knierim, 2015).

The hippocampus receives input also from subcortical areas, such as the Raphe nucleus, amygdala, or medial septum that are important for hippocampal rhythms and arousal. The EC layer II and III not only project to the DG but also directly to the CA1 and CA3 regions. Both, CA1 and CA3 have separated projections: The CA3 region projects via axonal bundles of the fimbria to the fornix which connect the mammillary bodies and further subcortical brain regions as the basal forebrain, thalamus, or high-order cortical areas. The CA3 region sends feedback to the DG, afferences to the prefrontal cortex and

amygdala but most importantly to recurrent collaterals within the CA3 region (Knierim, 2015; Witter et al., 2017).

3.3. Neurotransmitters

Neuronal activity and neurotransmission play a central role for functions and dysfunctions of the CNS. Among more than 200 known chemicals that amplify, transmit and convert signals to cells two main molecules drive and control neuronal activity in the CNS: Glutamate is the most important excitatory (Ju & Tam, 2022; Murley & Rowe, 2018) while γ-amino-butyric-acid (GABA) is the main inhibitory neurotransmitter in the mammalian brain. Additionally, acetylcholine is one important neurotransmitter that was shown to critically modulate glutamatergic and GABAergic signalling, linking brain stem and thalamic function to the limbic system (Wang et al., 2021).

3.3.1. Glutamatergic signalling

Glutamate is involved in both, regulating physiological processes, such as synaptic plasticity, spatiotemporal integrations and processing of sensory input, but also pathophysiological alterations such as epilepsy (Holmes, 1995) and neuronal excitotoxicity arising from prolonged exposure to glutamate (Choi, 1994). Within the synaptic cleft glutamate concentration of 1 to 2 µM is well maintained and raised up to 0.1 to 1 mM following complex action potential (AP)-mediated postsynaptic Ca^{2+} influx that leads to the secretion of vesicles that contain glutamate to the synaptic cleft (Anderson & Swanson, 2000; Attwell, 2000; Daikhin & Yudkoff, 2000).

3.3.2. Ionotropic glutamate receptors

Ionotropic glutamate receptors (iGluR) are a heterogeneous group of 15 different subunits encoded by 6 gene families building a functional receptor by homo- or hetero-tetramerization of subunits that consist of 3 α-helical transmembrane domain (TMD) I, III and IV (Traynelis et al., 2010). The allosteric ligand binding is possible at two separate extracellular subdomains: S1, which is located at the TMD I and SII, located between TMD III and IV (Stern-Bach et al., 1994). The iGluR can be classified by their agonists in three classes: N-methyl-D-aspartate-receptor (NMDA or GluN) (Wantkins, 1962), the α-amino-3-hydroxy-5-methyl-4-isoxazolepropionate receptor (AMPA or GluA) (Krogsgaard-Larsen et al., 1980) and Kainate receptor (GluK) (Shinozaki & Konishi, 1970). NMDA receptors are activated by NMDA and glutamate, AMPA receptors by AMPA, glutamate and Kainate, and Kainate receptors by Kainate and glutamate (Holmes, 1995). For each receptor type several subtypes are known which are made up of a combination

of pore-forming subunits forming heterotetramers: 9 NMDA receptors including GluN1, GluN2a to d, GluN3a to d; 4 AMPA receptors including GluA1 to 4, and 5 Kainate receptors comprising GluK1 to 5 (GluK1 – also termed GluR5; GluK2 – also termed GluR6; GluK3 – also termed GluR7; GluK4 – also termed KA1; GluK5 - also termed KA2) (Traynelis et al., 2010).

The most important differences are the permeability and activation kinetics of these receptor subtypes. NMDA receptors are permeable for mono -and bivalent cations like Na^+, K^+ and Ca^{2+}. Receptor activation is mediated by binding of its principal agonist glutamate to a GluN2 subunit, together with binding of glycine to a GluN1 or GluN3 subunit (Chatterton et al., 2002; Yao & Mayer, 2006). Due to a Mg^{2+}-mediated pore block at physiological neuronal membrane potentials between -95 to -60 mV the NMDA receptor coincidentally needs a membrane depolarization that ejects Mg^{2+}. Based on this complex activation pattern NMDA receptors are also called coincidence detectors (Dingledine et al., 1999). AMPA receptors are permeable predominantly for monovalent cations like Na^+ and K^+ but, depending on subunit composition, also Ca^{2+} permeability is possible. AMPA receptors are activated by glutamate binding and initiate the first membrane depolarization through the influx of Na^+, subsequently leading to the engagement of further NMDA receptors. Hence, AMPA receptors are most important for fast excitatory neurotransmission in the CNS, paving the way for further activities (Henley & Wilkinson, 2013). Also, by this function, AMPA receptors may trigger both long term depression and facilitation / potentiation of synaptic transmission (Ehlers, 2000). Kainate receptors are also permeable for monovalent cations but activated by glutamate and also Kainate binding (Dingledine et al., 1999; Traynelis et al., 2010) (see also Fig. 2).

A functional difference between GluN, GluA and GluK is a fast desensitization in the range of milliseconds during constant agonist exposure of Kainate receptors, while AMPA and NMDA receptors desensitize verry slowly (Armstrong et al., 2006; Sun et al., 2002). This fast desensitization is mainly mediated by the GluK1 subunit. Additionally, the agonists glutamate and Kainate have approximately 10 times higher potency at GluK subunits compared to AMPA (Hansen et al., 2021). Kinetics of the Kainate receptor are further regulated by its subunits: While GluK2 triggers, for instance, desensitization, GluK5 is important for fast activation (Mott et al., 2010).

Although the heteromerization of receptor subunits increases structural and functional variances, especially NMDA receptors contain one obligatory GluN1 subunit and several GluN2 and GluN3 (Dingledine et al., 1999; Vyklicky et al., 2014). The receptors pharmacological and functional properties, especially regarding Mg^{2+} pore block,

localization, agonist sensitivity and permeability are regulated mainly by GluN2 subunits (Dingledine et al., 1999; Traynelis et al., 2010; Wollmuth et al., 1998). NMDA receptors that also contain GluN2 and GluN3 subunits show a reduction in conductance, Ca^{2+} permeability and Mg^{2+} sensitivity (Madry et al., 2007). While GluN1 is expressed already early in embryonic development throughout the brain, GluN2 subunits are expressed differentially. GluN2a can be found in all brain regions despite the hypothalamus, GluN2b is expressed especially in the hippocampus and cortex and GluN2d is expressed mainly during embryonic development with gradual restriction to the hypothalamus in the adult brain.

AMPA receptors are frequently heteromeric resulting in various modulations of receptor functions. Additionally, each AMPA subunit exists in a so-called ‘flip’ or ‘flop’ splice variant further increasing functional variability. Flip variants desensitize slow and incomplete compared to flop variants (Mosbacher et al., 1994; Partin et al., 1994). Furthermore, the subunit GluA2 interferes the receptors permeability for Ca^{2+}, consequently GluA2-lacking AMPA receptors are usually Ca^{2+} permeable (Pellegrini-Giampietro et al., 1997). The pore region of the subunit contains a Q/R site at which, depending on posttranslational modifications of the pre-mRNA, either an arginine or a glutamine is located (Henley & Wilkinson, 2013; Seeburg, 1996). Depending on brain development stage, this exchange of arginine to glutamine lead to a drastically reduced Ca^{2+} permeability (Jonas et al., 1994). Additionally, in GluA2, 3 and 4 an arginine / glycine (R/G) site at the N-terminus can be modified. Exchange of R to G lead to a decreased desensitization and accelerated ability to reactivation (Wright & Vissel, 2012).

Physiologically, the GluK channels can be divided in the low affinity receptor subunits, GluK1, 2 and 3, and the high affinity receptor subunits, GluK4 and 5. All GluK subunits are expressed throughout the CNS, despite the subunits GluK2 and 5 are the most abundant in neurons (Hansen et al., 2021). An important role of GluK was found to be the modulation of presynaptic formation: Interestingly, over-expression of GluK1, 2 and 3 led to an increase in presynaptic puncta of cultured neurons, whereas knock-out of GluK2 or GluK5 led to a reduced density of presynaptic specializations (Hansen et al., 2021). The fast activation is still accompanied by GluK’s mediation of slow excitatory responses, that increase in amplitude among persistent and repetitive firing. A very interesting additive feature of GluK receptors, especially in hippocampal interneurons, is a coupling to metabotropic-protein mediated signalling, that reduces inhibitory signalling by inhibition of the voltage gated Ca^{2+} channel (VGCC) $Ca_V2.1$ (Rodríguez-Moreno & Lerma, 1998; Rozas et al., 2003; Rutkowska-Wlodarczyk et al., 2015). This interaction can also affect the excitability of CA1 neurons (Melyan et al., 2002). Hence, GluK signalling is directly

linked to inhibition and excitation of the hippocampus. Further subunit distribution and function is introduced in section 3.3.5.

3.3.3. Metabotropic glutamate receptors

The second group of glutamatergic receptors, metabotropic glutamate receptors (mGluR), are encoded by 8 genes, subunits for mGluR1 to mGluR8. All subunits consist of 7 TMD (Nakanishi & Masu, 1994), are G-protein coupled receptors (GPCR) and mediate their activation via G_q or G_i (Hollmann & Heinemann, 1994). mGluRs are separated into three subfamilies (Nakanishi & Masu, 1994). Group I includes mGluR1 and mGluR5 together with various splice variants that are predominantly located at the post-synapse (Pin & Duvoisin, 1995; Schoepp, 2001). Both receptors are coupled to a G_q, leading to well-known activation-cascades via activation of phospholipase C (PLC), hydrolysis of phosphatidylinositol-4,5-bisphosphat (PIP_2), increase in intracellular concentration of IP_3 -and Diacylglycerol (DAG), and final stimulation of Ca^{2+} release from intracellular Ca^{2+} stores, i.e., endoplasmic reticulum (ER). Rise in intracellular Ca^{2+} concentration together with DAG activation of the protein-kinase-C (PKC) can lead to phosphorylation of various targets as AMPA and NMDA receptors, that modulate receptor activity (Fukunaga et al., 1992; Hasham et al., 1997). Subfamily group II contains mGluR2 and 3 and group III contains mGluR4 and 6 to 8, which all are coupled to a G_i protein. Upon activation of group II or III mGluRs the adenylate cyclase (AC) activity is inhibited, leading to a decrease in intracellular cAMP levels. This ultimately leads to increased K^+ and decreased Ca^{2+} currents that hyperpolarize the cell membrane (Schoepp, 2001). In the CNS, mGluRs of group II and III are predominantly expressed pre-synaptically, where these receptors possess various physiological functions including the modulation of slow excitatory potentials (EPSPs) (Eaton et al., 1993; Glaum & Miller, 1992), inhibitory postsynaptic potentials (IPSPs) (Fiorillo & Williams, 1998) and transmitter release. Moreover, the function of mGluRs is also associated with epilepsy and fragile X syndrome (Ferraguti & Shigemoto, 2006).

3.3.4. The role of glutamate for epilepsy

Extracellular levels of glutamate are increased during seizures in humans. More precise, in patients with complex epilepsy or intractable epilepsies, an increased extracellular glutamate concentration within the hippocampus and amygdala before and during seizures was reported (During & Spencer, 1993; Lallement et al., 1991; Ronne-Engström et al., 1992). This increase of extracellular glutamate was also reported within the hippocampus for animal models of Pilocarpine-induced epilepsy (Millan et al., 1993) (see section 3.4.1.). Exposure of neurons to glutamate, even for a brief period, can lead to delayed cell death *in vitro* (Olney, 1989; Represa et al., 1989). Increase in extracellular levels of excitatory amino acids, when applied systemically or by focal injection, lead to hippocampal lesion that are similar to those of mesial temporal lobe sclerosis (Holmes, 1995) (see section 3.3.5.). As mentioned in section 3.1. mutations in ligand-gated ion channels account for 10% of genetic epilepsies. GluN subunits are affected frequently, and mutations reported and characterized especially for GluN1, GluN2a and GluN2b. The obligatory and glycine binding GluN1 subunit is encoded by *GRIN1* and linked by loss-of-function (LOF) mutations to early epileptic encephalopathy and intellectual disability (Oyrer et al., 2018). It was suggested that emerging pathogenesis secondarily lead to altered neuronal excitability and epilepsy (Oyrer et al., 2018). For both gain-of-function (GOF) and LOF mutation in the GluN2a subunit, encoded by GRIN2A, epilepsy and speech disorders are reported. Epilepsy occurs frequently during slow-wave sleep (Gao et al., 2017) and are linked to increased glutamate binding affinity, open probability (accounting for GOF), decreased Mg^{2+} pore block or protein expression level (accounting for LOF). As for LOF mutations in GluN1, decreased expression levels of GluN2a was suggested to secondary lead via emerging pathologies to altered neuronal excitability (Oyrer et al., 2018). Finally, also the *GRIN2B* encoded GluN2b subunit is linked by GOF and LOF mutations to infantile epileptic encephalopathy. Especially mutations that lead to decreased Mg^{2+} block or increased Ca^{2+} conductance are studied and characterized (Oyrer et al., 2018).

Localization, properties, and link to epilepsy of glutamatergic but also cholinergic and GABAergic receptors, introduced in the following sections 3.4., are summarized in Fig. 2.

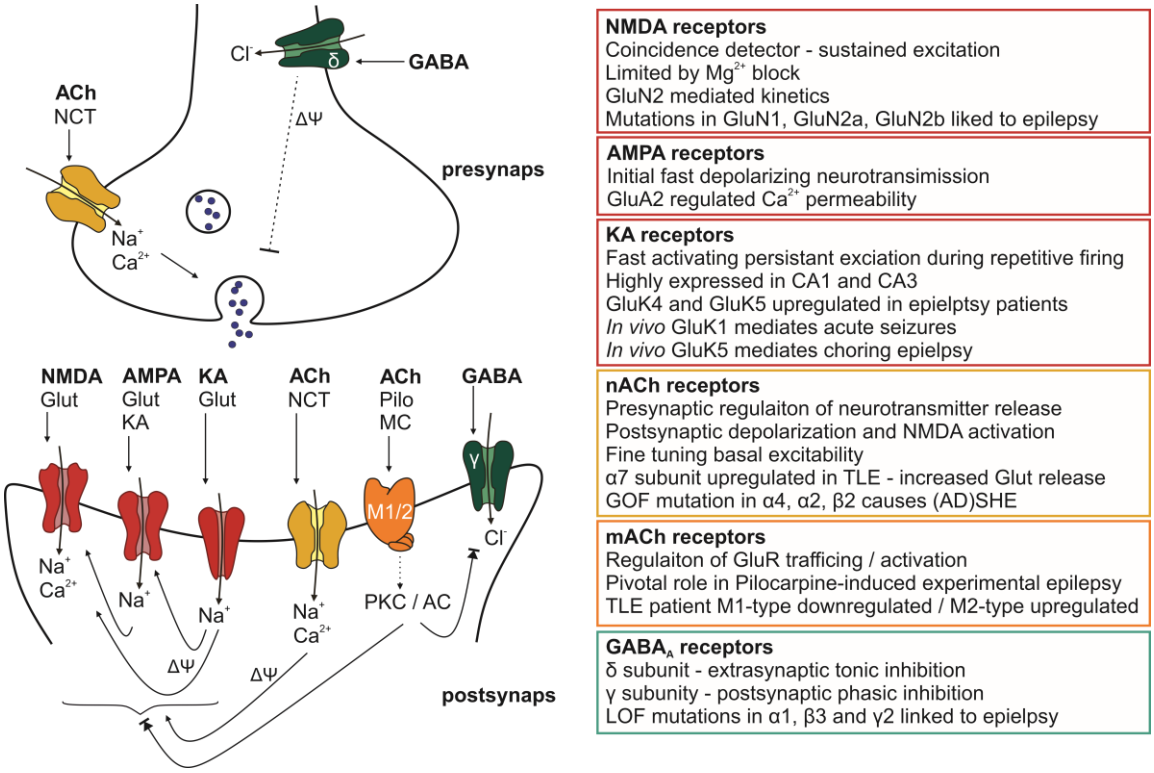

Figure 2: Neurotransmitter receptors involved in generation and balancing of neuronal activity.

The principal excitatory glutamatergic signalling is predominantly mediated by Na^+ and Ca^{2+} permeable NMDA and Na^+ permeable AMPA and KA receptors (KAR or GluK) (red symbols postsynaps) with depolarization mediated crosstalk between each receptor type (arrows with Δψ). Each receptor is activated by its specific agonist (NMDA, AMPA, KA) but also by glutamate (Glut). The principal inhibitory GABAergic neurotransmission is mediated by the $GABA_A$ receptor (green symbols) conveyed Cl^- influx. Depending on receptor subunit composition postsynaptic phasic (γ subunit) inhibition or extrasynaptic tonic inhibition (δ subunit) can be differentiated. Also, pre -and postsynaptic cholinergic signalling that is mediated by nicotinic (yellow symbol, Nicotine: NCT, nACh receptors) and muscarinic (orange symbol, Muscarine: MC, mACh receptors) acetylcholine receptors are modulating excitation. First, by modulating presynaptic neurotransmitter (blue circles) release and second, by postsynaptic depolarization (nACh receptor) or G-protein-mediated modulation (mACh receptor) of glutamatergic or GABAergic signalling. For all three receptor families mutations that cause temporal lobe epilepsy (TLE), *Autosomal Dominant Sleep-related Hypermotor Epilepsy* ((AD)SHE) and other epilepsy syndrome are known (depicted in respectively coloured text boxes on the right). Depicted receptors are not expressed and localized simultaneously in one postsynapse but just summarized for this figure.

3.3.5. The Kainic acid-induced model for epilepsy

Temporal lobe epilepsy (TLE) is the most common epilepsy disorder (Engel, 2001), and, similar to other epilepsy syndromes, also accompanied by heterogenous clinical manifestation(s) and pathophysiological alterations (Blümcke et al., 2013). To study TLE and other epilepsies KA was frequently used in the last decades to induce and model seizures, and histopathological alterations. Dealing with the fact that 60% of TLE patients display hippocampal sclerosis (HS, see below) with defined EEG pattern, the KA-based

model is a highly isomorphic model regarding the morpho-functional link between electrophysiological, clinical and histological presentation (Rusina et al., 2021).

KA is a cyclic analog of glutamate, activates GluK receptors that are expressed in the EC, amygdala, cerebellum, basal ganglia and especially hippocampus (Bloss & Hunter, 2010; Rusina et al., 2021) (see also 3.3.2.). Presynaptic GluK receptors modulate synaptic transmission bidirectionally with excitatory ionotropic and inhibitory non-canonical metabotropic function (Lerma & Marques, 2013). Postsynaptic GluK transmits excitatory signalling (Huettner, 2003). From the different GluK subunits, GluK4 is almost exclusively expressed in the CA3 region of the hippocampus with limited expression in the CA1 region (Darstein et al., 2003). GluK5 subunits are found to be expressed within GABAergic interneurons of the CA1 and CA3 region, together with cortex and striatum (Gallyas et al., 2003). In human patients, seizure provoked HS is linked to GluK5 upregulation (Li et al., 2010) that is also found in rodents (Bernard et al., 1999). Moreover, GluK1 and GluK2 are differentially expressed in the hippocampus, with abundant expression of GluK1 in the CA3 and GluK2 in the CA1 region (Bloss & Hunter, 2010). Previous work has shown that different GluK functions were directly linked to defined aspects of epilepsy: The GluK1 subunit was directly linked to induction of acute seizures (Fritsch et al., 2014). This is associated with GluK1 expression especially in inhibitory neurons of the hippocampus and evidence for alterations in inhibitory signalling, leading to acute epileptic seizures (Paternain et al., 2000). Chronic seizures were found to be directly linked to GluK2 and GluK5 subunits that are also found in mossy fibres, which, in turn, sprout among the chronic phase of epilepsy (Artinian et al., 2015; Rusina et al., 2021). Additionally, also in human patients specific GluK regulations can be determined: TLE patients reveal especially increased GluK4 expression levels (Lowry et al., 2013), that was also shown to mediate KA-provoked neurodegeneration (Das et al., 2012). Despite GluK subunits are linked to important elements of epilepsy and are most probably directly involved in seizure induction mediating excessive glutamatergic neuronal signalling, the detailed mechanisms how GluK mediate seizures and subsequently histopathological changes are not fully understood (Rusina et al., 2021). KA-induced seizures arise predominantly from the hippocampus (Ben-Ari & Cossart, 2000; Lévesque et al., 2009; Lothman et al., 1981), probably due to high GluK expression within the CA3 region that is especially prone to ictogenesis with its capacity to generate synchronized activity following KA exposure. This synchronized activity is due to activation of pyramidal cells via GluK of mossy fibres at the level of stratum lucidum (see Fig. 1).

In 88% of experiments intraperitoneal KA administration lead to generalized tonic-clonic convulsions that are highly isomorphic to human patient (Lévesque & Avoli, 2013).

Importantly, already 3 h after seizure induction, histopathological changes, which will be described in the following, occur. Mostly, these alterations are progredient for two weeks and are also highly isomorph to patients (Rusina et al., 2021). The behavioural spectrum of KA-induced seizures includes catatonic posture, myoclonus, mastication and automatisms, so called wet-dog-shakes and head nodding, rearing and frontlimb clonus, rearing with falling, jumping and cycling along the longitudinal axis, and finally SE with constant TCS (Raedt et al., 2009) leading to death in approximately 27% of cases. Consecutively, a latent period of 2 to 3 days without seizures separates acute seizures from SRS (Puttachary et al., 2015). This latent period is a central hallmark for human TLE and can prolong for years (Falco-Walter, 2020; Mathern et al., 1998). When SRS appear, the chronic period, representing principal epilepsy, is reached. Moreover, seizure provoked histopathological changes are isomorphic to human epilepsy patients. Upon KA administration extensive bilateral neuronal damage is provoked. Within the hippocampus, pyramidal cell loss is found especially within the CA3 but also CA1 region, together with astroglial reactivity and sprouting of mossy fibres, summarized as HS (Hu et al., 1998; McKhann et al., 2003; Mouri et al., 2008). Interestingly, parvalbumin positive (PV^+) interneurons are highly susceptible to KA-induced degeneration, especially within the CA1 region, EC and subiculum (Best et al., 1993; Drexel et al., 2012; Lévesque & Avoli, 2013). Additionally, cortical areas, the lateral amygdala and dorsal thalamus are affected, suggesting propagation of excessive neuronal activity to further brain regions, similar as in human patients (Hu et al., 1998; McKhann et al., 2003). Behavioural seizures are also characterized using electrophysiologic approaches. Following the systemic injection of KA to rats, typical EEG patterns like interictal spikes within the EC (Ben-Ari et al., 1981) 30 min after application, with subsequent ictal discharges within the hippocampal CA3 and amygdala appears and propagation to CA1, thalamus and frontal cortex (Lévesque & Avoli, 2013; Lothman et al., 1981). This is accompanied by rhythmic pattern like 30 - 90 Hz (gamma, γ) -oscillations within the hippocampus (Lévesque et al., 2009; Medvedev et al., 2000).

Together, the KA-based model for epilepsy includes all principal hallmarks of pathogenesis and clinical manifestation of human patients.

3.4. Other neurotransmitter systems in epilepsy

Beside glutamate, further neurotransmitters show an excitatory, inhibitory, and modulatory impact on neuronal activity. One important excitatory neurotransmitter represents acetylcholine, while GABA functions is the major inhibitory neurotransmitter in the CNS. In the following sections both are briefly introduced and related to clinical and experimental epilepsy.

3.4.1. Cholinergic signalling

Acetylcholine is mediating the so-called ”cholinergic signalling” that is transduced within the CNS by long-projection cholinergic neurons, located in the basal forebrain and brainstem, and local cholinergic interneurons, located for example in the striatum and hippocampus (Wang et al., 2021). Hence, cholinergic neurons especially from the medial septum, that is part of the basal forebrain, innervate limbic structures including hippocampus and amygdala, but also cortical regions (Allaway & Machold, 2017; Ballinger et al., 2016). The mesial septum extends GABAergic processes to the hippocampus, actively contributing to the maintenance of hippocampal θ-rhythm that plays a pivotal role in supporting cognitive functions (Nuñez & Buño, 2021; Yakel, 2013). Seizures can be provoked in the limbic system due to dysfunction in cholinergic tone. Cholinergic tone accelerates excitatory and limits inhibitory hippocampal signalling (somatostatin positive interneurons) thereby increasing excitatory output to the EC that further promotes EC-hippocampal network firing (Friedman et al., 2007).

Nicotinic acetylcholine receptors

As a homo- or hetero-pentamer comprising 16 known nicotinic acetylcholine receptor subunits (nACh), the functional receptor is a ligand gated ion channel, gating monovalent, but also bivalent cations. Subunits are named by Greek letter from α to ε. 9 different α, 4 different β and one member of each, γ, δ, and ε are known today, while ligand binding is mediated by α-subunits (Lukas et al., 1999). In the CNS, subunits α4, α7 and β2 are highly abundant, whereas within the hippocampus especially α7 and α4β2 subtypes are present (Yakel, 2013) and α4 in GABAergic interneurons (Son & Winzer-Serhan, 2006). Physiologically, activation of presynaptic nAChR can lead to accelerated release of neurotransmitters of both, glutamatergic and GABAergic neurons (see also Fig. 2). At the postsynapse, however, depolarization via nAChR can lead to a relive of the Mg^{2+} block of NMDA receptors and finally lead to increased excitability (Wang et al., 2021) (see also Fig. 2). In patients with TLE especially the α7 nAChR was found to regulate the hyperfunction of glutamatergic signalling within the hippocampus and amygdala

(Banerjee et al., 2020). Also, agonizing this α7 nAChR in the hippocampal CA1 region led to a decrease in seizure onset time in experimental epilepsy (Zhang et al., 2016). In epilepsy patients with *Autosomal Dominant Sleep-related Hypermotor Epilepsy* (see section 3.7.3) mutations in nAChR encoding *CHRNA2*, *CHRNA4* and *CHRNB2* were found to result in an increased expression density of this receptors in the midbrain, probably causing altered cholinergic signalling in the ascending arousal system (Picard et al., 2006). One of the (AD)SHE linked mutations causes spontaneous seizures, especially during periods of increased γ-waves, that are important for the non-REM-sleep phase (Picard et al., 2006). These pathologies result from increased nicotinic currents, which likely enhance neurotransmitter release from pre-synapses (De Fusco et al., 2000; Wang et al., 2021).

Muscarinic acetylcholine receptors and the Pilocarpine model for epilepsy

The muscarinic acetylcholine receptors (mAChRs) are GPCR encoded by 5 different genes M1 to M5 that build the 5 known receptor types. Functionally, the mAChRs can be grouped in M1-type receptors comprising M1, M3 and M5 that are coupled to a G_q protein, and M2-type receptors including M2 and M4 that signal through G_i (Caulfield & Birdsall, 1998) (for signal cascade see section 3.3.3.). Since mAChR are located on pre -and post-synapses of glutamatergic and GABAergic neurons, the functional properties can be very different. Especially the M1 receptor is important for a AMPA and NMDA mediated long term potentiation (Fernández de Sevilla & Buño, 2010). Neuronal rhythms like hippocampal γ -and θ-oscillations are mediated by mAChR expressed on both hippocampal pyramidal cells and GABAergic PV^+ interneurons, critically modulating experimental seizures (Dannenberg et al., 2017; Fisahn et al., 2002; Vandecasteele et al., 2014; Yakel, 2013).

Beside the KA-induced model for acute epilepsy (see 3.3.5.) the Pilocarpine (Pilo)-induced model is the most frequently used and established one (Curia et al., 2008). One favour of this model is that it mimics human patient isomorphic pattern and appearance of initial insult, development of seizures, latent period until SRS, progressive histopathological degenerations in certain brain areas, and EEG activity (Lévesque et al., 2021). As first described by Turski et al., 1983, Pilo i.p. injection provoke via M1 mAChR activation (Hamilton et al., 1997) convulsions and TCS that recure and lead to NMDA receptor driven SE in mice and rats (Müller et al., 2009; Nagao et al., 1996; Smolders et al., 1997). Following 30 min SE histopathological changes as neuronal cell loss within the piriform cortex, amygdala, thalamus, EC, subiculum, hippocampal CA regions, DG and substantia nigra can be detected (Lévesque et al., 2021). Furthermore, especially CA3

and DG neuronal sprouting into paragranular layer in TLE patient and mice (Cavazos et al., 2003) progressively occurring 10 days after SE (Becker et al., 2008). EEG recordings during latent period and adjected to SRS reveal interictal and ictal events that are isomorphic to human patients (Dudek & Staley, 2012; Perucca et al., 2014; Pitkänen et al., 2015; Weiss et al., 2016). Thos events are also linked to γ -and θ-osciullations within the CA3, CA1 and subiculum and are probably tuned by PV^+ but not somatostatin postitive inteneurons (Fujita et al., 2014; Jefferys et al., 2012; Salami et al., 2014; Toyoda et al., 2015). Also M2 type receptors were linked to epilepsies: In experimental models for epilepsy (Palomero-Gallagher et al., 2012) but also human TLE patients (Graebenitz et al., 2011), the expression of M2 and M4 were increased, while M1-type receptors are decreased (Müller-Gärtner et al., 1993) in patients with partial seizures, suggesting both to be compensatory regulated against epileptiform neuronal activity.

3.4.2. GABAergic signalling

The principal inhibitory neurotransmitter GABA mediate inhibitory neuronal signalling by ionotropic $GABA_A$ and metabotropic $GABA_B$ receptors (Owens & Kriegstein, 2002). These receptors were shown to recognize both, vesicular GABA in the synaptic cleft, which mediates phasic inhibition, and low concentrations of ‘ambient’ GABA, which regulates excitation by extra-synaptic receptors (Farrant & Nusser, 2005) thereby balancing excitability and temporal confidence of neuronal circuit activity. A dysfunction of GABA signalling is linked to a vast variety of epilepsy syndromes including TLE, childhood absence epilepsy and myoclonic atactic epilepsy (Cai et al., 2019).

$GABA_A$ type receptors (GARs) are pentameric and ligand gated ion channels composed of a hetero-pentamer of 19 possible subunit-encoding genes. Subunits can be divided into $\alpha_{1\text{-}6}$, $\beta_{1\text{-}3}$, $\gamma_{1\text{-}3}$, ε, δ, θ, π, $\rho_{1\text{-}3}$ with different pharmacological and biophysical properties (Chuang & Reddy, 2018; Sigel & Steinmann, 2012). Upon binding of GABA to the two binding sites at the interface between α and β subunits, channel opening leads to Cl^- influx and HCO_3^- efflux along concentration gradients (Voipio & Kaila, 2000). *In vivo*, 50 to 60% of GARs are composed of $\alpha_1/\beta_2/\gamma_2$, expressed throughout the CNS and at the post-synaptic membranes (Olsen & Sieghart, 2008; Pirker et al., 2000). Biophysical properties of GARs are determined especially by γ subunit mediates phasic inhibition by rapid activation kinetics, faster desensitization and higher EC_{50} (Baumann et al., 2002; Gingrich et al., 1995; Lavoie et al., 1997; Mody & Pearce, 2004) and δ subunit that mediate tonic inhibition by frequently extrasynaptic location, higher affinity, slower activation and low desensitization rates (Bianchi & Macdonald, 2002; Farrant & Nusser, 2005; Glykys & Mody, 2007; Haas & Macdonald, 1999) (see Fig. 2). One hippocampal

example is the post-synaptically located, slow kinetic and highly conducting δ containing GAR expressed within distal dendrites of pyramidal neurons, converting inhibitory signals from somatostatin positive interneurons. This enables control and modulation of NMDA mediated pyramidal firing and excitability (Schulz et al., 2018; Urban-Ciecko & Barth, 2016), i.e. feedback inhibition. Additionally, PV^+ modulation of pyramidal firing was found to be important for γ -and θ-oscillation and high frequency sharp waves (Dudok et al., 2022). Finally, also inhibitory interneurons are functionally connected: PV^+ interneurons of the hippocampal DG are densely packed with α_1 containing GARs allowing GABAergic disinhibition (Lin et al., 2015).

As members of the group of channelopathies mutations especially within *GABRA1* encoding α_1, *GABRAB3* encoded β_3 and *GABRG2* encoded γ_2 subunits are associated with early infantile epileptic encephalopathy (Oyrer et al., 2018). Predominantly LOF mutation lead to altered phasic and tonic GABAergic inhibition caused by decreased receptor expression, GABA sensitivity, and altered assembly resulting in aberrant network and disinhibition (Oyrer et al., 2018) (see also Fig. 2)

3.5. Voltage-gated sodium -and potassium channels in epilepsy

Glutamatergic, cholinergic, and GABAergic neurotransmission lead to gradual change in postsynaptic potential. Spatiotemporal sum of depolarization can lead to generation of action potentials (AP) at the soma and axonal initial segment (AIS), depending on neuron population with highly diverse AP kinetics, frequency, and pattern (Kress & Mennerick, 2009). The rise and fall of an AP is driven by voltage-sensitive Na^+ -and K^+ conductances with precisely tuned activity kinetics (Bezanilla, 2006b; González et al., 2012a; Johnston et al., 2010; Kaplan et al., 2016; Stafstrom, 2007) (see Fig. 3A and B) leading to the transient and regenerative 5-step AP that deflects the resting membrane potential (RMP) of -60 mV within 1 ms to +30 mV and return to RMP within 5 ms (Bezanilla, 2006a) (Fig. 3B). Beside channelopathies caused by mutations in ligand-gated ion channels (see Fig. 2), also voltage-gated ion channels that drive subsequent APs are known, mainly affecting voltage-gated Na^+ channels (Na_V) and voltage-gated K^+ channels (K_V).

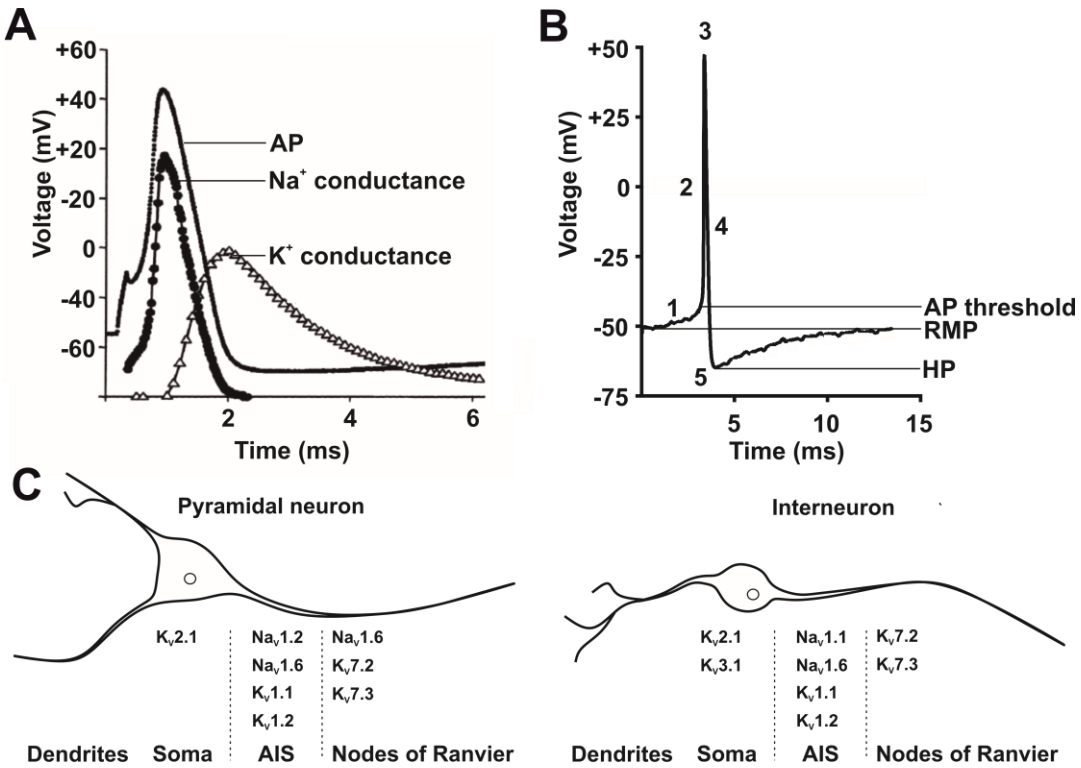

D

Channel	Contribuation	Impact	Epileptogenic mechanism
$Na_V1.1$	AP initiation	LOF	AP collaps at high firing frequencies
$Na_V1.2$	AP backpropagation	LOF / GOF	Increased I_{NaP}; increased excitability
$Na_V1.6$	AP initiation	GOF	Incoplete inactiavtion; increased I_{NaP}; increased excitability
$K_V1.1$	AP threshold; repol.	LOF	Broad AP support Ca^{2+} influx
$K_V1.2$	AP threshold; repol.	LOF / GOF	Shift in RMP; increased neurotransmission
$K_V2.1$	AP duration	LOF	Loss of K^+ sensitivity - increased depolarization
$K_V3.1$	AP duration	LOF	Decreased current amplitude limits AP firing
$K_V7.2/3$	AP duration	LOF	Loss of spiking adaptation

Figure 3: Phases of the action potential with pivotal ion channels and link to epilepsy.

The action potential (AP) is guided by differential opening of voltage-gated Na^+ channels (Na_V) that depolarize the resting membrane potential (RMP) by Na^+ influx (Na^+ conductance), followed by voltage-gated K^+ channels (K_V) that repolarized the RMP by K^+ efflux (K^+ conductance). Image adopted from Bezanilla, 2006b. **(B)** 5 phases of AP: (1) Upstroke – a sum of depolarizing stimuli causes an AP threshold to be reached at approximately -40 mV, and this results in the opening of Na_V leading to membrane potentials near 0 mV. (2) Over-shoot – Na_V reach their maximal conductance pushing membrane potential to positive values about +30 – +50 mV. (3) Peak – Na^+ influx approaches Na^+ equilibrium potential at approximately +50 mV. At this point Na_V channels are inactivated and slowly activating K_V open upon Na_V current removal. (4) Repolarization – Membrane potential rapidly returns to negative values, driven by delayed response of increasing K_V conductance that also fully inactivate Na_V. K^+ conductance stays elevated until Na^+ conductance reaches the resting status (see B) resulting in repolarization of the membrane potential. (5) Hyperpolarization – K_V mediated K^+ conductance remains present beyond the initial RMP, leading to transiently hyperpolarized membrane potentials. **(C)** For pyramidal neurons (left cell) and inhibitory neurons (right cell) several Na_V -and K_V are known to cause epilepsies in case of LOF or GOF mutations that are summarized as channelopathies. Depending on localization – dendrites, soma, axonal initial segment (AIS) or axon with nodes of Ranvier - these mutations affect basal excitability, channel opening and closing kinetics leading to increased excitatory or decreased inhibitory neuronal signalling (Oyrer et al., 2018). Illustration adopted from (Chow et al., 2020). **(D)** List of ion channels that are linked to epilepsy disorders by either GOF or LOF mutations including physiological (contribution) and pathophysiological (epileptic mechanism) properties. Repolarization is abbreviated as “repol.” Table adopted from (Oyrer et al., 2018).

3.5.1. Voltage-gated sodium channels in epilepsy

All 9 members of the 6 TMD spanning Na_V channels ($Na_V1.1$ to 1.9) are pivotal for setting the basal excitability e.g. AP threshold and initiate and propagate APs (Catterall et al., 2005) especially by so called “ball-and-chain” inactivation, mediating the open, closed and inactivated state of the channel that set the absolute and relative refractory period of the AP milliseconds after AP upstroke (see Fig. 3B) (Wisedchaisri et al., 2019; Yu & Catterall, 2003). Especially tetrodotoxin (TTX)-sensitive $Na_V1.1$, 1.2, 1.3 and 1.6 are expressed in the CNS that conduct transient (I_{NaT}) Na^+ currents with rapid gating in less than 1 ms driving AP upstroke. Additionally, following Na_V inactivation up to 1-3% of Na^+ currents can persist in activated state, called I_{NaP}. These persistent currents can be activated at an membrane potential of approximately -50 mV crucially modulating subthreshold voltages, neuronal excitability, and burst firing (Kaplan et al., 2016; Stafstrom, 2007).

Three members of Na_V channel family are directly linked to epilepsy, $Na_V1.1$, $Na_V1.2$ and $Na_V1.6$ all of which are sensitive to channel blocker TTX and important for AP upstroke and overshoot (see Fig. 3B). Different LOF and GOF mutations within the encoding genes lead to altered inactivation, reactivation or open-state kinetics frequently also depending on neuronal subtype. For example, $Na_V1.1$ is expressed predominantly in AIS of inhibitory neurons (see Fig. 3C) suggesting principal role for initiation and propagation of APs (Duflocq et al., 2008; Yu et al., 2006). There are several hundred primarily LOF variants in $Na_V1.1$ encoding gene *SCN1A* known (Oliva et al., 2012) leading to epilepsies most likely due to collapse of AP at higher firing frequencies in inhibitory neurons (Yu et al., 2006). Also, $Na_V1.2$ is expressed in the AIS but predominantly in excitatory neurons (see Fig. 3C) playing important roles for backpropagation to soma and dendrites (Hu et al., 2009). A variety of mutations in the $Na_V1.2$ encoding gene *SCN2A* are functionally either GOF or LOF (Oyrer et al., 2018). While LOF mutations are less well studied, GOF were associated with increased I_{NaP} and increased excitability of hippocampal pyramidal neurons (Kearney et al., 2001; Schattling et al., 2016). Finally, also $Na_V1.6$ is associated with GOF mutations in the encoding gene *KCN8A* to severe and early onset epilepsies (Oyrer et al., 2018). This channel is expressed within AIS and nodes of Ranvier (see Fig. 3C) and thereby important for AP initiation (Hu et al., 2009) and saltatory conductance (Gasser et al., 2012). GOF lead to incomplete channel inactivation and hyperpolarized voltage-dependence of activation (Oyrer et al., 2018). Thereby I_{NaP} currents was shown to be increased, together with unusual depolarizing events with excessive intracellular Na^+ concentrations (Lopez-Santiago et al., 2017). Interestingly, also $Na_V1.6$ deficiency can lead to epilepsies by altered GABAergic signalling within thalamic structures leading increased thalamic oscillation (Makinson et al., 2017).

3.5.2. Voltage-gated potassium channels in epilepsy

Beside Na_V channel, K_V channels are essential for AP kinetics in term of setting membrane potential, AP threshold and AP kinetics with subsequent regulation of spiking pattern making them prone to provoke epilepsies among altered function. K_V channels form one of the most diverse family of evolutionary conserved membrane proteins including 40 human K_V genes, categorized into 12 subfamilies (González et al., 2012b). Homo -or heterotetramers of six TMD (S1 to S6) form an α-subunit. A functional channel harbours its voltage sensor in the segment S1 to S4 and the pore forming domain between the flanking S5 and S6 segments (Attali et al., 2023; Kuang et al., 2015).

Based on their physiological characteristics, Kv channels can be divided in A-type channels with rapid activation and inactivation and classic delayed rectified channels that activate only partially and slowly and inactivate slowly. A-Type properties are evident for K_V1.4, K_V3.3 and 3.4, and K_V4.1 to 4.3. These channels affect AP duration during repetitive firing (González et al., 2012b). Most of the channels belonging to the K_V1, K_V2, K_V3, K_V7 and K_V10 subfamily are delayed rectifier channels with conductance in the range of 5 to 30 pS (Gutman et al., 2005). Further characteristics of K_V1 (especially1.2, 1.3 and 1.4) and Kv4 are activation following low levels of depolarization in the range of -35 mV (for K_V1.3) or -47 mV (for K_V4.1) and even lower in the range of the RMP, thereby fine tuning the timing of AP firing, the threshold for AP generation and the number of AP that are provoked during depolarization, but also shaping of waveforms of AP trains (Gutman et al., 2005; Johnston et al., 2010).

Delayed rectifier K_V1.1 and 1.2 are expressed within the AIS of excitatory and inhibitory neurons (see Fig. 3C) especially important for AP threshold, repolarization and waveform (Clark et al., 2009; Jan & Jan, 2012; Johnston et al., 2008). K_V1.1 is linked by LOF mutations of the encoding gene *KCNA1* to altered voltage-sensitivity and channel gating leading to lower peak amplitude and subsequent altered release of neurotransmitter by broadened AP and increased Ca^{2+} influx (Foust et al., 2011). This is linked to ataxia with increased seizure susceptibility (Simeone2013). LOF and GOF mutations in K_V1.2 encoding gene *KCNA2* are known to provoke early infantile epileptic encephalopathy (Allen et al., 2016; Maljevic & Lerche, 2013). Although the mechanism is not fully understood an altered neurotransmitter release due to shifted in RMP, limited high-pass filtering and gating of fast rising voltages triggering AP are likely involved (Oyrer et al., 2018).

K_V2 and K_V3 need more positive potentials to be activated in a range of +15 to +30 mV. This depolarization is achieved during AP and trains of APs. Thereby, they modulate the

AP duration and firing pattern of neurons supporting high and maintained firing (Johnston et al., 2010). Since K_V2 and K_V3 cannels additionally differ in their gating kinetics, with slow (K_V2) and fast activation (K_V3), respectively, K_V3 is especially important for AP duration and fast firing, fast after-HP (aHP) and reducing Na_V inactivation while K_V2 support inter-spike intervals to be more negative, thereby ensuring fast recovery of Na_V channels finally also maintaining firing within extended refractory periods (Johnston et al., 2010). Especially $K_V2.1$ and 3.1 are linked to epilepsies like infantile epileptic encephalopathy ($K_V2.1$) or progressive myoclonic epilepsies ($K_V3.1$) (Allen et al., 2016; Oliver et al., 2017). $K_V2.1$ is expressed in soma and AIS of excitatory and inhibitory neurons (Maljevic & Lerche, 2013; Trimmer, 2015). LOF mutations in the encoding gene *KCNB1* are associated with epilepsies probably due to loss of K^+ selectivity and altered gating that provoke increased cation influx and neuronal depolarization (Thiffault et al., 2015). While $K_V3.1$ related epilepsies are also linked predominantly to LOF mutations of the encoding gene *KCNC1* especially inhibitory neurons are affected by reduced current amplitude leading to limited fast spiking and increased network excitability (Oliver et al., 2017).

Finally, members of the K_V7 subfamily conduct the so called M-current, characterized by slow and non-inactivating K^+ current that critically regulate neuronal membrane potential hence excitability at subthreshold, also spiking adaptation and slow aHP (Brown & Passmore, 2009; Oyrer et al., 2018). Homo -and heterotetramers of $K_V7.1$ and 7.2 are expressed at the AIS and nodes of Ranvier (see Fig 3C) and linked to epileptic encephalopathy especially by LOF mutations within the encoding genes *KCNQ2* and *KCNQ3* that lead to loss of spiking adaption and increased excitability of excitatory neurons e.g., CA1 neurons (Maljevic & Lerche, 2013; Peters et al., 2005; Schwarz et al., 2006). Similarly, the M-current of $K_V7.5$ is important for lows aHP in CA1 neurons (Tzingounis et al., 2010) leading to epilepsies in case of LOF mutations in *KCNQ5*. Interestingly, as $K_V1.2$, also $K_V7.5$ is linked beside LOF to GOF provoked epilepsies (Lehman et al., 2017) making the underlying mechanism of $K_V7.5$ mutations, expressed in both excitatory neurons but also for example hippocampal PV^+ interneurons, more complex.

As a last example the *KCNMA1* encoded Slo1 is linked especially by LOF mutations to generalized epilepsies (Du et al., 2005). Slo conduct a large K^+ current that both can increase and decrease neuronal firing depending on context (Du et al., 2005). LOF lead to neuronal depolarization at rest leading to increased excitability and firing (Oyrer et al., 2018).

3.6. The Slo family of potassium channels

Beside Kv channels, the large superfamily of K^+ channels contain >70 genes, differentiated into 5 subfamilies. This 5 subfamilies include inward rectified K_{ir} channels and leak current 2-pore-loop K_{2P} channels that are essential for RMP, SK_{Ca} channels with intermediate K^+ conductance and finally the Slo family of K^+ channels (González et al., 2012b; Gutman et al., 2005; Kaczmarek et al., 2017).

Four members of ion sensing K^+ channels represent the Slo family of K^+ channels including the following: The Ca^{2+} sensing Slo1 (aka BK, maxi-K or $K_{Ca}1.1$), the Na^+ sensing Slo2.1 (aka Slick or $K_{Na}1.2$) and Slo2.2 (aka Slack or $K_{Na}1.1$) and the pH-sensing Slo3 (aka $K_{Ca}5.1$), all characterized by a high conductance following activation (Adelman et al., 1992; Atkinson et al., 1991; Butler et al., 1993). The individual members of this family differ in their structure and topology, leading to differences in functional and gating kinetics. Slo2.1, also called Slick (sequence like an intermediate conductance K^+ channel) and Slo2.2, also called Slack (sequence like a calcium activated K^+ channel) consist of six TMD. Slo1 and Slo3 have an additional S0 domain leading to seven TMD and an extracellular N-terminus (Meera et al., 1997; Salkoff et al., 2006). All members of the Slo family of K^+ channels share a prominent intracellular C-terminus of the α-subunit, which is responsible for sensing ions, metabolites, and other mediators, e.g. causing channel activation (Salkoff et al., 2006). Slo1 and Slo3 can be activated by membrane depolarization together with a second parameter, a rise in intracellular Ca^{2+} concentration for Slo1, and intracellular pH for Slo3. The amino acid sequence of the two Slo2 channels is 74% identical, leading to some similarities in structure, albeit a less abundant expression pattern (Schreiber et al., 1998). Slick is mostly expressed in brain, heart, skeletal muscle, kidney, liver, lung and testes, whereas the expression of Slack is restricted to excitatory tissues including the brain and heart, with testes as the only exception (Salkoff et al., 2006; Yuan et al., 2003). The main structural and functional divergence of Slick compared to Slack is the intracellular C-terminus. The Na^+ binding site is located at different positions, probably leading to their differences in Na^+ sensitivity, which is lower in Slack with an EC_{50} for Na^+ of ~40 mM, compared to Slick, with an EC_{50} for Na^+ of ~89 mM (Thomson et al., 2015). Also, when Na^+ is omitted from the experimental setup, Slick channels were shown to possess basal activity (Kaczmarek, 2013). This is probably due to a higher sensitivity of Slick for Cl^- ions (Kaczmarek, 2013; Yuan et al., 2000) and a C-terminal binding site for ATP.

3.7. The sodium-activated potassium channel Slack

Na^+-activated K^+ currents (K_{Na}) were first reported by Kameyama et al., 1984. Using patch-clamp recordings on guinea pig heart cells, those currents had a big conductance in the range of 210 pS and were depended on the intracellular Na^+ concentration ($[Na^+]_i$). Additionally, K_{Na} were independent from depolarizing voltages or increases in intracellular Ca^{2+} concentrations ($[Ca^{2+}]_i$). Interestingly, for K_{Na} activation, non-physiological $[Na^+]_i$ of up to 66 mM were required. In the next years K_{Na} were reported also for neuronal cell types (Bader et al., 1985; Dryer, 1991, 1994; Egan et al., 1992; Safronov & Vogel, 1996). Studies of Yuan et al., 2000 revealed an EC_{50} of 30 mM $[Na^+]_i$ and a conductance of 170 pS for neuronal K_{Na}. Under physiological conditions such high $[Na^+]_i$ are reached spatiotemporally very limited (Rose & Konnerth, 2001) making the physiological role of K_{Na} currents initially questionable. The term “sequence like and Ca^{2+} activated K^+ channel” (Slack) war first introduced by Joiner et al., 1998, who identified this new member of the Slo family upon a databank screening for the K^+ channel specific TXXTXGYG pore motif (Heginbotham et al., 1992) that is important for generating the K^+ selectivity. He found a Slo1 homolog in the genome of *Caenorhabditis elegans* (*C. elegans*). Based on this finding, a human homolog sequence was identified using the GenBank® (INSDC). Later, the homology of the new member was found to be restricted to 7% (Bhattacharjee & Kaczmarek, 2005a). Following this basal finding and characterization of Slack, studies on its structure and function were possible. In contrast to Slo1, Slack does not possess a S0 domain, hence, no modulatory β-subunits can associate with the channel through this domain. Also, the lack of positively charged amino acids in transmembrane domain S4 (see Fig. 4) leads to a voltage-insensitivity of the channel. Finally, in contrast to Slo1 channels, Slack is rather inhibited than activated by increasing $[Ca^{2+}]_i$ (Atkinson et al., 1991; Salkoff et al., 2006; Schreiber et al., 1998). Additionally, the Na^+ sensitivity of both, Slick and Slack, was reported to be increased by intracellular Cl^- leading to a left-shift in EC_{50} to 15 mM $[Na^+]_i$ among increased $[Cl^-]_i$ to 160 mM (Yuan et al., 2000).

From a structural point of view, the Slack channel consists of four identical α-subunits composed of six TMD S1 to S6 domains each. The K^+ selective pore forming loop-domain is located between TMD S5 and S6 (González et al., 2012b; Zhang et al., 2023). The prominent intracellular C-terminus adjacent to S6 harbours two regulator of conductance of K^+ (RCK) domains (Jiang et al., 2001; Yuan et al., 2003), several putative bindings sites for the protein kinase A (PKA), protein kinase C (PKC), as well as fragile mental retardation protein (FMRP) (Bausch et al., 2018; Brown et al., 2010; Nuwer et al., 2010;

Salkoff et al., 2006) and PDZ (postsynaptic density 95/disc large/zona occludes) bindings sites, which are also found in K_V, enabling localization and interaction with receptors at the postsynaptic site (Uchino et al., 2003) (see Fig. 4). PKC mediated phosphorylation of C-terminal S407 in the hinge region between S6 and RCK1 leads to increased current amplitude (Barcia et al., 2012; Santi, 2006). This S407 is also linked to protein phosphatase1 associated signal protein Phactr1, which dissociates from Slack upon channel activation and suggests, that further downstream signalling cascades are linked to Slack channel function and activation (Ali et al., 2020; Fleming et al., 2016).

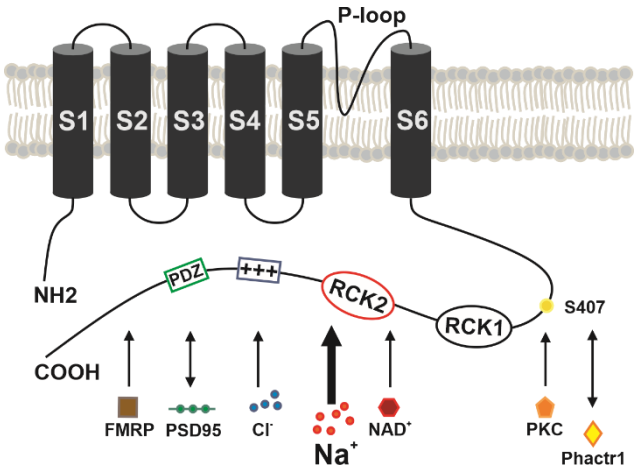

Figure 4: Slack channel topology with intracellular interaction partners.

The functional and pore forming α-subunit of Slack channels consists of 6 transmembrane domains, S1 to S6, carrying a pore-forming loop (P-loop) between S5 and S6 but no positively charged amino acids in S4, that are known for Slo1 and needed for voltage sensing, leading to Slack channels voltage-insensitivity. Four α-subunits must group together to form the pore. In contrast to Slo1 the N-terminus of Slack is located inside. The large intracellular C-terminus harbours modulatory phosphorylation sites (yellow circle S407) that can be phosphorylated by protein kinase C (PCK, yellow pentagon) and is linked to Phactr1 (yellow rhombus) binding and dissociation. Principal activation of Slack is mediated by Na^+ (red circles) via the RCK2 (regulators for conductance of K^+) domain. Among increased intracellular NAD^+ levels (red hexagon) Na^+ sensitivity of Slack is increased, similar to increased intracellular Cl^- concentrations (blue circles) that are recognized by positively charged amino acids (blue edged), a domain with functional similarity to Slo1's Ca^{2+}-bowl. Finally, PDZ interaction site (green edged, postsynaptic density 95/disc large/zona occludes) can interact with synaptic PSD95 and binding of fragile mental retardation protein (FMRP, brown rectangle) to the C-terminus can increase Slack currents. Arrows depict activating effect of intracellular ligand / factor / protein; double arrow depict interaction sites and partners.

Since the S6 domain does not contain positively charged amino acids as voltage sensor, it is not surprising that Slack function is independent from the cellular membrane potential, but predominantly regulated by the DX(R/K)XXH motive in the RCK2 domain that contains a highly conserved sequence of amino acids needed for Na^+ mediated activation of the channel (Thomson et al., 2015; Zhang et al., 2010). When this site is mutated Na^+ sensitivity is substantially reduced (Kaczmarek et al., 2017). This motive is similar to other

Na^+-sensing K^+ channels like $K_{ir}3.2$ and $K_{ir}3.4$ (Kaczmarek et al., 2017). The channel sensitivity towards Cl^- ions is mediated, at least in *C. elegans,* by a separate Cl^--bowl at the C-terminus, harbouring positively charged amino acids, which is similar to the Ca^{2+}-bowl in Slo1 (Yuan et al., 2000) and mediate increased Slack currents upon increased intracellular Cl^- concentrations. The Slo2.2 encoding gene *KCNT1* consists of 30 exons, allowing the alternative splicing of five different isoforms of Slack. These isoforms were found to mainly differ in their N-termini, kinetics, expression pattern and interaction with other channel subunits (Brown et al., 2008). The Slack-A and Slack-B isoforms differ in their exon 1 at the N-terminus and can be alternatively spliced to either Slack-Ax2 or Slack-Bx2, that both lack exon 2. Interestingly, the N-terminus of both, Slack-A and Slack-Ax2, show 78.1% similarity to the N-terminus of Slick, leading to similar fast activation kinetics of Slick and Slack-A. The N-terminus of Slack-B is more similar to Slo1 and shows delayed activation kinetics, due to fast but incomplete activation to an intermitted state that comes to a full conductance with a 100 ms delay. Additionally, Slack-B isoforms stay in their open configuration 6 times longer compared to Slack-A. The fifth isoform, Slack-M is less studies but reported to have a very different N-terminus that is encoded by a gene segment upstream of the Exon1 (Brown et al., 2008). By comparing conductances of Slack isoforms, again, probably due to the similarities in N-termini, the Slack-A isoform has a similar conductance compared to Slick. Still, the average conductance of all Slack isoforms is 180 pS and higher compared to Slick channels with 140 pS (Bhattacharjee et al., 2003a; Brown et al., 2008). As mentioned earlier, Slack is expressed almost exclusively in excitatory tissues (Joiner et al., 1998; Kameyama et al., 1984; Rizzi et al., 2016) with prominent expression in the olfactory bulb, midbrain and brain stem, cortex, cerebellum, and hippocampus (Bhattacharjee et al., 2002; Bhattacharjee & Kaczmarek, 2005b; Brown et al., 2008). More precise, Slack-A was reported to be expressed especially in hippocampal granular dendrites and DG, and Slack-A and Slack-B within the pyramidal cells of hippocampal CA regions (Brown et al., 2008).

The physiological role of Slack channel properties - $[Na^+]_i$ sensitivity and high conductance - was first studied by Bhattacharjee & Kaczmarek in 2005, and found to stabilize the neuronal resting membrane potential. In resting neurons the $[Na^+]_i$ is 4 to 15 mM (Kaczmarek, 2013; Rose, 2002). Based on this, Tamsett et al. 2009 also showed a functional impact of Slack channels in activated neurons, based on the shift in Na^+ sensitivity by increases in intracellular NAD^+ levels that reached physiological ranges. Besides modulating basal neuronal activity, Slack plays a prominent role during high frequent neuronal firing: Mediated by Na_V and glutamatergic receptors, repeated neuronal

high frequent spiking leads to increases in $[Na^+]_i$, suitable for Slack activation. Due to the persistent K^+ efflux mediated by Slack, the neuron can be hyperpolarized and inactivated for a long time (Kaczmarek, 2013; Kim & McCormick, 1998). The important contributions of Slack to this slow aHP was shown in pyramidal neurons of the cortex (Schwindt et al., 1989) and subsequently in various neuronal populations (Descalzo et al., 2005; Franceschetti et al., 2003; Kaczmarek, 2013; Kim & McCormick, 1998; Kubota & Saito, 1991; Sanchez-Vives et al., 2000; Sandler et al., 1998). Additionally, Slack channels play an important role in neuronal formations that generate and enable exact timing of firing: Timing of single AP in burst or spiking trains is fine-tuned by Slack, finally fitting rhythmic firing frequency (Kim & McCormick, 1998; Nuwer et al., 2010). Also, in the superior olivary body, neurons of the medial nucleus of the trapezoid body can fire at high frequencies of 800 Hz accurately tuned by Slo currents (Yang et al., 2007). Finally, Slack was very recently shown to physically interact with $Na_V1.6$ (Yuan et al., 2023), and it functionally interacts with GluA (Nanou et al., 2008) and GluN (Matt et al., 2021). These interactions link Slack currents directly to Na^+ sources thereby modulating neuronal activity and temporal accuracy.

Ultimately, the function of Slack is also linked to further physiological and pathological processes, including synaptic plasticity, nociception, excitotoxicity, and epilepsy.

The functions of Slack are briefly introduced below for nociception and excitotoxicity. Subsequently, Slack's role for epilepsy is further introduced in detail, which is relevant for the present work.

3.7.1. The role of Slack for neuropathic pain

Nociception is mediated by peripheral free nerve endings of afferent neurons, called nociceptors, that are responding to mechanic, thermic or chemical stimulation. Their electrical stimulation is emotionally evaluated in the CNS (Basbaum et al., 2009). Neuropathic pain is provoked by neuronal damage, leading to different expression and activity of ion channels and finally to accelerated excitability of sensory neurons (van Velzen et al., 2020; Waxman & Zamponi, 2014). The transmission of the peripheral signals to the CNS is mediated by sensory neurons of the dorsal root ganglia of the spinal cord (DRG) which were shown to express high levels of K_{Na} (Lu et al. 2015). Since spiking frequency and spiking adaption of DRG are directly linked to K_{Na} function, an important role of both, Slick and Slack, was postulated (Nuwer et al., 2010; Tamsett et al., 2009; Tomasello et al., 2015). Lu et al. 2015 provided first *in vivo* studies on global and DRG-specific Slack-KO mice, reporting enhanced nociception compared to wildtype animals. More recently, the underlying molecular and cellular mechanisms were

elucidated: by functional interaction with TRPA1 and P2X3 receptors Slack and Slick crucially modulate nociception (Lu et al., 2021; Zhou et al., 2022).

3.7.2. The role of Slack for excitotoxicity

Excitotoxicity refers to neuronal damage induced by toxically accelerated excessive and prolonged AMPA -and NMDA mediated glutamatergic signalling, leading to neuronal cell death (Gillessen et al., 2002; Olney, 1989). Glutamate accumulation in the synaptic cleft finally leads to necrotic and apoptotic cell death. This mode of neuronal degeneration is associated with neurodegenerative diseases and stroke provoked cerebral ischemia, which are intractable to date (Albensi et al., 2004). K^+ channels including Slack regulate neuronal excitability, hence, are suggested to provide neuroprotective counterparts of excitotoxic processes. In 2008 Nanou et al., induced excitotoxic synaptic transmission by AMPA-mediated activation. This neuronal activity was limited by Slack-mediated K^+ efflux. With these experiments, functional interaction of Slack channels with AMPA receptor-induced Na^+ influx was shown, as well as the capacity of Slack to limit excessive neuronal activity. Conformingly, also the NMDA-mediated neuronal activity was functionally linked to Slack channel function: Ehinger et al., 2021 reported exacerbated striatal lesion areas following NMDA injection to global Slack-KO mice compared to wildtype animals, or *in vitro,* by increased numbers of apoptotic Slack-KO cerebellar granular cells following NMDA exposure. These findings were functionally linked to Slack-mediated K^+ efflux that limited membrane depolarization, together with neuroprotective signalling of brain derived neurotrophic factor (BDNF) and its receptor TrkB, that was impaired in Slack-KO animals.

3.7.3. The role of Slack for epilepsy

Based on patient sequencing in 2012, the Slack channel was first linked to severe, early onset and refractory epilepsy disorders (Barcia et al., 2012; Heron et al., 2012). Subsequent multitudes of clinical reports constantly broadened the number of *KCNT1* variants linked to epilepsy. To date, 64 different pathogenic variants are known and described in a comprehensive study by Bonardi et al., in 2021 which distinguish between *Epilepsy of Infancy with Migration Focal Seizures* (EIMFS) and *Autosomal Dominant Sleep-related Hypermotor Epilepsy* (AD)SHE. Additionally, the patients that exhibit clinical manifestations comparable to EIMFS but differ in their seizure onset and migration were classified as no-EIMFS and linked to the wide group of heterogenous *Developmental and Epileptic Encephalopathy* (DEE). In general, most (61%) pathogenic variants of the Slack encoding gene, *KCNT1*, are linked to EIMFS, followed by (AD)SHE (21%) and non-EIMFS DEE (15%). Interestingly, all mutations share some characteristics as they

are almost exclusively missense mutations, located predominantly at the S5 pore region of the pore region, RCK1 or RCK2 domain (see Fig. 4), and are most frequently *de novo* mutations, which segregate autosomal dominant in case of inheritance (Bonardi, et al., 2021; Hansen et al., 2017; Ishii et al., 2013; Lim et al., 2016). Inherited cases are reported almost exclusively for (AD)SHE and segregate by both genders, paternally and maternally. Additionally, among all known mutations, 24 variants are repeatedly identified and reported, where G288S, A934T, R474H, R428Q, R398Q, and R950Q account for approximately half of all affected individuals. Two-thirds of (AD)SHE causing *KCNT1* mutations are located in the RCK2 domain, while EIMFS and non-EIMFS DEE provoking variants are found in all hot spot like regions, the pore region, RCK1 and RCK2 (Bonardi, et al., 2021). While EIMFS and non-EIMFS DEE are associated with an early onset of seizures and more severe intellectual disability starting at 1 month after birth, (AD)SHE shows later onset at approximately 54 months after birth. Still, all disorders are highly refractory to antiepileptic drugs (AED), leading to seizure freedom upon treatment in a minority of patients (6.4%) (Bonardi, et al., 2021).

Clinical characteristics of EIMFS include the following symptoms: (i) Migrating focal seizures, (ii) neurodevelopmental regression after seizure onset, (iii) high seizure frequency, (iv) heterogenous seizure types including tonic-clonic, focal impaired awareness, myoclonic, hemiclonic / clonic and tonic seizures that are (v) refractory to AED with (vi) an EEG revealing focal, multifocal and generalized interictal epileptic abnormalities (Aminkeng, 2013a; Barcia et al., 2012; Bonardi, et al., 2021). Besides *KCNT1* mutations, genomic aberrations in other genes, including the $Na_V1.1$ (see also section 3.5.1.) encoding gene *SCN1A* are reported to provoke EIMFS (Carranza Rojo et al., 2011; Milh et al., 2013). However, since 39% of all patients carry a mutation in *KCNT1*, this gene is the primary disease causing gene compared to other etiologies (Lim et al., 2016).

Clinical characteristics of non-EIMFS DEE are, despite not causing migrating seizures, greatly overlapping with EIMFS icluding (i) seizure onset in neonatal period, (ii) neurodevelopmental delay or regression, (iii) various seizure types including epileptic spasms, tonic-clonic, tonic, myoclonic seizures, (iv) refractory to AED and (v) an EEG with focal and multifocal epileptic abnormalities.

Clinical characteristics of (AD)SHE are the following: (i) Familiar inheritance in many cases, (ii) incomplete penetrance and variable intra-familiar presentation, (iii) seizure onset in early childhood, (iv) hypermotor and tonic asymmetric seizures with various seizure types, (v) in approximately one third of patient's seizures occur also during

daytime, (vi) are refractory to AED, and (vii) are linked to focal and multifocal ictal EEG onset, with additional (vii) cognitive impairment and psychiatric / behavioural problems (Aminkeng, 2013b, 2013a; Heron et al., 2012; Kim & Kaczmarek, 2014). Additionally, beside mutations in *KCNT1*, variants of other genes are known to cause (AD)SHE. Especially, mutations in *CHRNA4* encoding a nicotinic acetylcholine receptor subunit (see section 3.4.1) are linked to (AD)SHE together with mutations of *SCN2A*, encoding for $Na_V1.2$, and *KCNQ2*, encoding for $K_V7.2$ (see section 3.5.) (Kim & Kaczmarek, 2014; Møller et al., 2015). Interestingly, clinical presentation is different between KCNT1-related (AD)SHE and others. While mutations in *KCNT1* also lead to psychiatric, behavioural and intellectual impairments, these clinical alterations are not reported for other susceptibility genes.

In general, neurodevelopmental disorders are prominent in EIMFS and non-EIMFS DEE, while just fractions of (AD)SHE patients are affected by mild neurodevelopmental disorders (Bonardi, et al., 2021; Kim & Kaczmarek, 2014; Møller et al., 2015). Also, cardiovascular alterations are not frequent, but increased lethality of EIMFS and non-EIMFS DEE patients, which is probably linked to cardiac alterations.

Possible pathomechanism that lead to epilepsy syndromes caused by Slack mutations

Following first reports of *KCNT1* variants, underlying alterations in Slack channel function were extensively studied, especially in heterologous systems including HEK293 cells and *Xenopus laevis* oocytes. Interestingly, compared to wildtype Slack, an increased Slack-mediated current was found in all tested mutated Slack variants, leading to 3 to 12-fold increase in current amplitude (Barcia et al., 2012; Kim & Kaczmarek, 2014; Martin et al., 2014; Milligan et al., 2014). These amplitudes were provoked by increased open probability, limitation of intermediate conductance states, increase in Na^+ sensitivity and cooperativity between Slack channels (Barcia et al., 2012; McTague et al., 2018; Tang et al., 2016). The reasons for epileptiform neuronal activities can be variable and probably include circuitries of neuronal interactions and modulations. Still, especially K^+ channels were found to be linked to epilepsy syndromes by LOF, but also GOF mutations, leading to abnormal neuronal activity as reviewed by Niday & Tzingounis, 2018. Accordingly, Slack GOF variants were early discussed and suggested to drive epilepsy by different possible mechanisms (Kim & Kaczmarek, 2014): Slack GOF mutations can lead to epilepsies by (i) accelerated AP repolarization leading to shorter AP duration and higher rate of Na_V channel recovery to finally result in increased AP firing rates, (ii) accelerated hyperpolarization resulting in increased activation of hyperpolarization activated cation channels (HCN; I_h) triggering network hyperexcitability, (iii) increased hyperpolarizing K^+

currents, especially in inhibitory neurons, leading to network disinhibition by altered balance between excitation and inhibition, and (iv) increasing K^+ currents in early developmental stages and subsequent alterations of proper circuitry wiring.

Interestingly, also a LOF variant of *KCNT1* was reported to cause severe leukoencephalopathy, accompanied by delayed myelination and epilepsy (Vanderver et al., 2014). More precise, patient suffer from myoclonic, generalized-tonic seizures and frequently SE one month after birth. This pathogenic mutation is a heterozygous P932I *de novo* point mutation at a highly conserved C-terminal position downstream of the RCK2 domain. In contrast to EIMFS, seizures caused by the P932I mutation are not migrating and clinical overlap to (AD)SHE is mainly restricted to refractory myoclonic seizures. Still, delayed myelination can also be found in approximately 34% of EIMFS and 8% of (AD)SHE patients (Bonardi, et al., 2021) reflecting, together with refractory seizures, common features of Slack related epileptic disorders. Based on experiments using a heterologous Chinese hamster ovary (CHO) cell model, the LOF variant was further characterized and found to result in altered localization of Slack channels: Mutant Slack was expressed to an equal level as the wildtype channel, but not located at the plasma membrane. This was functionally confirmed by insensitivity of mutant LOF-Slack to non-specific “Slack activator” Loxapine in voltage-clamped cells (Evely et al., 2017). Together, both, too much but also too little Slack function leads to severe epilepsy and underlying pathomechanism were consecutively studied in the recent years.

Current research and evidence for the role of Slack in epilepsy

An increasing number of research articles provides *in vivo* and *in vitro* findings concerning Slack LOF and GOF knock-in mice leading to several highly sophisticated characterizations of the role of Slack in epilepsy. Mice with a global Slack knock-out (KO) were reported to display impaired motor learning, reversal learning and anxiety (Bausch et al., 2015; Quraishi et al., 2020; Zhang et al., 2022) in line with psychiatric and behavioural symptoms, especially in (AD)SHE (Bonardi, et al., 2021). Still, no spontaneous seizures were reported, and also EEG recordings revealed no interictal discharges in Slack deficient mice or *Drosophila* (Byers et al., 2021; Quraishi et al., 2020; Zhang et al., 2022). Four different GOF variants of Slack were generated and studied to date: (i) the mouse R455H which corresponds to human R474H located in the RCK1 domain (Quraishi et al., 2020), (ii) the mouse Y777H which corresponds to human Y796H located near the NAD^+ binding site of the RCK2 domain (Shore et al., 2020; Zhang et al., 2022), (iii) the mouse P905L which corresponds to human P924L located downstream adjacent to the RCK2 domain (Burbano et al., 2022; Quraishi et al., 2019), and (iv) a L456F mutation located at the RCK1 domain (Gertler et al., 2022). These *KCNT1* variants

are repeatedly found in EIMFS patients - R474H and P905L – or (AD)SHE patients – Y796H – excepted from L456F, which is not related to human patients, but still provokes *in vivo* and *in vitro* pathologic phenotypes (Gertler et al., 2022). Interestingly, while human patients with spontaneous recurrent seizures carry heterozygous *KCNT1* variants, Slack GOF penetrance is more diverse in animal models. Homozygous L456F do not lead to spontaneous seizures. Homozygous R455H is lethal *in uteri*, together with spontaneous seizures in heterozygous mice (Gertler et al., 2022; Quraishi et al., 2020). The Y777H and P905L variant lead to SRS in homozygous but not heterozygous mice, although the authors discussed occurrence of sporadic seizures that are frequently not detectable due to rare occurrence (Burbano et al., 2022; Shore et al., 2020). In Table 1 *in vivo* findings of Slack-deficient ($Slack^{-/-}$) and Slack-knock-in (KI) mice and *Drosophila* are summarized.

Table 1: *Differential role of Slack variants for spontaneous and provoked convulsions*

				Seizure susceptibiliyt and severety				
Species	**KCNT1 varinat**	**Functional cause**	**SRS**	**KA**	**PTZ**	**mA**	**Bang / Heat**	
C57Bl/6N	$Slack^{-/-}$	LOF	no	↑	↔	↑ *		*Susceptibility↑ mortality ↓
Drosophila	$Slack^{-/-}$	LOF	no	-	-	-	↑	↑ - Increased
C57Bl/6NJ	$Slack^{Y777H/Y777H}$	GOF	yes	-	-	-	-	↓ - Decreased
C57Bl/6J	$Slack^{+/R455H}$	GOF	yes	-	↑	-	-	SRS - Spontaneous recurrent seizures
C57Bl/6J	$Slack^{L456F/L456F}$	GOF	no	↑	↑	-	-	KA - Kainic acid
C57Bl/6J	$Slack^{P905L/P905L}$	GOF	Yes	-	-	-	-	PTZ - Pentylenetetrazole
								mA - Current induced seizures

Beside basal seizure occurrence and activity, mice and *Drosophila* with either Slack-KO or KI were tested in several models of acute seizures. In two studies, the $GABA_A$ and $GABA_B$ blocker Pentylenetetrazol (PTZ) was tested: Both, R455H and L456F lead to increased seizure severity upon PTZ injection to heterozygous (R455H) or homozygous (L456F) mice (Gertler et al., 2022; Quraishi et al., 2020) (see also Table 1). Interestingly, using the $GABA_A$ blocker Flurothyl to provoke acute seizures, no genotype specific differences were found in L456F transgenic mice. *Vice versa*, these animals responded with drastically increased seizure susceptibility and severity to a KA-induced model of acute seizures (Gertler et al., 2022). Together, mutant *KCNT1* leads to various phenotypes and finally, the seizure susceptibility varies between *KCNT1/Kcnt1* variant, seizure model and species. This complexity is to some extend confirmed by reports derived from Slack-KO animal models, showing increased seizure susceptibility in several *Drosophila* epilepsy models (Byers et al., 2021), but unchanged vulnerability to PTZ in Slack-KO mice, that are even protected from death in a electro-shock induced model for seizures (Quraishi et al., 2020).

The *in vivo* phenotype and seizure susceptibility depend on the Slack status, with complex differences between the studied Slack variants. Still, increased, as well as decreased Slack function may cause altered seizure susceptibility. The underlying mechanisms were studied in detail using both Slack-KO and Slack-KI animal models. As summarized in Table 2 different Slack-state lead to differential impact on neuronal subpopulations and AP properties.

Table 2: *Differential role of Slack variants for brain regions, neuronal population, and action potential property.*

	Cortical neurons		**Hippocampal neurons**		**BLA neurons**		**DRG**	
KCNT1 varinat	**Affected neurons**	**Alteration**	**Affected neurons**	**Alteration**	**Affected neurons**	**Alteration**	**Affected neurons**	**Alteration**
KO	-		Glut	AP frequ. ↑ AP thresh. ↓ AP slope ↑	Glut	AP frequ. ↑ RMP ↓ AP thresh. ↔	Glut	AP frequ. ↑ AP thresh. ↓ RMP ↑
Y777H	NFS	AP frequ. ↓ Rheo ↑ I_{NaP} ↓	-		Glut	AP frequ. ↓ RMP ↓ AP thresh. ↔	-	
P905L	iPSC	AP frequ. ↑ aHP ampl. ↑ AP thresh. ↔	-		-			
L456F	-		PV^+	AP frequ. adapt.↑ RMP ↔ AP thresh. ↔				

FS: Non fast spiking interneuron
iPSC: Induced pluripotent stemm cell derived cortical neuron
Glut: Glutamatergic neuron
PV^+: Parvalbumin positive inhibitory neuron
AP: Action potential
frequ.: Frequency
thresh.: Threshold
↑ / ↓ / ↔: Upregulated / downregulated / not altered

For cortical and hippocampal neuros carrying Slack-KI channel based on current-clamp and multi-electrode-array measurements, an increase in single cell and tissue circuitry firing was reported (Gertler et al., 2022; Shore et al., 2020). This was primarily linked to increased hyperpolarizing Slack currents in GABAergic non-fast-spiking (NFS) cortical neurons and PV^+ positive hippocampal interneurons, while firing patterns of glutamatergic neurons were unaltered. In other studies contradicting findings gave rise to the idea that Slack channel function is highly brain region-, cell type- and activation dependent: While induced pluripotent stem cell (iPSC) derived neurons, that are probably glutamatergic and carrying a Slack GOF variant, respond with increased AP firing to stimulation also glutamatergic Slack-KO neurons isolated from the lateral amygdala or DRG respond with increased spiking to stimulation (Martinez-Espinosa et al., 2015; Quraishi et al., 2019; Zhang et al., 2022). Within the amygdala, Zhang et al. 2022 was able to determine effects of both, Slack LOF and Slack GOF, on firing frequency of glutamatergic neurons. They observed increased firing frequency in Slack null neurons, and, *vice versa*, a decreased spiking frequency in Sack GOF neurons (Zhang et al., 2022). In all experimental systems,

changes in neuronal activity were accompanied by at least one alteration in RMP, AP threshold or AP amplitude (three main alterations summarized for all Slack variants in Table 2), hence directly linking electrophysiological parameters to AP firing frequency, and finally *in vivo* manifestation. Together, depending on the neuronal circuitry, too much, as well as too little Slack activity promoted neuronal activity and finally seizure susceptibility and severity. Systemic disinhibition can lead to accelerated neuronal activity, but also a loss of Slack can increase glutamatergic firing.

Targeting Slack to treat epilepsy

Slack related epilepsies were found to be provoked by GOF mutations in the *KCNT1* gene. This common feature led to the idea of treating patients with Slack inhibitors. Quinidine is a Na^+ channel blocker and used for treatment of arrhythmia, but also found to be a non-specific blocker of both, wildtype and mutated Slack channels (Milligan et al., 2014). Starting with a first EIMFS patient who benefited from Quinidine treatment with seizure free periods and improved psychomotor development (Bearden et al., 2014; Mikati et al., 2015), several studies found inconsistent results as recently reviewed by Xu et al., 2022. Accordingly, approximately 50% of patients that benefit from Quinidine had cardiac adverse effects (Bonardi, et al., 2021; Xu et al., 2022). Recently, Yuan et al. 2023 provided evidences of physical interactions of $Na_V1.6$ and Slack channels, suggesting Quinidine function to target both, Slack and its Na^+ sources. Additionally, further compounds were found to modulate Slack function in ortholog systems (Biton et al., 2012; Yang et al., 2006), which is important at least for pharmacological modulations of Slack function, and raises opportunities to further study the role of Slack in epilepsy. Spitznagel et al. found a highly potent Slack antagonist VU0606170 that is potent to block Slack at 10 µM *in vitro*, which needs to be further evaluated in an animal model-based approach, but gives rise to new and further Slack specific treatments of *KCNT1* related epilepsy (Spitznagel et al., 2020). Also Griffin et al. reported a highly Slack specific antagonist, compound 31, with the striking advantage of per-oral administration (Griffin et al., 2021). Together, patient and laboratory-based evidence suggest Slack to be a valid pharmacological target to treat *KCNT1*-related, but also other epilepsy syndromes. To complete new pharmacological options, also a Slack activator, compound 6, was successfully designed and tested *in vivo* (Balzulat et al., 2023). Robust reduction of itch in mouse modes for both histamine-independent and chronic itch were reported. This confirms the Slack channel as a pharmacological target and expands the pharmacological possibilities to modulate Slack channel function.

4. Aims and Objectives

Given the importance of Slack channel function in setting the RMP and neuronal excitability, the following goals were set to further elucidate the role of Slack in epilepsy:

(1) To determine whether seizure susceptibility and severity is increased in Slack-deficient mice, comparable to human patients carrying a LOF mutation of Slack.

This was approached by subjecting Slack-KO mice to a KA-induced model for epilepsy. Seizures were scored and subsequently seizure-provoked changes in hippocampal mRNA expression levels determined.

(2) To transfer *in vivo* findings (1) to *in vitro* studies by determining the potentially altered vulnerability of Slack-deficient hippocampal tissue and dissociated neurons in response to KA-exposure.

This was approached by culturing hippocampal slices and dissociated cells, followed by KA exposure and PI-based quantification of cell death.

(3) To elucidate underlying mechanism of altered vulnerability against excessive neuronal activity in Slack-deficient versus -proficient neurons.

This was assessed in dissociated hippocampal neurons allowing for an optimal spatial resolution of the real-time live cell imaging experiments. Ion fluxes essential for neuronal excitability and activity were measured upon KA exposure or electrical stimulation. In detail, Fura2 was applied to monitor Ca^{2+} fluxes as surrogate for neuronal activity. Using a FRET-based sensor K^+ fluxes were studied to link neuronal activity with Slack-mediated activity. Voltage-induced TTX-sensitive inward and outward currents were recorded to determine Slack-currents and activation induced inward-currents that reflect basal excitability.

(4) To link neuronal excitability and ion fluxes to altered firing pattern and kinetics.

This was approached by current-clamp on dissociated hippocampal neuros in the presence or absence of KA or current injections to evoke AP and determine fringing frequency and spiking kinetics.

(5) To confirm KA-based findings using a second (*in vitro*) model of epilepsy.

This was analysed by PI-based cell death quantification and Fura2 based measurements of Ca^{2+} transients induced by Pilocarpine exposure. This combined approach enabled the

analysis of the role of Slack in the context of over-activated cholinergic stimulation in hippocampal slice cultures and cells.

5. Material and Methods

5.1. Slack mouse model

All experimental procedures were conducted in accordance with animal protection law in Germany approved by the Ethics Committee for Animal Research (Regierungspräsidium Tübingen) and were approved by study protocols PZ08/18M, PZ01/21M, PZ04/22M and PZ03/20G. Animals were maintained on a 12/12 h light/dark cycle (light on 6 a.m. to 6 p.m.) with access to food and water *ad libitum* and 22 ± 2 °C with 55 ± 5% humidity in an open specific pathogen free (SPF) animal facility of the Institute of Pharmacy, University of Tübingen. For breeding two females were housed with one male in a Makrolon type III cage. Following 21 postpartal days and genotyping new pups were separated to a maximum of three males or females per Makrolon type II cage enriched with bedding, nesting material, and plastic house for females. To avoid ranking fights, male mice were housed with no plastic houses. *In vivo* studies were conducted by using wildtype ($Slack^{+/+}$) animals as a control for animals with a global Slack deficiency ($Slack^{-/-}$) (Table 3). $Slack^{-/-}$ animals carry an Exon 11 deletion in the *Kcnt1* gene encoding the functional pore-domain of the channel (Lu et al., 2015). Founders were backcrossed to a C57BL/6N background for at least nine generations prior to subsequent experiments.

Table 3: *Genotypes of experimental mice and Slack mouse strain of maintenance.*

International nomenclature	Internal nomenclature
C57BL/6N	$Slack^{+/+}$; Slack WT
B6-Kcnt1^{tm1Ruth}/RuLu	$Slack^{-/-}$; Slack KO
Heterozygous for breeding	$Slack^{-/+}$

KA *in vivo* epilepsy models (see also section 3.3.5.) were performed with either 4 weeks-old (juvenile) or 8 to 12 weeks-old (adult) male litter-matched offspring from heterozygous ($Slack^{+/-}$) parental breeding. Due to the high number of pups needed and the limited time available for genotyping, hippocampal tissue and dissociated cell-based *in vitro* studies were established from age-matched offspring pups generated by mating of either homozygous $Slack^{+/+}$ or $Slack^{-/-}$ breeding. To maintain $Slack^{+/+}$ and $Slack^{-/-}$ genetic background and to avoid genetic drift(s) crossings of animals for *in vitro* experiments derived from a F2 generations were from same heterozygous breeding's as used for *in vivo* experiments.

5.2. Genotyping

Genotypes were determined by DNA extraction and polymerase chain reaction (PCR) with KAPA2G Fast HotStart Genotyping Kit (KAPA Biosystems, KK5621, Sigma-Aldrich Chemie GmbH, Taufkirchen) of tissue specimen collected from the animal's ear. Briefly, 100 µl extraction buffer, containing 1/50 *KAPA Express Extract Enzyme* and 1/10 *KAPA Extraction Buffer* in H_2O were added to each sample. Following 10 min proteinase-based tissue digestion at 75 °C, extract enzyme was inactivated for 5 min at 95 °C and DNA containing supernatant was separated from pellet by centrifugation for 1 min at 14,000 rpm. For PCR-based amplification, primer pairs were designed which allow the distinction of the $Slack^{+/+}$ or $Slack^{-/-}$ allele (see Table 4 and Figure 5). Slack DNA was amplified from 1 µl supernatant using 24 µl of a master mix containing 12.5 µl KAPA Fast Hot Start DNA Polymerase, 1 µl of a 4 µM Slack primer mix and 10.5 µl H_2O. Following 30 PCR cycles (see Table 5) amplicons were loaded on a 2 % agarose gel in Tris-Borat-EDTA buffer (see Table 6), containing 1/1000 Ethidium bromide (2218.2, Carl Roth GmbH + Co. KG, Karlsruhe, Germany) and subsequently imaged on a UVP GelStudioPLUS (Jena Analytics, Jena). Subsequently, the $Slack^{+/+}$ band was detected at 277 bp, whereas the pore-region deficient $Slack^{-/-}$ DNA band was detected at 210 bp (see Figure 5) using the 1 kb DNA ladder for sizing (BioLabs, N32200S).

Table 4: *Primers used for genotyping PCR.*

Allele	Primer sequence 5'-to-3' direction		Amplicon size (bp)
$Slack^{+/+}$	Forward	AGG GGC TGA GAG GGG TCT CG	277
	Reverse 1	TGG GTA GGG CTG CCA CAA GC	
$Slack^{-/-}$	Forward	AGG GGC TGA GAG GGG TCT CG	210
	Reverse 2	GCC ACA ATC TGT TCC TTG GCA	

Table 5: *PCR grogram for genotyping*.

Step	Temperature (°C)	Time (sec)	
T1	95.0	180	
T2	95.0	15	
T3	59.7	15	30 cycles
T4	72.0	15	
T5	72.0	300	

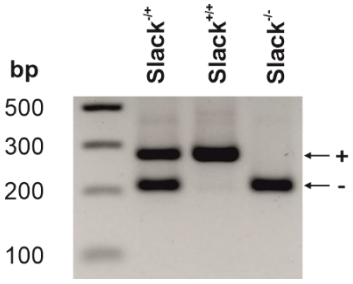

Figure 5: Genotyping result of different Slack alleles.

Representative gel electrophoresis of PCR amplified Slack$^{+/+}$ allele, detected at 277 bp (middle) and Slack$^{-/-}$ allele detected at 210 bp (right line). In Slack$^{+/-}$ mice both alleles can be detected (left line).

Table 6: *Composition of TBE buffer for gel electrophoresis.*

Chemical	Company	Ref. Nr.	Concentration (mM)
TRIS	Carl Roth GmbH + Co.	5429.2	89
Boric acid	Carl Roth GmbH + Co.	6943.3	89
EDTA	Carl Roth GmbH + Co.	3054.1	2

5.3. Kainic acid-induced model for acute epilepsy

The kainic acid (KA) model for acute epilepsy is a well-established and characterized model for epileptic seizures provoked by activation of glutamatergic neuronal signalling especially in the limbic system, with propagation to cortex and other brain regions (Ben-Ari et al., 1981; Lévesque & Avoli, 2013) (see also 3.3.5.). Hereby, seizures and seizure-provoked pathological correlates are highly isomorphic to human frontal lobe epilepsy, the most frequent subtype of epilepsy (Drexel et al., 2012; K. Haas et al., 2001; Wang et al., 2015). Litter-matched 4-weeks juvenile or 12-weeks old adult male Slack$^{+/+}$ and Slack$^{-/-}$ animals were checked for their habitus and phenotype to verify their health status and to ensure a normal development status. Following weighing 15 to 30 mg/kg KA (ab120100, abcam, Berlin, Germany) in sterile saline was intraperitonially (i.p.) applied using a 3 mg/kg stock solution. Leak-out of KA from the application-site was thoroughly avoided by brief pause following injection until removal of the canula. Injected animals were transferred to a vivarium equipped with bedding for optimal observation and video recording for 90 min. Seizure susceptibility and severity was measured on an adopted Racine Scale (Racine et al., 1972) as highest seizure score (SSc) reached in a 5 min interval. Score criteria ranged from 0 – no response, to 6 – tonic-clonic-seizures (TCS) with status epilepticus (SE) and 7 – seizures leading to death (see Table 7 and Figure 6).

Table 7: *Modified Racine scale for seizure scoring of KA-induced epilepsy* (Lévesque & Avoli, 2013; Racine et al., 1972).

Seizure Score	Phenotype
0	No response
1	Immobile / rigid
2	Myoclonic jerks / head nodding
3	Straub tail / front limb clonus
4	Rearing / Rearing with front limb clonus
5	Falling / Jumping
6	Tonic clonic seizures / Status epilepticus
7	Death following status epilepticus

Typical onset and progression of seizures started with SSc of 1 to 2 approximately during first 10 min post injection. Seizure serials that occur following next 60 min are frequently not isolated but in a close chronology starting with increased rigidity (SSc 1), stretching of longitudinal body axis, leading to head nodding (SSc 2), escalating in front limb clonia (SSC3), and reaching rearing with falling (SSc 4 and 5). Finally, convulsions are not self-sustaining and return to SSc 2 and 3. Convulsive events are frequently intermitted by minutes of constant SSc 2 to rearing of SSc 4. For all doses, seizure severity tends to lower after 90 min with less convulsions, more constant rearing (SSc 4) and low intense front limb clonia (SSc 3).

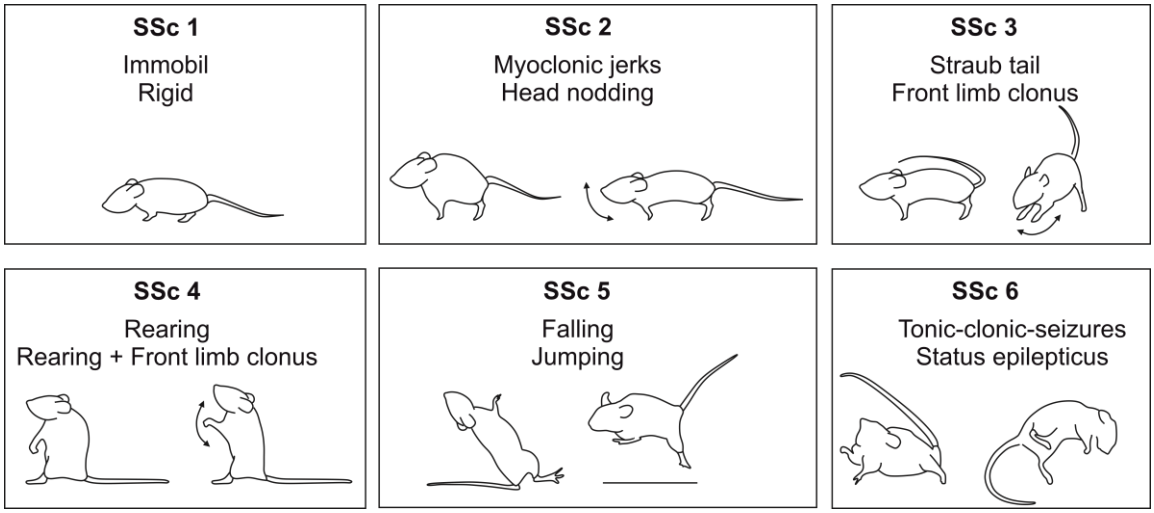

Figure 6: Illustration of KA-induced seizures.

Following KA administration non-convulsive (seizure score, SSc1 and 2) and convulsive seizures (SSc3 to 6) can be classified in 6 levels. **SSc1**: Immobility with stretched and flattened habitus. **SSc2**: Myoclonic jerks with crouched habitus and / or head nodding with prominent stretched body and neck followed by rhythmic head movements. **SSc3**: Straub tail postured straight near the back and / or convulsions of the frond limbs with stretched body and limbs and elongated hindlimbs. **SSc4**: rearing with sitting on the hindlimbs, round back and stiff frond limbs and / or stretched back with convulsions of the front limbs. **SSc5**: Falling with loss of righting ability during rearing or sitting and / or wild jumping. **SSc6**: Tonic-clonic-seizures (TCS) characterized by rhythmic convulsions all over the body, prominent front, and hind limb clonus with loss of righting ability and stereotype head shaking during constant rigid or contracted body.

Following observation, animals recovered in their home cage for 24 h before euthanasia and mRNA was isolated according to 5.6.

5.4. Hippocampus dissection

For analysis of seizure provoked changes in hippocampal mRNA expression levels of involved and related genes, hippocampi were dissected 24 h post KA injection in ice-cold DPBS (14190-094, Thermo Fisher Scientific, Waltham, US). To this end, head of mice was decapitated with a large scissor and scalp withdrawn following midsagittal incision from the skull-basis to the nose. Skull was opened following one midsagittal and two lateral cuts and brain isolated by iris spatula. Hippocampi were dissected by gentle midsagittal division of the hemispheres and lateral roll-out from dorsal to ventral apex of hippocampi using an iris spatula. Required materials are listed in Table 8. Hippocampi were snap frozen in liquid nitrogen for subsequent mRNA isolation (see section 5.6.).

Table 8: *Specific material needed for Kainic acid-induced model and hippocampal dissection.*

Material	Company	Ref. Nr. / Type
Large scissor	Fine science tools GmbH, Heidelberg, Germany	14101-14
Fine scissor	Fine science tools GmbH, Heidelberg, Germany	14058-11
Spring Scissor	Fine science tools GmbH, Heidelberg, Germany	15003-08
Iris spatula	Fine science tools GmbH, Heidelberg, Germany	10093-13
Forceps	Fine science tools GmbH, Heidelberg, Germany	11231-30
Fine forceps	Fine science tools GmbH, Heidelberg, Germany	11254-20
Binocular	KERN Optics GmhB, Balingen, Germany	OZL463

5.5. Organotypic hippocampal slice cultures

Hippocampal slice cultures (HSC) were obtained from postnatal day 5 (P5) pups from homozygous breeding pairs of either $Slack^{+/+}$ or $Slack^{-/-}$ parental animals and were preparated as previously reported (Skrabak et al., 2023). Pups of both sexes were decapitated with a large scissor and brains were removed following one midsagittal and two lateral cuts through skin plus skull from skull-basis to rostral end with a spring scissor. Hippocampi were dissected in ice-cold preparation medium (see Table 9) by fixing the brain at the cerebellar side using forceps and gentle midsagittal separation of the hemispheres using iris spatula. From slightly divided hemispheres hippocampi were rolled-out from dorsal to ventral end again with the help of an iris spatula (for tools see Table 8). Torsion or flexion of hippocampal formation during the dissections was carefully avoided. Next, hippocampi were transferred using snipped pipettes to a Teflon plate and

remaining dissection medium was removed. Following copping to 400 µm on a McIlwain tissue chopper (Quantum 98 Design GmbH, Darmstadt, Germany) transversal hippocampal slices were selected in preparation medium if they were complete and undamaged i.e., included EC, fimbria (Fb), intact DG, and clearly visible and undamaged CA regions. To provide comparable sections, especially slices of the middle hippocampus were selected and dorsal or ventral slices withdrawn. 5 slices were placed onto 0.4 µm membrane inserts (PICM03050, Merck Millipore, Darmstadt, Germany) in 6-well plates with 1 ml of culturing medium (see Table 10). Medium was exchanged after 3 h and subsequently every 3 days for up to 14 days *in vitro* (div). Cultures were maintained in a humidified incubator (HeraCell150 Incubator, Thermo Fisher Scientific) at 37 °C with 5% CO_2. Slices underwent flattening during the first 10 days and appeared transparent with clearly visible hippocampal compartments and outgrowing edges until 14 div (see Fig. 7).

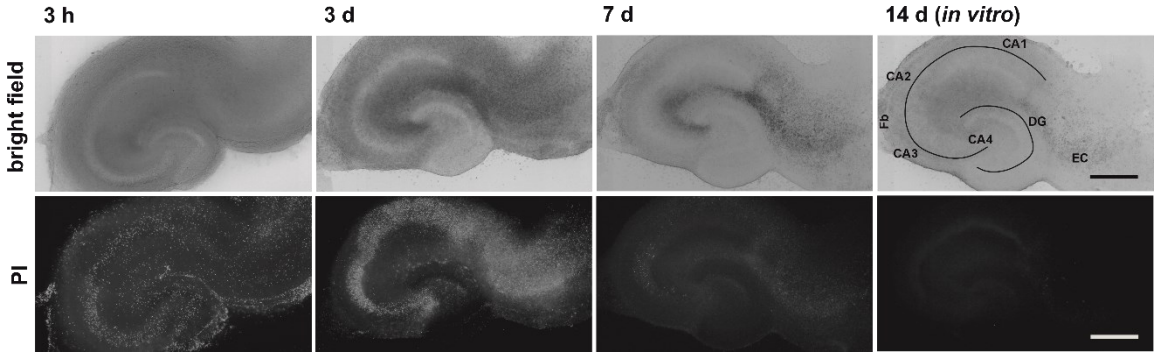

Figure 7: Exemplary images of hippocampal slice cultures over time.

Hippocampal slice cultures (HSC) were cultures up to 14 days thereby developing a mature and organotypic neuronal network (Holopainen, 2005). Through cultivation HSC become transparent and flattened (see bright field images, top) by losing cells in the first days as indicated by Propidium iodide (PI) staining (see also section 5.8.1.). Following cultivation of 14 d hippocampal compartments as fimbria (Fb), CA regions, DG and EC are undamaged and clearly visible (see bright field, top left). Scale bar equals 500 µM.

Table 9: *Preparation medium components.*

Compound	Company	Ref. Nr. / Type	Concentration
HBSS	Thermo Fisher Scientific	14025	-
HEPES	Sigma Aldrich Chemie GmbH	H4034	20%
D-glucose	Sigma Aldrich Chemie GmbH	16301	20 mM

Table 10: *Culturing medium components.*

Compound	Company	Ref. Nr. / Type	Concentration
MEM	Thermo Fisher Scientific	32360034	-
Horse serum	Thermo Fisher Scientific	26050088	20%
GlutaMAX	Thermo Fisher Scientific	35050061	1 mM
Ascorbic acid	Sigma Aldrich Chemie GmbH	A92902	0.000125%
Insulin	Sigma Aldrich Chemie GmbH	I2643	0.001 mg/ml
$CaCl_2 \cdot 2\ H_2O$	Carl Roth GmbH + Co.	5239.2	1 mM
$MgSO_4 \cdot 6\ H_2O$	Merck, Darmstadt	A914133	2 mM
D-glucose	Sigma Aldrich Chemie GmbH	16301	20 mM
penicillin/streptomycin	Thermo Fisher Scientific	15140122	100 U/ml

5.6. Quantitative RT-PCR

Relative mRNA expression levels were determined as previously described (Skrabak et al., 2023). In brief, hippocampi were isolated 24 h after KA-induced seizures (see section 5.4.), homogenized (Polytron PT 1200E) and RNA was extracted using 1 ml Peq-GOLD RNApure (VWR International GmbH, Darmstadt, Germany) according to manufacturer's instructions. mRNA was extracted from 20 pooled hippocampal brain slice cultures (see 5.5.) using the NucleoSpin kit (MACHEREY-NAGEL GmbH & Co. KG, Düren, Germany) according to the protocols provided with the kit. Genomic DNA was digested using DNase I (04716728001, Sigma Aldrich Chemie GmbH,) at 54 °C for 30 min. 500 ng RNA were reversely transcribed by iScript cDNA Synthesis Kit (170-8896, Bio-Rad Laboratories GmbH, Feldkirchen, Germany). Real-time quantitative PCR (RT-PCR) was performed in triplicates with 7.5 ng/µl mRNA and 333 nmol/l of corresponding primers. Each run included water and RT negative controls (where reverse transcriptase was omitted during reverse transcription). Reactions were performed using SSoAdvanced Universal SYBR Green Supermix (1725274, Bio-Rad Laboratories GmbH) on a CFX Connect Real-Time PCR Detection System (Bio-Rad Laboratories GmbH) by incubating RT-PCR reactions at 92 °C for 2 min, followed by 40 cycles of 5 s at 95 °C and 30 s at 58 °C. Expression of targeted genes was calculated by the $2^{-\Delta\Delta Ct}$ method relative to hypoxanthine-guanine phosphoribosyl transferase (HPRT). Primer sequences (see Table 11) were designed by Primer3 and PrimerBLAST software and are based on gene sequences listed on Ensembl, considering key criteria such as spanning an exon-exon junction, melting temperatures between 58 to 64 °C and a GC-content of 40 to 60%.

Table 11: *Oligonucleotides for RT qPCR.*

RT-qPCR target	Primer	Sequence '5'-to-3'
HPRT	Forward	CCT TCA TGA CAT CTC GAG CA
	Reverse	CAT TAT GCC GAG GAT TTG GA
Slack	Forward	CTG CTG TGC CTG GTC TTC A
	Reverse	AAG GAG GTC AGC AGG TTC AA
Slick	Forward	CTC GCG CTT TCA AAA CTG GA
	Reverse	ACT CTT CCC GCA GCA AAA GG
BK	Forward	GAC GCC TCT TCA TGG TCT TC
	Reverse	TAG GAG CCC CCG TAT TTC TT
GluK4	Forward	GCC TCA TGA ACT ACC TTC GCA
	Reverse	GTT GGA CCT CTG GCC TTT GC
GluK5	Forward	CCG TGT GGC TCT TCA TGC TT
	Reverse	TGT ACC ACT CAT AAG GGC TCA G
GluA1	Forward	GGT TGG CGA GGA TGT AGT GG
	Reverse	TGG TGG TGG TGG ACT GTG AA
GluA2	Forward	AGC ACT CCT TAG CTT GAT TGA GT
	Reverse	CCA CTT CTT CTC CGC AGC AG
GluN1	Forward	AGG AAG ATC ATC TGG CCA GGA
	Reverse	GGG CTT GAC ATA CAC GAA GGG
GluN2A	Forward	GAG ACC CCG CTA CAC ACT C
	Reverse	TCA GCA CGA TCA CCA CAA GC
GluN2B	Forward	CGC CCA GAT CCT CGA TTT CA
	Reverse	ACT GGA AGA ACA TGG AGG ACT CA
BDNF	Forward	GAC GAC ATC ACT GGC TGA CA
	Reverse	GTC CGC GTC CTT ATG GTT TT
TrkB	Forward	TTT CCG CCA CCT TGA CTT GT
	Reverse	TCC TGG AGA GTC TTG AGC CA
GFAP	Forward	TGC AAG AGA CAG AGG AGT GGT
	Reverse	GTG CTT GGC TTG GCG GAG

5.7. Dissociated hippocampal neuronal cultures

Primary hippocampal neurons (PHN) were prepared and cultured from P0 Slack$^{+/+}$ and Slack$^{-/-}$ pups as previously described (Skrabak et al., 2023). Pups were decapitated, brains and hippocampi isolated in ice cold dissecting medium (see Table 12) as defined for HSC (section 5.5.). Hippocampi were liberated from meninges especially the hippocampal concave side by gently pulling meninges from the distal, cortical edge to the hippocampal proximal compartments. After washing thrice in 10 ml dissecting medium, hippocampi were incubated in 4.5 ml dissecting medium with 0.5 ml of 2.5% trypsin (15090, Thermo Fisher Scientific) at 37 °C for 20 min before 0.5 ml of 0.1%

Desoxyribonuclease I (DN25, Sigma Aldrich Chemie GmbH) was added for another 5 min at room temperature. Next, hippocampi were washed twice in dissecting and twice in plating medium (see Table 13) before dissociation by gentle trituration in 2.5 ml plating medium in three steps using fire-polished Pasteur pipets of incrementally decreasing diameter. Subsequently, cells were counted and seeded onto coverslips pre-coated with 0.5 mg/ml poly-L-lysine (P2636, Sigma Aldrich 123 Chemie GmbH) in borate buffer (see Table 15). 110,000 cells in plating medium were either plated on 32 mm diameter coverslips (KHY0.1, Carl Roth GmbH + Co.) restricted by silicon culture inserts (80466, ibidi GmbH, Graefelfing, Germany) to reduce growth area, or on 12 mm coverslips (ECN631-1577, VWR, Darmstadt). 2 h after seeding, medium was changed to maintenance medium (see Table 14) and isolated PHN were kept in culture for 8 to 14 days. During the first 5 days culture media remained unchanged to limit media change induced stress and enable neuronal and astroglial modulation of growth factors as BDNF. Subsequently, only 30% of the volume was changed every 4 days.

Table 12: *Dissecting medium composition.*

Compound	Company	Ref. Nr. / Type	Concentration
HBSS	Thermo Fisher Scientific	14175-053	-
HEPES	Sigma Aldrich Chemie GmbH	H4034	10 mM
D-glucose	Sigma Aldrich Chemie GmbH	16301	0.1%
Sodium pyruvate	Thermo Fisher Scientific	11360-070	1 mM

Table 13*: Plating medium composition.*

Compound	Company	Ref. Nr. / Type	Concentration
BME with EBSS	Thermo Fisher Scientific	41010-026	-
Fetal bovine serum	Thermo Fisher Scientific	16140071	10%
D-glucose	Sigma Aldrich Chemie GmbH	16301	0.5%
Sodium pyruvate	Thermo Fisher Scientific	11360-070	1 mM
GlutaMAX	Thermo Fisher Scientific	35050-038	2 mM
P/S	Thermo Fisher Scientific	15140-122	100 U/ml

Table 14: *Maintenance medium composition.*

Material	Company	Ref. Nr. / Type	Concentration
Neurobasal	Thermo Fisher Scientific	21103049	-
B-27	Thermo Fisher Scientific	17504044	10%
GlutaMAX	Thermo Fisher Scientific	35050-038	2 mM

Table 15: *Borate buffer composition.*

Material	Company	Ref. Nr. / Type	Concentration (mM)
H_3BO_3	Carl Roth GmbH + Co.	6949.3	50
$Na_2B_4H_7$	Carl Roth GmbH + Co.	T880.1	12.5

Adjust do pH 8.7

5.8. Imaging

5.8.1. Propidium iodide-based cell death assay

KA, Pilo and PTZ-induced cell death in HSC or PHN was assessed using propidium iodide (PI) staining. PI can intercalate to nucleic acid, thereby emitting bright fluorescence at 535 nm. Since especially in apoptotic cells membrane integrity is altered, polar PI can enter the cell, hence, it is commonly used as a maker for non-viable necrotic or apoptotic cells. Accordingly, cell death in HSC and PHN has been found to correlate with PI fluorescence intensity (Crowley et al., 2016; Noraberg et al., 1999). Thus, PI fluorescence can offer an effective estimate of neuronal cell death for HSC and PHN (Happ & Tasker, 2016; Jiajia et al., 2017).

5.8.2. Assessing PI uptake in HSC

Imaging of PI uptake was conducted as described previously (Skrabak et al., 2023). For all PI based experiments in HSC, imaging was performed with an RFP filter block in a Nikon Eclipse Ts2R microscope (Nikon Instruments Inc., Melville, US) equipped with a Plan Fluor OFN25 4x objective (Nikon Instruments Inc.) and a DMK 33Ux174 camera (OEM cameras, Middletown, US). Illumination was adjusted manually and kept unchanged for all experiments. Images were made with IC Capture 2.5 software using the noise reduction function layering 32 images to optimize resolution. For KA or Pilo treatment, PI staining and imaging was assessed in close relation to Noraberg et al., 1999 and Poulsen et al., 2002. First, basal viability of 14 div HSC was measured after 10 min incubation with 2 µg/ml PI (P4864, Sigma-Aldrich Chemie GmbH). Subsequently 5 or 10 µM KA was added to culturing medium and PI uptake was imaged consecutively after 1 and 2 days. In a second set of experiments, HSC were exposed to 20 µM KA for 1 h and media was replaced to fresh culturing medium followed by PI imaging over a total of 7 days post KA exposure. In case of Pilo treatment, HSC were exposed either to 4 -or 8 mM Pilo and PI uptake was imaged after 1, 2 and 3 days. In case of PTZ treatment, HSC were exposed either to 10 -or to 20 µM PTZ and PI uptake was imaged after 1 and 2 days. As a positive control for the PI uptake, culturing medium was replaced for 1 ml of

80% EtOH for 1 h at -20 °C at the end of each experiment before new PI was applied for a final set of images. Relative PI uptake for each HSC was quantified as described by Happ & Tasker, 2016 using Fiji (Schindelin et al., 2012). As shown in Figure 8 three circular regions of interest (ROI, 80x80 pixels) were placed on each CA1/2, CA3/4, and DG (yellow circles). Differentiation of CA regions was possible by extrapolating DG branches to the distal CA regions. An additional tenth region (orange circle) was placed adjacent to the slice for background subtraction. Background subtracted integrated densities of each region were averaged for each region, CA1, CA3 and DG. KA, Pilo -and PTZ-induced PI uptake was calculated relative to the positive control for each slice following subtraction of basal PI uptake. HSC with ≥2% PI uptake under basal conditions (i.e., prior to KA, Pilo or PTZ exposure) were excluded from analysis.

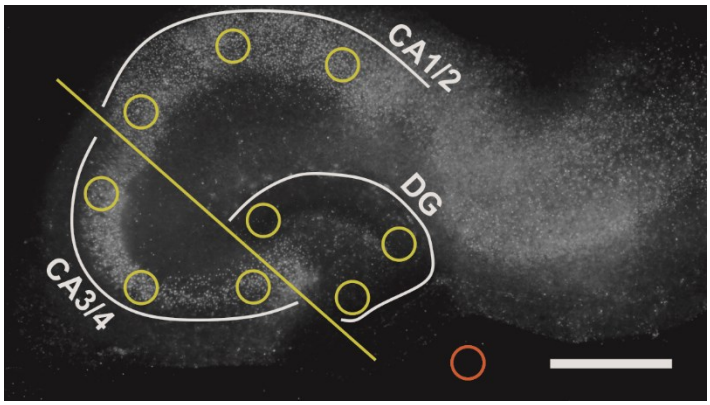

Figure 8: Exemplary PI stained HSC with ROI for PI quantification.

Relative PI uptake of HSC was quantified densitometrically using three circular RIO for each, CA1/CA2, CA3/CA4 and DG (yellow circles). Respective localization was determined by extrapolating edges of DG leaflets (diagonal line between CA1/2 and CA3/4). Final ROI was calculated by considering background intensity adjacent to the HSC (orange circle). Scale bar equals 500 µM.

5.8.3. Assessing PI uptake in PHN

For cell death detection of dissociated hippocampal neurons, PHN were plated on ibidi 8 well Slides (80826, ibidi GmbH) and cultured for 8 to 10 days with a special interest to work on cultures showing low fibroblast contamination and confluent neuron distribution. For measurements, 2 µg/ml PI and KA at a final concentration of 5 or 10 µM were added to each well for 24 h. In a second set of experiments PHN were treated with high doses of 50 to 500 µM KA for 15 h. To functionally connect KA-induced cell death and KA-mediated increase in neuronal activity a co-stimulation experiments was carried out. Therefore, PHN were exposed either to 10 µM KA alone or in combination to 50 or 100 µM GABA antagonist Picrotoxin (PiTX) to accelerate and disinhibit KA-provoked neuronal firing (Corner & Ramakers, 1992; Thompson et al., 1996). As described previously

(Skrabak et al., 2023) slides were placed into a prewarmed stage top incubation system (10722, 11922-DL, 10918-DL, ibidi GmbH) maintaining 5% CO_2, 21% O_2 and 80% humidity at 37 °C by IncuControl (ibidi GmbH) software. A temperature of 37°C in culture medium was achieved by setting lid temperature to 42 °C and plate temperature to 38 °C. For each well, time courses of 4 ROI were automatically imaged over-time using a BioPrecision2 automated XY-table (Ludl Electronic Products Ltd., Hawthorne, US) on a Zeiss Axio Observer Z1 inverted microscope equipped with a Zeiss EC-Plan-Neofluar 20x/0.5 objective (440340-9904, Carl Zeiss AG, Oberkochen, Germany) and a LedHUB LED light-engine equipped with 505–600 nm LED (Omicron Laserage Laserprodukte GmbH, Dudenhofen, Germany). Excitation was trimmed to 575/15 nm (AHF Analysentechnik, Tübingen, Germany). The microscope contained the following filter set: 475/543/702 nm emission filter and 459/526/596 dichroic, which were obtained from AHF Analysentechnik. For each well five different ROI were determined and calculated as sample size. PI emission of all ROI was automatically detected every 30 min for either 24 h (5 and 10 µM KA and 10 µM KA with PiTX) or 15 h (50 to 500 µM) with a PCO panda 4.2bi camera (Excelitas PCO GmbH, Kelheim, Germany) controlled by VisiView software (Visitron Systems GmbH, Puchheim, Germany). Fiji (Schindelin et al., 2012) was used to count particles in each ROI over time after background subtraction using a constant threshold to calculate relative PI uptake. In detail, PI images of all time points were staked, background subtracted from total stack and PI particles were counted automatically. To calculate relative PI uptake per ROI, the number of particles of the first image, was counted and number of particles of the last image calculated as relative fold-change of each ROI. For each experimental condition, one ROI was counted as one sample size.

5.8.4. Immunofluorescence staining

PHN were stained as previously reported (Skrabak et al., 2023). General maturity, neuronal attributes, and Slack expression pattern of PHN were verified by immunofluorescence staining of 8 and 14 div cultures. First, cells were washed twice with warm HBSS (1475-053, Thermo Fisher Scienticic) and fixed for 10 min with warm fixation solution (DPBS with 4% Paraformaldehyde and 4% Sucrose). Cells were washed twice for 5 min in HBSS and incubated for 2 h at room temperature with blocking buffer (see Table 16). Subsequently, cells were incubated with primary antibodies (see Table 17) in blocking buffer for 24 h at 4 °C. Next, cells were washed thrice for 5 min with washing solution (DPBS with 0.01% Triton x-100) and incubated for 2 h at room temperature with secondary antibodies (see Table 17) and Hoechst 33342 (14533, Sigma-Aldrich Chemie GmbH) in blocking buffer. Cells were washed in washing solution thrice for 5 min, once with DPBS for 5 min and once with water for 5 min. Cells were mounted with PermaFluor

aqueous mounting medium (TA-030-FM, Thermo Fisher Scientific) and imaged the next day with a Zeiss Axiovert 200M equipped with a colour camera (AxioCam MRc Rev 3) and ZEN 3.4 software (Carl Zeiss AG).

To generate reliable images for all experimental trials, a negative control incubated exclusively with the corresponding secondary antibody was carried out. Images were captured following automated illumination-detection of Zeiss ZEN 3.4 program and negative control was imaged under same illuminations to finally subtract corresponding background or non-specific staining of the secondary antibody from the fluorescence images. To provide Slack-specific immunofluorescence images, comparative imaging between genotypes was performed. To this end, illumination conditions were adjusted to $Slack^{+/+}$ cultures and $Slack^{-/-}$ samples were illuminated under the same conditions to finally subtract non-specific fluorescence.

Table 16: *Blocking buffer composition.*

Compound	Company	Ref. Nr. / Type	Dilution
DPBS	Thermo Fisher Scientific	14190-094	-
Glycerol	Carl Roth GmbH + Co.	3783.1	2%
Triton X-100	Carl Roth GmbH + Co.	3051.2	0.3%
NH_4Cl	Carl Roth GmbH + Co.	K298.2	50 mM
Normal goat serum	Vector Labs	S-1000	5%
Bovine serum albumin	Carl Roth GmbH + Co.	0163.2	2%

Table 17: *Antibodies used for immunofluorescence imaging.*

Antibody	Company	Ref. Nr. / Type	Dilution
Slack	Sigma Aldrich Chemie GmbH	SAB5200036	1/300
βIII-tubulin	R&D Systems	MAB1195	1/1000
MAP2	Cell Signalling Leiden	D5G1	1/1500
GFAP	Dako	Z0334	1/1500
Synapsin	SynapticSystems	106-002	1/1000
GluA1 / GluR1	NeuroMab	TA326534	1/1000
GluN1 / MR1	NeuroMab	TA326536	1/1000
Alexa555 α IgG1	Thermo Fisher Scientific	A21127	1/800
Alexa555 α IgG2a	Thermo Fisher Scientific	A21137	1/800
Alexa488 α IgG1	Thermo Fisher Scientific	A21131	1/800
Alexa488 α IgG2a	Thermo Fisher Scientific	A21121	1/800
Alexa555 α rb	Thermo Fisher Scientific	A11055	1/800
Alexa488 α rb	Thermo Fisher Scientific	A11008	1/800

5.8.5. Ca^{2+} life cell imaging

To asses neuronal activity, dynamic changes of the intracellular Ca^{2+} concentration ($[Ca^{2+}]_i$) were imaged as a surrogate parameter as described previously. This was based on the functional link between neuronal depolarization and opening of selective and non-selective cation channels like AMPA, NMDA or VGCC leading to influx and accumulation of free $[Ca^{2+}]_i$ from the extracellular space (Guatteo et al., 2004; Matt et al., 2021; Simms & Zamponi, 2014). To detect $[Ca^{2+}]_i$ the commonly used fluorescent dye Fura2AM (21021, Biomol GmbH, Hamburg, Germany) was used. Fura2AM contains an acetoxy-methyl (AM)-ester, which is able to cross the plasma membrane (Figure 9, left). Intracellularly, the AM-residue is removed by esterases leading to more hydrophilic Fura2, thereby accumulating within the intracellular space (Figure 9, middle). Since Fura2 is a Ca^{2+} specific chelator and changes the emission maximum following binding of Ca^{2+} from 380 nm to 340 nm (Figure 9 right graph) $[Ca^{2+}]_i$ can be determined ratiometrically by alternating excitation of both wavelengths during real time imaging.

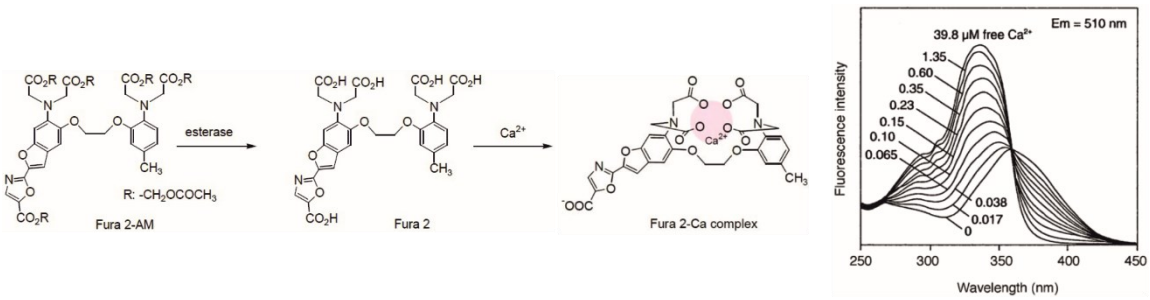

https://www.dojindo.com/EUROPE/products/F015/
https://www.vetmeduni.ac.at/hochschulschriften/bakk-biomed-biotechn/AC08392020.pdf

Figure 9: Fura2AM structure and function.

(A) Fura2AM shuttles to intracellular space and AM residue is hydrolysed. **(B)** Fura2 can complex Ca^{2+} ions, thereby shifting its emission maximum from an excitation at 380 nm to 340 nm.

As reported previously (Skrabak et al., 2023) 8 to 10 div PHN were loaded with 2.5 µM Fura2 in maintenance medium for 40 min and cells were subsequently transferred to a PC30 perfusion chamber (NGFI GmbH, Graz, Austria) connected to a gravity-based perfusion system (NGFI GmbH) to obtain constant perfusion with prewarmed recording buffer (see Table 18). $[Ca^{2+}]_i$ was measured using a Zeiss Axiovert 200 equipped with a Zeiss Fluar 440255 40x/1.30 oil immersion objective (Carl Zeiss AG) and illuminated by a CoolLED *p*E-340^{fura} (CoolLED Ltd, Andover, US). Light was filtered by AHF Analysentechnik F39-380 and F39-343 nm BrightLine filters, passed the dichroic filter AT515LP and emission was finally filtered by CmF 525/15. Fura2 was imaged at 1 Hz, with a binning of 4 using a PCO panda 4.2 camera (Excelitas PCO GmbH) and VisiView

software (Visitron Systems GmbH) with background correction. ROI was set to bundles of intermitted and small neurons grouped to lose collections but not dense round shaped insula and loaded to intermediate amounts of Fura2. Very large and highly loaded neurons were excluded from measurements, since $[Ca^{2+}]_i$ was basally at a very high level and cells were found to be less viable. After 5 min of equilibration under constant perfusion and 2 min of measuring basal $[Ca^{2+}]_i$, PHN were superfused for 2 min with recording buffer additionally containing 1 to 100 µM KA before washout for 3 min. In a second set of experiments PHN were superfused with combinations of KA and 10 µM AMPA antagonist NBQX, 100 µM NMDA antagonist DL-AP5 or 5 µM non-specific "Slack activator" Loxapine. To isolate non-responding or late responding glial cells from analysis, maximal Ca^{2+} influx at the end of each measurement was determined by administration of 50 µM glutamate. This control stimulus was excluded from statistical analysis. Maximum change in fluorescence emission ratio between 340 nm and 380 nm was calculated followed by background subtraction. All cells from one recording were averaged and data was analysed using GraphPad Prism 8 software (GraphPad Software, Boston, US).

Table 18: *Recording buffer composition.*

Compound	Company	Ref. Nr. / Type	Concentration (mM)
NaCl	Carl Roth GmbH + Co.	3957.2	138
KCl	Sigma Aldrich Chemie GmbH	P9541	5
$CaCl_2$	Carl Roth GmbH + Co.	5239.2	2
$MgCl_2$	Merck	1.05833.1000	1
HEPES	Sigma Aldrich Chemie GmbH	H4034	10
D-glucose	Sigma Aldrich Chemie GmbH	16301	10

5.8.6. K^+ life cell imaging

To relate measurements of Ca^{2+} fluxes with modulated K^+ dynamics potentially also caused by Slack, thereby linking Slack channel function to neuronal activity, a K^+ sensitive genetically encoded FRET-based probe (GEPII) was utilized. Designed by Bischof et al., 2017, this GEPII biosensors are composed of a bacterial K^+ binding protein (Kbp) consisting of a K^+ binding BON domain and a second Lysin rich motif (LysM), which is essential for binding of K^+ and a subsequent conformational change (Bischof et al., 2017). The Kbp was flanked by an optimized, monomeric super-enhanced cyan fluorescent protein (CFP), mseCFP, and an optimized, circularly permuted yellow fluorescent protein (YFP), cpV. Upon K^+ binding to Kbp, a conformational change brings both fluorescent probes in close proximity, and CFP transfers energy to cpV to finally emit FRET-signals

with a wavelength of 530 nm (FRET) instead of 475 nm (CFP). With this system, the ratio between FRET/CFP reveals the intracellular K^+ concentration ($[K^+]_i$).

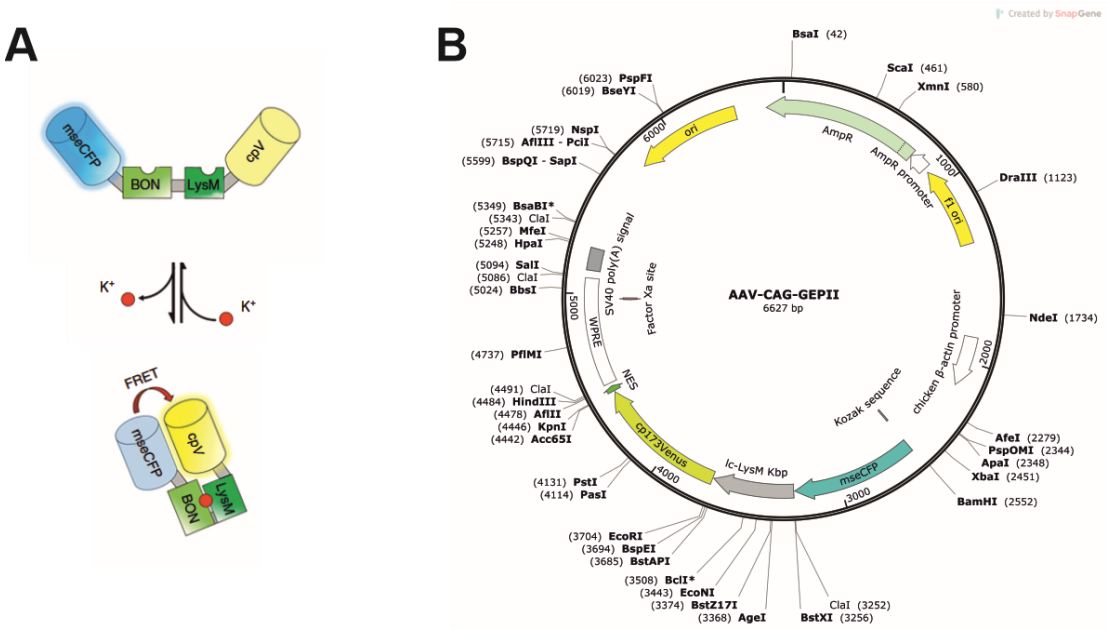

Figure 10: K^+-sensitive, genetically encoded, FRET-based probe GEPII.

(A) Scheme of GEPII with K^+ binding site (Kbp) fused to a CFP and YFP variant, thereby allowing FRET-based measurements of K^+. **(B)** Vector map of GEPII encoding vector carried by an adeno associated virus (AAV-DJ/8) under the control of a CAG promotor (Pham et al., 2023).

To deliver the biosensor to the PHN, cells were transduced with an adeno-associated virus (AAV-DJ/8) (Pham et al., 2023). Cytoplasmatic localization of the sensor was achieved by attachment of a nuclear export signal (NES) to the sensor, and expression was under control of a CAG promotor. As also described previously (Skrabak et al., 2023) PHN were virally transduced at 7 to 8 div at a multiplicity of infection (MOI) of 100. After 3 days, the FRET-based K^+ biosensor was expressed to a sufficient extend, and PHN were imaged in a PC30 perfusion chamber (NGFI GmbH) under constant perfusion with prewarmed imaging buffer (see Table 19) by a gravity-based perfusion system (NGFI GmbH). Imaging was performed using a Zeiss Axio Observer Z1 inverted microscope equipped with a Zeiss EC Plan-NEOFLUAR 40x/1.3 Oil 420460-9900 objective (Carl Zeiss AG) and connected to a LedHUB LED light-engine producing excitation light at a wavelength of 430 nm (Omicron Laserage Laserprodukte GmbH), which was trimmed to 427/10 nm by an excitation filter (AHF Analysentechnik). The microscope was equipped with a 459/526/596 dichroic and a 475/543/702 emission filter (AHF Analysentechnik). Emission light of lc-LysM GEPII 1.0 was collected simultaneously at 475 and 530 nm using an Optosplit II optical image splitter (Cairn Research, Faversham, UK) equipped with a T505lpxr (AHF Analysentechnick) connected to a PCO panda 4.2bi camera

(Excelitas PCO GmbH). Images were acquired at 1 Hz with a binning of 4 using VisiView software (Visitron Systems GmbH).

To provide antiparallel signals of CFP and FRET, especially PHN with prominent transduction and fluorescence intensity were chosen for imaging. Additionally, neural cells in small groups were considered to be viable, and therefore represented neurons for optimal measurements. Regions with grid-like distribution, low transduction efficiency and bold neurite morphology were considered to be astroglia and not used for experimental trials. Following 2 min of basal recording, PHN were exposed to 1, 3 and 5 µM KA for 2 min each with 3 min of washout. After KA exposure, a 50 µM glutamate control stimulus was used to validate the general glutamatergic responsiveness of the cells measured. Cells that did not respond to the control stimulus were considered non-neuronal and excluded from analysis. Ratios were calculated after background correction by dividing FRET by CFP emission and ratio was normalized for first 2 min of baseline recording to obtain maximal changes in FRET/CFP ratios during KA stimulations. Cells of one measurement were averaged and delta rations provoked by glutamate control stimulus not included to statistical analysis. Further data analysis was performed using GraphPad Prism 8 software (GraphPad Software).

Table 19: *Imaging buffer compositions.*

Antibody	Company	Ref. Nr. / Type	Concentration (mM)
NaCl	Carl Roth GmbH + Co.	3957.2	126.5
KCl	Sigma Aldrich Chemie GmbH	P9541	2
$CaCl_2$	Carl Roth GmbH + Co.	5239.2	2
$MgCl_2$	Merck	1.05833.1000	2
HEPES	Sigma Aldrich Chemie GmbH	H4034	10
D-glucose	Sigma Aldrich Chemie GmbH	16301	30
Sodium-pyruvate	Thermo Fisher Scientific	11360-070	10

5.9. Electrophysiological analysis of PHN

As described previously (Skrabak et., al., 2023) patch-clamp electrophysiology was performed using ≥14 div PHN cultured on 12 mm glass cover slips. Viable cultures were selected by the following morphological criteria: Few pycnotic cells, individually visible medium-sized, plastic and high-contrast cells and few tangles of neurites. Cultures with strongly separated or strongly clustered cells, thick neurite tangles or grid-like distribution patterns were omitted from experimental trials. Experimental implementation is also described in Skrabak et al., 2023. PHN were transferred to a submerged-type recording chamber (Warner Instruments, USA) with constant perfusion (Gilson Minipuls 2, Gilson

Middleton USA) of extracellular buffer (see Table 20) supplied by a peristaltic pump (Gilson Minipuls 2, Gilson Middleton USA). Cells were visualized by a Nikon Tc2R equipped with a Nikon S Plan Fluor 40x/0.6 objective with EMBOSS contrast and a DFK 33Ux174 camera (Nikon Instruments Inc.). 3.5 to 4 MΩ micropipettes were pulled from borosilicate glass (BM150-10P, Science Products GmbH, Hofheim, Germany) using a P-1000 Micropipette Puller (Sutter Instruments, Novato, US), thoroughly polished by a MF-830 Micro Forge (Narishige International Ltd., London, UK) and filled with intracellular buffer (see Table 21). After achieving whole-cell configuration, whole-cell capacitance and series resistance were compensated for current-clamp recordings using an EPC10 amplifier (HEKA Elektronik GmbH, Lambrecht, Germany) and PatchMaster software. Recordings were sampled at 5 kHz and analysed using FitMaster software. Cells with changes in access resistance exceeding 20% during recording were excluded from analysis.

For voltage-clamp recordings, neurons were held at -60 mV and whole-cell current responses to 500 ms voltage steps from -60 to +80 mV in 20 mV increments were recorded before and after perfusion of extracellular buffer containing 10 µM TTX, Carl Roth GmbH + Co. KG) to block voltage gated Na^+ channels and thereby Na^+-dependent activation of Na^+-activated K^+ channels like Slack. Amplitudes of transient inward and persistent outward currents were measured as minimum in a 15 ms window at the beginning or as mean of a 25 ms window at the end of the voltage step, respectively.

For current-clamp recordings, neurons were held at a membrane potential near -60 mV before perfusion of 5 µM KA. Starting from the first KA-induced AP, the number of APs per 1 s bin was counted for 30 s. Additionally, AP threshold (membrane potential at AP initiation) and amplitude (from threshold to peak) was calculated from the first evoked AP. For current injections, cells were held near -60 mV in current-clamp mode and depolarized by 10 current injections in increments of 20 pA for 500 ms. AP number per depolarization was counted for each current injection. Additionally, AP threshold (membrane potential at AP initiation), AP amplitude (from threshold to peak), afterhyperpolarization (aHP) duration (time from HP peak to resting potential, Fourcaud-Trocmé et al., 2022) and amplitude (aHP, peak minus resting potential) were measured for the first AP. By using Clampfit 10.7 also the kinetics of first provoked APs were analysed automatically by define AP maximal rise slope and AP halfwidth.

Table 20: *Extracellular buffer compositions.*

Antibody	Company	Ref. Nr. / Type	Concentration (mM)
NaCl	Carl Roth GmbH + Co.	3957.2	140
KCl	Sigma Aldrich Chemie GmbH	P9541	2.5
$CaCl_2$	Carl Roth GmbH + Co.	5239.2	2
$MgCl_2$	Merck	1.05833.1000	4
HEPES	Sigma Aldrich Chemie GmbH	H4034	10
D-glucose	Sigma Aldrich Chemie GmbH	16301	10

pH 7.4 and 310 mOsm/kg

Table 21: *Intracellular buffer compositions.*

Antibody	Company	Ref. Nr. / Type	Concentration (mM)
K-gluconate	Sigma Aldrich Chemie GmbH	P1847	136
$MgCl_2$	Merck	1.05833.1000	0.6
HEPES	Sigma Aldrich Chemie GmbH	H4034	17.8
EGTA	Carl Roth GmbH + Co.	3054.1	1
Na_2-ATP	Carl Roth GmbH + Co.	HN35.2	4
Na_2-GTP	Carl Roth GmbH + Co.	K056.1	0.3

pH 7.4 and 310 mOsm/kg

5.10. Data analysis

Analysis of all data was performed as described in Skrabak et al., 2023. Data were analysed using GraphPad Prim version 8 software (GraphPad Software). First, D'Agostino & Pearson test for normality distribution was performed. Genotype-dependent effects were analysed by unpaired t-test (Fig. 11B, 12A-F, 13D-F, 14B, 16C, 21C and E, 22F and H) including Welch's correction in case of different variance (Fig.21D), Mann-Whitney test in case of non-parametric data (Fig. 16B, 22C, D, G, I, K and L) and two-way ANOVA in case of time course related data (Fig.11C and F, 13A, 14C and D, 17D and F, 18A-C, 19C, 20C and D, 21B, 22B, 23B and C), Log-rank test for latency to reach convulsive seizures among KA-injection (Fig. 11D and G, 3B) and Chi-square test for fraction of animals reaching defined SSc (Fig.11E and H, 3C). Juvenile mice also died following KA-induced seizures, so mRNA transcript levels were analysed between surviving and dead animals. Since no differences in mRNA levels between survived and dead animals were found, all $Slack^{-/-}$ samples were pooled (Fig. 13D-F). Since no $Slack^{+/+}$ animal died following KA-induced SE (Fig. 13C) this procedure was not needed here. In case of Fura2 measurements with increasing KA concentrations, a non-linear, sigmoidal curve fit was performed to determine the logEC50 and goodness of curve fit (Fig. 17D). Sample size (n) was defined as number of animals for KA epilepsy testing (Fig. 11 and

13). For quantification of KA-induced PI uptake in HSC, n was defined as mean of three ROI placed to each, CA1, CA3 and DG of 5 slices per well. Slices of 3 to 6 preparations were analysed (Fig. 14 and 23). For quantification of KA-induced PI uptake in PHN sample size, n was defined as ROI with four to five ROI per well and recording. Recordings were performed from 3 preparations (Fig. 16). For Fura2-based Ca^{2+} measurements, cells of each measurement were averaged to one experimental sample n. Data were acquired from 12 to 13 wells of 8 to 10 preparation (Fig. 17). Also FRET-based K^+ measurements cells of one well were averaged and defined as sample size n with 8 to 10 wells from 5 to 6 preparations (Fig. 19). For patch-clamp experiments, each cell was defined as sample size n with 6 to 7 preparations for voltage-clamp data (Fig. 20) and 8 to 9 preparations for current-clamp data (Fig. 21 and 22). All data are represented as mean ± SEM. In figures, significance is indicated by asterisks (*p <0.05, **p <0.01, ***p <0.001). n.s. denotes non-significant results (p ≥0.05). Statistics are summarized in Supplementary Tables 1 to 16.

6. Results

6.1. Slack modulates Kainic acid-induced seizure severity in adult mice

To unravel the role of Slack in epilepsy, we induced epileptic seizures in Slack$^{+/+}$ and Slack$^{-/-}$ mice *in vivo*. For this purpose, the well-established and widely used KA-based model for acute epilepsy was used, as this model has been shown to be highly isomorphic to human epilepsies (Lévesque & Avoli, 2013) and previous studies revealed a functional interaction of Slack and the glutamatergic transmitter system (Matt et al., 2021; Nanou et al., 2008). Seizures were induced by intraperitoneal (i.p.) application of a single KA dose as outlined (section 5.3.). The subsequent occurrence of seizures was scored by using an adopted Racine scale (Racine et al., 1972) that rates the highest reached seizure score (SSc) within 5 min intervals over a total duration of 90 min (Fig. 11A). Scores ranged from SSc 0, no symptoms, to SSc 1 to 3, mild convulsions, up to SSc 5 and 6, characterised by prominent convulsions and TCS, while SSc 7 indicated death provoked by seizures (see section 5.3. and Fig. 6). In a first set of experiments, seizure severity of adult 8 to 12 weeks old male mice was analysed upon injection of increasing doses of KA, starting from 15 mg/kg up to 30 mg/kg (Fig. 11B). Comparison of the highest reached SSc over the total scoring time of 90 min unveiled mild convulsions in the range of SSc 1 to 2 (non-convulsive seizures) in both genotypes upon injection of the lowest KA dose (15 mg/kg). With increasing doses, both genotypes reached severe seizures in the rage of SSc ≥5. Interestingly, injection of 30 mg/kg KA provoked significantly higher SSc values in Slack$^{-/-}$ compared to Slack$^{+/+}$ (Fig. 11B). At a single interval level, analysis of KA-provoked seizures revealed a different time course of the responses for Slack$^{-/-}$ vs Slack$^{+/+}$: In particular, 40 to 90 min following injection of 20 mg/kg KA i.p., Slack$^{+/+}$ mice showed significantly more severe convulsive seizures (CS, SSc ≥3) (Fig. 11C). Onset of CS, however, was faster in Slack$^{-/-}$ (Fig. 11D) and accordingly the fraction of animals reaching SSc 5 was also higher in Slack$^{-/-}$ compared to Slack$^{+/+}$ (Fig. 11E; SSc 5: Slack$^{-/-}$ 2 of 5 mice, SSc 5: Slack$^{+/+}$ 4 of 6 mice). Thus, the higher seizure score over time was likely due to a large fraction of Slack$^{+/+}$ mice that reach SSc 4 and remained at this level throughout several intervals compared to Slack$^{-/-}$. For Slack$^{-/-}$ in turn, more mice reached CS rapidly and with higher fraction i.e., SSc 5. Interestingly, both genotypes reacted, at least regarding some key responses to KA, contrarily SSc following injection of 30 mg/kg, which provoked significantly higher SSc over time in Slack$^{-/-}$ compared to Slack$^{+/+}$ mice (Fig. 11F). As previously for 20 mg/kg KA, Slack$^{-/-}$ animals showed a tendency to reach

CS more rapidly (Fig. 11G). Also, with 30 mg/kg KA high SSc of 6 and 7 (SE and death following SE) were reached by $Slack^{-/-}$ more frequently (Fig. 11H; SSc 6: $Slack^{+/+}$ 1 out of 7 mice, $Slack^{-/-}$ 4 out of 7 mice, Chi-square, $p = 0.094$; SSc 7: $Slack^{+/+}$ 0 out of 7 mice, $Slack^{-/-}$ 3 out of 7, Chi-square, $p = 0.0507$). To summarize these findings, we observed an increased seizure susceptibility of $Slack^{-/-}$ compared to $Slack^{+/+}$ mice at higher KA doses. Since principal aim of KA-based model for epilepsy is to reach epilepsy like high SSc and high doses of 30 mg/kg KA are reported in literature (Gertler et al., 2022; Kang et al., 2015; Nasrallah et al., 2022; Wang et al., 2009; Wu et al., 2005) findings based on 30 mg/kg KA are of principal significance.

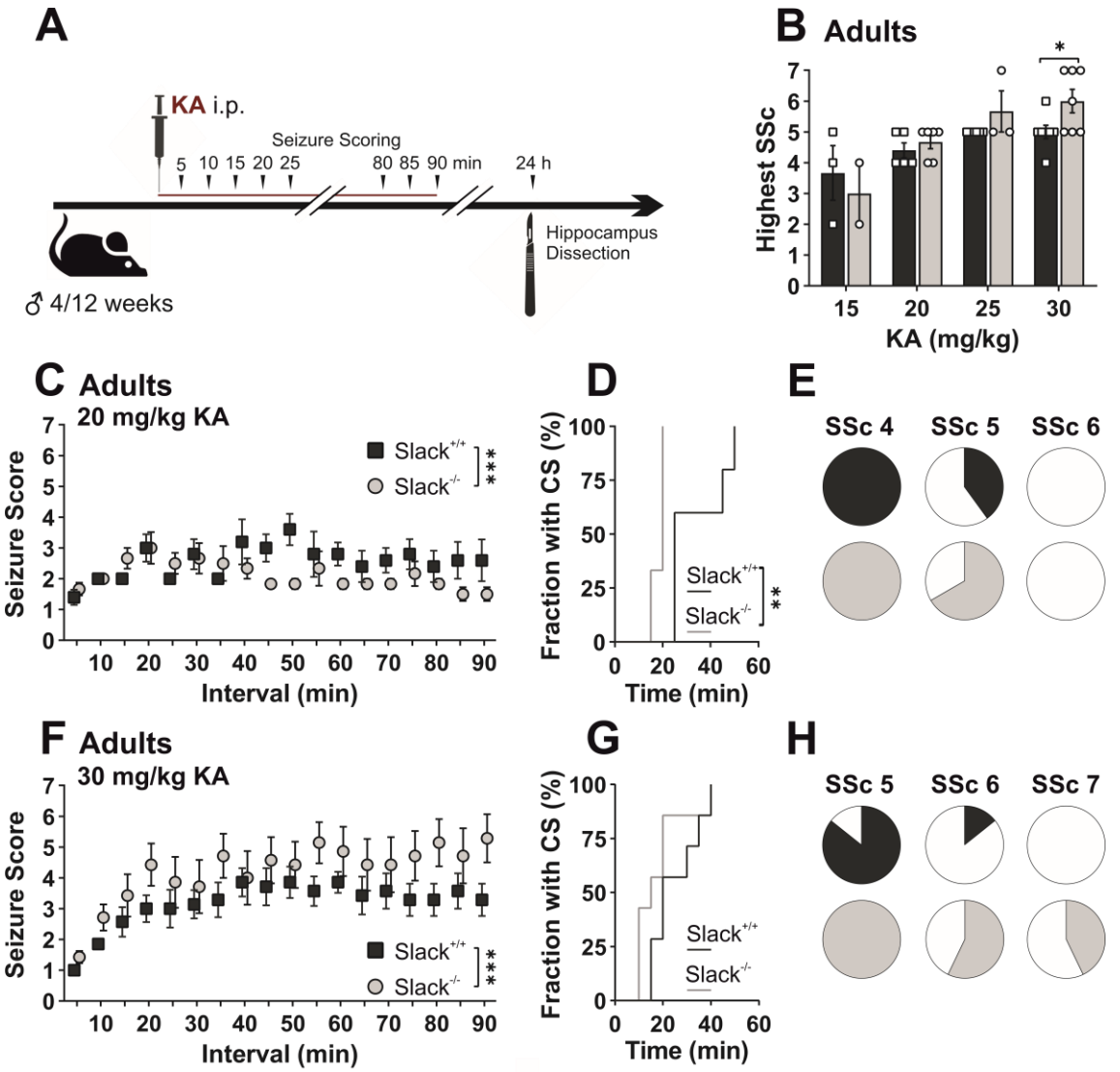

Figure 11: Slack modulates seizures and lethality in KA-induced model of acute epilepsy.

(A) Schematic representation of the experimental protocol used for adult 8-12 weeks old mice (Fig. 11 and 12) and juvenile 4 weeks old mice (see Fig. 13). Male wildtype (Slack$^{+/+}$) and Slack knock-out (Slack$^{-/-}$) mice were tested for seizure susceptibility and severity by intraperitoneal injection of 15 to 30 mg/kg Kainic acid (KA). Subsequently, seizures were scored by employing the highest score within a 5 min interval for a total of 90 min using an adopted Racine scale (Racine et al., 1972), ranging from seizure score (SSc) 0, no seizures, SSc 5, severe seizures with rearing and falling, to SSc 6, TCS, and SSc 7, death following seizures. **(B)** Dose-finding study using male, 8 to 12 weeks old adult mice was performed by injection of increasing KA doses ranging from 15 to 30 mg/kg. Compared to Slack$^{+/+}$, highest SSc reached over a total of 90 min is a significantly more frequent event in Slack$^{-/-}$ animals following injection of 30 mg/kg (Slack$^{+/+}$ black bars, n = 7, Slack$^{-/-}$ grey bars, n = 7, unpaired t-test p = 0.040), while at lower KA doses no differences were observed between genotypes. **(C)** Compared to Slack$^{+/+}$ (n = 5), Slack$^{-/-}$ (n = 6) animals are protected from KA (20 mg/kg) provoked convulsions over a total time course of 90 min ($F_{1/162}$ =11.96, p = 0.0007). **(D)** Yet, Slack$^{-/-}$ animals reach convulsive seizures earlier (Log-rang test p = 0.0024) and **(E)** fraction of animals reaching SSc 5 tended to be higher in Slack$^{-/-}$ (black and grey sections represent affected fraction, white sections unaffected fraction of animals; Slack$^{+/+}$ 2 out of 5 animals, Slack$^{-/-}$ 4 out of 6 animals, Chi-square, p = 0.37). **(F)** Following injection of 30 mg/kg KA Slack$^{-/-}$ animals (n = 7) exhibit significantly (two-way ANOVA $F_{1/216}$ = 24.32, p < 0.001) increased seizure severity over time compared to respective Slack$^{+/+}$ siblings (n = 7) with **(G)** a similar onset of CS but **(H)** a higher frequency of status epilepticus (SE) and death following SE (SSc 6: Slack$^{+/+}$ 1 of 7animals, Slack$^{-/-}$ 4 of 7 animals, Chi-square, p = 0.094; SSc 7: Slack$^{+/+}$ 0 of 7 animals, Slack$^{-/-}$ 3 of 7 animals, Chi-square, p = 0.0507). All data are presented as mean values ± SEM with ***P <0.001. For detailed statistics also consult Supplementary Table 1. Figure modified from Skrabak et al., 2023.

Since in particular the hippocampal formation is affected in epilepsy and in the KA-induced model of temporal lobe epilepsy (Lévesque & Avoli, 2013; Sendrowski & Sobaniec, 2013), pathophysiological corelates were analysed in hippocampal mRNA samples by determining transcript levels of Slack, related K^+ channels, and epilepsy-relevant genes 24 h post KA injection. Expression levels of Slick and BK, which are also members of the Slo-gene family of K^+-channels and conduct large K^+-currents (see also section 3.6.), were not different in $Slack^{+/+}$ vs $Slack^{-/-}$ hippocampus 24 h post injection of 20 mg/kg KA, suggesting these channels functionally do not compensate for loss of Slack in $Slack^{-/-}$ (Fig. 12A). Also, obligatory receptor subunits of KA-, AMPA- and NMDA-type glutamatergic signalling were not differentially expressed in $Slack^{-/-}$ compared to $Slack^{+/+}$ hippocampus (Fig. 12B). Since BDNF signalling was previously reported to be altered following glutamatergic excitotoxicity in Slack-deficient cerebellar granular cells (Ehinger et al., 2021), also expression levels of BDNF and its receptors TrkB was assesses. Interestingly, transcript levels of BDNF and TrkB as well as the astroglia marker GFAP were not different in $Slack^{-/-}$ compared to $Slack^{+/+}$ (Fig. 12C). Hippocampal mRNA expression levels of these genes were also assessed for adult animals 24 h post injection of 30 mg/kg KA. Again, neither the related K^+ channels Slick and BK (Fig. 12D), nor receptor subunits of glutamatergic signalling GluK, GluA and GluN (Fig. 12E) were Slack dependently modulated. Accordingly, BDNF and TrkB expression were not different between genotypes, whereas GFAP was upregulated in $Slack^{+/+}$ animals 24 h post injection of 30 mg/kg KA (Fig. 12F), indicating an enhanced glial response to the KA-induced seizures.

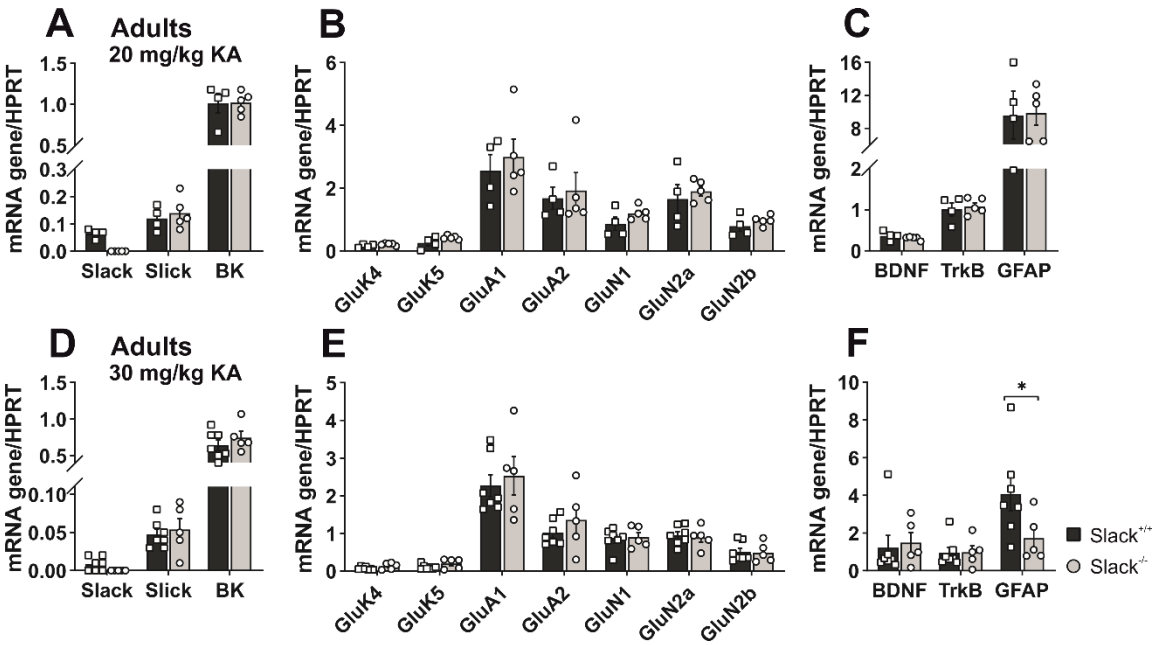

Figure 12: KA-induced epilepsy does not induce compensatory or regulatory changes in hippocampal mRNA transcription levels of Slack and other "epilepsy" related genes.

(A to C) Compared to adult Slack$^{+/+}$ (n = 4, black bars), Slack$^{-/-}$ (n = 5, grey bars) hippocampal mRNA expression levels of **(A)** related K^+ channels, subunits of **(B)** glutamatergic receptor subunits and **(C)** neurotrophic factors are not altered 24 h following injection of 20 mg/kg KA. **(D to F)** Compared to adult Slack$^{+/+}$ (n = 7, black bars), Slack$^{-/-}$ (n = 5, grey bars) hippocampal mRNA expression levels of **(D)** related K^+ channels or **(E)** subunits of glutamatergic receptor are not altered 24 h following injection of 30 mg/kg KA, while Slack$^{+/+}$ hippocampi responded with a significant increase in **(F)** GFAP mRNA expression to KA induced convulsions (unpaired t-test p = 0.013). Data represented as mean ± SEM with *P <0.05. For detailed statistics also consult Supplementary Table 2. Figure modified from Skrabak et al., 2023.

Together, these data raise evidence for a differential role of Slack during KA-induced seizures, as Slack function prolonged mild convulsions (Fig. 11C) but limited occurrence of SE (Fig. 11H) and prevented death following SE (Fig. 11H) in adult animals. Additionally, analysis of hippocampal mRNA expression levels following injection of 20 or 30 mg/kg KA revealed no prominent compensatory regulation of related and involved genes, despite increased glial response to high KA does in Slack$^{+/+}$ (30 mg/kg) (Fig. 12F). These findings suggest an acute protective role of Slack K^+ channels during KA-provoked cellular events that cause seizures and/or affect seizure susceptibility and severity, but this is not associated with different mRNA expression levels of glutamatergic receptors.

6.2. Slack$^{-/-}$ juvenile mice show increased seizure susceptibility and impaired BDNF signalling upon KA-provoked epilepsy

Pathogenic variants of the Slack-encoding gene *Kcnt1* lead to epilepsy syndromes with an early onset (Evely et al., 2017). Thus, we adopted the experimental setup of KA-induced acute epilepsy to more patient-relevant conditions by using 4-weeks-old juvenile male mice (see also Fig. 13A), and challenged these young animals with 20 mg/kg KA to score seizures for 90 min.

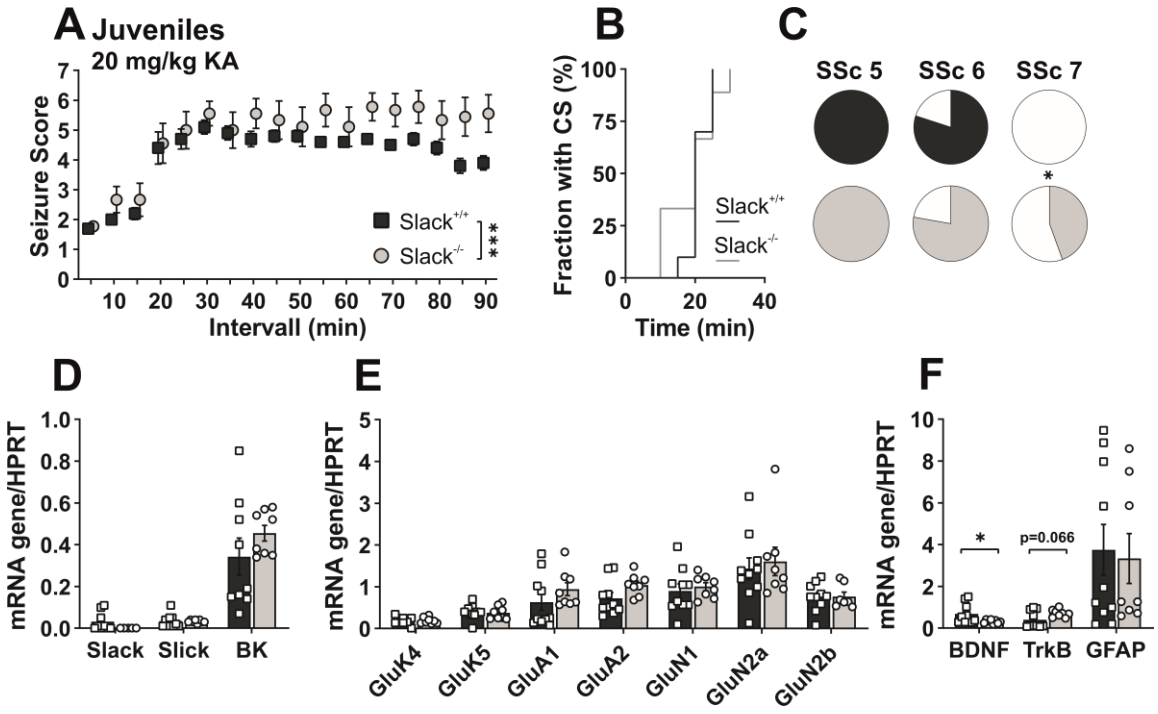

Figure 13: Juvenile Slack$^{-/-}$ animals respond with increased seizure-provoked lethality to KA injection and show impaired BDNF signalling 24 h post seizures.

(A) Seizure susceptibility and severity were analysed in 4-weeks-old juvenile mice upon 20 mg/kg KA i.p. injection, followed by seizure scoring. Compared to Slack$^{+/+}$ (n = 10, black squares and bars), Slack$^{-/-}$ (n = 9, grey circles and bars) mice exhibit significantly (two-way ANOVA $F_{1/144} = 30.63$, $p < 0.001$) increased seizure severity over time with **(B)** similar onset of CS but **(C)** more frequent death following SE (SSc 7: Slack$^{+/+}$ 0 of 10 animals, Slack$^{-/-}$ 4 of 9 animals, Chi-square, p = 0.048). **(D and E)** Hippocampal mRNA expression levels of **(D)** related K^+ channels are unchanged between Slack$^{+/+}$ and Slack$^{-/-}$, comparable to **(E)** subunits of glutamatergic receptors, that are similar in Slack$^{-/-}$ compared to Slack$^{+/+}$ 24 h following seizures. **(F)** Transcript levels of the neurotrophic factor BDNF was decreased in Slack$^{-/-}$ (Slack$^{+/+}$ n = 10, Slack$^{-/-}$ n = 8; unpaired t-test, BDNF p = 0.048) 24 h after seizures. Data represented as mean ± SEM with *P <0.05, **P <0.01, ***P <0.001. For detailed statistics also consult Supplementary Table 3. Figure modified from Skrabak et al., 2023.

Compared with the groups of adult mice studied previously (Fig. 11), juvenile mice of both genotypes responded with more severe seizures following KA injection with SSc ≥4 20 min post injection (Fig. 13A). Importantly, SSc values that were achieved in Slack$^{-/-}$ were significantly higher compared to Slack$^{+/+}$ siblings over the total scoring period of 90 min. While onset of CS (Fig. 13B) and fraction of animals reaching SE (Fig. 13C, SSc 6: Slack$^{+/+}$ 8 of 10, Slack$^{-/-}$ 7 of 9) was similar in both genotypes, epilepsies were frequently lethal for Slack$^{-/-}$ but not Slack$^{+/+}$ mice (Fig. 13C, SSc 7: Slack$^{+/+}$ 0 of 10, Slack$^{-/-}$ 4 of 9; Chi-square, $p = 0.048$), suggesting a severely impaired intrinsic ability to limit the KA-induced seizures in the absence of Slack channels. Accordingly, Slack$^{+/+}$ tended to show decreased SSc after approximately 1 h, where they returned to a SSc ≤4 in average (Fig. 13A 80 to 90 min). Confirming our findings in adult mice, KA-provoked convulsions did not lead to differential hippocampal mRNA expression levels of Slack-related K^+ channels such as Slick and BK 24 h post KA injection (Fig. 13D). Also, expression of GluK, GluA and GluN subunits in Slack$^{+/+}$ and Slack$^{-/-}$ were equal (Fig. 13E). Moreover, 24 h after the seizures, Slack$^{-/-}$ animals expressed significantly reduced levels of the neuroprotective BDNF, while TrkB transcripts showed a trend to higher levels in Slack deficient hippocampus (Fig. 13F).

Together with data obtained in adult mice, *in vivo* findings of juvenile mice emphasize that Slack limits high intense epileptic seizures and reduces seizure provoked death. In both, adult and juvenile mouse groups, aberrant regulation of Slack-related K^+ channels were not associated with the increased seizure scores of Slack$^{-/-}$. Finally, Slack was apparently important counteracting the KA-induced hippocampal hyperactivation; here, upregulation of BDNF, among other factors, may play a role, that is in line with previous findings of altered BDNF signalling in Slack-deficient cerebellar granular cells (Ehinger et al., 2021).

6.3. Slack$^{-/-}$ hippocampal tissue and single cells are more prone to KA-induced cell death

Slack channels (Bhattacharjee & Kaczmarek, 2005b; Ehinger et al., 2021; Rizzi et al., 2016) and Kainate-type glutamatergic receptors (Lévesque & Avoli, 2013; Rusina et al., 2021) are highly expressed in the hippocampal formation, especially the CA3 region. Also, the limbic system, and in particular the hippocampal formation, is highly prone to the migration and propagation of ictal events, which may even begin here (Mikati et al., 2003; Sendrowski & Sobaniec, 2013; Weinstein, 2016; Yaari & Beck, 2002). As a consequence, so called hippocampal scleroses (HS) can be found in epilepsy patients with atrophy of hippocampus and cell loss predominantly in the CA3 region (Sendrowski & Sobaniec, 2013). Hence, to transfer *in vivo* findings to a valid *in vitro* model, hippocampal slice

cultures (HSC) from 5P Slack$^{+/+}$ and Slack$^{-/-}$ pups were generated and cultured for 14 days, which retained intact intra-hippocampal connections (Holopainen, 2005; Humpel, 2015). Indeed, following organotypic culture, both, Slack$^{+/+}$ and Slack$^{-/-}$ HSC showed morphologically intact hippocampal layers (Fig. 14A left, brightfield). Also, mRNA expression levels of Slack-related K^+ channels Slick and BK were assessed, and no aberrant regulations were found at transcript level (Fig. 14B). HSC were exposed for 2 days to 5 or 10 µM KA, and cell death provoked by this treatment was quantified relative to the positive control by PI staining (Fig. 14A middle and right).

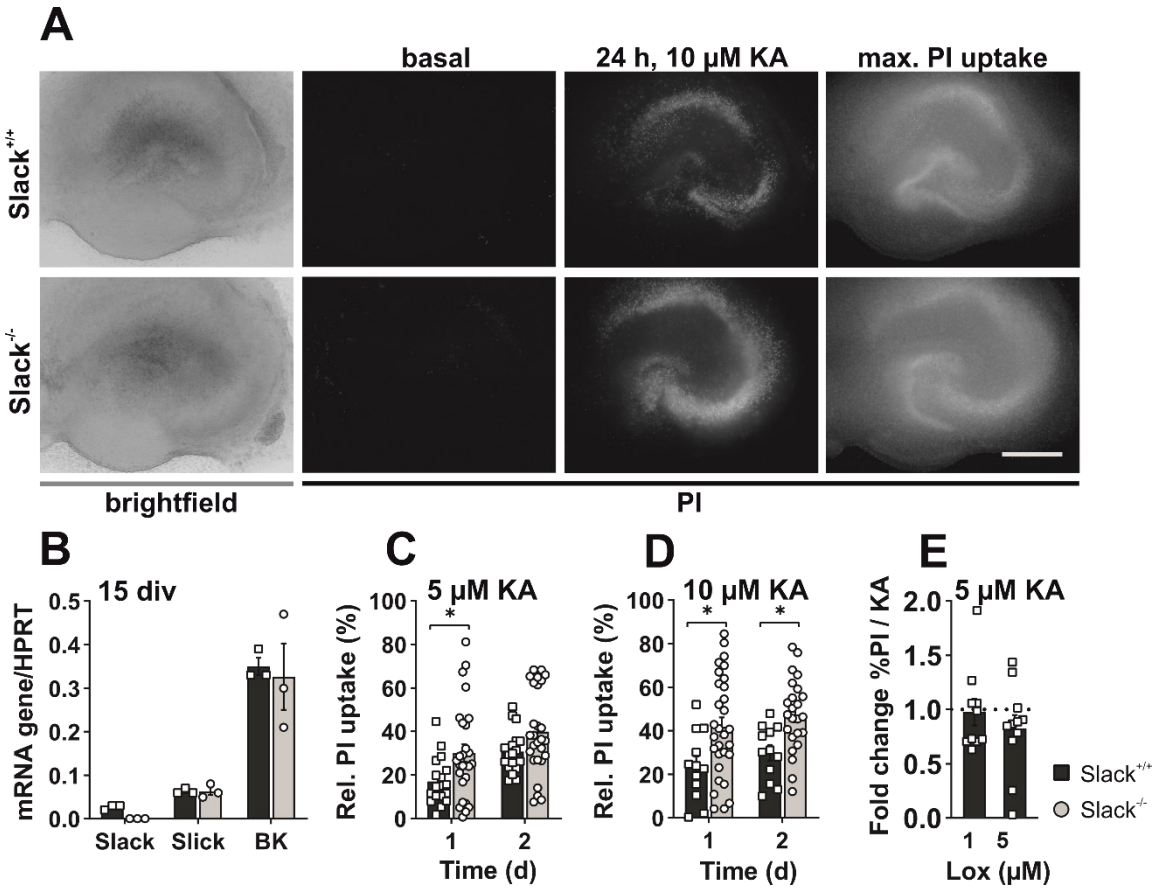

Figure 14: Increased KA-induced cell death in Slack$^{-/-}$ HSC.

(A) Images of representative 14 div hippocampal slice cultures (HSC) from Slack$^{+/+}$ (upper images) and Slack$^{-/-}$ (lower images) prior treatment (basal), after 24 h exposure to 10 µM KA (24 h 10 µM KA) or after application of 80% ethyl-alcohol (max. PI uptake). Scale bar: 500 µm. **(B)** mRNA expression levels of 14 div Slack$^{+/+}$ (black bars) and Slack$^{-/-}$ hippocampal slice cultures (grey bars). As expected, no Slack mRNA transcripts were detectable in Slack$^{-/-}$. Slick and BK mRNA levels are similar in Slack$^{+/+}$ and Slack$^{-/-}$. **(C and D)** Compared to Slack$^{+/+}$, Slack$^{-/-}$ HSC showed significantly increased PI uptake (normalized to maximum) in response to 5 and 10 µM KA (24 h). At 10 µM KA, this difference was still significant after 48 h (5 µM KA: Slack$^{+/+}$ n = 18 ROI out of 3 to 4 wells from 4 preparations, Slack$^{-/-}$ n = 27 ROI out 8 to 9 wells from 6 preparations, two-way-ANOVA with Sidak´s multiple comparison, p = 0.027 for 1d, p = 0.079 for 2 d; 10 µM KA: Slack$^{+/+}$ n = 12, Slack$^{-/-}$ n = 24, two-way-ANOVA with Sidak´s multiple comparison, p = 0.012 for 1d, p = 0.022 for 2 d). **(E)** In Slack$^{+/+}$ HSC KA co-treatment with non-specific “Slack activator” Loxapine tendentially reduces PI uptake. Data is represented as mean ± SEM with *P <0.05. For detailed statistics also consult Supplementary Table 4. Figure modified from Skrabak et al., 2023.

Both KA concentrations, 5 and 10 µM, induced significantly increased PI uptake in Slack$^{-/-}$ HSC following 1 d and 2 d exposure (Fig. 14C and D), predominantly due to dye accumulation in the CA3 layer (Fig. 14A, middle).

Moreover, short-time (1 h) high-dose exposure of 20 µM KA followed by subsequent PI imaging for 7 d confirmed an increased vulnerability of Slack$^{-/-}$ HSC (Supplementary Fig. 1A). Hence, both, acute and chronic KA-exposure caused increased PI uptake in Slack$^{-/-}$ HSC indicative of more cell death in the absence of neuronal Slack channels.

In a parallel approach, we aimed to pharmacologically target Slack to modulate KA-induced PI uptake. Using the non-specific “Slack activator” Loxapine (Biton et al., 2012) alone or together with 5 µM KA, PI uptake in Slack$^{+/+}$ HSC was quantified. PI uptake was slightly reduced by Loxapine co-exposure (Fig. 4E) confirming Slack´s potentially protective role in hippocampal tissue that can be exploited pharmacologically. However, Loxapine interacts with multiple receptors such as dopamine D2/D3 receptor, histamine H1, serotonin 5-HT2 and adrenergic α1 (Chakrabarti et al., 2007; Popovic et al., 2015), and therefore it is not surprising that the co-treatment performed here did not yield a prominent difference. Nevertheless, to strengthen these findings, experiments were repeated with the “Slack activator” Bithionol and the “Slack inhibitor” Quinidine (Bhattacharjee et al., 2003b; Yang et al., 2006), but these treatments did not modulate the KA-indued PI uptake (Supplementary Fig. 1B and C) suggesting again multiple off-target effects and/or an insufficient Slack-specificity of the compounds, somehow in line with principal application for cardiac dysfunctions (Yang et al., 2009) and Helminth infections (Keiser & Utzinger, 2010).

In summary, in line with *in vivo* findings, Slack seems to play a protective role in hippocampal circuitries of isolated HSC *in vitro*, as it limits KA-induced PI uptake in CA regions and the DG.

Following our in-depth analysis of HSC with intact hippocampal circuitry, primary dissociated hippocampal neurons (PHN) were engaged to determine the role of Slack for KA-induced epileptiform activation on a single cell level, independent from hippocampal wiring, projections, and topography. PHN were cultured from Slack$^{+/+}$ and Slack$^{-/-}$ new-born pups for 8 to 10 days. Using immunofluorescence imaging, prominent Slack expression was detected in Slack$^{+/+}$ PHN but not Slack$^{-/-}$ (Fig. 15 A). Additionally, expression of functional corelates like synapses and obligatory AMPA and NMDA receptor subunits such as GluA1 and GluN1, were expressed in the same extend and pattern in both, Slack$^{+/+}$ and Slack$^{-/-}$ PHN (Fig. 15B to D).

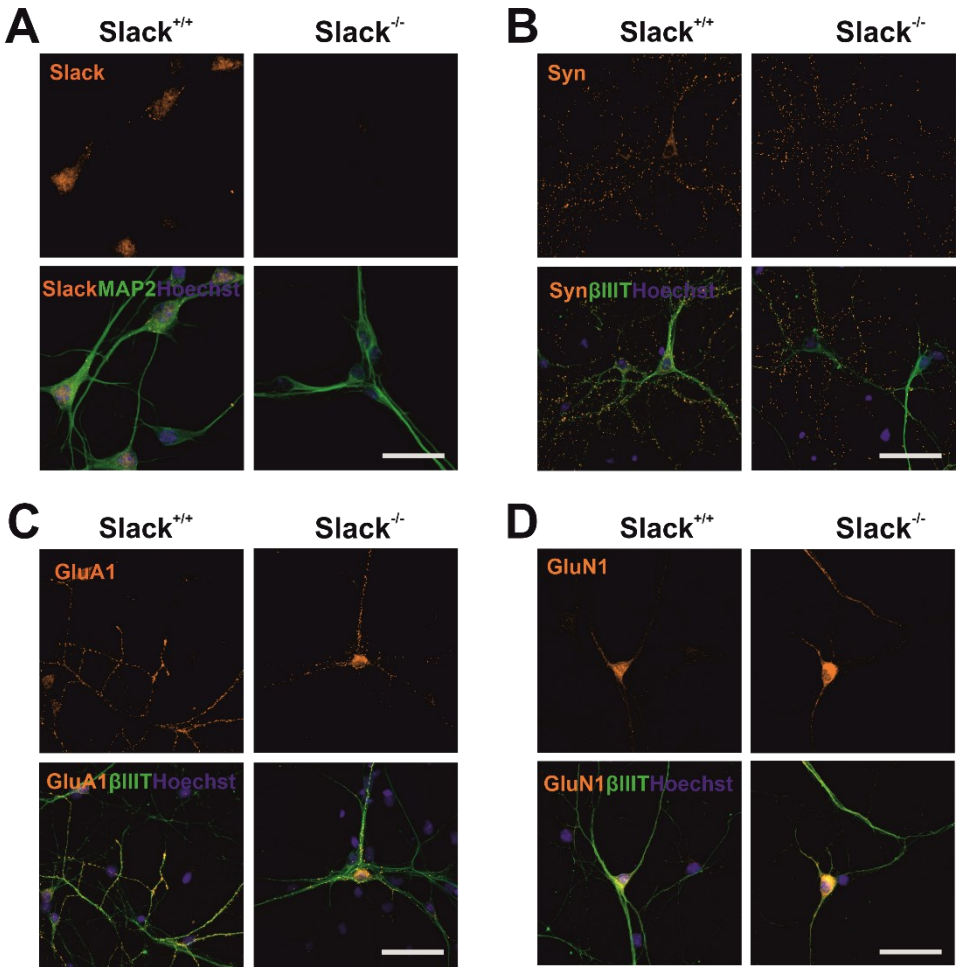

Figure 15: Primary hippocampal neuron cultures express Slack, synapsin and glutamate receptor subunits following cultivation.

(A) Representative fluorescence images of 8 to 10 div hippocampal Slack$^{+/+}$ (left images) and Slack$^{-/-}$ primary neurons (right images) stained with specific antibodies against Slack (orange) and neuronal marker MAP2 (green). Slack immunoreactivity is not detected in Slack$^{-/-}$. **(B to D)** Representative fluorescence images of 8 div hippocampal Slack$^{+/+}$ (left images) and Slack$^{-/-}$ neurons (right images) stained with antibodies directed against **(B)** synapse-associated proteins (synapsin, Syn), **(C)** AMPA-type glutamate receptor subunit GluA1 or **(D)** NMDA-type glutamate receptor subunit GluN1 (orange), together with the neuron-specific cytoskeletal protein marker βIIItubulin (green). Both, Slack$^{+/+}$ and Slack$^{-/-}$ neurons express βIIItubulin with no gross differences in protein levels or marker distribution. **(A to D)** Nuclei are visualized with Hoechst 33342 (blue). Scale bars: 40 µm. Figure modified from Skrabak et al., 2023.

The dominant fraction of isolated and cultured cells were neurons, as verified by staining for the neuronal and axonal markers MAP2 and βIIItubulin (Fig. 15A to D), although few glial cells were detected using antibodies raised against GFAP (Supplementary Fig. 2A). Analogous cell viability studies in organotypic HSC, single cells were stained with PI after KA exposure. Following determination of the baseline viability as number of basally PI positive particles (Fig. 16A middle) PHN were exposed to 5 or 10 µM KA for 24 h and KA-induced PI uptake was quantified relative to the basal levels (Fig. 16A, right).

In accordance with HSC, Slack$^{-/-}$ PHN showed a significantly increased PI uptake compared to Slack$^{+/+}$ in response to 10 µM KA exposure (Fig. 16B). Shorter exposure of PHN to high KA concentrations of 50 to 500 µM KA for 15 h confirmed these results (Supplementary Fig. 2B).

Next, we tried to establish a functional link between KA-induced cell death and neuronal activity. Therefore, PHN were exposed to 10 µM KA alone or cells were co-treated with 10 µM KA and 50 or 100 µM of the $GABA_A$ antagonist picrotoxin (PiTX) to further disinhibit KA-induced neuronal firing.

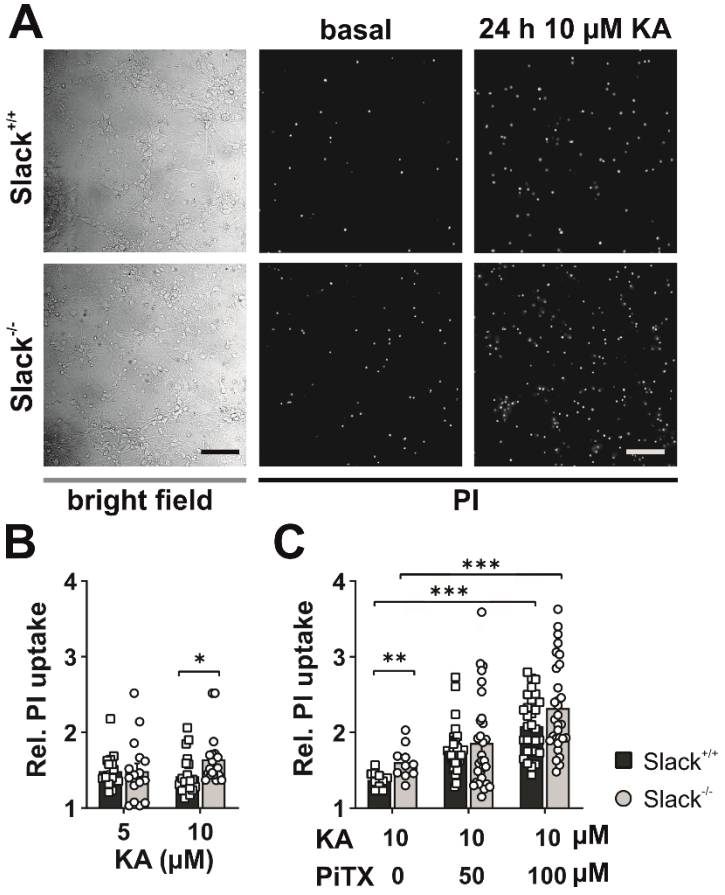

Figure 16: Increased KA-induced cell death in dissociated Slack$^{-/-}$ hippocampal neurons.

(A) Left, representative brightfield images of 8 div PHN. Right, representative images of PI uptake in 8 div Slack$^{+/+}$ (upper images) or Slack$^{-/-}$ hippocampal neurons (lower images) before (basal) and after 24 h exposure to 10 µM KA. Scale bars: 500 µm. **(B)** Cell death is significantly (Mann-Whitney test, p = 0.0016) increased in Slack$^{-/-}$ (n = 22 ROI out of 4 wells from 3 preparations) compared to Slack$^{+/+}$ neurons (n = 20 ROI out of 4 wells from 3 preparations) as measured by PI uptake (normalized to basal) after 24 h exposure to 10 µM KA. **(C)** In both, Slack$^{+/+}$ (n = 30 ROI out of 4 to 5 wells from 3 preparations) and Slack$^{-/-}$ neurons (n = 30 ROI out of 4 to 5 wells from 3 preparations) KA-provoked PI-uptake is significantly exacerbated by co-treatment with 100 µM Picrotoxin (PiTX) (Sidak's multiple comparison p = 0.0008 for Slack$^{+/+}$ and p = 0.0007 for Slack$^{-/-}$). Additionally, by comparing groups over all treatment conditions, Slack$^{-/-}$ neurons are tendentially more affected than Slack$^{+/+}$ (two-way-ANOVA, $F_{1/116} = 3.23$, p = 0.075). Data in B represented as mean ± SEM with *P <0.05, **P <0.01, ***P <0.001. For detailed statistics also consult Supplementary Table 5. Figure modified from Skrabak et al., 2023.

As expected, PiTX mediated loss of GABAergic signalling in PHN led to exacerbated KA-induced PI uptake. In particular at high concentrations of 100 µM PiTX the PI uptake in both, Slack$^{+/+}$ and Slack$^{-/-}$ was significantly increased compared to KA alone (Fig. 16C). Within each co-treatment groups, no genotype-related differences were found, suggesting that the protection afforded by Slack could prevent KA to excite nerve cells to their death only if $GABA_A$ signalling was intact. Nevertheless, by comparing the PI uptake of both genotypes throughout all co-treatment conditions, Slack$^{-/-}$ tend to respond with increased PI uptake.

To sum up, PI-based approaches revealed an enhanced cell death in Slack$^{-/-}$ HSC (Fig. 14C and D) and PHN (Fig. 16B) supporting Slack's neuroprotective role during KA-induced epileptiform activity *in vivo* (Fig. 11 and 13). Moreover, the accelerated cell death under conditions of concomitant treatment with PiTX (Fig. 16C) suggests that excessive neuronal activity was the underlying cause for the KA-induced PI uptake.

6.4. Slack$^{-/-}$ hippocampal neurons respond with increased Ca^{2+} influx but decreased K^+ efflux to KA-provoked activation

Subsequently, we aimed to elucidate the potential underlying molecular mechanisms explaining the increased susceptibility to KA-induced activation in Slack$^{-/-}$ mice *in vivo* and of Slack$^{-/-}$ hippocampal tissue and neurons *in vitro*. To this end, live-cell imaging of changes in the $[Ca^{2+}]_i$ and $[K^+]_i$ concentration was performed. First, 8 to 10 div PHN were loaded with the Ca^{2+} sensitive fluorescent dye Fura2 (Fig. 17A) to enable real-time measurements of KA-induced Ca^{2+} fluxes as surrogate for neuronal activation. Therefore, Slack$^{+/+}$ and Slack$^{-/-}$ neurons were first exposed to KA followed by co-exposure to KA and Ca^{2+}-free recording buffer additionally containing 100 µM Ca^{2+} chelating EGTA to omit Ca^{2+} from the extracellular space. Since the KA-induced increase in Fura2 ratio was abolished by co-exposure with the Ca^{2+} chelator EGTA (Fig. 17B), the KA-induced increase in $[Ca^{2+}]_i$ was considered to originate from extracellular sources. Subsequently, PHN were superfused with increasing KA concentrations ranging from 1 to 100 µM, intermitted by washout sequences using recoding buffer (Fig. 17C), and sigmoidal concentration-response curves were fitted to maximal Fura2 delta ratios (Fig. 17D). Interestingly, the EC_{50} of $[Ca^{2+}]_i$ response to KA was equal for Slack$^{+/+}$ (EC_{50} = 13.05 µM) and Slack$^{-/-}$ (EC_{50} = 12.56 µM) cells, suggesting unaltered general density of KA-receptors (GluK) in Slack$^{-/-}$ and Slack$^{+/+}$ PHN. Yet, at low KA concentration of 1 µM KA, Ca^{2+}-influx tended to be increased in Slack$^{-/-}$ (Sidak's multiple comparison p = 0.40).

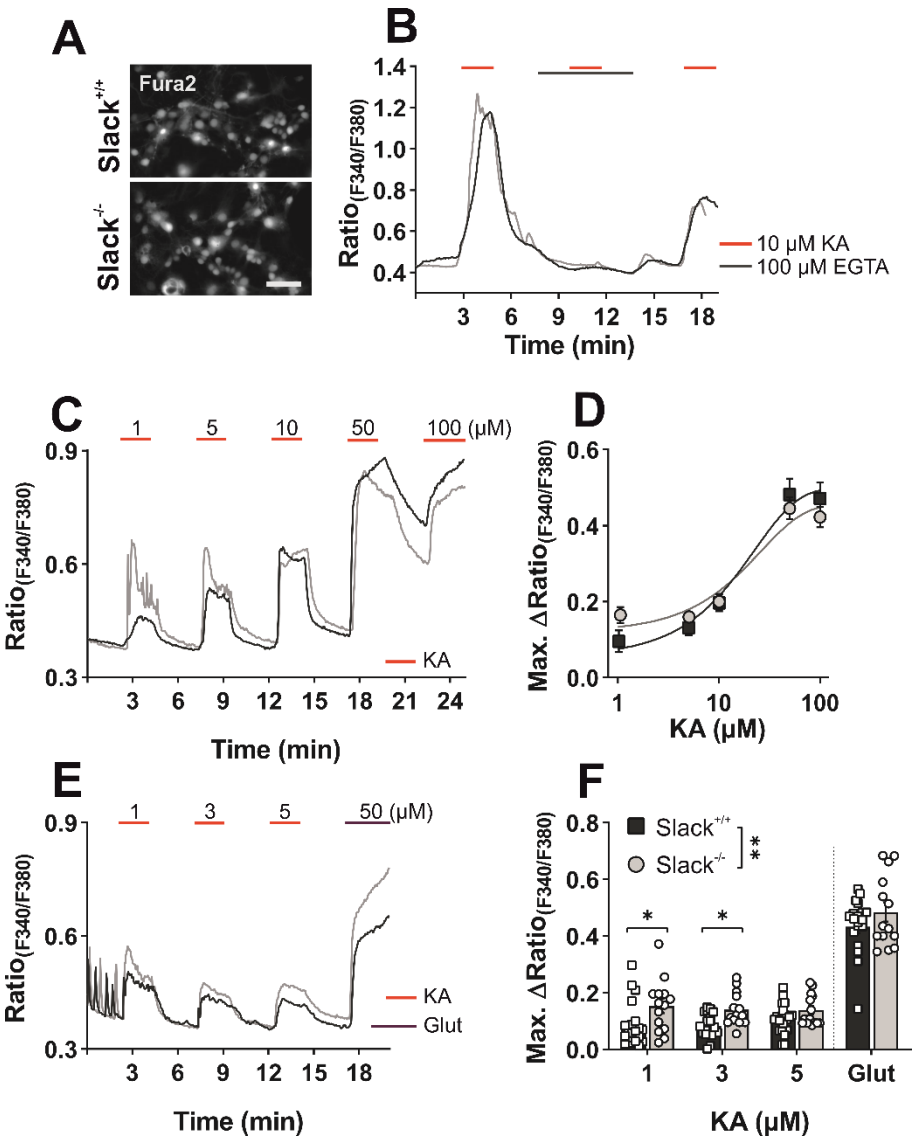

Figure 17: Increased KA-induced Ca^{2+} influx in Slack$^{-/-}$ hippocampal neurons.

(A) Representative images of 8 div Slack$^{+/+}$ (upper image) or Slack$^{-/-}$ hippocampal neurons (lower images) loaded with Fura2. Images were captured at an excitation of 380 nm. Scale bar: 50 µm **(B)** Representative Fura2 based recording of Ca^{2+} influx following exposure of Slack$^{+/+}$ (black curve) or Slack$^{-/-}$ hippocampal neurons (grey curve) to 10 µM KA alone or in combination with Ca^{2+} free and 100 µM EGTA containing recording buffer suggests extracellular Ca^{2+} to be responsible for KA-induced changes in Fura2 signal. **(C)** Exemplary time course of Fura2 recordings from Slack$^{+/+}$ (black curve) or Slack$^{-/-}$ primary hippocampal neurons (grey curve) treated with 1 to 100 µM KA as indicated by the red lines above the curves. **(D)** Sigmoidal concentration-response fit of Fura2 maximum delta ratios following exposure to increasing KA concentrations ranging from 1 to 100 µM (see traces in C) reveal no significant changes in EC_{50} (Slack$^{+/+}$, black squares, n = 12 wells out of 9 preparations, EC_{50} = 13.05; Slack$^{-/-}$, grey circles, n = 13 wells out of 8 preparations, EC_{50} = 12.56). **(E)** Exemplary Fura2 ratio signals over time of PHN treated with lower concentrations of KA (red lines) and a final glutamate control stimulus (purple line). **(F)** Quantification of maximal Fura2 delta ratio signals following PHN exposure to low KA concentrations ranging from 1-3 µM (see traces in E). Slack$^{-/-}$ PHN (grey bars) respond with increased Ca^{2+} influx to these treatments compared to Slack$^{+/+}$ cells (black bars) (Slack$^{+/+}$ n = 20 wells out of 9 preparations, Slack$^{-/-}$ n = 14 wells out of 10 preparations, two-way-ANOVA $F_{1/96}$ = 15.38, p = 0.0002, Sidak's multiple comparison 1 µM KA p = 0.014, 3 µM KA p = 0.036). Glutamate control stimulus is not included in the statistics. Data represented as mean ± SEM with *P <0.05, **P <0.01. For detailed statistics also consult Supplementary Table 6. Figure modified from Skrabak et al., 2023.

Based on this trend, a second set of experiments was carried out by exposing PHN to lower KA concentrations i.e., 1, 3 and 5 µM (Fig. 17E). By assessing Fura2 maximal delta ratios of these low KA concentrations, we were able to determine that, compared to Slack$^{+/+}$, Slack$^{-/-}$ responded with significantly increased Ca^{2+} influx to these stimuli (Fig. 17F).

Due to the previously reported interactions between Slack with AMPA-type receptors (Nanou et al., 2008) and NMDA-type receptors (Matt et al., 2021), the functional basis of Slack's regulatory contribution to the KA-induced Ca^{2+} influx was studied in the presence and absence of AMPA -and NMDA receptor modulation. This approach is important as the ability of Slack to affect the AMPA receptor and/or NMDA receptor driven Ca^{2+} influx would directly contribute to the KA-induced cell death and potential changes in cellular activity. To this end, neuronal activation induced by 5 µM KA was either modulated by treatment of KA with 10 µM AMPA receptor antagonist NBQX (Fig. 18A), 100 µM of the NMDA receptor antagonist DL-AP5 (Fig. 18B) or 10 µM non-specific "Slack activator" Loxapine (Fig. 18C, Lox).

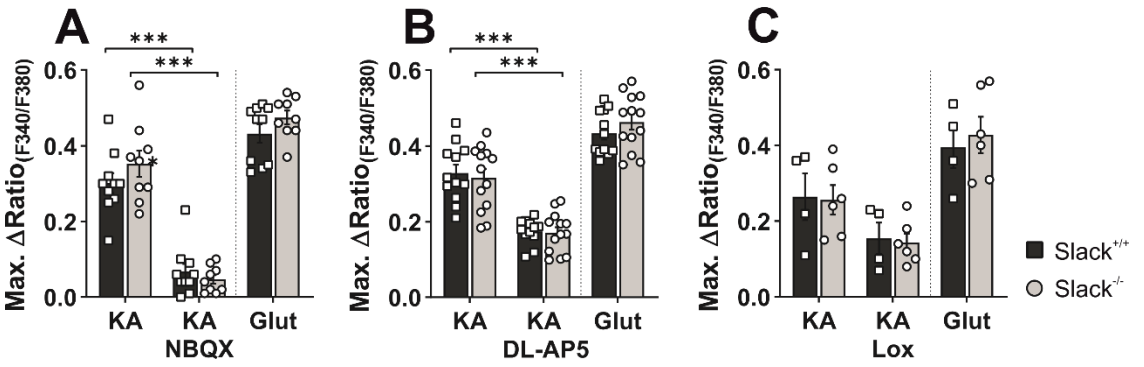

Figure 18: KA-induced Ca^{2+} influx is carried by NMDA and AMPA components that are not modulated by Slack.

Quantification of maximal Fura2 delta ratio signals following PHN exposure to 5 µM KA or co-treatment with KA and AMPA receptor blocker NBQX, NMDA receptor blocker DL-AP5 or Slack activator Loxapine (Lox). **(A)** NBQX reduced KA-induced increase in Fura2 maximal ratio both Slack$^{+/+}$ (n = 10 wells out of 5 preparations) and Slack$^{-/-}$ (n = 9 wells out of 4 preparations) significantly (Sidak's multiple comparison, Slack$^{+/+}$ p <0.0001, Slack$^{-/-}$ p <0.0001) **(B)** DL-AP5 reduced KA-induced increase in Fura2 maximal ratio both Slack$^{+/+}$ (n = 12 wells out of 7 preparations) and Slack$^{-/-}$ (n = 13 wells out of 7 preparations) significantly (Sidak's multiple comparison, Slack$^{+/+}$ p <0.0001, Slack$^{-/-}$ p <0.0001). **(C)** Loxapine did not modulate KA-induced increase in Fura2 maximal ration of either Slack$^{+/+}$ (n = 4 wells out of 3 preparations) or Slack$^{-/-}$ (n = 6 wells out of 3 preparations). Data represented as mean ± SEM with ***P <0.001. For detailed statistics also consult Supplementary Table 7. Figure modified from Skrabak et al., 2023.

As previously (Fig. 17D), 5 µM KA provoked similar maximal Fura2 delta ratios in Slack$^{+/+}$ and Slack$^{-/-}$ neurons with a tendency towards higher influx in the absence of Slack (Fig. 18A). This is consistent with the experiments shown in Fig. 17F. There, the genotypes differed only for 1 and 3 µM KA or when all concentrations were tested in the

1-5 µM KA range. Again, this suggests that the Ca^{2+} influx is dependent on Slack in particular at low level glutamatergic stimulation. Following co-treatment of 5 µM KA together with NBXQ or DL-AP5 Fura2 maximal delta ratio was strongly decreased (Fig. 18A and B) suggesting prominent AMPA -and NMDA-mediated components of the KA-induced Ca^{2+} influx. AMPA -and NMDA components might be due to direct KA-mediated activation of AMPA receptors, but also by the recruitment of NMDA receptors that apparently support the KA-induced Ca^{2+} influx. Interestingly, neither blockers of glutamatergic receptor subtypes (Fig. 18A and B), nor the activation of Slack (Fig. 18C) induced genotype dependent differences in response to KA stimulation. Together, Slack's contribution to the Ca^{2+} influx in PHN is moderate, restricted to a narrow KA concentration range of 1 to 3 µM, and with Fura2 the slack modulation of glutamatergic signalling can probably not be sufficiently resolved. Accordingly, the "Slack activator" Loxapine did not affect the Ca^{2+} signals obtained by KA co-stimulation, which is consistent with the marginal effects of this compound on the PI uptake in HSC (Fig. 14E).

Next, we tried to link the altered Ca^{2+} entry under KA stimulated conditions with dynamic K^+ alterations, i.e., Slack K^+ channel function. For this purpose, $[K^+]_i$ was monitored in 8 to 10 div PHN after viral transduction with a genetically encoded K^+ ion sensor NES lc-LysM GEPII 1.0 (Bischof et al., 2017; Pham et al., 2023) under control of a common CAG promotor (Fig. 19A). Repeating the Fura2 based experimental setups (Fig. 17E and F), PHN were perfused with imaging buffer with or without 1, 3 and 5 µM KA (Fig. 19B) and FRET ratio measured under control of antiparallel CFP and FRET values (Supplementary Fig. 3). Interestingly, $Slack^{-/-}$ PHN responded with a significantly increased and not as expected lower K^+ efflux to 1, 3 and 5 µM KA (Fig. 19C) suggesting other, yet to be identified, K^+ currents that are critically involved in the KA response of $Slack^{-/-}$ PHN, for example K_V channels.

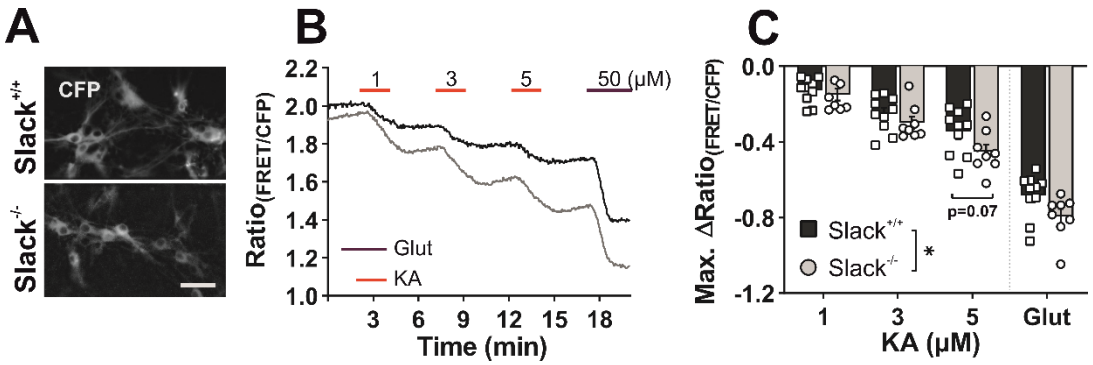

Figure 19: Increased KA-induced K^+ efflux in Slack$^{-/-}$ hippocampal neurons.

(A) Representative images of 8 div hippocampal Slack$^{+/+}$ (upper image) or Slack$^{-/-}$ neurons (lower image) virally transduced with the FRET-based K^+ sensitive sensor Ic LysM GEPII 1.0. Scale bar: 50 µm. **(B)** Exemplary FRET-ratio signals over-time of hippocampal Slack$^{+/+}$ (black curve) or Slack$^{-/-}$ neurons (grey curve) treated with the indicated concentrations of KA (red lines above the panel), or 50 µM of glutamate (purple line). **(C)** Delta FRET-ratio signals as recorded by Ic-LysM GEPII 1.0 expressed in Slack$^{+/+}$ (n = 8 wells obtained from 6 preparations) and Slack$^{-/-}$ (n = 10 wells obtained from out of 8 preparations) hippocampal neurons exposed to 1, 3 and 5 µM KA (indicated as red line), and the final glutamate control stimulus (indicated in purple). Counterintuitively, Slack$^{-/-}$ neurons respond with significant (two-way-ANOVA $F_{1/48} = 4.8$, $p = 0.031$) enhanced $[K^+]_i$ reduction to KA perfusion. Glutamate control stimulus is not included in these statistics, albeit responses obtained in Slack$^{+/+}$ and Slack$^{-/-}$ PHN were not different. Data represented as mean ± SEM with *P <0.05. For detailed statistics also consult Supplementary Table 8. Figure modified from Skrabak et al., 2023.

In sum, the assessment of cellular Ca^{2+} and K^+ dynamics demonstrated that the distribution of both ions across the plasma membrane is depending on Slack. Although the effects are rather mild overall, an increased Ca^{2+} influx and increased concomitant K^+ efflux are seen in Slack$^{-/-}$ neurons. These alterations are functionally not linked to total AMPA- or NMDA-receptor type signalling, but potentially rather reflect a shift in neuronal sensitivity engaging more specific GluK, GluA or especially GluN subunits (i.e. GluN2b) (Matt et al., 2021) or even link other parameters of neuronal excitability, such as changes in functionality of other ion channel. For instance, alterations in K^+ dynamics emphasized an accelerated activity of other K^+ channels, potentially K_V channels, in the absence of Slack currents, while the latter must still be confirmed by suitable patch-clamp approaches.

6.5. Slack$^{+/+}$ neurons show increased TTX-sensitive outward but decreased inward currents

To consecutively check whether alterations in Ca^{2+} and K^+ homeostasis would translate in altered neuronal activity i.e., changes in Na^+ currents, Slack$^{+/+}$ and Slack$^{-/-}$ primary hippocampal neurons were cultured for 14 days, followed by patch-clamp analysis. First, inward an outward whole-cell currents were assessed using voltage-clamp technique. To this end, neurons were voltage-clamped, and 8 incremental depolarizing voltage-steps of 20 mV were injected to the cells starting from -60 mV to +80 mV. Inward rectified currents, as maximal deflection of the first 15 ms, and steady state outward currents, as mean current density of the last 25 ms of the stimulus, were quantified. After basal stimulation (Fig. 20A left) Tetrodotoxin (TTX), an inhibitor of Na_V, was superfused to the cells, followed by repeated stimulation (Fig. 20A middle) to digitally separate (Fig. 20A right, difference) transient inward rectified currents and to identify Na^+-dependent K^+ outward, i.e., Slack, currents. By calculating basal inward currents, no Slack-specific alterations were found (Supplementary Fig. 4) suggesting no gross structural deregulation of Na_V channels in Slack$^{-/-}$ neurons. TTX-sensitive inward currents, likely representing Na_V channel-driven currents, were significantly amplified in Slack$^{-/-}$ compared to Slack$^{+/+}$ (Fig. 20B and C). Also, TTX-sensitive steady-state outward currents were significantly higher in Slack$^{+/+}$ (Fig. 10D, 0 to +80 mV), likely representing a major component contributed by the Na^+-activated K^+ channel Slack. Furthermore, a prominent inward deflection of steady-state currents, especially in Slack$^{-/-}$, was detected (Fig. 20D red line and E higher magnitude) at voltages between -20 and 0 mV. This currents probably represent persistent Na^+ currents (I_{NaP}) which were previously reported to be increased in Slack analogue Slo2 deficient *Drosophila* neurons (Byers et al., 2021) and also in mammalian neurons of the olfactory bulb (Hage & Salkoff, 2012), medium spiny neurons of the striatum, tufted-mitral cells of the olfactory bulb and cortical pyramidal cells (Budelli et al., 2009).

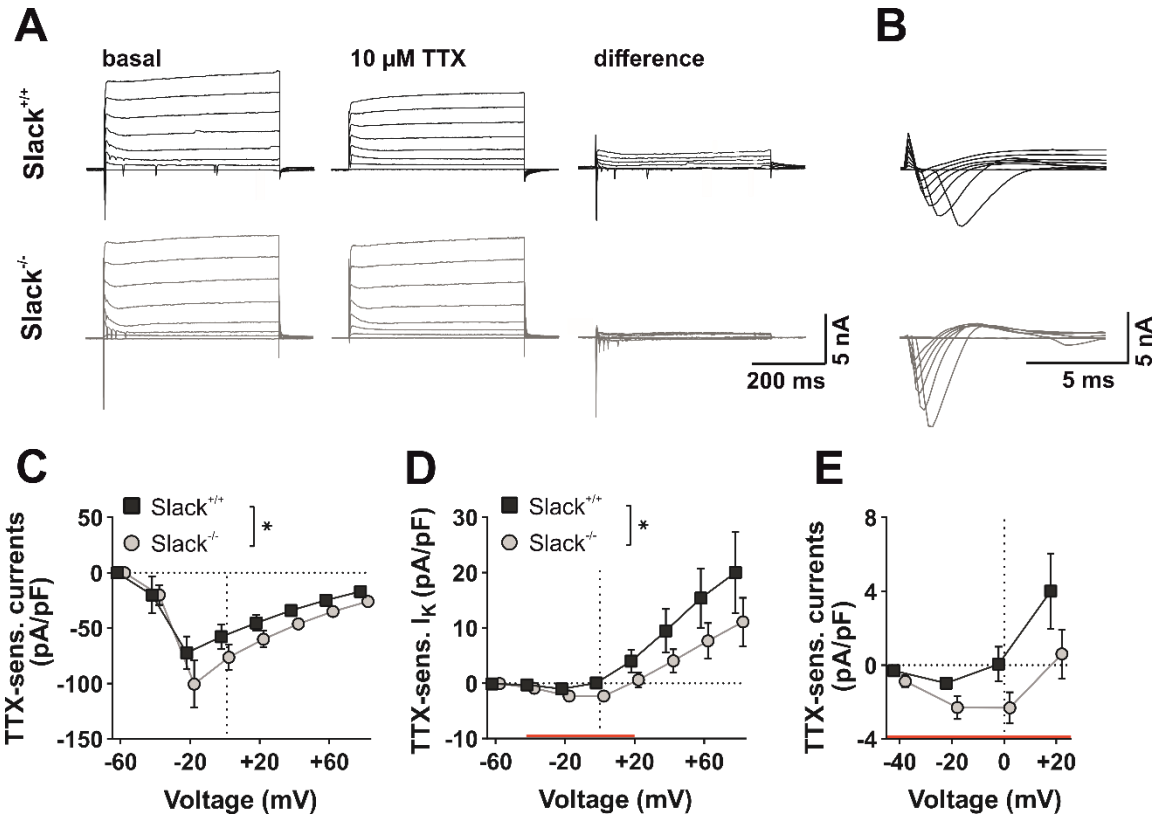

Figure 20: TTX-sensitive outward and inward currents are amplified in Slack$^{-/-}$ neurons.

(A) Representative current traces of voltage-clamp Slack$^{+/+}$ (top, black) and Slack$^{-/-}$ (bottom, grey) hippocampal neuron at 14 div, stimulated with 8 increments of depolarizing voltage-injections from -60 to +80 mV. Neurons were investigated before (basal, left) and following TTX superfusion (TTX, middle) to pharmacologically isolate (difference. right) voltage-gated Na^+ and Na^+-dependent Slack currents. **(B)** TTX-sensitive inward currents of (A), with higher magnitude. **(C)** Slack$^{-/-}$ hippocampal neurons (n = 20 neurons from 6 preparations) respond with significantly (two-way-ANOVA $F_{1/280}$ = 5.791, p = 0.0168) increased TTX-sensitive inward currents to depolarizing voltage steps compared to Slack$^{+/+}$ (n = 17 neurons from 7 preparation). **(D)** Compared to Slack$^{-/-}$ (n = 24), TTX-sensitive steady state outward currents – K^+ currents (I_K) were significantly (two-way-ANOVA $F_{1/312}$ = 5.122, p = 0.0243) higher in Slack$^{+/+}$ (n = 17) hippocampal neurons. **(E)** Steady state currents provoked by voltages from -20 to 0 mV of (D) (indicated by red line) display an amplified inward-directed current component in Slack$^{-/-}$ neurons, likely representing persistent Na^+ currents. Data represented as mean ± SEM with *P <0.05. For detailed statistics also consult Supplementary Table 9. Figure modified from Skrabak et al., 2023.

Together, this data indicates that Slack$^{-/-}$ hippocampal neurons lack TTX-sensitive (outward) K^+ currents and exhibit accelerated transient and persistent TTX-sensitive Na^+ currents.

6.6. Absence of Slack increases neuronal excitability and action potential frequency

In the next series of experiments, we tried to clarify how alterations in Na^+ currents and Ca^{2+} and K^+ dynamics affect the neuronal firing properties of $Slack^{-/-}$ PHN. For that purpose, $Slack^{+/+}$ and $Slack^{-/-}$ 14 div PHN were perfused with 5 µM KA during whole-cell current-clamp recording and action potential (AP) firing rate per 1 s was counted for a total of 30 s (Fig. 21A). As expected, KA-induced spiking frequency over a total of 30 s (Fig. 21B), but also averaged over time (Fig. 21C) was significantly increased in $Slack^{-/-}$ compared to $Slack^{+/+}$ neurons. Also, threshold potential required to provoke the first AP was tendentially more negative in $Slack^{-/-}$ (Fig. 21D), while the amplitude was unchanged (Fig. 21E). Both findings suggest increased excitability and capacity for high frequency firing during constant expression of relevant Na^+ and K^+ ion channels in $Slack^{-/-}$ neurons.

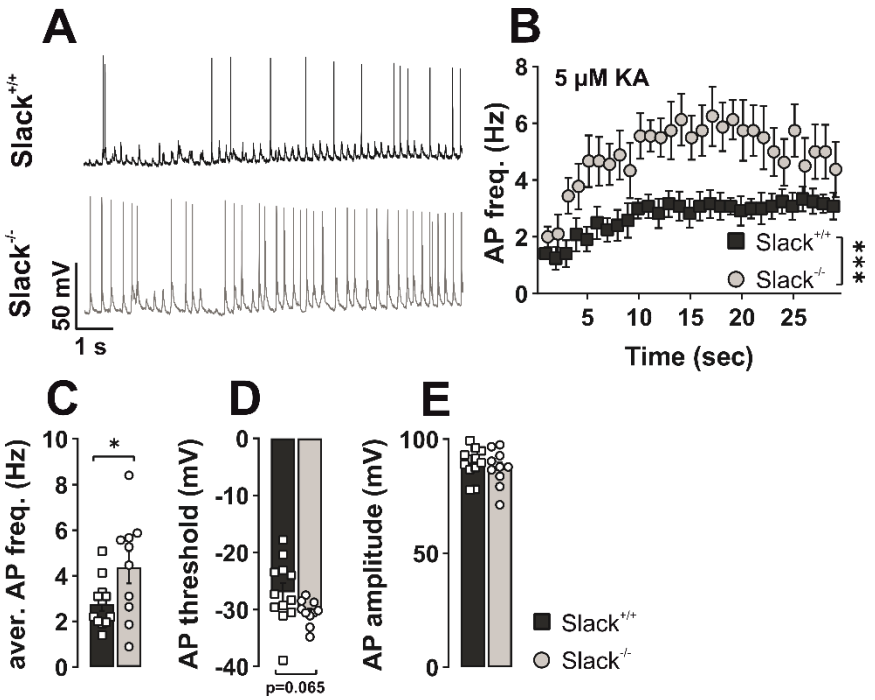

Figure 21: Increased KA-induced AP frequencies in $Slack^{-/-}$ hippocampal neurons.

(A) Representative current-clamp recordings from 14 div $Slack^{+/+}$ (upper curve) and $Slack^{-/-}$ PHN (lower curve) after treatment with 5 µM KA. **(B)** Number of action potentials (AP) per 1 s after KA application is significantly (two-way ANOVA, $F_{1/551}$ = 175.4, p <0.001) increased in $Slack^{-/-}$ (n = 12 neurons from 6 preparations) compared to $Slack^{+/+}$ (n = 9 from 4 preparations). **(C)** Average number of KA-provoked APs during the first 30 sec (see trace in B) following KA-perfusion is significantly increased in $Slack^{-/-}$ PHN ($Slack^{+/+}$ n = 12, $Slack^{+/+}$ n = 10, unpaired t-test p = 0.039). **(D)** Minimal required membrane depolarization to provoke first AP (AP threshold) is slightly, but not significantly, shifted to more negative voltages in $Slack^{-/-}$ compared to $Slack^{+/+}$ ($Slack^{+/+}$ n = 12, $Slack^{-/-}$ n = 10, unpaired t-test Welch´s corrected, p = 0.065). **(E)** Amplitude of KA-provoked AP is similar in both, $Slack^{+/+}$ and $Slack^{-/-}$ PHN. Data represented as mean ± SEM with *P <0.05, **P <0.01, ***P <0.001. For detailed statistics also consult Supplementary Table 10. Figure modified from Skrabak et al., 2023.

Finally, to confirm changes in Slack$^{-/-}$ excitability and firing on a KA-independent basis, 10 consecutive depolarizing current steps of 20 pA increment were injected to current-clamped Slack$^{+/+}$ and Slack$^{-/-}$ hippocampal neurons and the number of elicited APs was counted for each current injection. Again, Slack$^{-/-}$ neurons responded with significantly increased AP frequency to the current injection protocol (Fig. 22A and B). This effect was not accompanied by changes in resting membrane potential (RMP) of Slack$^{-/-}$ (Fig. 22C), while AP threshold was shifted significantly to more negative potentials (Fig. 22D). Also, by analysing AP kinetics (Fig. 22E) the AP rise slope was found to be significantly steeper (Fig. 22F), together with a tendency of decreased AP half-width (Fig. 22G) in Slack$^{-/-}$ compared to Slack$^{+/+}$ neurons, confirming voltage-clamp based findings of increased TTX-sensitive currents likely I_{Na}. Yet, in line with KA-provoked APs, the AP amplitude was not altered in Slack$^{-/-}$ upon current injection (Fig. 22H). Fittingly, by analysing the kinetics of after hyperpolarization (aHP) (Fig. 22I), again, the amplitude was found to be similar for both genotypes (Fig. 22J), while the duration of the aHP was significantly shortened in Slack$^{-/-}$, compared to Slack$^{+/+}$ (Fig. 22K), with faster returning time to resting potential. Although the underlying mechanistic details are unclear, this links the accelerated KA-induced K^+ efflux in Slack$^{-/-}$ (Fig. 19), to the patch-clamp data, suggesting other K^+ sources, i.e., K_V currents, to accelerate repolarizing K^+ efflux, leading to faster excitable membrane potential. Hence, Slack limit neuronal firing by prolonging aHP and thereby prevent follow-up APs.

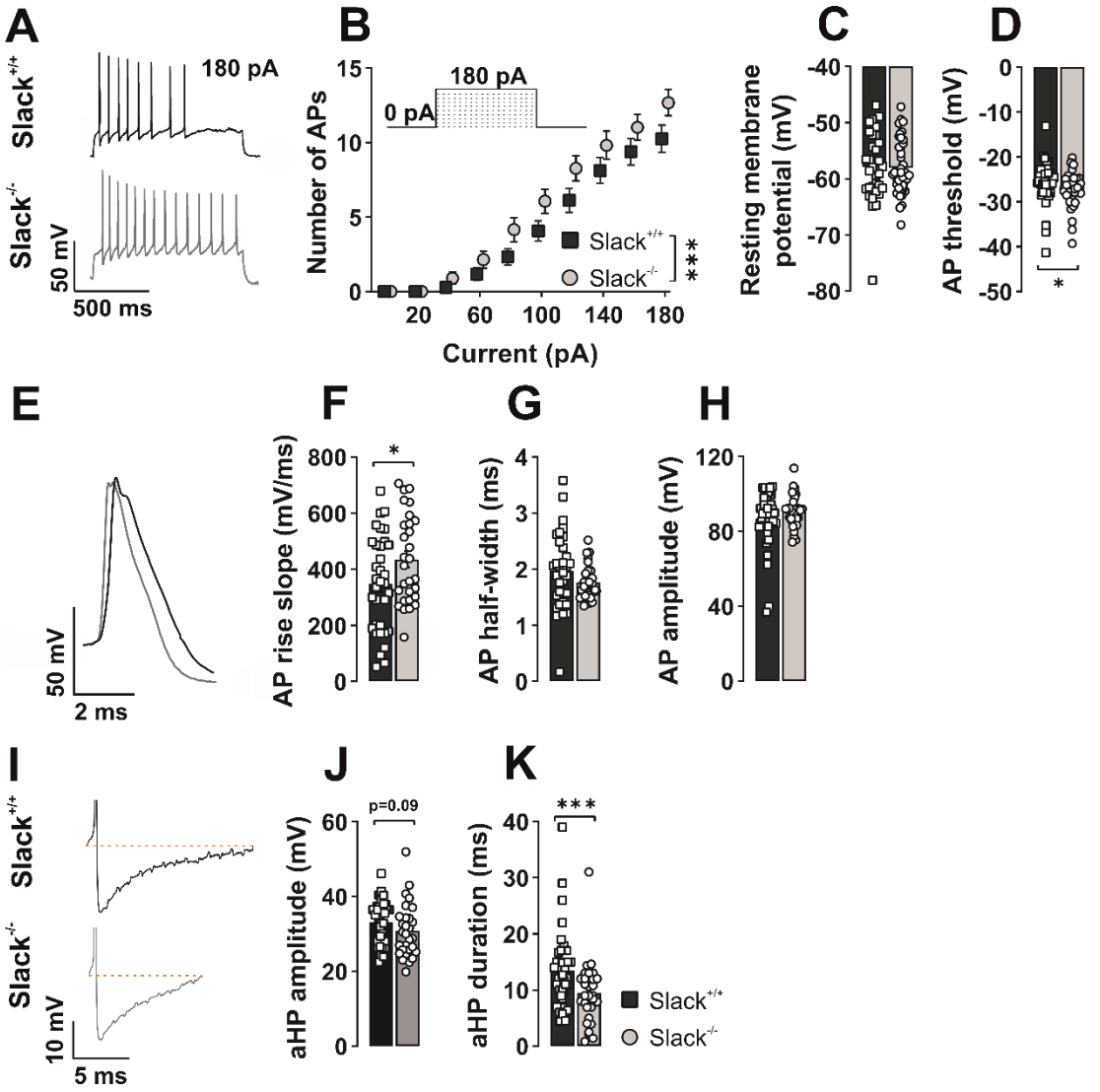

Figure 22: Increased AP frequencies following current injections in Slack$^{-/-}$ hippocampal neurons.

(A) Representative current-clamp recordings from Slack$^{+/+}$ (top) and Slack$^{-/-}$ (bottom) neurons during 180 pA current injection. **(B)** AP frequency in response to incremental current injection is significantly (two-way-ANOVA $F_{1/668} = 20.50$, $p < 0.0001$) increased in Slack$^{-/-}$ (n = 33 neurons obtained from 8 preparations) compared to Slack$^{+/+}$ cells (n = 38 neurons obtained from 9 preparations). **(C)** Resting membrane potential is not different between genotypes. **(D)** Slack$^{-/-}$ neurons display significantly (Mann-Whitney test p = 0.043) more negative threshold potential for initiation of AP firing compared to Slack$^{+/+}$ neurons. **(E)** While amplitude of AP and **(F)** after hyperpolarization (aHP) is not different in Slack$^{-/-}$ PHN, **(G)** the duration of aHP is significantly shorter (Mann Whitney test p = 0.0009) in Slack$^{-/-}$ neurons. **(H)** Exemplary trace of a single AP from current-clamped Slack$^{+/+}$ (black) and Slack$^{-/-}$ (grey) neurons illustrating differences in kinetics. **(I)** Slack$^{-/-}$ (n = 29) AP have significantly (Mann-Whitney test p = 0.001) steeper action potential rise slope compared to Slack$^{+/+}$ (n = 34). **(J)** AP half-width is similar comparing neurons of both genotypes. **(K)** Representative traces of Slack$^{+/+}$ (black) and Slack$^{-/-}$ (grey) current-clamped hippocampal neurons depicting differences in after hyperpolarization duration. **(L)** Slack$^{-/-}$ hippocampal neurons reveal significantly (Mann-Whitney test p = 0.0009) shortened duration of aHP compared to Sack$^{+/+}$. Data represented as mean ± SEM with *P <0.05, **P <0.01, ***P <0.001. For detailed statistics also consult Supplementary Table 11. Figure modified from Skrabak et al., 2023.

In summary, Slack deficient hippocampal neurons are more prone to be activated and respond with higher AP-firing and repolarization-timing to KA and current induced stimulations. Hence, presence of Slack can limit neuronal firing by adjusting neuronal excitability and by prolonging neuronal repolarization.

Based on *in vivo* and *in vitro* data of the KA-induced epilepsy model, the role of Slack channels for neuronal activity can be summarized: Herein, Slack´s role seems to be in a close functional interplay between Na_V and K_V channels. Following KA-mediated activation of GluK and subsequent membrane depolarization, Na_V channels are activated and inactivated by cycles of repolarization mediated by K_V and Slack channels. Since Slack channels provide a long lasting aHP, Slack is suggested to prolong these cycles for Na_V-induced activity causing depolarization, presumably by increasing the inactivated sate of the Na_V via prolonged K^+ efflux. Based on accelerated K^+ efflux and decreased aHP duration found in $Slack^{-/-}$ neurons, the accelerated repolarization-depolarization circuit between Na_V and K_V is postulated to render epileptiform seizures due to the lack of an important “activity brake” provided Slack channels.

6.7. $Slack^{+/+}$ hippocampal tissue is more prone to Pilo-induced cell death

The epilepsy syndromes EIMFS and (AD)SHE are linked to variances of the Slack encoding gene *KCNT1,* as well as mutations of cholinergic receptors like *CHRNA4* (Heron et al., 2007, 2012). Also, occurrence of seizures in (AD)SHE patients is sleep-related (Combi et al., 2004) and in turn sleep predominantly modulated by cholinergic neurons of the brain stem (Eretz & Avie, 2001). Together with evidence for functional coupling of Slack and the cholinergic receptor system (Santi, 2006), the Pilocarpine (Pilo)-based model for epileptic neuronal activity was employed to confirm KA-based *in vitro* findings and elucidate the role of Slack in an additional model for cholinergic epileptogenic activity. The Pilo-induced model for *in vivo* epilepsy is widely used and well-established, provoking epilepsies by agonizing the muscarine M1 receptor (Ahmed Juvale & Che Has, 2020; Gröticke et al., 2007; Lévesque et al., 2021) (see section 3.4.1.). Also, Pilo is used *in vitro* on cultured hippocampal slices (Poulsen et al., 2002) to modulate epileptogenic neuronal activity. Hence, again HSC were engaged to study consequences of Pilo-induced epileptiform neuronal activity. $Slack^{+/+}$ and $Slack^{-/-}$ HSC were exposed for 3 days to 4 -and 8 mM Pilo, and cell death was quantified by measuring relative PI uptake (Fig. 23A). Surprisingly, compared to $Slack^{-/-}$ Pilo provoked significantly increased PI uptake in $Slack^{+/+}$ HSC especially following two days of Pilo-exposure for both, 4 -and 8 mM Pilo

(Figure 23B and C). This was predominantly due to PI uptake in the CA1 region, the hippocampal region containing most of hippocampal cholinergic neurons (Blusztajn & Rinnofner, 2016; Frotscher et al., 1986). This result was unexpected and contrasts with KA-based findings (Fig. 14).

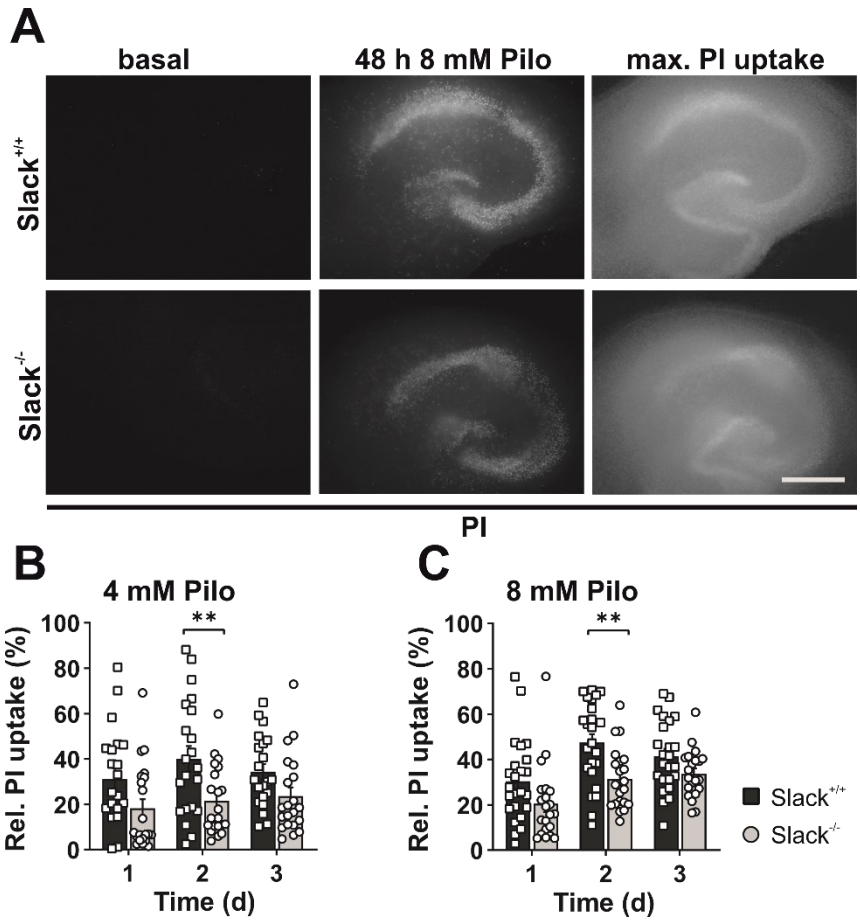

Figure 23: Increased Pilo-induced cell death in Slack$^{+/+}$ HSC.

(A) Representative images of 14 div hippocampal slice cultures (HSC) from Slack$^{+/+}$ (upper images) and Slack$^{-/-}$ (lower images) prior treatment (basal), after 24 h exposure to 8 mM Pilo (48 h 8 mM Pilo) or after application of 80% ethyl-alcohol (max. PI uptake). Scale bar: 500 µm. **(B and C)** Compared to Slack$^{-/-}$ (n = 21 - 24 ROI from 7 wells generated by 5 preparations), Slack$^{+/+}$ (n = 21 ROI from 8 wells generated by 5 preparations) HSC showed significantly increased PI uptake (normalized to maximum) among 48 h exposure to 4 -and 8 mM Pilo. (4 mM Pilo: two-way-ANOVA with Sidak´s multiple comparison, p = 0.007; 8 mM Pilo: two-way-ANOVA with Sidak´s multiple comparison, p = 0.003). Data is represented as mean ± SEM with **P <0.01. For detailed statistics also consult Supplementary Table 12. Figure modified from Skrabak et al., 2023.

Again, the link between PI uptake and neuronal activity was assessed by measuring changes in $[Ca^{2+}]_i$ via Fura2. Since very high Pilo concentrations of 50 and 100 mM were needed to provoke Fura2 based Ca^{2+} fluxes in PHN (Supplementary Figure 5), also these findings are unexpected but somehow in line with PI-based findings that differ from expectations. Cholinergic neurons were reported to be rarely abundant in the

hippocampal formation (Frotscher et al., 1986), present just in distinct locations of the hippocampus (Teles-Grilo Ruivo & Mellor, 2013) and especially important for efferent and afferent hippocampal brain regions (Haam et al., 2018; Teles-Grilo Ruivo & Mellor, 2013). Hence, we conclude that the hippocampus is not an appropriate model to study the role of Slack during Pilo-induced epileptogenic neuronal activity using PI -and Fura2 imaging with their limited specificity in resolving distinct cellular processes. Our results suggest that, for instance, thalamic neurons or neurons of the brain stem could be more interesting to study Slack´s role for Pilo-induced epilepsy, especially using patch-clamp techniques, together with *in vivo* experiments that engage all brain areas and physiologically reflects Slack´s role for Pilo-induced epilepsy.

To sum up Pilo-based findings, the hippocampal formation plays differential roles for Slack-mediated regulation of neuronal activity. Apparently, Slack is limiting the activity of KA-induced glutamatergic signalling, but counterintuitively, its activity appears to be adverse during cholinergic overstimulation.

7. Discussion

7.1. The KA-induced model for acute epilepsy

The Slack channel is linked to severe, early onset and refractory epilepsies by mutations within the encoding gene *KCNT1* that primarily lead to GOF by enhancing channel gating and conductance (Bonardi, et al., 2021; Lim et al., 2016; McTague et al., 2017). Based on this, in the past nonspecific “Slack-inhibitors” were used in explorative approaches to treat patients (Bonardi et al., 2021; Xu et al., 2022). In the last years, Slack-inhibitors were designed that show promising and verry specific effects *in vitro* and *in vivo* (Griffin et al., 2021; Spitznagel et al., 2020). Since a LOF mutation of Slack has also been found, the underlying mechanisms leading to epilepsies in both GOF and LOF mutations need to be urgently elucidated, especially for the clinical use of highly specific Slack inhibitors. To this end, Slacks role for epilepsy was studies using global Slack deficient mice, hippocampal tissue, and single neurons.

Using the KA-induced model for acute epilepsy in adult mice a new and partly unexpected role of Slack for seizure severity was found. Following injection of rather low KA doses (20 mg/kg), Slack$^{-/-}$ animals reached CS more rapidly (Fig. 11D) and TCS more frequently compared to their Slack$^{+/+}$ littermates (Fig. 11E), suggesting Slack confers protection against severe seizures, while primarily *KCNT1* GOF variants are causative for rare and severe epileptic syndromes such as (AD)SHE and EIMFS (see section 3.7.3.). Surprisingly, in Slack$^{+/+}$ animals seizure behaviour sustained for a longer period, leading to increased SSc over time (Fig. 11C). Since the experimental setup did not resolve involved brain regions or differentiate between the involved neuronal subtypes, a distinct role of Slack in different brain regions or cell types cannot be excluded. Yet, it can be suggested that at 20 mg/kg KA Slack function was opposing the progressive synchronization of neuronal tissue and protects against generalization of network firing. Besides, Slack activity seems to limit the potency to terminate moderate seizures. However, following injection of a higher dose of KA (30 mg/kg), Slack$^{-/-}$ adult mice respond with significantly increased seizure severity over time (Fig. 11F), with a higher fraction of animals reaching SE or even died following SE (Fig. 11H). This confirms that seizure severity and fatality are beneficially modulated by Slack, especially at high seizure activity. Moreover, this finding is in line with patients that carry a LOF Slack variant, leading to severe epilepsy and demyelination (Evely et al., 2017; Vanderver et al., 2014), and with experimental data implying that loss of Slack function results in an increased seizure susceptibility in Slo-deficient *Drosophila* or electro-shock induced seizures in Slack-KO

mice (Byers et al., 2021; Quraishi et al., 2020) (see Table 1 section 3.7.3.). Similar onset of CS (Fig. 11G) in Slack$^{+/+}$ and Slack$^{-/-}$ receiving a high dose of KA, allows the conclusion that a Slack-dependent modulation or reduction of seizure severity was somewhat limited in this experimental setup.

24 h post KA injection, the mRNA expression levels of family members Slick, BK, glutamatergic receptors subunits and BDNF with related receptors were investigated. Following both, injection of 20 or 30 mg/kg KA, no compensatory regulations of other Slo genes including Slick and BK was found (Fig. 12A and D). This finding makes it less likely that genetic compensation is underlining a Slack-specific modulation of KA-induced seizures. Still, beside structural changes in expression, functional compensation could not be excluded, an aspect that will be further discussed below. Also, the expression of important glutamate receptor subunits was unaltered between Slack$^{+/+}$ and Slack$^{-/-}$ mice after KA injection (Fig. 12B and E), which argues against increased seizure severity in Slack$^{-/-}$ due to differential receptor expression or Slack-dependent changes during brain development. Although, GluK4 and GluK5 expression was found to be altered in TLE patients (Li et al., 2010; Lowry et al., 2013) and both are expressed to a high extend in the hippocampus, GluK1 and GluK2 were linked to distinct phases of KA-provoked epilepsy (see section 3.3.5.) but not analysed here. Hence, increased seizure severity in Slack$^{-/-}$ mice due to different expression levels of GluK1 and GluK2 can't be excluded. In addition to expression analyses of glutamate receptor subunits, BDNF and its receptor TrkB expression levels were analysed. Both, however, were not differentially regulated in Slack$^{+/+}$ and Slack$^{-/-}$ animals, despite GFAP, upregulated in gliosis following CNS injury (Vargas-Sánchez et al., 2018) was significantly upregulated in Slack$^{+/+}$ following injection of 30 mg/kg KA (Fig. 12F). Since seizure severity was limited in Slack$^{+/+}$, it could be interpreted as a more competent regenerative astroglial response and repair following seizure-induced neuronal excitotoxicity. As variants in *KCNT1* result in epilepsy with very early onset, KA-based *in vivo* experiments were repeated in 4 weeks old juvenile animals to adopt experimental conditions to those found in patients. Consistently, juvenile Slack$^{-/-}$ animals responded with significantly increased SSc over time compared to Slack$^{+/+}$ (Fig. 13A), which was predominantly due to a larger fraction of animals that died following seizures (Fig. 13C). This finding fits to the animal data deriving from adult mice, highlighting the role of Slack in limiting severe seizures and seizure related death also in juvenile mice. In contrast, Slack$^{-/-}$ display protection from death following electro-convulsive seizures (Quraishi et al., 2020). This discrepancy could be explained by different mechanism of seizure induction. Accordingly, the KA-based model for epilepsy is triggering seizures predominantly by activation of the limbic system, especially the

hippocampus, subsequently propagating to distal brain regions (see section 3.3.5.), while electro-convulsions may primarily affect cortical regions, hence involving interconnections and actions of different inhibitory and excitatory cell types and regions. The hippocampus is highly connected to subcortical brain regions as the thalamus and brain stem structures that also modulate general hippocampal excitability (see section 3.2. and 3.4.1.). KA-based activation of the hippocampus that is linked to brain stem structures might additionally explain the higher death rate of Slack$^{-/-}$ adult and juvenile mice, which suffered from TCS that are predominantly mediated by brain stem structures (Browning et al., 1993; Wang et al., 2021). Following electro-convulsion, the propagation pattern of seizure events might be different and affect hippocampal or brain stem structures to a different extend, leading to altered lethality in the KA or electro-convulsive model for seizures in the absence of Slack. Also recently, Gertler et al., 2022 investigated the role of Slack in different models for acute epilepsy. In this study, first, L457F GOF Slack-KI mice responded with increased SSc to the KA-induced model of epilepsy. This finding again emphasizes that Slack crucially modulates neuronal network excitability, as increased Slack function, but also Slack deficiency, as shown herein, led to increased seizure scores following KA injection. Second, using the $GABA_A$ specific antagonist Flurothyl to provoke epileptic seizures, this Slack-KI mice did not respond with different seizure severity to the treatment. However, following injection of the non-specific GABA antagonist PTZ, the Slack-KI displayed increased SSc confirming earlier reports (Quraishi et al., 2020). Hence, rather PTZ-induced block of $GABA_B$, but not $GABA_A$, mediated extrasynaptic and parasynaptic 'ambient' GABA signalling (see section 3.4.2. and Fig. 2) was modulated by Slack and secondary general excitatory properties of nervous tissues. Interestingly, Slack-deficient mice do not respond with different SSc to PTZ injection (Quraishi et al., 2020). Based on evidence that suggest GABAergic signalling to be predominantly affected by Slack GOF (see section 3.7.3. and Table 1 and 2), two Slack-mediated susceptibilities are recognized: First, GOF Slack variants that are disinhibited under basal conditions lead to increased seizure severity involving altered GABAergic inhibition, and a decreased potency to limit KA-induced excitation. Second, LOF Slack variant that affect mainly excitatory systems, promote KA-mediated excitation without Slack-mediated seizure block.

Although in adult animals the mRNA transcription levels of glutamate receptor subunits or BDNF and TrkB were not altered between genotypes (Fig. 12), a Slack-dependent modulation of BDNF mRNA expression was observed in juvenile animal. Accordingly, Slack$^{-/-}$ mice showed decreased BDNF levels 24 h post KA-induced seizures (Fig. 13E and F). This finding suggest altered neurotrophic signalling following ictal events and is in

line with previous findings of an altered BDNF signalling in Slack-KO cerebellar granular cells following excessive glutamatergic activation (Ehinger et al., 2021). Together, besides similar seizure susceptibility, increased seizure severity and lethality was shown for both, adult and juvenile Slack$^{-/-}$ mice, confirming the proposed role of Slack acting as a "seizure-terminator" (Igelström, 2013), and one reported LOF variant of Slack in an epilepsy patient (Vanderver et al., 2014). However, most studies *KCNT1* variants associated with detrimental seizures and neuronal hyperexcitability result from Slack GOF mutations (Bonardi, et al., 2021; Burbano et al., 2022; Gertler et al., 2022; Lim et al., 2016; Quraishi et al., 2020; Shore et al., 2020). As also presented in section 3.7.3., this was proposed to relate to several mechanisms (Kim & Kaczmarek, 2014) including: (i) limitation of Na_V channel inactivation by Slack mediated acceleration of repolarization, (ii) altered development and wiring due to increased Slack channel function, and (iii) disinhibition of neuronal circuitries due to increased Slack channel function, especially in inhibitory neurons that are limited in function. Especially the last aspect was supported by three different Slack-KI mouse models recapitulating the human phenotype(s) (Gertler et al., 2022; Shore et al., 2020; Wu et al., 2023). Slack may play a different role in excitatory and inhibitory neurons, as recently suggested by Wu et al., 2023, making it difficult to draw clear conclusions about the role of Slack LOF or GOF mutations in the development of epilepsies. Accordingly, a prediction of the cellular consequences resulting from Slack LOF or GOF activities remains difficult at present.

Based on proposed mechanism (Igelström, 2013; Kim & Kaczmarek, 2014), clinical reports (Bonardi, et al., 2021; Vanderver et al., 2014) and experimental studies (Quraishi et al., 2020; Shore et al., 2020), a damped or over-activate Slack function my differentially affect the brain's inhibitory and excitatory systems, and thereby regions involved in ictogenesis.

7.2. KA-induced cell death in hippocampal tissue cultures and single neurons

While Slack GOF variants have been characterized more widely *in vivo* and *in vitro,* the underlying mechanism of increased seizure severity in Slack LOF variants are largely elusive. Therefore, in this study we further explored the importance of Slack by using *in vitro* hippocampal slice preparations. Although epileptic seizures of EIMFS or (AD)SHE patients were predominantly characterized by cortical EEG (Bonardi, et al., 2021), the hippocampus was assessed in our approaches because previous work reported that seizure development induced by KA arises from hippocampal formations (Lévesque & Avoli, 2013) likely also due to the prominent GluK expression in this brain region

(see section 3.3.5.). Additionally, Slack is highly enriched in this brain region (Brown et al., 2008; Rizzi et al., 2016). Finally, the most frequent epileptic syndrome, the TLE, leads to extensive, well studied histopathological changes within the hippocampus (see section 3.3.5.). This makes the hippocampal formation an optimal system for investigating the role of Slack in epilepsy. First, hippocampal slices were cultures for 14 days to become organotypic and stable following preparations. Although slices underwent cell death following preparation, deafferentation and flattening (Holopainen, 2005), the preservation of the hippocampal compartments and the viability of the cells (Fig. 14A brightfield and PI basal), together with representative transcript levels of Slack-related channels such as Slick and BK (Fig. 14B) were similar in both $Slack^{+/+}$ and $Slack^{-/-}$, suggesting Slack is not involved in the protection of nervous tissues against mechanic stress or deafferentation. Following chronic (Fig. 14C and D) and transient (Supplementary Fig. 1A) KA exposures, $Slack^{-/-}$ hippocampal tissues respond with increased cell death, predominantly due to increased susceptibility of the CA3 region (Fig. 14 PI, 24 h 10 µM KA). According to literature, this compartment has recurrent collaterals (see section 3.2. and Fig. 1) and high levels of Slack and GluK expression (see section 3.3.5. and 3.7.), potentially linking hippocampal circuits with accelerated KA-based signalling and protective Slack channel function. Moreover, these findings link Slack-mediated limitation of severe seizures *in vivo* to neuronal survival *in vitro*. Furthermore KA-provoked PI uptake, predominantly within the CA3 region, was reported earlier (Noraberg et al., 1999). In a subsequent pharmacological approach, however, neither nonspecific “Slack-activators” Loxapine and Bithionol (Fig. 14E and Supplementary Fig. 1B) nor the inhibitor Quinidine (Supplementary Fig. 1C) modulate the KA-induced PI uptake in a Slack dependent manner. This might be due to insufficient Slack specificity of all used compounds, but also caused by the poor temporal resolution of the PI based cell death readout. Interestingly, Loxapine at a rather low concentration of 5 µM tended to limit the PI uptake in $Slack^{+/+}$ hippocampal cultures (Fig. 14E). It will therefore be interesting to test Loxapine-based more specific activators currently under development by Balzulat et al., 2023 as new antiepileptic therapy targeting LOF Slack. To make this possible, the new activators must be able to cross the blood-brain barrier, which seems to be the case at least for some of the candidates with no obvious effects on the normal mouse behaviour.

Following investigations of Slack’s role for epileptic seizures *in vivo* and neuronal tissue activity *in vitro*, the spatiotemporal resolution was further increased by using dissociated hippocampal neuron cultures. After 8 days *in vitro*, neurons were considered to be mature since both $Slack^{+/+}$ and $Slack^{-/-}$ neurons generated synapses (Fig. 15B), expressed mandatory receptor subunits of glutamatergic signalling (Fig. 15C and D) and astroglia

appeared only at a low number (Supplementary Fig. 2A). No apparent differences for all stained neuronal markers or in brightfield appearance (Fig. 16A brightfield) were found by comparing Slack$^{+/+}$ to Slack$^{-/-}$ neurons, confirming an unaltered maturation of hippocampal cultures following cultivation. Similar to the findings derived from hippocampal circuitries, also Slack$^{-/-}$ dissociated hippocampal neurons responded with increased cell death to low (Fig. 16A and B) or high (Supplementary Fig. 2B) doses of KA treatment. Hence, the protectivity against KA-induced excessive neuronal activity mediated by Slack channels is not limited to the CA3 region with intact hippocampal circuitries but is also present at the single cell level. This corresponds with the neuroprotective role Slack confers in previous studies using mouse striatum *in vivo* or cerebral granular cell *in vitro* against NMDA-induced excitotoxity (Ehinger et al., 2021). PiTX-induced disinhibition of KA-based neuronal activity led to exacerbated cell death in both Slack$^{+/+}$ and Slack$^{-/-}$ neurons (Fig. 16C). This indicated that cause of PI uptake is excessive neuronal activity in response to KA exposure that can be exacerbated by PiTX induced disinhibition. Interestingly, the extend of cell death exacerbation was similar in Slack$^{+/+}$ and Slack$^{-/-}$ neuron cultures, when individual treatment conditions, KA with 50 µM PiTX or KA with 100 µM PiTX, were evaluated separately. Nevertheless, by comparing both co-treatment conditions on a group level, Slack$^{-/-}$ dissociated hippocampal neurons only tendentially respond with higher cell death rates compared to Slack$^{+/+}$ (see also Supplementary Table 5C). One explanation for this almost even cell death level following KA plus PiTX exposure might be: first, neuronal firing that is limited to some extend on a molecular level, and harsh excitation by KA in the presence of PiTX probably led to saturated activation of neuronal firing in both genotypes, masking potential differences in vulnerability. Second, antagonizing GABA signalling by PTZ resulted in a similar extend of cell loss also in HSC (Supplementary Fig. 6). Interestingly, also *in vivo* injection of PTZ to Slack-KO mice did not promote different seizure susceptibilities compared to wildtype control mice (Quraishi et al., 2020). Based on these data, one can speculate, that on the level of hippocampal circuitries, but also *in vivo*, Slack channel-mediated protectivity is not caused by general GABAergic inhibitory signalling and circuitry synchronisation. Since GOF variants of Slack were reported to primarily affect function of inhibitory neurons rather than excitatory neurons (Gertler et al., 2022; Quraishi et al., 2020; Shore et al., 2020), these findings suggest Slack functions to be closely related to neuronal subtypes as inhibitory and excitatory and model system.

7.3. Imaging of KA-induced Ca^{2+} and K^+ fluxes

PI staining is an indicator for late stages of cell death and suffers from limited specificity and low temporal resolution. Due to this limitation, neuronal activity was further investigated using the Ca^{2+} sensitive dye Fura2. In a first set of experiments, the Ca^{2+} influx was not different between genotypes upon cell treatment with increasing KA concentrations (Fig. 17C). Although not significant, at the lowest concentration of 1 µM KA, $Slack^{-/-}$ neurons tended to respond with increased Ca^{2+} influx compared to $Slack^{+/+}$ neurons. Subsequently, experiments were repeated with a focus on lower KA concentrations, which reproducibly provoked a significantly increased Ca^{2+} influx in $Slack^{-/-}$ compared to $Slack^{+/+}$ neurons (Fig. 17F). This links KA-induced neuronal signalling to subsequent Ca^{2+} sources as NMDA receptors. Also, confirming the augmented cell death in the presence of KA and PiTX, KA-provoked increases of intracellular Ca^{2+} link excessive activity and KA signalling to cell death. Since Slack was reported to functionally interact with AMPA and NMDA receptor subunits (Matt et al., 2021; Nanou et al., 2008), and to confirm and better dissect Slack-dependent KA-induced Ca^{2+} fluxes, an additional set of experiments was performed using the AMPA blocker NBQX, the NMDA blocker DL-AP5 and Loxapine as pharmacological tool to activate Slack. Treatment of hippocampal neurons with KA alone or KA in combination with NBQX, DL-AP5 or Loxapine did not reveal any genotype specific differences in Ca^{2+} influx (Fig. 18) suggesting first comparable global expression of AMPA and NMDA receptors and second limited efficacy of Loxapine to modulate KA-induced Ca^{2+} influx. Further, expression of GluK, GluA and GluN receptors in hippocampal neurons, indicated by measuring transcript levels in hippocampi isolated from adult mice (Fig. 12 and 13D to F) and by immunofluorescence using dissociated hippocampal neurons (Fig. 15), were unaltered. Surprisingly, $Slack^{+/+}$ and $Slack^{-/-}$ neurons responded with a similar Ca^{2+} influx to an initial stimulus of 5 µM KA (Fig. 18A to C). This further supports the idea of increased Ca^{2+} influx to $Slack^{-/-}$ neurons to be restricted to low KA concentrations of 1 and 3 µM KA (Fig. 17F). This in turn reflects that Slack modulates neuronal threshold and timing of excitatory signals, but not so much maximum response amplitudes. A summary of the Fura2-based fluorescence report of many APs (and potential differences in signalling) might be covered under such conditions i.e., when KA concentration is high. For instance, Nanou et al., 2008 reported Slack-mediated sharpening and shortening of AMPA EPSPs, detected at the level of several milliseconds, while the Fura2 measurements are carried out in a different temporal range (1 Hz imaging rate). Finally, the present data confirm previous findings of $Slack^{+/+}$ and $Slack^{-/-}$ hippocampal neurons, that responded with similar Fura2 maximal delta ratios to glutamate treatment, or co-treatment with glutamate and NBQX

and / or DL-AP5 (Matt et al., 2021). Interestingly, Matt et al. recently demonstrated functional interaction between Slack and the receptor subunit GluN2b using the specific GluN2b blocker Ro25-6981. Overall, Slack-dependent modulation of glutamatergic signalling appears to be well coordinated and specific to one (or more) receptor subunits, and therefore cannot be beneficially modulated by NBQX or DL-AP5 which in general block all AMPAR are NMDAR complexes, respectively. Importantly, both NBQX and DL-AP5 reduced KA-induced Ca^{2+} influx drastically (Fig. 18A and B). This finding suggests large AMPA and NMDA components of KA-induced Ca^{2+} influx. First, probably due to direct AMPA receptors activation by KA and second by subsequent recruitment of NMDA receptors. Especially KA-mediated NMDA activation may directly link excessive neurons signalling to Ca^{2+} influx that finally led to cell death (Fig. 16) and also is in line increased neuronal vulnerability of Slack-deficient mice and neurons following NMDA treatment (Ehinger et al., 2021).

Also, co-treatment of KA and Loxapine did not result in changes of Ca^{2+} fluxes in both $Slack^{+/+}$ and $Slack^{-/-}$ neurons. Since Loxapine targets multiple dopaminergic receptors besides Slack (Balzulat et al., 2023) and it failed to reduce KA-induced cell death in $Slack^{+/+}$ HSC (Fig. 14E), it is concluded that Loxapine-mediated Slack modulation i.e. the activation of the channel occurs at a level that may be inadequate to modulate Ca^{2+}-dependent KA signalling. Additionally, since acute hippocampal slice-based experiments with field-potential recordings found evidence for a Slack-mediated decrease in AP firing upon Loxapine exposure (Gertler et al., 2022), it cannot ultimately be ruled out, as already explained, that the temporal resolution of the Fura2 assay is insufficient to uncover with the required sensitivity how Slack affects the glutamatergic Ca^{2+} signalling. Taken together, Slack's contribution to the Ca^{2+} influx in PHN is moderate, likely restricted to a narrow (low) KA concentration range, and KA-mediated Ca^{2+} influx is essentially driven by AMPA and NMDA-type receptors, but largely independent from Slack function.

Beside Ca^{2+} influxes, also K^+ effluxes were assessed in hippocampal neurons. Surprisingly, upon KA exposure, $Slack^{-/-}$ neurons responded with increased K^+ efflux compared to $Slack^{+/+}$ (Fig. 19C). This finding is explained by another K^+ conductance that is structurally or functionally upregulated in $Slack^{-/-}$ neurons. Since mice carrying a global $K_V1.3$ KO reportedly upregulated Slack currents (Lu et al., 2010) compensatory regulation between specific K_V channels and Slack seems possible and likely. According to literature, $K_V1.3$ exhibits rather slow kinetics and activates at negative potentials, shifting AP threshold to more positive potentials (see section 3.5.2.). This $K_V1.3$ modulation of AP threshold is, however, in contrast to the present Fura2 measurements, that suggest a Slack-dependent sensitization to KA-induced Ca^{2+} influx, and hence, a sensitized current

threshold for AP generation eliciting this type of electrical activity at a more negative membrane potential. Other K_V channels, for example K_V2 or K_V3 have faster activation kinetics (see section 3.5.2) (Johnston et al., 2010) mediating fast repolarization during fast AP firing and could therefore represent potential candidates for the compensatory increased K^+ efflux in Slack$^{-/-}$ neurons in response to KA exposure. More importantly, FRET-based findings of increased K^+ efflux in Slack$^{-/-}$ contrasts with previous studies reporting decreased K^+ efflux in Slack-deficient cerebral granular cells upon NMDA exposure (Ehinger et al., 2021). This discrepancy could be explained by high KA sensitivity of hippocampal neurons, especially withing the CA regions, or alternatively by different subsets of further ion channels that contribute to the K^+ conductance, causing fundamental differences in the two cellular systems studied.

7.4. Electrophysiological measurements

To increase the spatiotemporal resolution and gain more precise insights on relevant currents in Slack$^{-/-}$ hippocampal neurons, voltage-clamp and patch-clamp recordings were carried out. During incremental voltage steps TTX was used to block Na^+ currents and thereby Slack activation. First, as expected, Slack$^{+/+}$ neurons respond with higher TTX-sensitive steady state currents to depolarizing voltages compared to Slack$^{-/-}$, confirming Slack specific currents in Slack$^{+/+}$ but not Slack$^{-/-}$ neurons (Fig. 20D), a finding which is in line with previous studies (Byers et al., 2021; Ehinger et al., 2021; Martinez-Espinosa et al., 2015). Second, transient TTX-sensitive inward currents were amplified in Slack$^{-/-}$ neurons (Fig. 20C). Due to the presence of Na^+ in the bath solution and lack of K_V channel blockers like Tetraethylammonium (TEA) or 4-amminupyridine (4-AMP), these currents could not be ascertained as I_{NaT}. Yet, these currents were transient, appearing only during approximately 2.5 ms of the voltage stimuli, reflecting highly transient Na_V kinetics (Catterall et al., 2005; Kaplan et al., 2016), and a direct biophysical interaction between Slack and $Na_V1.6$, the most abundant sodium channel in the brain involved mediating I_{NaT} (Goldin, 2001), was reported recently (Yuan et al., 2023). Furthermore, it could be speculated that Na_V mediated Na^+ currents provide the initial driving force for VGCC recruitment, leading to increased KA-induced Ca^{2+} influx in Slack$^{-/-}$ neurons, as detected by Fura2 measurements (Fig. 17). Finally, increased Na^+ currents that accelerate neuronal depolarization could potentially also lead to increased K_V channel activation, resulting in accelerated K^+ efflux, as detected by FRET-based measurements (Fig. 19). Besides the increased transient inward currents, also TTX-sensitive steady state currents displayed an amplified net inward-directed current component at -20 to +20 mV, probably reflecting I_{NaP} (Fig. 20E). Interestingly, I_{NaP} has functionally been linked to Slack

currents in mammalian neurons (Budelli et al., 2009; Hage & Salkoff, 2012). Since Slack deficient *Drosophila* neurons also exhibit increased I_{NaP} (Byers et al., 2021) and GABAergic neurons that carry a GOF Slack variant respond with decreased I_{NaP} to voltage steps (Shore et al., 2020), Slack activity seems to be coupled to I_{NaP} and is limiting this Na_V current component likely by its persistent hyperpolarizing K^+ efflux.

To ultimately assess whether Slack-mediated changes of currents and ion fluxes translate into altered AP firing properties, hippocampal neurons were current-clamped, and APs analysed in response to KA exposure or current injections. As expected, $Slack^{-/-}$ hippocampal neurons responded with a significantly increased AP firing frequency to both, KA exposure or current injection (Fig. 21B and 22B). This finding of increased AP firing bridges the gap between changes in ion fluxes, *in vitro* exacerbation of cell death and higher *in vivo* severity in the KA-induced model of epilepsy. Also, the presented AP analysis is in line with results deriving from electrophysiological recordings of Slack-deficient DRG and glutamatergic neurons of the basolateral amygdala (Lu et al., 2015a; Martinez-Espinosa et al., 2015; Zhang et al., 2022) as both cell types responded with increased AP firing to depolarizing current injections. Moreover, these studies found a depolarized RMP in the absence of Slack, while RMP or amplitudes of AP and aHP were not significantly altered in a Slack-dependent manner in hippocampal neurons (Fig. 21E, 22C, 22H and 22J). Interestingly, cortical GABAergic neurons that carry a Slack GOF exhibited a similar RMP compared to wildtype (Shore et al., 2020), and hippocampal CA1, but not PV^+ interneurons with a Sack GOF mutation (Gertler et al., 2022) showed a depolarized RMP, which corresponds to the previously mentioned Slack deficient DRG and amygdala neurons (Miguel Sanz et al., 2023; Zhang et al., 2022). These controverse findings again emphasize that the role of Slack for neuronal activity is highly dependent on the cell and tissue type (see section 3.7.3. Table 2), as confirmed by different responses of Slack LOF and GOF animals in different *in vivo* models for epilepsy (see section 2.7.3. Table 1). The amplitude of both, AP and aHP, was unchanged in $Slack^{-/-}$ compared to $Slack^{+/+}$ hippocampal neurons (Fig. 22H and J), which is in line with similar basal inward currents in $Slack^{+/+}$ and $Slack^{-/-}$ neurons (Supplementary Fig. 4), and to findings deriving from Slo-deficient DRG neurons (Martinez-Espinosa et al., 2015). Following analysis of AP amplitudes, differences in AP firing frequency were expected to be mediated by AP kinetics and the duration of distinct AP components (see section 3.5. Fig. 3). Indeed, compared to $Slack^{+/+}$ neurons, the $Slack^{-/-}$ AP was elicited at a more negative membrane potential (Fig. 22D) together with increases in AP rise slope (Fig. 22F). Hence, the increased TTX-sensitive inward currents of $Slack^{-/-}$ (Fig. 20C) may be explained by a steeper AP rise slope, increased steady state TTX-sensitive inward

currents, and an increased KA-induced K^+ efflux (Fig. 19) to eventually change the threshold for AP-generation. AP-threshold can be modulated by K_V or Na_V channels (Johnston et al., 2010; Kaplan et al., 2016). K_V channels, like K_V1.3 or 1.4 that activate near the RMP would limit initiation of APs (see section 3.5.2.) (Gutman et al., 2005; Johnston et al., 2010), hence are probably not causing hyperpolarized AP-threshold in Slack$^{-/-}$. More likely TTX-sensitive Na_V1.3 or Na_V1.6, that were reported to conduct principal components of I_{NaP} (Kaplan et al., 2016; Köhling, 2002; Stafstrom, 2007) are candidates to explain altered AP-threshold in Slack$^{-/-}$. First I_{NaP} can boost subthreshold currents and are half maximal activated at approximately -50 mV thereby hyperpolarizing AP-threshold (Köhling, 2002). Second, increased TTX-sensitive inward transient and persistent currents could reflect increased Na_V activity that led to both altered AP-threshold (Fig. 22D) and AP rise-slope (Fig. 22F). In glutamatergic iPSC derived neurons or inhibitory neurons that carried a GOF Slack variant, respectively, AP initiation was reported to be unaffected or even depolarized. This is consistent with data obtained from Slack$^{-/-}$ hippocampal neurons, which exhibit a hyperpolarized AP-threshold, and further supports the idea that Slack modulates AP threshold directly or via further subconductance states. Finally, the duration of aHP was found to be shorter in Slack$^{-/-}$ hippocampal neuros (Fig. 22K), further supporting the idea of changes in AP initiation and timing, rather than shifts in amplitudes. In line, the increased K^+ efflux seen in Slack$^{-/-}$ hippocampal neurons using FRET imaging (Fig. 19) probably links shortened aHP duration and accelerated K^+ efflux to Kv channel function. Although Slick or BK were only assessed at the transcriptional level and these channels were found to be unaltered in hippocampal tissues obtained from Slack$^{-/-}$ (Fig. 12 and 13), the function of BK or possible K_V candidate channels that was not yet analysed in detail in the present model, could potentially reinforce fast aHP and repolarize the neurons faster. Together with further Kv channels that reportedly support fast AP firing as K_V3 (see section 3.5.2.), but in the absence of Slack-mediated slow and persistent aHP, neuronal AP firing could be accelerated, which was herein confirmed for KA-treated and current-injected Slack$^{-/-}$ neurons ultimately leading to increase seizure severity *in vivo* (Fig. 11 and 13).

To summarize the electrophysiological data a Slack mediated persistent K^+ current, basal active or activated by Na^+ sources like GluK receptors and Na_V channels, eventually sets Na_V activation and AP threshold. The subthreshold (leakage) Slack current might be activated by persistent Na_V currents like Na_V1.6. Slack channel function limits AP generation and prolongs aHP, ultimately leading to persistently refractory Na_V channel currents and a delayed generation of follow-up AP, which together limit ictal events *in vitro* and *in vivo*. However, in Slack$^{-/-}$, AP are evoked faster, due to subthreshold I_{NaP} and faster

reactivated I_{NaT}, facilitating K_V channel activity that in turn conduct a fast repolarization leading to Na_V channel reactivation and consequently to a boost of Ca^{2+} conductance and ictal activity. This triggers cell death and seizures mediated by glutamatergic activity (Fig. 24). Yet, by comparing Slack$^{-/-}$ to Slack GOF mouse variants causing spontaneous seizures or even death in uteri (Quraishi et al., 2020; Shore et al., 2020), this contrasts with unaffected homozygous Slack$^{-/-}$ animals and cultured hippocampal tissues or dissociated cells. A potential explanation for unaffected Slack$^{-/-}$ mice could be further K^+ channels as principal driving force for aHP as shown previously for BK, K_v1.1. or K_V7.5 (González et al., 2012b; Tzingounis et al., 2010). Particularly LOF variants of the latter one are, like Slack, linked to epilepsy (Krüger et al., 2022; Lehman et al., 2017), and LOF of K_V7.5 is accompanied by a loss of aHP. Hence, the general functionality of the nervous tissue is ensured by a set of other K^+ conductance and their activity are balanced and modulated by Slack channel function. Without Slack, neuronal networks are functional, at least in principle, but they are also very susceptible to changes in the balance between excitation and inhibition.

To elucidate the role of Slack for a second type of experimental epilepsy, Pilo was applied. As briefly introduced in section 3.4.1. Pilo-induced seizures are a widely applied and well-established model for epilepsy. Apart of *in vivo* models using Pilo, also HSC were used to study limbic seizures provoked by Pilo (Poulsen et al., 2002). Unexpectedly, following Pilo exposure, Slack$^{+/+}$ HSC responded with significantly increased cell death to Pilo treatment compared to Slack$^{-/-}$ (Fig. 23), which is in contrast to the results of the KA-based model (Fig. 14). Applying Fura2, acute Pilo-induced Ca^{2+} fluxes from intracellular stores were measured, but hippocampal neurons responded only to very high Pilo concentrations (Supplementary Fig. 5). Together these findings suggest that certain sub-populations of hippocampal neurons are vulnerable to Pilo, especially upon acute exposure. This is consistent with literature, stating cholinergic hippocampal neurons, that are predominantly interneurons, as the Pilo sensitive cell fraction (Frotscher et al., 1986). Since hippocampal excitability is modulated by basal forebrain and brain stem, deafferented HSC are probably only of limited importance for studying cholinergic functions in the hippocampus. Both GABAergic and glutamatergic hippocampal neurons can have pre-synaptic choline receptors that modulate the release of neurotransmitters (see section 3.4.1. and Fig. 2). Based on the *in vitro* data, several mechanisms can be speculated to be responsible for the increased neuronal cell death in Slack$^{+/+}$ HSC after Pilo exposure: First, Pilo treatment over days may promote neuronal rhythms like θ -or γ-oscillation that affect Slack$^{+/+}$ and Slack$^{-/-}$ HSC to a different extend. Second, basal expression of mAChR could be altered in Slack$^{-/-}$, leading to changes in Pilo-induced

epileptic activity. Third, as described in section 3.4.1. Pilo binds to cholinergic M1 receptors that mediate activation of PKC. Slack was shown to be phosphorylated at S407 by PCK leading to 2 – 6 fold increase in current amplitude and slower activation kinetics (Barcia et al., 2012; Kaczmarek, 2013; Santi, 2006) (Fig. 4). Considering expression of cholinergic receptors especially in GABAergic neurons within the hippocampus increased Slack currents could inhibit inhibitory signalling by limiting excitability of GABAergic neurons leading to pathological causes similar to reports on GOF Slack mutations (Gertler et al., 2022; Shore et al., 2020). To further study this, field potential recordings on acute hippocampal slices and single neurons and in-depth expression analysis are needed in the future. However, increased vulnerability of Slack$^{+/+}$ HSC implies a region specific and even trigger or signalling pathway specific role of Slack, that is also evident for different epilepsy models in Slack-KI and Slack-KO mice (Gertler et al., 2022; Quraishi et al., 2020).

7.5. Conclusions

Considering all reported and discussed data deriving from Slack$^{-/-}$ mice, hippocampal tissue and single neurons, the herein presented discrepancy to seizures provoked by Slack GOF mutations in human patients remains unresolved. So far, different Slack-KI or Slack-KO mice have been studied, focussing on multiple brain regions and cell types (Table 1 and 2). These analyses resulted in different and partly contradictory findings regarding Slack's role for epilepsy. Depending on the used model for epilepsy, neuronal network or cell type, Slack function was associated with different phenotypes and epilepsy syndromes. One example is the Y777H GOF variant of *KCNT1*, which is linked to (AD)SHE in human patients and SRS in mice. Neurons from different brain regions of mice carrying this mutation show very different neuronal properties: Analyses of cortical neurons revealed a decreased excitability of GABAergic neurons, but unchanged firing properties of glutamatergic neurons (Shore et al., 2020). Conversely, in neuronal of the basolateral amygdala decreased excitability of glutamatergic neurons was observed (Zhang et al., 2022). One explanation for this difference was recently given by Wu and Kaczmarek (Wu et al., 2023). These authors argue that two different splice variants of Slack exist, the rapidly activating Slack-A, and the slowly activating Slack-B (see section 3.7.). While the rapidly activating Slack-A variant might promote fast repolarization and faster AP, the relatively slow activating Slack-B variant was rather contributing to RMP and prolong aHP, leading to a lower AP firing rate. This heterogeneity might explain differential roles of Slack in different cells and brain regions. Furthermore, especially the Slack-B can form heteromeric channels with Slick leading to increased expression at the

plasma membrane and subsequent highly increased peak current amplitudes. Formation of heteromers is followed by activation kinetics that are slower than Slack-B or Slick homomers (Chen et al., 2009; Kaczmarek, 2013). Considering this, one can speculate about different roles of Slack during KA -and Pilo-induced excessive neuronal firing: Based on the current data, endogenous Slack activity functions as seizure blocker, especially in KA-induced models of acute epilepsy. Following KA exposure within excitatory glutamatergic neurons, Slack-B properties in particular may act protectively to limit AP firing frequency likely through a delayed and sustained hyperpolarizing K^+ efflux. As the results based on Pilo-treated HSCs show, slack properties can also have a detrimental effect on neuronal viability. In this context, Slack-mediated K^+ currents might limit (potentially protective) GABA signalling causing neuronal cell loss.

Because EIMFS and (AD)SHE patients suffer from GOF mutations, while LOF variants of *KCNT1* are rare, Slack inhibitors are designed as potential anti-epileptic drugs in the last years (Griffin et al., 2021; Spitznagel et al., 2020). However, based on the herein studied KA-based model for epilepsy, Slack activity must be modulated very carefully, since a complete block of Slack channels may lead to an increased seizure susceptibility. Combined with the rare LOF *KCNT1* variants this confirms that caution is required when central Slack activity is pharmacologically targeted. Furthermore, brain damage exacerbates and may occur even hours or days after ictal events (Lipton & Rosenberg, 1994; Sheardown et al., 1993). Hence, considering Slack's potential role as intrinsic "seizure blocker" pharmacological modulation (i.e. stimulation) might also be interesting to ameliorate or even prevent post-ictal pathologies.

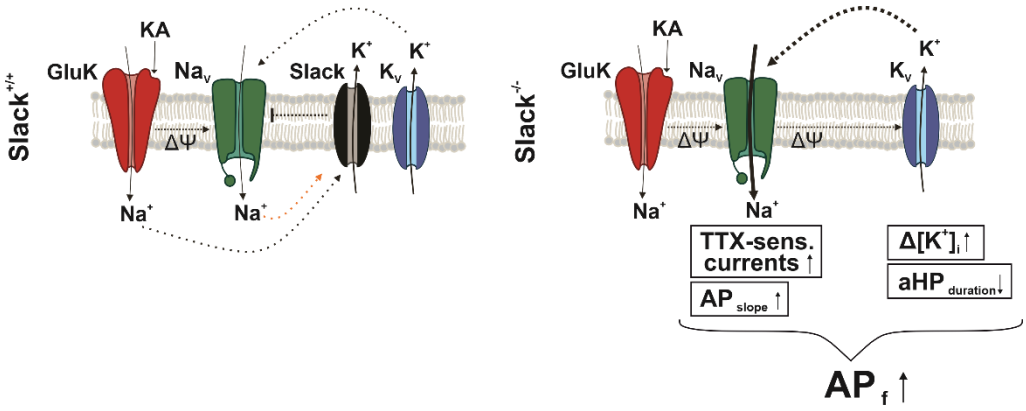

Figure 24: Schematic illustration of proposed Slack function during KA-induced neuronal activation.

Proposed mechanism explaining Slack's function in KA-exposed mouse brains and neurons. Loss of Slack function led to i.) disinhibited Na_V channels, ii.) a shift of the AP threshold, iii.) in repolarization-depolarization circuitry, and iv.) in higher K_V channel activity eventually accelerating AP firing (AP_f) upon glutamatergic activation. Together, this results in the absence of Slack in increased seizure severity in KA-induced acute epilepsies.

As recently discussed in Skrabak et al., 2023, during KA-induced neuronal depolarization Slack-mediated sustained outward K^+ current is involved in Na_V activation and AP threshold limitation (Fig. 21D and 22D). A subthreshold Slack current is likely to be activated by I_{NaP} (Fig. 20E) (Budelli et al., 2009; Hage & Salkoff, 2012) finetuning both AP rise and aHP duration and thereby AP frequency (Fig. 24 left hand side).

Within $Slack^{-/-}$, however, there is no limitation of Na_V activation, and the Na_V-mediated currents already reach the AP threshold at more negative membrane potentials. Subsequently, increased depolarizing Na^+ currents significantly enhanced the Ca^{2+} influx, mediated by NDMA receptors or VGCC (Fig. 17) to ultimately cause neuronal cell death (Fig. 14 and 16). Furthermore, increased depolarization can lead to increased activation of K_V channels that support faster repolarization and subsequent high frequency of neuronal firing, which is consistent with the finding of an increased K^+ efflux following KA treatment (Fig. 19). This in turn explains neuronal demise in hippocampal tissue and single cell cultures and increased seizure severity in $Slack^{-/-}$ mice implying Slack K_{Na} channels are critical modulators of seizures.

7.6. Limitations and Outlook

Several limitations of this study can be defined.

First, exclusively male mice were used for *in vivo* experiments, which means from a translational perspective that the findings can only be transferred to female test subjects or patients to a limited extend.

Second, Slack$^{-/-}$ animal carry a global deletion of the Slack channel. By this, alterations in brain development and wiring, together with compensatory changes in protein expressions, cell-type abundance or topology cannot be excluded. Since pathomechanism of Slack-KI *in vivo* and *in-vitro* were reported to affect especially GABAergic interneurons further experiments using cell-type specific Slack-KO, for instance in GABAergic interneurons, should be verry informative.

Third, for all *in vitro* experiments hippocampal tissue or dissociated cells were used. The hippocampus is a crucial formation for epileptogenesis and heavily affected in the KA-induced model for epilepsy. Since Slack-related epilepsies are mainly characterized and studied based on cortical EEG recordings, and seizures of especially (AD)SHE occurs frequently within the frontal cortex this model system is somewhat limited. Especially for patch-clamp based findings confirmatory experiments using cortical neurons would strengthen the presented findings, which are based on hippocampal neurons.

Fourth, mRNA expression levels were analysed 24 h post KA injection and only on hippocampal tissues. Neuronal and glial alteration might occur, however, earlier or even days later and within another brain region making this isolated analysis spatiotemporally limited.

Fifth, further experiments, especially proofing altered neuronal excitability by current-clamp experiments, should include neurons from different brain region and differentiate between neuronal subtypes.

Sixth, evidence for changes in Na^+ or K^+ currents need to be further confirmed. Along this line, Na^+ currents need to be recorded under appropriate recording conditions that specifically isolate I_{Na}; and K^+ fluxes need to be further confirmed and characterized using different K_V channel blocker and a voltage-clamp approach.

Finally, pharmacological experiments that confirm results obtained from the genetic Slack$^{-/-}$ model are limited or not successful in the study. Hence, a more specific Slack inhibitor and/or activator to test their impact on seizure severity *in vivo* or AP firing

properties *in vitro* must be carried out in future. Importantly, such approaches will demonstrate whether pharmacological targeting of Slack reduces the KA-induced seizure severity *in vivo*.

8. Supplementary data

8.1. Supplementary Figures

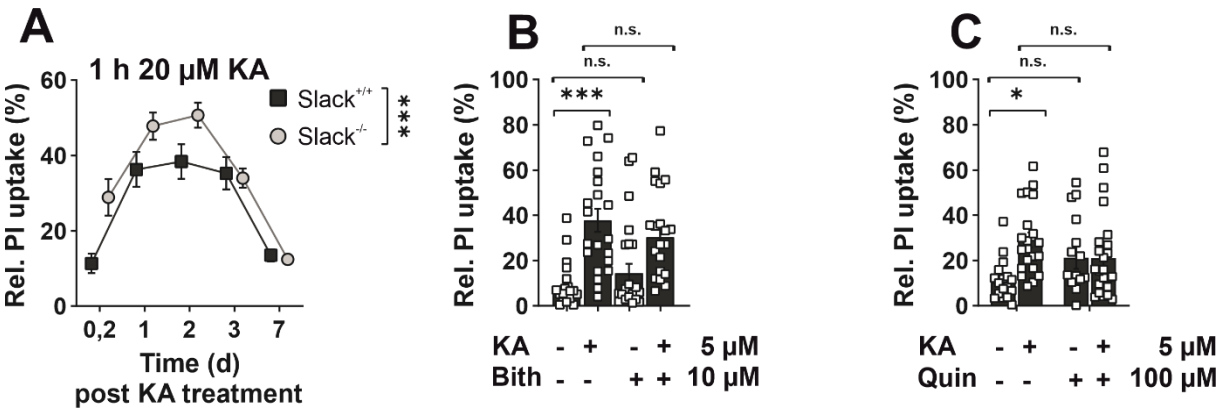

Supplementary Figure 1: Increased cell death in Slack$^{-/-}$ HSC among transient high dose KA-exposure but no Slack-mediated modulation of KA-induced PI uptake.

(A) Compared to Slack$^{+/+}$ (n = 15 to 24 ROI out of 8 wells from 4 preparations), Slack$^{-/-}$ HSC (n = 21 to 30 ROI out of 8 wells from 4 preparations) showed significantly (two-way-ANOVA, $F_{1/233} = 12.44$, p = 0.005) increased PI uptake (normalized to maximum) in response to transient 1 h 20 µM KA treatment and subsequent PI imaging over 7 d in culturing medium without KA. **(B)** In Slack$^{+/+}$ HSC (n = 18 to 24 ROI out of 8 wells from 2 preparations) KA co-treatment with non-specific "Slack activator" Bithionol (Bith) for 24 h did not modulate KA-induced PI uptake (untreated to 5 µM KA: unpaired t-test p <0.0001). **(C)** Also, by co-treating Slack$^{+/+}$ HSC with KA and the non-specific "Slack inhibitor" Quinidine (Quin) for 24 h, no modulation of KA-induced PI uptake was detected (untreated to 5 µM KA: unpaired t-test p = 0.0139). Data represented as mean ± SEM with *P <0.05, **P <0.01, ***P <0.001. For detailed statistics also consult Supplementary Table 13.

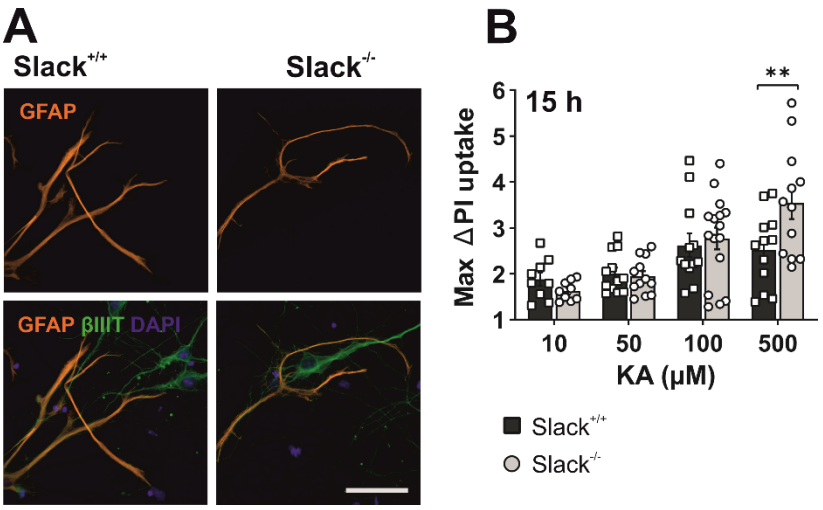

Supplementary Figure 2: PHN cultures also contain astroglia and Slack$^{-/-}$ PHN respond with increased PI uptake to short time exposure of high KA concentration.

(A) Exemplary immunofluorescence images of Slack$^{+/+}$ (top) and Slack$^{-/-}$ (bottom) PHN sained against astroglial marker GFAP (orange) and neuronal marker βIIIt (green) together with nucleus with Hoechst (blue). PHN of both, Slack$^{+/+}$ and Slack$^{-/-}$ contain astroglia to approximately same levels. Scale bar: 40 µm. **(B)** Slack$^{-/-}$ PHN respond with increased PI uptake to 15 h exposure to high KA concentration of 500 µM (unpaired t-test, p = 0.002). Data represented as mean ± SEM with *P <0.05, **P <0.01, ***P <0.001. For detailed statistics also consult Supplementary Table 14.

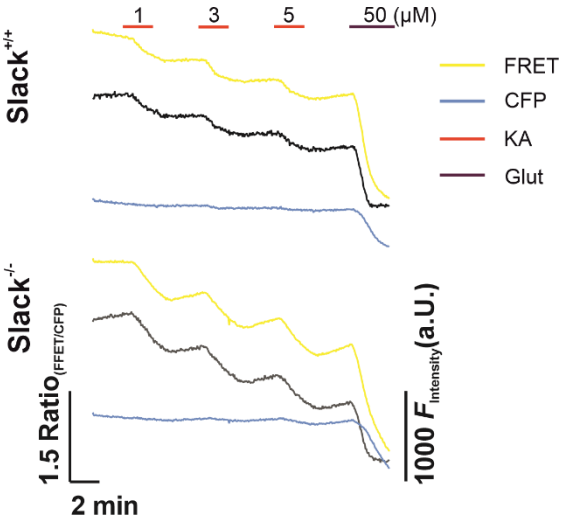

Supplementary Figure 3: Exemplary traces of FRET-based K$^+$ live cell imaging.

Following viral transduction of Slack$^{+/+}$ and Slack$^{-/-}$ PHN KA-provoked (KA, red lines) K$^+$ efflux was measured as ration (black line) of FRET (yellow line) and CFP (blue line) intensity (*F* intensity in arbitrary units) that need to show antiparallel courses. To validate neuronal responses a final 50 µM glutamate stimulus (purple line) was carried out. CFP is constant or slightly antiparallel to FRET signals among KA exposure. Strong glutamate induced deflection of FRET is not followed by antiparallel CFP signals, probably due to kinetics of the biosensor. Still, since glutamate was not included to statistics, properties of FRET-measurements were validated successfully.

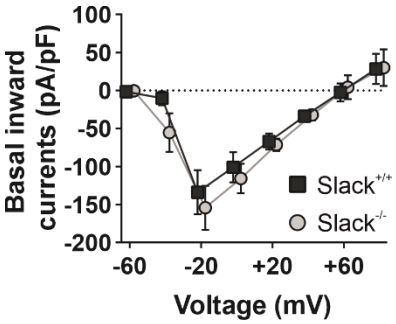

Supplementary Figure 4: Similar basal voltage-step provoked inward currents of PHN.

Among incremental voltage steps in voltage-clamped Slack$^{+/+}$ (n = 34 derived from 6 preparations) and Slack$^{-/-}$ (n = 33 derived from 7 preparations) PHN similar basal inward currents were detected especially between -40 and +40 mV. Data is represented as mean ± SEM. For detailed statistics also consult Supplementary Table 15.

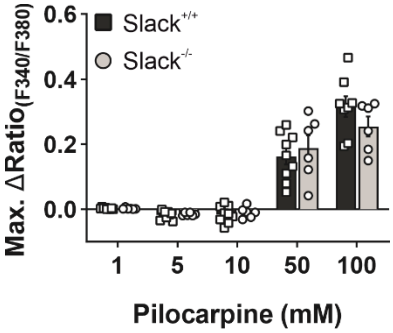

Supplementary Figure 5: Similar Pilo-induced Ca^{2+} dynamics in Slack$^{+/+}$ and Slack$^{-/-}$ PHN.

Slack$^{+/+}$ and Slack$^{-/-}$ PHN were loaded with Fura2 and Ca^{2+} dynamics imaged among exposure to increasing Pilo concentration (1 to 100 mM Pilo). Verry high Pilo concentrations were needed to provoke Ca^{2+} fluxes, that are similar in both Slack$^{+/+}$ (n = 9 wells derived from 2 preparations) and Slack$^{-/-}$ (n = 6 wells derived from 2 preparations) PHN. Data is represented as mean ± SEM. For detailed statistics also consult Supplementary Table 16.

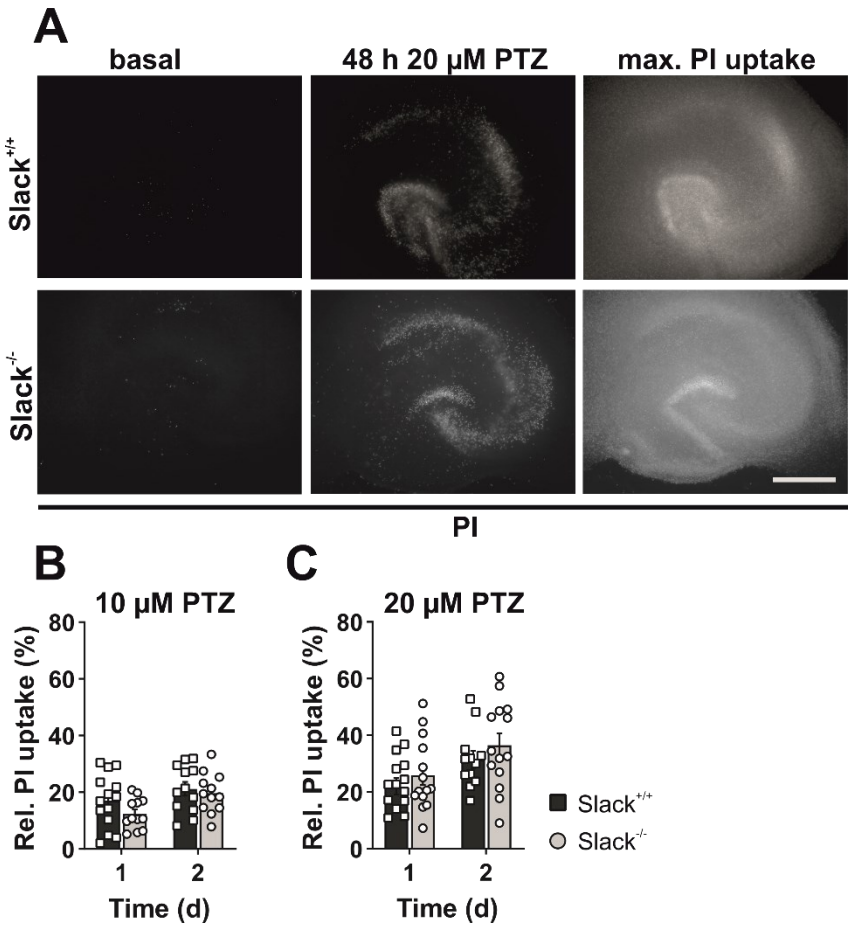

Supplementary Figure 6: Similar cell death in Slack$^{+/+}$ and Slack$^{-/-}$ HSC following PTZ exposure.

(A) Images of representative 14 div hippocampal slice cultures (HSC) from Slack$^{+/+}$ (upper images) and Slack$^{-/-}$ (lower images) prior treatment (basal), after 48 h exposure to 20 µM PTZ (48 h 20 µM PTZ) or after application of 80% ethyl-alcohol (max. PI uptake). Scale bar: 500 µm. **(B and C)** Among exposure of 10 µM PTZ (B) or 20 µM PTZ (C) Slack$^{+/+}$ (n = 12 to 15 from 6 wells derived from 3 preparations) and Slack$^{-/-}$ (n = 12 to 14 from 6 wells derived from 3 preparations) HSC respond with similar PI uptake to treatment. Data is represented as mean ± SEM. For detailed statistics also consult Supplementary Table 17.

8.2. Supplementary Tables

Supplementary Table 1: *Values and statistics of Figure. 11*

B	KA (mg/kg)	Genotype	Rel. PI uptake	**n** = mice	Statistics	p
	15	Slack$^{+/+}$	3.67 ± 0.88	3	Unpaired t-test	0.66
		Slack$^{-/-}$	3 ± 1	2		
	20	Slack$^{+/+}$	4.40 ± 0.24	5	Unpaired t-test	0.85
		Slack$^{-/-}$	4.67 ± 0.21	6		
	25	Slack$^{+/+}$	5 ± 0	6	Unpaired t-test	0.17
		Slack$^{-/-}$	5.67 ± 0.67	3		
	30	Slack$^{+/+}$	5 ± 0.22	7	Unpaired t-test	**0.04**
		Slack$^{-/-}$	6 ± 0.38	7		

C		Genotype			
		Slack$^{+/+}$		**Slack$^{-/-}$**	
	Time	**SSc**	**n** = mice	**SSc**	**n** = mice
	5	1.40 ± 0.24	5	1.67 ± 0.21	6
	10	2.00 ± 0.00		2.00 ± 0.00	
	15	2.00 ± 0.00		2.67 ± 0.33	
	20	3.00 ± 0.45		3.00 ± 0.52	
	25	2.00 ± 0.00		2.50 ± 0.34	
	30	2.80 ± 0.49		2.67 ± 0.49	
	35	2.00 ± 0.00		2.50 ± 0.56	
	40	3.20 ± 0.73		2.33 ± 0.33	
	45	3.00 ± 0.45		1.83 ± 0.17	
	50	3.60 ± 0.51		1.83 ± 0.17	
	55	2.80 ± 0.73		2.33 ± 0.56	
	60	2.80 ± 0.37		1.83 ± 0.17	
	65	2.40 ± 0.51		1.83 ± 0.17	
	70	2.60 ± 0.40		1.83 ± 0.17	
	75	2.80 ± 0.49		2.17 ± 0.40	
	80	2.40 ± 0.51		1.83 ± 0.17	
	85	2.60 ± 0.60		1.50 ± 0.22	
	90	2.60 ± 0.68		1.50 ± 0.22	
	Statistics: two-way-ANOVA $F_{1/162}$ = 11.96 **p = 0.0007**				

D

n = mice	**Genotype**	
	Slack$^{+/+}$	**Slack$^{-/-}$**
	CS (min)	
1	25	20
2	25	15
3	25	20
4	45	15
5	50	20
6		20
Kapplan-Meyer: Log rank test, **p = 0.0024**		

E

SSc	**Genotype**	**Fraction**	**% of all**	**Chi-Square**
4	Slack$^{+/+}$	5/5	100	-
	Slack$^{-/-}$	6/6	100	
5	Slack$^{+/+}$	2/5	40	0.37
	Slack$^{-/-}$	4/6	66.67	
6	Slack$^{+/+}$	0/5	0	-
	Slack$^{-/-}$	0/6	0	

F

	Genotype			
	Slack$^{+/+}$		**Slack$^{-/-}$**	
Time	**SSc**	**n** = mice	**SSc**	**n** = mice
5	1.00 ± 0.00	7	1.43 ± 0.20	7
10	1.86 ± 0.14		2.71 ± 0.42	
15	2.57 ± 0.48		3.43 ± 0.69	
20	3.00 ± 0.44		4.43 ± 0.69	
25	3.00 ± 0.62		3.86 ± 0.83	
30	3.14 ± 0.46		3.71 ± 0.87	
35	3.29 ± 0.57		4.71 ± 0.71	
40	3.86 ± 0.46		4.00 ± 0.87	
45	3.71 ± 0.61		4.57 ± 0.75	
50	3.86 ± 0.51		4.43 ± 0.75	
55	3.57 ± 0.48		5.14 ± 0.67	
60	3.86 ± 0.34		4.86 ± 0.80	
65	3.43 ± 0.61		4.43 ± 0.84	
70	3.57 ± 0.57		4.43 ± 0.90	
75	3.29 ± 0.52		4.71 ± 0.81	
80	3.29 ± 0.52		5.14 ± 0.77	
85	3.57 ± 0.57		4.71 ± 0.89	
90	3.29 ± 0.52		5.29 ± 0.78	
Statistics: two-way-ANOVA $F_{1/216}$ = 24.32 **p <0.001**				

G

n = mice	Genotype	
	Slack$^{+/+}$	**Slack$^{-/-}$**
	CS (min)	
1	20	15
2	20	40
3	40	10
4	15	20
5	15	10
6	30	10
7	35	20
Kapplan-Meyer: Log rank test, **p = 0.36**		

H

SSc	Genotype	Fraction	% of all	Chi-Square
5	Slack$^{+/+}$	6/7	85.7	0.299
	Slack$^{-/-}$	7/7	100	
6	Slack$^{+/+}$	1/7	14.28	0.094
	Slack$^{-/-}$	4/7	57.14	
7	Slack$^{+/+}$	0/7	0	**0.0507**
	Slack$^{-/-}$	3/7	42.86	

Supplementary Table 2: *Values and statistics of Figure. 12*

	Parameter	Genotype	Data	n = hippocampi	Statistics	p
A	**Slack**	$Slack^{+/+}$	0.07 ± 0.01	4	Unpaired t-test	0.39
		$Slack^{-/-}$	0.00 ± 0.00	5		
	Slick	$Slack^{+/+}$	0.12 ± 0.02	4	Unpaired t-test	0.79
		$Slack^{-/-}$	0.14 ± 0.03	5		
	BK	$Slack^{+/+}$	1.02 ± 0.12	4	Unpaired t-test	0.93
		$Slack^{-/-}$	1.02 ± 0.06	5		
B	**GluK4**	$Slack^{+/+}$	0.17 ± 0.03	4	Unpaired t-test	0.91
		$Slack^{-/-}$	0.21 ± 0.02	5		
	GluK5	$Slack^{+/+}$	0.26 ± 0.09	4	Unpaired t-test	0.71
		$Slack^{-/-}$	0.43 ± 0.03	5		
	GluA1	$Slack^{+/+}$	2.57 ± 0.50	4	Unpaired t-test	0.34
		$Slack^{-/-}$	3.00 ± 0.57	5		
	GluA2	$Slack^{+/+}$	1.69 ± 0.36	4	Unpaired t-test	0.58
		$Slack^{-/-}$	1.93 ± 0.57	5		
	GluN1	$Slack^{+/+}$	0.87 ± 0.21	4	Unpaired t-test	0.46
		$Slack^{-/-}$	1.20 ± 0.10	5		
	GluN2a	$Slack^{+/+}$	1.66 ± 0.46	4	Unpaired t-test	0.58
		$Slack^{-/-}$	1.91 ± 0.15	5		
	GluN2b	$Slack^{+/+}$	0.79 ± 0.17	4	Unpaired t-test	0.69
		$Slack^{-/-}$	0.97 ± 0.07	5		
C	**BDNF**	$Slack^{+/+}$	0.37 ± 0.06	4	Unpaired t-test	0.97
		$Slack^{-/-}$	0.31 ± 0.02	5		
	TrkB	$Slack^{+/+}$	1.01 ± 0.16	4	Unpaired t-test	0.97
		$Slack^{-/-}$	1.08 ± 0.09	5		
	GFAP	$Slack^{+/+}$	9.58 ± 2.91	4	Unpaired t-test	0.89
		$Slack^{-/-}$	9.82 ± 1.44	5		
D	**Slack**	$Slack^{+/+}$	0.008 ± 0.003	7	Unpaired t-test	0.89
		$Slack^{-/-}$	0.000 ± 0.000	5		
	Slick	$Slack^{+/+}$	0.047 ± 0.007	7	Unpaired t-test	0.92
		$Slack^{-/-}$	0.054 ± 0.014	5		
	BK	$Slack^{+/+}$	0.64 ± 0.070	7	Unpaired t-test	0.12
		$Slack^{-/-}$	0.74 ± 0.087	5		
E	**GluK4**	$Slack^{+/+}$	0.074 ± 0.015	7	Unpaired t-test	0.82
		$Slack^{-/-}$	0.13 ± 0.04	5		
	GluK5	$Slack^{+/+}$	0.11 ± 0.02	7	Unpaired t-test	0.73
		$Slack^{-/-}$	0.20 ± 0.058	5		
	GluA1	$Slack^{+/+}$	2.272 ± 0.289	7	Unpaired t-test	0.33
		$Slack^{-/-}$	2.534 ± 0.509	5		
	GluA2	$Slack^{+/+}$	1.022 ± 0.129	7	Unpaired t-test	0.21
		$Slack^{-/-}$	1.36 ± 0.374	5		
	GluN1	$Slack^{+/+}$	0.854 ± 0.104	7	Unpaired t-test	0.86
		$Slack^{-/-}$	0.9 ± 0.125	5		
	GluN2a	$Slack^{+/+}$	0.948 ± 0.095	7	Unpaired t-test	0.84
		$Slack^{-/-}$	0.896 ± 0.128	5		
	GluN2b	$Slack^{+/+}$	0.508 ± 0.095	7	Unpaired t-test	0.96
		$Slack^{-/-}$	0.494 ± 0.116	5		
F	**BDNF**	$Slack^{+/+}$	1.218 ± 0.653	7	Unpaired t-test	0.76
		$Slack^{-/-}$	1.486 ± 0.537	5		
	TrkB	$Slack^{+/+}$	0.951 ± 0.288	7	Unpaired t-test	0.97
		$Slack^{-/-}$	0.982 ± 0.345	5		
	GFAP	$Slack^{+/+}$	4.078 ± 0.899	7	Unpaired t-test	**0.013**
		$Slack^{-/-}$	1.732 ± 0.556	5		

Supplementary Table 3: *Values and statistics of Figure. 13*

A

	Genotype			
	Slack$^{+/+}$		**Slack$^{-/-}$**	
Time	**SSc**	**n** = mice	**SSc**	**n** = mice
5	1.70 ± 0.15	10	1.78 ± 0.15	9
10	2.00 ± 0.00		2.67 ± 0.44	
15	2.20 ± 0.20		2.67 ± 0.55	
20	4.40 ± 0.54		4.56 ± 0.67	
25	4.70 ± 0.33		5.00 ± 0.62	
30	5.10 ± 0.23		5.56 ± 0.41	
35	4.90 ± 0.23		5.00 ± 0.60	
40	4.70 ± 0.26		5.56 ± 0.50	
45	4.80 ± 0.20		5.33 ± 0.65	
50	4.80 ± 0.20		5.11 ± 0.65	
55	4.60 ± 0.16		5.67 ± 0.55	
60	4.60 ± 0.16		5.11 ± 0.65	
65	4.70 ± 0.15		5.78 ± 0.46	
70	4.50 ± 0.17		5.67 ± 0.55	
75	4.70 ± 0.21		5.78 ± 0.55	
80	4.40 ± 0.22		5.33 ± 0.65	
85	3.80 ± 0.25		5.44 ± 0.65	
90	3.90 ± 0.23		5.56 ± 0.63	
Statistics: two-way-ANOVA $F_{1/144}$ = 30.63 **p <0.001**				

B

	Genotype	
	Slack$^{+/+}$	**Slack$^{-/-}$**
n = mice	**CS (min)**	
1	25	25
2	20	25
3	15	20
4	25	10
5	20	30
6	20	10
7	20	20
8	20	10
9	20	20
10	25	
Kapplan-Meyer: Log rank test, **p = 0.94**		

C	SSc	Genotype	Fraction	% of all	Chi-Square
	5	$Slack^{+/+}$	10/10	100	-
		$Slack^{-/-}$	9/9	100	
	6	$Slack^{+/+}$	8/10	80	0.905
		$Slack^{-/-}$	7/9	77.78	
	7	$Slack^{+/+}$	0/10	0	0.017
		$Slack^{-/-}$	4/9	44.44	

D	Parameter	Genotype	Data	n = hippocampi	Statistics	p
	Slack	$Slack^{+/+}$	0.031 ± 0.014	10	Unpaired t-test	0.15
		$Slack^{-/-}$	0.000 ± 0.000	8		
	Slick	$Slack^{+/+}$	0.034 ± 0.009	10	Unpaired t-test	0.89
		$Slack^{-/-}$	0.032 ± 0.002	8		
	BK	$Slack^{+/+}$	0.342 ± 0.088	10	Unpaired t-test	0.28
		$Slack^{-/-}$	0.455 ± 0.037	8		
E	**GluK4**	$Slack^{+/+}$	0.191 ± 0.028	10	Unpaired t-test	0.98
		$Slack^{-/-}$	0.19 ± 0.026	8		
	GluK5	$Slack^{+/+}$	0.39 ± 0.055	10	Unpaired t-test	0.87
		$Slack^{-/-}$	0.377 ± 0.056	8		
	GluA1	$Slack^{+/+}$	0.635 ± 0.200	10	Unpaired t-test	0.26
		$Slack^{-/-}$	0.942 ± 0.157	8		
	GluA2	$Slack^{+/+}$	0.724 ± 0.131	10	Unpaired t-test	0.07
		$Slack^{-/-}$	1.045 ± 0.090	8		
	GluN1	$Slack^{+/+}$	0.901 ± 0.168	10	Unpaired t-test	0.63
		$Slack^{-/-}$	1.003 ± 0.095	8		
	GluN2a	$Slack^{+/+}$	1.434 ± 0.258	10	Unpaired t-test	0.68
		$Slack^{-/-}$	1.607 ± 0.339	8		
	GluN2b	$Slack^{+/+}$	0.758 ± 0.107	10	Unpaired t-test	0.95
		$Slack^{-/-}$	0.767 ± 0.107	8		
F	**BDNF**	$Slack^{+/+}$	0.678 ± 0.148	10	Unpaired t-test	**0.047**
		$Slack^{-/-}$	0.316 ± 0.030	8		
	TrkB	$Slack^{+/+}$	0.403 ± 0.127	10	Unpaired t-test	0.066
		$Slack^{-/-}$	0.708 ± 0.065	8		
	GFAP	$Slack^{+/+}$	3.747 ± 1.214	10	Unpaired t-test	0.81
		$Slack^{-/-}$	3.333 ± 1.198	8		

Supplementary Table 4: *Values and statistics of Figure. 14*

B	Gene	Genotype	Rel. mRNA expression	**n** = preparation/ slices	Statistics	p
	Slack	$Slack^{+/+}$	0.03 ± 0.00	3/30	Unpaired t-test	**0.0013**
		$Slack^{-/-}$	0.00 ± 0.00	3/30		
	Slick	$Slack^{+/+}$	0.06 ± 0.00	3/30		>0.99.
		$Slack^{-/-}$	0.06 ± 0.00	3/30		
	BK	$Slack^{+/+}$	0.35 ± 0.02	3/30		0.78
		$Slack^{-/-}$	0.033 ± 0.08	3/30		

C	KA (µM)	Time (d)	Genotype	Rel. PI uptake	**n** = preparation/well/ROI	Statistics	p
	5	1	$Slack^{+/+}$	16.97 ± 2.54	6/3/18	two-way-ANOVA Sidak´s multiple comparison	**0.027**
			$Slack^{-/-}$	30.05 ± 4.11	6/9/27		
		2	$Slack^{+/+}$	30.66 ± 2.31	6/3/18		0.152
			$Slack^{-/-}$	39.89 ± 3.69	6/9/27		
D	10	1	$Slack^{+/+}$	23.60 ± 4.55	3/4/12	two-way-ANOVA Sidak´s multiple comparison	**0.012**
			$Slack^{-/-}$	41.94 ± 4.24	6/8/24		
		2	$Slack^{+/+}$	29.92 ± 3.60	3/4/12		**0.022**
			$Slack^{-/-}$	47.39 ± 3.40	6/8/24		

E	Lox (µM)	Genotype	Fold change % PI / KA	**n** = slices
	1	$Slack^{+/+}$	0.98 ± 0.12	10
	5	$Slack^{+/+}$	0.83 ± 0.12	11

Supplementary Table 5: *Values and statistics of Fig. 16*

B	KA (µM)	Genotype	Rel. PI uptake	**n** = preparation/well/ROI	Statistics	p
	5	$Slack^{+/+}$	1.49 ± 0.23	3/4/17	Mann Whitney test	0.67
		$Slack^{-/-}$	1.49 ± 0.41	3/4/16		
	10	$Slack^{+/+}$	1.42 ± 0.25	3/5/22	Mann Whitney test	**0.0016**
		$Slack^{-/-}$	1.65 ± 0.33	3/5/20		

C	Treatment (µM)	Genotype	Rel. PI uptake	**n** = preparation/ well/ROI	Statistics	p	
	10 KA	Slack$^{+/+}$	1.38 ± 0.03	2/1/10	Unpaired t test	**0,008**	
		Slack$^{-/-}$	1.61 ± 0.07	2/1/10			
	10 KA + 50 PiTX	Slack$^{+/+}$	1.77 ± 0.06	3/6/30	Unpaired t test	0,5	
		Slack$^{-/-}$	1.86 ± 0.11	3/6/30			
	10 KA + 100 PiTX	Slack$^{+/+}$	2.08 ± 0.07	3/6/30	Unpaired t test	0,069	
		Slack$^{-/-}$	2.32 ± 0.10	3/6/30			
	10 KA vs. 10 KA + 100 PiTX	Slack$^{+/+}$	1.38 ± 0.03	3/6/30	two-way-ANOVA with Sidak's multiple comparison	**0,0008**	Statistics: two-way-ANOVA $F_{1/116}$ = 3.23 p = 0.075
		Slack$^{+/+}$	2.08 ± 0.07				
	10 KA vs. 10 KA + 100 PiTX	Slack$^{-/-}$	1.61 ± 0.07	3/6/30		**0,0007**	
		Slack$^{-/-}$	2.32 ± 0.10				

Supplementary Table 6: *Values and statistics of Figure 17*

D		Genotype		
		Slack$^{+/+}$		
	KA (µM)	Max. ΔRatio$_{(340/380)}$	**n** = preparation/well	Statistics
	1	0.09 ± 0.02	9/12	Non-linear fit R = 0.74 95 % IC 8.40 - 20.21 EC_{50} = 13.03
	5	0.12 ± 0.01	9/12	
	10	0.19 ± 0.02	9/12	
	50	0.48 ± 0.042	9/12	
	100	0,47 ± 0.043	9/12	
		Slack$^{-/-}$		
	KA (µM)	Max. ΔRatio$_{(340/380)}$	**n** = preparation/well	Statistics
	1	0.16 ± 0.02	8/13	Non-linear fit R = 0.75 95 % IC 8.32 - 18.96 EC_{50} = 12.56
	5	0.15 ± 0.01	8/13	
	10	0.20 ± 0.02	8/13	
	50	0.45 ± 0.03	8/13	
	100	0.42 ± 0.02	8/13	

D	Treatment (µM)	Genotype	Max. ΔRatio$_{(340/380)}$	**n** = preparation/well	Statistics	p
	1 KA	Slack$^{+/+}$	0.10 ± 0.03	9/12	two-way-ANOVA Sidak´s multiple comparison	0.35
		Slack$^{-/-}$	0.16 ± 0.02	8/13		
	5 KA	Slack$^{+/+}$	0.13 ± 0.02	9/12		0.96
		Slack$^{-/-}$	0.16 ± 0.01	8/13		
	10 KA	Slack$^{+/+}$	0.19 ± 0.02	9/12		>0.99
		Slack$^{-/-}$	0.20 ± 0.02	8/13		
	50 KA	Slack$^{+/+}$	0.48 ± 0.042	9/12		0.89
		Slack$^{-/-}$	0.45 ± 0.03	8/13		
	100 KA	Slack$^{+/+}$	0,47 ± 0.043	9/12		0.69
		Slack$^{-/-}$	0.42 ± 0.02	8/13		

F	Treatment (µM)	Genotype	Max. $\Delta Ratio_{(340/380)}$	n = preparation/well	Statistics	p	
	1 KA	$Slack^{+/+}$	0.09 ± 0.02	9/20	two-way-ANOVA Sidak´s multiple comparison	**0.014**	two-way-ANOVA $F_{1/96}$ = 15.38, **p = 0.0002**
		$Slack^{-/-}$	0.15 ± 0.02	10/14			
	3 KA	$Slack^{+/+}$	0.09 ± 0.01	9/20		**0.036**	
		$Slack^{-/-}$	0.14 ± 0.02	10/14			
	5 KA	$Slack^{+/+}$	0.11 ± 0.01	9/20		0.454	
		$Slack^{-/-}$	0.14 ± 0.01	10/14			
	50 Glut	$Slack^{+/+}$	0.43 ± 0.02	9/20	-	-	
		$Slack^{-/-}$	0.48 ± 0.03	10/14			

Supplementary Table 7: *Values and statistics of Figure 18*

A	**Treatment (µM)**	**Genotype**	**Max. ΔRatio$_{(340/380)}$**	**n** = preparation/well	**Statistics**	**p**
	5 KA	Slack$^{+/+}$	0.30 ± 0.03	5/10	two-way-ANOVA Sidak´s multiple comparison	0.28
		Slack$^{-/-}$	0.35 ± 0.04	4/9		
	5 KA + 10 NBQX	Slack$^{+/+}$	0.07 ± 0.02	5/10		0.81
		Slack$^{-/-}$	0.05 ± 0.01	4/9		
	50 Glut	Slack$^{+/+}$	0.43 ± 0.02	5/10	-	-
		Slack$^{-/-}$	0.47 ± 0.02	4/9		
	5 KA vs. 5 KA + 10 NBQX	Slack$^{+/+}$	0.30 ± 0.03	5/10	two-way-ANOVA with Sidak's multiple comparison	**<0.0001**
		Slack$^{+/+}$	0.07 ± 0.02	5/10		
		Slack$^{-/-}$	0.35 ± 0.04	4/9		**<0.0001**
		Slack$^{-/-}$	0.05 ± 0.01	4/9		

B	**Treatment (µM)**	**Genotype**	**Max. ΔRatio$_{(340/380)}$**	**n** = preparation/well	**Statistics**	**p**
	5 KA	Slack$^{+/+}$	0.33 ± 0.02	7/12	two-way-ANOVA Sidak´s multiple comparison	0.86
		Slack$^{-/-}$	0.32 ± 0.02	7/13		
	5 KA + 100 DL-AP5	Slack$^{+/+}$	0.17 ± 0.01	7/12		0.99
		Slack$^{-/-}$	0.17 ± 0.01	7/13		
	50 Glut	Slack$^{+/+}$	0.43 ± 0.02	7/12	-	-
		Slack$^{-/-}$	0.46 ± 0.02	7/13		
	5 KA vs. 5 KA + 100 DL-AP5	Slack$^{+/+}$	0.33 ± 0.02	7/12	two-way-ANOVA with Sidak's multiple comparison	**<0.0001**
		Slack$^{+/+}$	0.17 ± 0.01	7/12		
		Slack$^{-/-}$	0.32 ± 0.02	7/13		**<0.0001**
		Slack$^{-/-}$	0.17 ± 0.01	7/13		

C	**Treatment (µM)**	**Genotype**	**Max. ΔRatio$_{(340/380)}$**	**n** = preparation/well	**Statistics**	**p**
	5 KA	Slack$^{+/+}$	0.27 ± 0.06	3/4	two-way-ANOVA Sidak´s multiple comparison	0.99
		Slack$^{-/-}$	0.26 ± 0.04	3/6		
	5 KA + 5 Lox	Slack$^{+/+}$	0.16 ± 0.04	3/4		0.98
		Slack$^{-/-}$	0.14 ± 0.02	3/6		
	50 Glut	Slack$^{+/+}$	0.40 ± 0.05	3/4	-	-
		Slack$^{-/-}$	0.43 ± 0.05	3/6		
	5 KA vs. 5 KA + 10 Lox	Slack$^{+/+}$	1.38 ± 0.03	3/4	two-way-ANOVA with Sidak's multiple comparison	0.87
		Slack$^{+/+}$	2.08 ± 0.07	3/4		
		Slack$^{-/-}$	1.61 ± 0.07	3/6		0.59
		Slack$^{-/-}$	2.32 ± 0.10	3/6		

Supplementary Table 8: *Values and statistics of Figure 19*

G	Treatment (µM)	Genotype	Max. ΔRatio$_{(FRET/CFP)}$	**n** = preparation/well	Statistics	p
	untreated	Slack$^{+/+}$	2.05 ± 0.06	6/10	Unpaired t-test	0.425
		Slack$^{-/-}$	1.98 ± 0.06	5/8		
	1 KA	Slack$^{+/+}$	-0.13 ± 0.21	6/10	two-way-ANOVA	$F_{1/48}$ = 4.8 p = **0.031**
		Slack$^{-/-}$	-0.15 ± 0.03	5/8		
	3 KA	Slack$^{+/+}$	-0.25 ± 0.03	6/10		
		Slack$^{-/-}$	-0.29 ± 0.03	5/8		
	5 KA	Slack$^{+/+}$	-0.34 ± 0.04	6/10		
		Slack$^{-/-}$	-0.45 ± 0.04	5/8		
	50 Glut	Slack$^{+/+}$	-0.68 ± 0.04	6/10	-	-
		Slack$^{-/-}$	-0.79 ± 0.04	5/8		

Supplementary Table 9: *Values and statistics of Figure 20*

C		Genotype			
		Slack$^{+/+}$		Slack$^{-/-}$	
	Voltage (mV)	**inward current (pA/pF)**	**n** = preparation/cell	**inward current (pA/pF)**	**n** = preparation/cell
	-60	-0.01 ± 0.04	6/20	-0.08 ± 0.08	7/17
	-40	-19.89 ± 16.71		-19.99 ± 8.92	
	-20	-72.29 ± 14.87		-100.52 ± 21.30	
	0	-57.82 ± 11.23		-76.52 ± 11.68	
	20	-45.28 ± 7.23		-59.87 ± 7.55	
	40	-34.10 ± 3.97		-46.23 ± 4.57	
	60	-24.79 ± 2.39		-35.05 ± 3.23	
	80	-16.84 ± 2.53		-25.83 ± 3.09	
	Statistics: Two-Way-ANOVA. $F_{1/280}$ = 5.791, **p = 0.0168**				

D		Genotype			
		Slack$^{+/+}$		Slack$^{-/-}$	
	Voltage (mV)	**steady-state current (pA/pF)**	**n** = preparation/cell	**steady-state current (pA/pF)**	**n** = preparation/cell
	-60	-0.11 ± 0.09	6/24	-0.06 ± 0.04	7/17
	-40	-0.30 ± 0.10		-0.88 ± 0.31	
	-20	-0.99 ± 0.28		-2.30 ± 0.62	
	0	-0.06 ± 0.94		-2.32 ± 0.85	
	20	-4.00 ± 2.05		-0.60 ± 1.33	
	40	-9.47 ± 3.91		-4.05 ± 2.11	
	60	-15.37 ± 5.35		-7.67 ± 3.20	
	80	-20.00 ± 7.31		-11.08 ± 4.38	
	Statistics: Two-Way-ANOVA. $F_{1/312}$ = 5.122, **p = 0.0243**				

Supplementary Table 10: *Values and statistics of Figure 21*

B		Genotype			
		Slack$^{+/+}$		**Slack$^{-/-}$**	
	Time (s)	**Nr. of AP´s**	**n** = preparation/cell	**Nr. of AP´s**	**n** = preparation/cell
	1	1.42 ± 0.19		2.00 ± 0.37	
	2	1.25 ± 0.39		2.11 ± 0.68	
	3	1.42 ± 0.47		3.44 ± 0.63	
	4	2.08 ± 0.58		3.78 ± 0.80	
	5	1.92 ± 0.43		4.67 ± 0.91	
	6	2.50 ± 0.57		4.67 ± 0.85	
	7	2.25 ± 0.41		4.56 ± 0.73	
	8	2.42 ± 0.54		4.89 ± 0.86	
	9	2.58 ± 0.61		4.33 ± 0.97	
	10	3.00 ± 0.35		5.56 ± 0.80	
	11	3.08 ± 0.42		5.56 ± 0.56	
	12	2.83 ± 0.52		5.50 ± 0.68	
	13	3.17 ± 0.46		5.75 ± 1.01	
	14	3.08 ± 0.51		6.13 ± 0.91	
	15	2.83 ± 0.51	4/12	5.50 ± 0.78	4/9
	16	3.08 ± 0.50		5.75 ± 0.90	
	17	3.17 ± 0.49		6.25 ± 1.05	
	18	3.08 ± 0.48		5.88 ± 0.85	
	19	3.08 ± 0.29		6.13 ± 0.69	
	20	2.92 ± 0.51		5.75 ± 1.06	
	21	3.00 ± 0.35		5.75 ± 0.90	
	22	3.00 ± 0.55		5.50 ± 1.12	
	23	3.08 ± 0.45		5.00 ± 0.85	
	24	3.25 ± 0.43		4.63 ± 0.82	
	25	3.08 ± 0.48		5.75 ± 0.92	
	26	3.33 ± 0.43		4.50 ± 0.98	
	27	3.25 ± 0.45		5.00 ± 0.96	
	28	3.17 ± 0.32		5.00 ± 0.94	
	29	3.08 ± 0.47		4.38 ± 0.98	
	30	3.67 ± 0.43		5.00 ± 1.05	
	Statistics: two-way-ANOVA $F_{1/551}$ = 175.4 **p <0.001**				

	Parameter	Genotype	Data	n = preparation/cell	Statistics	p
C	**aver. AP freq. (Hz)**	Slack$^{+/+}$	2.77 ± 0.30	4/12	Unpaired t-test	**0.039**
		Slack$^{-/-}$	4.37 ± 0.71	4/10		
D	**AP thresh. (mV)**	Slack$^{+/+}$	-26.98 ± 1.63	4/12	Unpaired t test with Welch's correction	0,06
		Slack$^{-/-}$	-30.50 ± 0.69	4/10		
E	**AP ampl. (mV)**	Slack$^{+/+}$	89.57 ± 1.89	4/12	Unpaired t-test	0,48
		Slack$^{-/-}$	87.37 ± 2.52	4/10		

Supplementary Table 11: *Values and statistics of Figure 22*

B		Genotype			
		Slack$^{+/+}$		**Slack$^{-/-}$**	
	Time (s)	**Nr. of AP´s**	**n** = preparation/cell	**Nr. of AP´s**	**n** = preparation/cell
	0	0.00 ± 0.00	10/38	0.00 ± 0.00	7/33
	20	0.00 ± 0.00		0.00 ± 0.00	
	40	0.29 ± 0.16		0.91 ± 0.39	
	60	1.18 ± 0.42		2.16 ± 0.57	
	80	2.34± 0.56		4.16 ± 0.81	
	100	4.08 ± 0.68		6.07 ± 0.80	
	120	6.13 ± 0.81		8.28 ± 0.85	
	140	8.13 ± 0.86		9.83 ± 0.94	
	160	9.39 ± 0.88		11.03 ± 0.86	
	180	10.26 ± 0.90		12.69 ± 0.88	
	Statistics: Two-Way-ANOVA. $F_{1/668}$ = 20.50, **p < 0.0001**				

C	**Parameter**	**Genotype**	**Data**	**n** = preparation/cell	**Statistics**	**p**
	RMP (mV)	Slack$^{+/+}$	-54.20 ± 3.77	10/33	Mann Whitney test	0.62
		Slack$^{-/-}$	-52.93 ± 3.84	7/41		
D	**AP thresh. (mV)**	Slack$^{+/+}$	-25.78 ± 0.77	10/38	Mann Whitney test	**0.043**
		Slack$^{-/-}$	-27.46 ± 0.72	7/32		
F	**AP rise slope (mV)**	Slack$^{+/+}$	348.19 ± 29.27	10/34	Unpaired t-test	**0,041**
		Slack$^{-/-}$	434.84 ± 29.08	7/29		
G	**AP half-width (ms)**	Slack$^{+/+}$	2.27 ± 0.24	10/34	Mann Whitney test	0,094
		Slack$^{-/-}$	1.76 ± 0.06	7/29		
H	**AP ampl. (mV)**	Slack$^{+/+}$	86.92 ± 2.46	10/38	Mann Whitney test	0,59
		Slack$^{-/-}$	90.76 ± 1.52	7/32		
J	**aHP (mV)**	Slack$^{+/+}$	33.13 ± 0.96	10/36	Mann Whitney test	0.089
		Slack$^{-/-}$	30.87 ± 1.32	7/29		
K	**aHP duration (ms)**	Slack$^{+/+}$	138.59 ± 11.96	10/38	Mann Whitney test	**0.0009**
		Slack$^{-/-}$	84.87 ± 7.32	7/32		
	AP intervall (ms)	Slack$^{+/+}$	0.83 ± 0.16	10/29	Mann Whitney test	0,98
		Slack$^{-/-}$	0.87 ± 0.24	7/29		

Supplementary Table 12: *Values and statistics of Figure 23*

B	Pilo (mM)	Time (d)	Genotype	Rel. PI uptake	n = preparation/well/ROI	Statistics	p
	4	1	Slack$^{+/+}$	31.18 ± 4.80	5/8/21	two-way-ANOVA Sidak´s multiple comparison	0.097
			Slack$^{-/-}$	18.26 ± 4.05	5/7/21		
		2	Slack$^{+/+}$	40.11 ± 5.60	5/8/21		**0.007**
			Slack$^{-/-}$	21.54 ± 3.30	5/7/21		
		3	Slack$^{+/+}$	34.38 ± 3.45	5/8/21		0.213
			Slack$^{-/-}$	23.67 ± 3.81	5/7/21		
C	8	1	Slack$^{+/+}$	30.38 ± 3.71	5/8/21	two-way-ANOVA Sidak´s multiple comparison	0.112
			Slack$^{-/-}$	20.51 ± 3.63	5/7/24		
		2	Slack$^{+/+}$	47.52 ± 3.75	5/8/21		**0.003**
			Slack$^{-/-}$	31.46 ± 2.95	5/7/24		
		3	Slack$^{+/+}$	41.52 ± 3.15	5/8/21		0.277
			Slack$^{-/-}$	33.73 ± 2.33	5/7/24		

Supplementary Table 13: *Values and statistics of Supplementary Figure. 1*

A	KA (µM)	Time (d)	Genotype	Rel. PI uptake	n = preparation/well/ROI	Statistics	p
	1 h 20 µM	0.2	Slack$^{+/+}$	11.37 ± 2.57	4/8/21	two-way-ANOVA Sidak´s multiple comparison	$F_{1/233}$ = 12.44, **p = 0.0005**
			Slack$^{-/-}$	28.92 ± 4.85	4/8/24		
		1	Slack$^{+/+}$	36.29 ± 4.62	4/8/24		
			Slack$^{-/-}$	47.78 ± 3.59	4/8/30		
		2	Slack$^{+/+}$	38.42 ± 4.57	4/8/15		
			Slack$^{-/-}$	50.72 ± 3.30	4/8/21		
		3	Slack$^{+/+}$	35.28 ± 4.27	4/8/24		
			Slack$^{-/-}$	34.01 ± 2.56	4/8/30		
		7	Slack$^{+/+}$	13.28 ± 1.58	4/8/24		
			Slack$^{-/-}$	12.45 ± 1.36	4/8/30		

B	Treatment (µM)	Genotype	Data	n = preparation/well/ROI	Statistics	p
	Ctrl	Slack$^{+/+}$	4.32 ± 1.39	2/8/22	-	-
	5 KA	Slack$^{+/+}$	31.44 ± 4.36	2/8/18		
	10 Bith	Slack$^{+/+}$	14.50 ± 4.13	2/8/24		
	5 KA + 10 Bith	Slack$^{+/+}$	30.38 ± 4.53	2/8/21		
	Ctrl vs 5 KA	Slack$^{+/+}$	4.32 ± 1.39	2/8/22	Unpaired t-test	**<0.0001**
			31.44 ± 4.36	2/8/18		
	Ctrl vs 10 Bith	Slack$^{+/+}$	4.32 ± 1.39	2/8/22	Unpaired t-test	0.104
			14.50 ± 4.13	2/8/24		
	5 KA vs 5 KA + 10 Bith	Slack$^{+/+}$	31.44 ± 4.36	2/8/18	Unpaired t-test	0.286
			30.38 ± 4.53	2/8/21		

C	Treatment (µM)	Genotype	Data	n = preparation/well/ROI	Statistics	p
	Ctrl	Slack$^{+/+}$	10.56 ± 2.22	2/8/18	-	-
	5 KA	Slack$^{+/+}$	21.24 ± 4.99	2/8/15		
	100 Quin	Slack$^{+/+}$	29.10 ± 3.38	2/8/21		
	5 KA + 100 Quin	Slack$^{+/+}$	21.11 ± 3.82	2/8/24		
	Ctrl vs 5 KA	Slack$^{+/+}$	10.56 ± 2.22	2/8/18	Unpaired t-test	**0.0139**
			21.24 ± 4.99	2/8/15		
	Ctrl vs 100 Quin	Slack$^{+/+}$	10.56 ± 2.22	2/8/18	Unpaired t-test	0.122
			29.10 ± 3.38	2/8/21		
	5 KA vs 5 KA + 100 Quin	Slack$^{+/+}$	21.24 ± 4.99	2/8/15	Unpaired t-test	0.129
			21.11 ± 3.82	2/8/24		

Supplementary Table 14: *Values and statistics of Supplementary Figure. 2*

B	KA (µM)	Genotype	Data	n = preparation/well/ROI	Statistics	p
	10	Slack$^{+/+}$	1.88 ± 0.15	3/4/9	Unpaired t-test	0.482
		Slack$^{-/-}$	1.63 ± 0.07	3/4/9		
	50	Slack$^{+/+}$	2.01 ± 0.13	3/6/12	Unpaired t-test	0.847
		Slack$^{-/-}$	1.95 ± 0.11	3/6/12		
	100	Slack$^{+/+}$	2.62 ± 0.26	3/6/12	Unpaired t-test	0.616
		Slack$^{-/-}$	2.77 ± 0.24	3/6/12		
	500	Slack$^{+/+}$	2.53 ± 0.23	3/6/12	Unpaired t-test	**0.002**
		Slack$^{-/-}$	3.54 ± 0.34	3/6/12		

Supplementary Table 15. *Values and statistics of Supplementary Figure. 4*

C		Genotype			
		Slack$^{+/+}$		**Slack$^{-/-}$**	
	Voltage (mV)	**inward current (pA/pF)**	**n** = preparation/cell	**inward current (pA/pF)**	**n** = preparation/cell
	-60	-1.82 ± 1.11	6/34	-0.23 ± 0.10	7/33
	-40	-10.25 ± 9.21		-55.39 ± 25.43	
	-20	-133.82 ± 28.96		-154.20 ± 28.96	
	0	-100.91 ± 19.67		-115.72 ± 19.37	
	20	-67.14 ± 10.53		-71.16 ± 8.06	
	40	-33.78 ± 6.77		-31.98 ± 7.13	
	60	-2.50 ± 11.98		-4.20 ± 15.60	
	80	-28.25 ± 19.88		-30.24 ± 24.10	
	Statistics: Two-Way-ANOVA. $F_{1/516}$ = 1.093, p = 0.296				

Supplementary Table 16: *Values and statistics of Supplementary Figure. 5*

	Treatment (mM)	**Genotype**	**Max. ΔRatio$_{(340/380)}$**	**n** = preparation /well	**Statistics**
	1 Pilo	Slack$^{+/+}$	0.00 ± 0.00	4/9	two-way-ANOVA, $F_{1/64}$ = 0.2074, p =0.65
		Slack$^{-/-}$	0.00 ± 0.00	3/6	
	5 Pilo	Slack$^{+/+}$	-0.02 ± 0.00	4/9	
		Slack$^{-/-}$	-0.02 ± 0.00	3/6	
	10 Pilo	Slack$^{+/+}$	-0.02 ± 0.01	4/9	
		Slack$^{-/-}$	-0.01 ± 0.01	3/6	
	50 Pilo	Slack$^{+/+}$	0.16 ± 0.02	4/9	
		Slack$^{-/-}$	0.19 ± 0.04	3/6	
	100 Pilo	Slack$^{+/+}$	0.32 ± 0.03	4/9	
		Slack$^{-/-}$	0.25 ± 0.03	3/6	

Supplementary Table 17: *Values and statistics of Supplementary Figure. 6*

B	**KA (µM)**	**Time (d)**	**Genotype**	**Rel. PI uptake**	**n** = preparation/well/ROI	**Statistics**	**p**
	10	1	Slack$^{+/+}$	22.00 ± 2.90	3/6/15	two-way-ANOVA Sidak´s multiple comparison	0.64
			Slack$^{-/-}$	25.94 ± 3.39	3/6/14		
		2	Slack$^{+/+}$	31.49 ± 2.98	3/6/12		0.52
			Slack$^{-/-}$	36.61 ± 4.09	3/6/14		
C	20	1	Slack$^{+/+}$	17.02 ± 2.52	3/6/14	two-way-ANOVA Sidak´s multiple comparison	0.26
			Slack$^{-/-}$	12.42 ± 1.57	3/6/12		
		2	Slack$^{+/+}$	21.22 ± 2.40	3/6/12		0.86
			Slack$^{-/-}$	19.68 ± 2.03	3/6/12		

9. References

Adelman, J. P., Shen, K. Z., Kavanaugh, M. P., Warren, R. A., Wu, Y. N., Lagrutta, A., Bond, C. T., & North, R. A. (1992). Calcium-activated potassium channels expressed from cloned complementary DNAs. *Neuron*, *9*(2), 209–216. https://doi.org/10.1016/0896-6273(92)90160-f

Ahmed Juvale, I. I., & Che Has, A. T. (2020). The evolution of the pilocarpine animal model of status epilepticus. *Heliyon*, *6*(7), e04557. https://doi.org/10.1016/j.heliyon.2020.e04557

Albensi, B. C., Igoechi, C., Janigro, D., & Ilkanich, E. (2004). Why do many NMDA antagonists fail, while others are safe and effective at blocking excitotoxicity associated with dementia and acute injury? *American Journal of Alzheimer's Disease and Other Dementias*, *19*(5), 269–274. https://doi.org/10.1177/153331750401900502

Ali, S. R., Malone, T. J., Zhang, Y., Prechova, M., & Kaczmarek, L. K. (2020). Phactr1 regulates Slack (KCNT1) channels via protein phosphatase 1 (PP1). *FASEB Journal*, *34*(1), 1591–1601. https://doi.org/10.1096/fj.201902366R

Allaway, K. C., & Machold, R. (2017). Developmental specification of forebrain cholinergic neurons. *Developmental Biology*, *421*(1), 1–7. https://doi.org/10.1016/j.ydbio.2016.11.007

Allen, N. M., Conroy, J., Shahwan, A., Lynch, B., Correa, R. G., Pena, S. D. J., McCreary, D., Magalhães, T. R., Ennis, S., Lynch, S. A., & King, M. D. (2016). Unexplained early onset epileptic encephalopathy: Exome screening and phenotype expansion. *Epilepsia*, *57*(1), e12-7. https://doi.org/10.1111/epi.13250

Aminkeng, F. (2013a). KCNT1 mutations in ADNFLE and MMPSI: A new driver in the etiology and pathophysiology of early-onset epileptic syndromes. *Clinical Genetics*, *83*(4), 319–320. https://doi.org/10.1111/cge.12082

Aminkeng, F. (2013b). KCNT1 mutations in ADNFLE and MMPSI: A new driver in the etiology and pathophysiology of early-onset epileptic syndromes. *Clinical Genetics*, *83*(4), 319–320. https://doi.org/10.1111/cge.12082

Anderson, C. M., & Swanson, R. A. (2000). Astrocyte glutamate transport: review of properties, regulation, and physiological functions. *Glia*, *32*(1), 1–14.

Armstrong, N., Jasti, J., Beich-Frandsen, M., & Gouaux, E. (2006). Measurement of conformational changes accompanying desensitization in an ionotropic glutamate receptor. *Cell*, *127*(1), 85–97. https://doi.org/10.1016/j.cell.2006.08.037

Artinian, J., Peret, A., Mircheva, Y., Marti, G., & Crépel, V. (2015). Impaired neuronal operation through aberrant intrinsic plasticity in epilepsy. *Annals of Neurology*, *77*(4), 592–606. https://doi.org/10.1002/ana.24348

Atkinson, N. S., Robertson, G. A., & Ganetzky, B. (1991). A component of calcium-activated potassium channels encoded by the Drosophila slo locus. *Science (New York, N.Y.)*, *253*(5019), 551–555. https://doi.org/10.1126/science.1857984

Attali, B., Chandy, K. G., Giese, M. H., Grissmer, S., Gutman, G. A., Jan, L. Y., Lazdunski, M., Mckinnon, D., Nerbonne, J., Pardo, L. A., & Robertson, G. A. (2023). *Voltage-gated potassium channels (K v) in GtoPdb v . 2023 . 1*.

Attwell, D. (2000). Brain uptake of glutamate: food for thought. *The Journal of Nutrition*, *130*(4S Suppl), 1023S-5S. https://doi.org/10.1093/jn/130.4.1023S

Bader, C. R., Bernheim, L., & Bertrand, D. (1985). Sodium-activated potassium current in cultured avian neurones. *Nature*, *317*(6037), 540–542. https://doi.org/10.1038/317540a0

Ballinger, E. C., Ananth, M., Talmage, D. A., & Role, L. W. (2016). Basal Forebrain Cholinergic Circuits and Signaling in Cognition and Cognitive Decline. *Neuron*, *91*(6), 1199–1218. https://doi.org/10.1016/j.neuron.2016.09.006

Balzulat, A., Zhu, W. F., Flauaus, C., Hernandez-Olmos, V., Heering, J., Sethumadhavan, S., Dubiel, M., Frank, A., Menge, A., Hebchen, M., Metzner, K., Lu, R., Lukowski, R., Ruth, P., Knapp, S., Müller, S., Steinhilber, D., Hänelt, I., Stark, H., Schmidtko, A. (2023). Discovery of a new activator of Slack potassium channels with robust efficacy in models of histamine-independent and chronic itch. *BioRxiv*, 2023.10.05.560997. https://doi.org/10.1101/2023.10.05.560997

Banerjee, J., Dey, S., Dixit, A. B., Tripathi, M., Doddamani, R., Sharma, M. C., & Chandra, P. S. (2020). α7 nicotinic receptors contributes to glutamatergic activity in the hippocampus of patients with mesial temporal lobe epilepsy with hippocampal sclerosis (MTLE-HS). *Journal of Neural Transmission (Vienna, Austria : 1996)*, *127*(10), 1441–1446. https://doi.org/10.1007/s00702-020-02239-2

Barcia, G., Fleming, M. R., Deligniere, A., Gazula, V. R., Brown, M. R., Langouet, M., Chen, H., Kronengold, J., Abhyankar, A., Cilio, R., Nitschke, P., Kaminska, A., Boddaert, N., Casanova, J. L., Desguerre, I., Munnich, A., Dulac, O., Kaczmarek, L. K., Colleaux, L., & Nabbout, R. (2012). De novo gain-of-function KCNT1 channel mutations cause malignant migrating partial seizures of infancy. *Nature Genetics*, *44*(11), 1255–1259. https://doi.org/10.1038/ng.2441

Basbaum, A. I., Bautista, D. M., Scherrer, G., & Julius, D. (2009). Cellular and molecular mechanisms of pain. *Cell*, *139*(2), 267–284. https://doi.org/10.1016/j.cell.2009.09.028

Baulac, M., De Grissac, N., Hasboun, D., Oppenheim, C., Adam, C., Arzimanoglou, A., Semah, F., Lehéricy, S., Clémenceau, S., & Berger, B. (1998). Hippocampal developmental changes in patients with partial epilepsy: Magnetic resonance imaging and clinical aspects. *Annals of Neurology*, *44*(2), 223–233. https://doi.org/10.1002/ana.410440213

Baumann, S. W., Baur, R., & Sigel, E. (2002). Forced subunit assembly in alpha1beta2gamma2 GABAA receptors. Insight into the absolute arrangement. *The Journal of Biological Chemistry*, *277*(48), 46020–46025. https://doi.org/10.1074/jbc.M207663200

Bausch, A. E., Dieter, R., Nann, Y., Hausmann, M., Meyerdierks, N., Kaczmarek, L. K., Ruth, P., & Lukowski, R. (2015). The sodium-activated potassium channel Slack is required for optimal cognitive flexibility in mice. *Learning and Memory*, *22*(7), 323–335. https://doi.org/10.1101/lm.037820.114

Bausch, A. E., Ehinger, R., Straubinger, J., Zerfass, P., Nann, Y., & Lukowski, R. (2018). Loss of Sodium-Activated Potassium Channel Slack and FMRP Differentially Affect Social Behavior in Mice. *Neuroscience*, *384*, 361–374. https://doi.org/10.1016/j.neuroscience.2018.05.040

Bearden, D., Strong, A., Ehnot, J., DiGiovine, M., Dlugos, D., & Goldberg, E. M. (2014). Targeted treatment of migrating partial seizures of infancy with quinidine. *Annals of Neurology*, *76*(3), 457–461. https://doi.org/10.1002/ana.24229

Becker, A. J., Pitsch, J., Sochivko, D., Opitz, T., Staniek, M., Chen, C.-C., Campbell, K. P., Schoch, S., Yaari, Y., & Beck, H. (2008). Transcriptional upregulation of Cav3.2 mediates epileptogenesis in the pilocarpine model of epilepsy. *The Journal of Neuroscience : The Official Journal of the Society for Neuroscience*, *28*(49), 13341–13353. https://doi.org/10.1523/JNEUROSCI.1421-08.2008

Beghi, E. (2020). The Epidemiology of Epilepsy. *Neuroepidemiology*, *54*(2), 185–191. https://doi.org/10.1159/000503831

Ben-Ari, Y., & Cossart, R. (2000). Kainate, a double agent that generates seizures: two decades of progress. *Trends in Neurosciences*, *23*(11), 580–587. https://doi.org/https://doi.org/10.1016/S0166-2236(00)01659-3

Ben-Ari, Y., Tremblay, E., Riche, D., Ghilini, G., & Naquet, R. (1981). Electrographic, clinical and pathological alterations following systemic administration of kainic acid, bicuculline or pentetrazole: Metabolic mapping using the deoxyglucose method with special reference to the pathology of epilepsy. *Neuroscience*, *6*(7), 1361–1391. https://doi.org/10.1016/0306-4522(81)90193-7

Bernard, A., Ferhat, L., Dessi, F., Charton, G., Represa, A., Ben-Ari, Y., & Khrestchatisky, M. (1999). Q/R editing of the rat GluR5 and GluR6 kainate receptors in vivo and in vitro: evidence for independent developmental, pathological and cellular regulation. *The European Journal of Neuroscience*, *11*(2), 604–616. https://doi.org/10.1046/j.1460-9568.1999.00479.x

Best, N., Mitchell, J., Baimbridge, K. G., & Wheal, H. V. (1993). Changes in parvalbumin-immunoreactive neurons in the rat hippocampus following a kainic acid lesion. *Neuroscience Letters*, *155*(1), 1–6. https://doi.org/https://doi.org/10.1016/0304-3940(93)90660-D

Bezanilla, F. (2006b). The action potential: from voltage-gated conductances to molecular structures. *Biological Research*, *39*(3), 425–435. https://doi.org/10.4067/s0716-97602006000300005

Bhattacharjee, A., Gan, L., & Kaczmarek, L. K. (2002). Localization of the Slack potassium channel in the rat central nervous system. *The Journal of Comparative Neurology*, *454*(3), 241–254. https://doi.org/10.1002/cne.10439

Bhattacharjee, A., Joiner, W. J., Wu, M., Yang, Y., Sigworth, F. J., & Kaczmarek, L. K. (2003a). Channel Inhibited by ATP. *Bioinformatics*, *23*(37), 11681–11691.

Bhattacharjee, A., Joiner, W. J., Wu, M., Yang, Y., Sigworth, F. J., & Kaczmarek, L. K. (2003b). Slick (Slo2.1), a rapidly-gating sodium-activated potassium channel inhibited by ATP. *The Journal of Neuroscience : The Official Journal of the Society for Neuroscience*, *23*(37), 11681–11691. https://doi.org/10.1523/JNEUROSCI.23-37-11681.2003

Bhattacharjee, A., & Kaczmarek, L. K. (2005a). For K+ channels, Na+ is the new Ca2+. *Trends in Neurosciences*, *28*(8), 422–428. https://doi.org/10.1016/j.tins.2005.06.003

Bhattacharjee, A., & Kaczmarek, L. K. (2005b). For K+ channels, Na+ is the new Ca2+. *Trends in Neurosciences*, *28*(8), 422–428. https://doi.org/10.1016/j.tins.2005.06.003

Bianchi, M. T., & Macdonald, R. L. (2002). Slow phases of GABA(A) receptor desensitization: structural determinants and possible relevance for synaptic function. *The Journal of Physiology*, *544*(Pt 1), 3–18. https://doi.org/10.1113/jphysiol.2002.020255

Bischof, H., Rehberg, M., Stryeck, S., Artinger, K., Eroglu, E., Waldeck-Weiermair, M., Gottschalk, B., Rost, R., Deak, A. T., Niedrist, T., Vujic, N., Lindermuth, H., Prassl, R., Pelzmann, B., Groschner, K., Kratky, D., Eller, K., Rosenkranz, A. R., Madl, T., Malli, R. (2017). Novel genetically encoded fluorescent probes enable real-Time detection of potassium in vitro and in vivo. *Nature Communications*, *8*(1), 1–11. https://doi.org/10.1038/s41467-017-01615-z

Biton, B., Sethuramanujam, S., Picchione, K. E., Bhattacharjee, A., Khessibi, N., Chesney, F., Lanneau, C., Curet, O., & Avenet, P. (2012). The Antipsychotic Drug Loxapine Is an Opener of the Sodium-Activated Potassium Channel Slack (Slo2.2). *Journal of Pharmacology and Experimental Therapeutics*, *340*(3), 706–715. https://doi.org/10.1124/jpet.111.184622

Bloss, E. B., & Hunter, R. G. (2010). Hippocampal kainate receptors. *Vitamins and Hormones*, *82*, 167–184. https://doi.org/10.1016/S0083-6729(10)82009-6

Blümcke, I., Thom, M., Aronica, E., Armstrong, D. D., Bartolomei, F., Bernasconi, A., Bernasconi, N., Bien, C. G., Cendes, F., Coras, R., Cross, J. H., Jacques, T. S., Kahane, P., Mathern, G. W., Miyata, H., Moshé, S. L., Oz, B., Özkara, Ç., Perucca, E., Spreafico, R. (2013). International consensus classification of hippocampal sclerosis in temporal lobe epilepsy: a Task Force report from the ILAE Commission on Diagnostic Methods. *Epilepsia*, *54*(7), 1315–1329. https://doi.org/10.1111/epi.12220

Blusztajn, J. K., & Rinnofner, J. (2016). Intrinsic cholinergic neurons in the hippocampus: Fact or artifact? *Frontiers in Synaptic Neuroscience*, *8*(MAR), 6–11. https://doi.org/10.3389/fnsyn.2016.00006

Bonardi, C. M., Heyne, H. O., Fiannacca, M., Fitzgerald, M. P., Gardella, E., Gunning, B., Olofsson, K., Lesca, G., Verbeek, N., Stamberger, H., Striano, P., Zara, F., Mancardi, M. M., Nava, C., Syrbe, S., Buono, S., Baulac, S., Coppola, A., Weckhuysen, S., Rubboli, G. (2021). KCNT1-related epilepsies and epileptic encephalopathies: phenotypic and mutational spectrum. *Brain : A Journal of Neurology*, *144*(12), 3635–3650. https://doi.org/10.1093/brain/awab219

Brown, D. A., & Passmore, G. M. (2009). Neural KCNQ (Kv7) channels. *British Journal of Pharmacology*, *156*(8), 1185–1195. https://doi.org/10.1111/j.1476-5381.2009.00111.x

Brown, M. R., Kronengold, J., Gazula, V.-R., Chen, Y., Strumbos, J. G., Sigworth, F. J., Navaratnam, D., & Kaczmarek, L. K. (2010). Fragile X mental retardation protein controls gating of the sodium-activated potassium channel Slack. *Nature Neuroscience*, *13*(7), 819–821. https://doi.org/10.1038/nn.2563

Brown, M. R., Kronengold, J., Gazula, V. R., Spilianakis, C. G., Flavell, R. A., von Hehn, C. A. A., Bhattacharjee, A., & Kaczmarek, L. K. (2008). Amino-termini isoforms of the Slack K+ channel, regulated by alternative promoters, differentially modulate rhythmic firing and adaptation. *Journal of Physiology*, *586*(21), 5161–5179. https://doi.org/10.1113/jphysiol.2008.160861

Browning, R., Maggio, R., Sahibzada, N., & Gale, K. (1993). Role of Brainstem Structures in Seizures Initiated from the Deep Prepiriform Cortex of Rats. *Epilepsia*, *34*(3), 393–407. https://doi.org/10.1111/j.1528-1157.1993.tb02579.x

Budelli, G., Hage, T. a, Wei, A., Rojas, P., Jong, I. Y., Malley, K. O., Salkoff, L., & Mo, L. (2009). *Current in Neurons During Normal Physiology*. *12*(6), 745–750. https://doi.org/10.1038/nn.2313.Na

Burbano, L. E., Li, M., Jancovski, N., Jafar-Nejad, P., Richards, K., Sedo, A., Soriano, A., Rollo, B., Jia, L., Gazina, E. V., Piltz, S., Adikusuma, F., Thomas, P. Q., Kopsidas, H., Rigo, F., Reid, C. A., Maljevic, S., & Petrou, S. (2022). Antisense oligonucleotide therapy for KCNT1 encephalopathy. *JCI Insight*, *7*(23). https://doi.org/10.1172/jci.insight.146090

Butler, A., Tsunoda, S., McCobb, D. P., Wei, A., & Salkoff, L. (1993). mSlo,a complex mouse gene encoding “Maxi” calcium-activated potassium channels. *Science*, *261*(7), 221–224.

Byers, N., Hahm, E. T., & Tsunoda, S. (2021). Slo2/KNa Channels in drosophila protect against spontaneous and induced seizure-like behavior associated with an increased persistent na1 current. *Journal of Neuroscience*, *41*(43), 9047–9063. https://doi.org/10.1523/JNEUROSCI.0290-21.2021

Cai, K., Wang, J., Eissman, J., Wang, J., Nwosu, G., Shen, W., Liang, H.-C., Li, X.-J., Zhu, H.-X., Yi, Y.-H., Song, J., Xu, D., Delpire, E., Liao, W.-P., Shi, Y.-W., & Kang, J.-Q. (2019). A missense mutation in SLC6A1 associated with Lennox-Gastaut syndrome impairs GABA transporter 1 protein trafficking and function. *Experimental Neurology*, *320*, 112973. https://doi.org/10.1016/j.expneurol.2019.112973

Carranza Rojo, D., Hamiwka, L., McMahon, J. M., Dibbens, L. M., Arsov, T., Suls, A., Stödberg, T., Kelley, K., Wirrell, E., Appleton, B., MacKay, M., Freeman, J. L., Yendle, S. C., Berkovic, S. F., Bienvenu, T., De Jonghe, P., Thorburn, D. R., Mulley, J. C., Mefford, H. C., & Scheffer, I. E. (2011). De novo SCN1A mutations in migrating partial seizures of infancy. *Neurology*, *77*(4), 380–383. https://doi.org/10.1212/WNL.0b013e318227046d

Catterall, W. A., Goldin, A. L., & Waxman, S. G. (2005). International Union of Pharmacology. XLVII. Nomenclature and structure-function relationships of voltage-gated sodium channels. *Pharmacological Reviews*, *57*(4), 397–409. https://doi.org/10.1124/pr.57.4.4

Caulfield, M. P., & Birdsall, N. J. M. (1998). International union of pharmacology. XVII. Classification of muscarinic acetylcholine receptors. *Pharmacological Reviews*, *50*(2), 279–290.

Cavazos, J. E., Zhang, P., Qazi, R., & Sutula, T. P. (2003). Ultrastructural features of sprouted mossy fiber synapses in kindled and kainic acid-treated rats. *The Journal of Comparative Neurology*, *458*(3), 272–292. https://doi.org/10.1002/cne.10581

Chakrabarti, A., Bagnall, A., Chue, P., Fenton, M., Palaniswamy, V., Wong, W., & Xia, J. (2007). Loxapine for schizophrenia. *Cochrane Database of Systematic Reviews*, *4*. https://doi.org/10.1002/14651858.CD001943.pub2

Chatterton, J. E., Awobuluyi, M., Premkumar, L. S., Takahashi, H., Talantova, M., Shin, Y., Cui, J., Tu, S., Sevarino, K. A., Nakanishi, N., Tong, G., Lipton, S. A., & Zhang, D. (2002). Excitatory glycine receptors containing the NR3 family of NMDA receptor subunits. *Nature*, *415*(6873), 793–798. https://doi.org/10.1038/nature715

Chen, H., Kronengold, J., Yan, Y., Gazula, V. R., Brown, M. R., Ma, L., Ferreira, G., Yang, Y., Bhattacharjee, A., Sigworth, F. J., Salkoff, L., & Kaczmarek, L. K. (2009). The N-terminal domain of slack determines the formation and trafficking of slick/slack heteromeric sodium-activated potassium channels. *Journal of Neuroscience*, *29*(17), 5654–5665. https://doi.org/10.1523/JNeurosci.5978-08.2009

Choi, D. W. (1994). Glutamate receptors and the induction of excitotoxic neuronal death. *Progress in Brain Research*, *100*, 47–51. https://doi.org/10.1016/s0079-6123(08)60767-0

Chow, C. Y., Absalom, N., Biggs, K., King, G. F., & Ma, L. (2020). Venom-derived modulators of epilepsy-related ion channels. *Biochemical Pharmacology*, *181*(May), 114043. https://doi.org/10.1016/j.bcp.2020.114043

Chuang, S.-H., & Reddy, D. S. (2018). Genetic and Molecular Regulation of Extrasynaptic GABA-A Receptors in the Brain: Therapeutic Insights for Epilepsy. *The Journal of Pharmacology and Experimental Therapeutics*, *364*(2), 180–197. https://doi.org/10.1124/jpet.117.244673

Clark, B. D., Goldberg, E. M., & Rudy, B. (2009). Electrogenic tuning of the axon initial segment. *The Neuroscientist : A Review Journal Bringing Neurobiology, Neurology and Psychiatry*, *15*(6), 651–668. https://doi.org/10.1177/1073858409341973

Combi, R., Dalprà, L., Tenchini, M. L., & Ferini-Strambi, L. (2004). Autosomal dominant nocturnal frontal lobe epilepsy. *Journal of Neurology*, *251*(8), 923–934. https://doi.org/10.1007/s00415-004-0541-x

Corner, M. A., & Ramakers, G. J. (1992). Spontaneous firing as an epigenetic factor in brain development--physiological consequences of chronic tetrodotoxin and picrotoxin exposure on cultured rat neocortex neurons. *Brain Research. Developmental Brain Research*, *65*(1), 57–64. https://doi.org/10.1016/0165-3806(92)90008-k

Crowley, L. C., Scott, A. P., Marfell, B. J., Boughaba, J. A., Chojnowski, G., & Waterhouse, N. J. (2016). Measuring cell death by propidium iodide uptake and flow cytometry. *Cold Spring Harbor Protocols*, *2016*(7), 647–651. https://doi.org/10.1101/pdb.prot087163

Curia, G., Longo, D., Biagini, G., Jones, R. S. G., & Avoli, M. (2008). The pilocarpine model of temporal lobe epilepsy. *Journal of Neuroscience Methods*, *172*(2), 143–157. https://doi.org/10.1016/j.jneumeth.2008.04.019

Daikhin, Y., & Yudkoff, M. (2000). Compartmentation of brain glutamate metabolism in neurons and glia. *The Journal of Nutrition*, *130*(4S Suppl), 1026S-31S. https://doi.org/10.1093/jn/130.4.1026S

Dannenberg, H., Young, K., & Hasselmo, M. (2017). Modulation of hippocampal circuits by muscarinic and nicotinic receptors. *Frontiers in Neural Circuits*, *11*(December), 1–18. https://doi.org/10.3389/fncir.2017.00102

Darstein, M., Petralia, R. S., Swanson, G. T., Wenthold, R. J., & Heinemann, S. F. (2003). Distribution of kainate receptor subunits at hippocampal mossy fiber synapses. *The Journal of Neuroscience : The Official Journal of the Society for Neuroscience*, *23*(22), 8013–8019. https://doi.org/10.1523/JNEUROSCI.23-22-08013.2003

Das, A., Wallace, G. C. 4th, Holmes, C., McDowell, M. L., Smith, J. A., Marshall, J. D., Bonilha, L., Edwards, J. C., Glazier, S. S., Ray, S. K., & Banik, N. L. (2012). Hippocampal tissue of patients with refractory temporal lobe epilepsy is associated with astrocyte activation, inflammation, and altered expression of channels and receptors. *Neuroscience*, *220*, 237–246. https://doi.org/10.1016/j.neuroscience.2012.06.002

De Fusco, M., Becchetti, A., Patrignani, A., Annesi, G., Gambardella, A., Quattrone, A., Ballabio, A., Wanke, E., & Casari, G. (2000). The nicotinic receptor beta 2 subunit is mutant in nocturnal frontal lobe epilepsy. *Nature Genetics*, *26*(3), 275–276. https://doi.org/10.1038/81566

Descalzo, V. F., Nowak, L. G., Brumberg, J. C., McCormick, D. A., & Sanchez-Vives, M. V. (2005). Slow adaptation in fast-spiking neurons of visual cortex. *Journal of Neurophysiology*, *93*(2), 1111–1118. https://doi.org/10.1152/jn.00658.2004

Dingledine, R., Borges, K., Bowie, D., & Traynelis, S. F. (1999). The glutamate receptor ion channels. *Pharmacological Reviews*, *51*(1), 7–61.

Drexel, M., Preidt, A. P., & Sperk, G. (2012). Sequel of spontaneous seizures after kainic acid-induced status epilepticus and associated neuropathological changes in the subiculum and entorhinal cortex. *Neuropharmacology*, *63*(5), 806–817. https://doi.org/10.1016/j.neuropharm.2012.06.009

Dryer, S. E. (1991). Na(+)-activated K+ channels and voltage-evoked ionic currents in brain stem and parasympathetic neurones of the chick. *The Journal of Physiology*, *435*, 513–532. https://doi.org/10.1113/jphysiol.1991.sp018522

Dryer, S. E. (1994). Na+-activated K+ channels: a new family of large-conductance ion channels. *Trends in Neurosciences*, *17*(4), 155–160. https://doi.org/10.1016/0166-2236(94)90093-0

Du, W., Bautista, J. F., Yang, H., Diez-Sampedro, A., You, S.-A., Wang, L., Kotagal, P., Lüders, H. O., Shi, J., Cui, J., Richerson, G. B., & Wang, Q. K. (2005). Calcium-sensitive potassium channelopathy in human epilepsy and paroxysmal movement disorder. *Nature Genetics*, *37*(7), 733–738. https://doi.org/10.1038/ng1585

Dudek, F. E., & Staley, K. J. (2012). *The Time Course and Circuit Mechanisms of Acquired Epileptogenesis.* (J. L. Noebels, M. Avoli, M. A. Rogawski, R. W. Olsen, & A. V Delgado-Escueta (eds.)).

Dudok, B., Klein, P. M., & Soltesz, I. (2022). Toward Understanding the Diverse Roles of Perisomatic Interneurons in Epilepsy. *Epilepsy Currents*, *22*(1), 54–60. https://doi.org/10.1177/15357597211053687

Duflocq, A., Le Bras, B., Bullier, E., Couraud, F., & Davenne, M. (2008). Nav1.1 is predominantly expressed in nodes of Ranvier and axon initial segments. *Molecular and Cellular Neurosciences*, *39*(2), 180–192. https://doi.org/10.1016/j.mcn.2008.06.008

During, M. J., & Spencer, D. D. (1993). Extracellular hippocampal glutamate and spontaneous seizure in the conscious human brain. *Lancet (London, England)*, *341*(8861), 1607–1610. https://doi.org/10.1016/0140-6736(93)90754-5

Eaton, S. A., Jane, D. E., Jones, P. L., Porter, R. H., Pook, P. C., Sunter, D. C., Udvarhelyi, P. M., Roberts, P. J., Salt, T. E., & Watkins, J. C. (1993). Competitive antagonism at metabotropic glutamate receptors by (S)-4-carboxyphenylglycine and (RS)-alpha-methyl-4-carboxyphenylglycine. *European Journal of Pharmacology*, *244*(2), 195–197. https://doi.org/10.1016/0922-4106(93)90028-8

Egan, T. M., Dagan, D., Kupper, J., & Levitan, I. B. (1992). Na(+)-activated K+ channels are widely distributed in rat CNS and in Xenopus oocytes. *Brain Research*, *584*(1–2), 319–321. https://doi.org/10.1016/0006-8993(92)90913-t

Ehinger, R., Kuret, A., Matt, L., Frank, N., Wild, K., Kabagema-Bilan, C., Bischof, H., Malli, R., Ruth, P., Bausch, A. E., & Lukowski, R. (2021). Slack K+ channels attenuate NMDA-induced excitotoxic brain damage and neuronal cell death. *FASEB Journal*, *35*(5), 1–20. https://doi.org/10.1096/fj.202002308RR

Ehlers, M. D. (2000). Reinsertion or degradation of AMPA receptors determined by activity-dependent endocytic sorting. *Neuron*, *28*(2), 511–525. https://doi.org/10.1016/s0896-6273(00)00129-x

Engel, J. J. (2001). Mesial temporal lobe epilepsy: what have we learned? *The Neuroscientist : A Review Journal Bringing Neurobiology, Neurology and Psychiatry*, *7*(4), 340–352. https://doi.org/10.1177/107385840100700410

Eretz, P., & Avie, L. (2001). Sleep Disturbances in the Wake of Traumatic Events. *N Engl J Med*, *345*(25), 137–146. doi: 10.1056/NEJMra012893

Evely, K. M., Pryce, K. D., & Bhattacharjee, A. (2017). The Phe932Ile mutation in KCNT1 channels associated with severe epilepsy, delayed myelination and leukoencephalopathy produces a loss-of-function channel phenotype. *Neuroscience*, *351*, 65–70. https://doi.org/10.1016/j.neuroscience.2017.03.035

Falco-Walter, J. (2020). Epilepsy-Definition, Classification, Pathophysiology, and Epidemiology. *Seminars in Neurology*, *40*(6), 617–623. https://doi.org/10.1055/s-0040-1718719

Farrant, M., & Nusser, Z. (2005). Variations on an inhibitory theme: Phasic and tonic activation of GABA A receptors. *Nature Reviews Neuroscience*, *6*(3), 215–229. https://doi.org/10.1038/nrn1625

Fernández de Sevilla, D., & Buño, W. (2010). The muscarinic long-term enhancement of NMDA and AMPA receptor-mediated transmission at Schaffer collateral synapses develop through different intracellular mechanisms. *The Journal of Neuroscience : The Official Journal of the Society for Neuroscience*, *30*(33), 11032–11042. https://doi.org/10.1523/JNEUROSCI.1848-10.2010

Ferraguti, F., & Shigemoto, R. (2006). Metabotropic glutamate receptors. *Cell and Tissue Research*, *326*(2), 483–504. https://doi.org/10.1007/s00441-006-0266-5

Fiest, K. M., Sauro, K. M., Wiebe, S., Patten, S. B., Dykeman, J., Pringsheim, T., & Lorenzetti, D. L. (2017). Fiest KM, Sauro KM, Wiebe S, Patten SB, Kwon CS, Dykeman J, et al. Prevalence and Incidence of Epilepsy: A Systematic Review and Meta-analysis of International Studies. Neurology. January 2017; 88(3): 296-303. *Neurology*, *88*(3), 296–303.

Fiorillo, C. D., & Williams, J. T. (1998). Glutamate mediates an inhibitory postsynaptic potential in dopamine neurons. *Nature*, *394*(6688), 78–82. https://doi.org/10.1038/27919

Fisahn, A., Yamada, M., Duttaroy, A., Gan, J.-W., Deng, C.-X., McBain, C. J., & Wess, J. (2002). Muscarinic induction of hippocampal gamma oscillations requires coupling of the M1 receptor to two mixed cation currents. *Neuron*, *33*(4), 615–624. https://doi.org/10.1016/s0896-6273(02)00587-1

Fisher, R. S., Cross, J. H., French, J. A., Higurashi, N., Hirsch, E., Jansen, F. E., Lagae, L., Moshé, S. L., Peltola, J., Roulet Perez, E., Scheffer, I. E., & Zuberi, S. M. (2017). Operational classification of seizure types by the International League Against Epilepsy: Position Paper of the ILAE Commission for Classification and Terminology. *Epilepsia*, *58*(4), 522–530. https://doi.org/10.1111/epi.13670

Fisher, R. S., Van Emde Boas, W., Blume, W., Elger, C., Genton, P., Lee, P., & Engel, J. (2005). Response: Definitions proposed by the International League Against Epilepsy (ILAE) and the International Bureau for Epilepsy (IBE) [4]. *Epilepsia*, *46*(10), 1701–1702. https://doi.org/10.1111/j.1528-1167.2005.00273_4.x

Fleming, M. R., Brown, M. R., Kronengold, J., Zhang, Y., Jenkins, D. P., Barcia, G., Nabbout, R., Bausch, A. E., Ruth, P., Lukowski, R., Navaratnam, D. S., & Kaczmarek, L. K. (2016). *Stimulation of Slack K+ channels alters mass at the plasma membrane by triggering dissociation of a phosphatase- regulatory complex Matthew*. *16*(9), 2281–2288. https://doi.org/10.1016/j.celrep.2016.07.024.Stimulation

Fourcaud-Trocmé, N., Zbili, M., Duchamp-Viret, P., & Kuczewski, N. (2022). Afterhyperpolarization Promotes the Firing of Mitral Cells through a Voltage-Dependent Modification of Action Potential Threshold. *ENeuro*, *9*(2), 1–21. https://doi.org/10.1523/ENEURO.0401-21.2021

Foust, A. J., Yu, Y., Popovic, M., Zecevic, D., & McCormick, D. A. (2011). Somatic membrane potential and Kv1 channels control spike repolarization in cortical axon collaterals and presynaptic boutons. *The Journal of Neuroscience : The Official Journal of the Society for Neuroscience*, *31*(43), 15490–15498. https://doi.org/10.1523/JNEUROSCI.2752-11.2011

Franceschetti, S., Lavazza, T., Curia, G., Aracri, P., Panzica, F., Sancini, G., Avanzini, G., & Magistrett, J. (2003). Na+-activated K+ current contributes to postexcitatory hyperpolarization in neocortical intrinsically bursting neurons. *Journal of Neurophysiology*, *89*(4), 2101–2111. https://doi.org/10.1152/jn.00695.2002

Friedman, A., Behrens, C. J., & Heinemann, U. (2007). Cholinergic dysfunction in temporal lobe epilepsy. *Epilepsia*, *48 Suppl 5*, 126–130. https://doi.org/10.1111/j.1528-1167.2007.01300.x

Fritsch, B., Reis, J., Gasior, M., Kaminski, R. M., & Rogawski, M. A. (2014). Role of GluK1 kainate receptors in seizures, epileptic discharges, and epileptogenesis. *The Journal of Neuroscience : The Official Journal of the Society for Neuroscience*, *34*(17), 5765–5775. https://doi.org/10.1523/JNEUROSCI.5307-13.2014

Frotscher, M., Schlander, M., & Léránth, C. (1986). Cholinergic neurons in the hippocampus. *Cell and Tissue Research*, *246*(2), 293–301. https://doi.org/10.1007/bf00215891

Fujita, S., Toyoda, I., Thamattoor, A. K., & Buckmaster, P. S. (2014). Preictal activity of subicular, CA1, and dentate gyrus principal neurons in the dorsal hippocampus before spontaneous seizures in a rat model of temporal lobe epilepsy. *The Journal of Neuroscience : The Official Journal of the Society for Neuroscience*, *34*(50), 16671–16687. https://doi.org/10.1523/JNEUROSCI.0584-14.2014

Fukunaga, K., Soderling, T. R., & Miyamoto, E. (1992). Activation of Ca2+/calmodulin-dependent protein kinase II and protein kinase C by glutamate in cultured rat hippocampal neurons. *The Journal of Biological Chemistry*, *267*(31), 22527–22533.

Gallyas, F. J., Ball, S. M., & Molnar, E. (2003). Assembly and cell surface expression of KA-2 subunit-containing kainate receptors. *Journal of Neurochemistry*, *86*(6), 1414–1427. https://doi.org/10.1046/j.1471-4159.2003.01945.x

Gao, K., Tankovic, A., Zhang, Y., Kusumoto, H., Zhang, J., Chen, W., XiangWei, W., Shaulsky, G. H., Hu, C., Traynelis, S. F., Yuan, H., & Jiang, Y. (2017). A de novo loss-of-function GRIN2A mutation associated with childhood focal epilepsy and acquired epileptic aphasia. *PloS One*, *12*(2), e0170818. https://doi.org/10.1371/journal.pone.0170818

Gasser, A., Ho, T. S.-Y., Cheng, X., Chang, K.-J., Waxman, S. G., Rasband, M. N., & Dib-Hajj, S. D. (2012). An ankyrinG-binding motif is necessary and sufficient for targeting Nav1.6 sodium channels to axon initial segments and nodes of Ranvier. *The Journal of Neuroscience : The Official Journal of the Society for Neuroscience*, *32*(21), 7232–7243. https://doi.org/10.1523/JNEUROSCI.5434-11.2012

Gertler, T. S., Cherian, S., DeKeyser, J. M., Kearney, J. A., & George, A. L. (2022). KNa1.1 gain-of-function preferentially dampens excitability of murine parvalbumin-positive interneurons. *Neurobiology of Disease*, *168*. https://doi.org/10.1016/j.nbd.2022.105713

Gillessen, T., Budd, S. L., & Lipton, S. A. (2002). Excitatory amino acid neurotoxicity. *Advances in Experimental Medicine and Biology*, *513*, 3–40. https://doi.org/10.1007/978-1-4615-0123-7_1

Gingrich, K. J., Roberts, W. A., & Kass, R. S. (1995). Dependence of the GABAA receptor gating kinetics on the alpha-subunit isoform: implications for structure-function relations and synaptic transmission. *The Journal of Physiology*, *489 (Pt 2*(Pt 2), 529–543. https://doi.org/10.1113/jphysiol.1995.sp021070

Glaum, S. R., & Miller, R. J. (1992). Metabotropic glutamate receptors mediate excitatory transmission in the nucleus of the solitary tract. *The Journal of Neuroscience : The Official Journal of the Society for Neuroscience*, *12*(6), 2251–2258. https://doi.org/10.1523/JNEUROSCI.12-06-02251.1992

Glykys, J., & Mody, I. (2007). Activation of GABAA receptors: views from outside the synaptic cleft. *Neuron*, *56*(5), 763–770. https://doi.org/10.1016/j.neuron.2007.11.002

Goldberg, E. M., & Coulter, D. A. (2013). Mechanisms of epileptogenesis: A convergence on neural circuit dysfunction. *Nature Reviews Neuroscience*, *14*(5), 337–349. https://doi.org/10.1038/nrn3482

Goldin, A. L. (2001). Resurgence of Sodium Channel Research. *Annual Review of Physiology*, *63*(1), 871–894. https://doi.org/10.1146/annurev.physiol.63.1.871

González, C., Baez-Nieto, D., Valencia, I., Oyarzún, I., Rojas, P., Naranjo, D., & Latorre, R. (2012a). K+ channels: Function-structural overview. *Comprehensive Physiology*, *2*(3), 2087–2149. https://doi.org/10.1002/cphy.c110047

Graebenitz, S., Kedo, O., Speckmann, E.-J., Gorji, A., Panneck, H., Hans, V., Palomero-Gallagher, N., Schleicher, A., Zilles, K., & Pape, H.-C. (2011). Interictal-like network activity and receptor expression in the epileptic human lateral amygdala. *Brain : A Journal of Neurology*, *134*(Pt 10), 2929–2947. https://doi.org/10.1093/brain/awr202

Griffin, A. M., Kahlig, K. M., Hatch, R. J., Hughes, Z. A., Chapman, M. L., Antonio, B., Marron, B. E., Wittmann, M., & Martinez-Botella, G. (2021). Discovery of the First Orally Available, Selective KNa1.1 Inhibitor: In Vitro and in Vivo Activity of an Oxadiazole Series. *ACS Medicinal Chemistry Letters*, *12*(4), 593–602. https://doi.org/10.1021/acsmedchemlett.0c00675

Gröticke, I., Hoffmann, K., & Löscher, W. (2007). Behavioral alterations in the pilocarpine model of temporal lobe epilepsy in mice. *Experimental Neurology*, *207*(2), 329–349. https://doi.org/10.1016/j.expneurol.2007.06.021

Guatteo, E., Bengtson, C. P., Bernardi, G., & Mercuri, N. B. (2004). Voltage-gated calcium channels mediate intracellular calcium increase in weaver dopaminergic neurons during stimulation of D2 and GABA B receptors. *Journal of Neurophysiology*, *92*(6), 3368–3374. https://doi.org/10.1152/jn.00602.2004

Gutman, G. A., Chandy, K. G., Grissmer, S., Lazdunski, M., McKinnon, D., Pardo, L. A., Robertson, G. A., Rudy, B., Sanguinetti, M. C., Stühmer, W., & Wang, X. (2005). International Union of Pharmacology. LIII. Nomenclature and molecular relationships of voltage-gated potassium channels. *Pharmacological Reviews*, *57*(4), 473–508. https://doi.org/10.1124/pr.57.4.10

Haam, J., Zhou, J., Cui, G., & Yakel, J. L. (2018). Septal cholinergic neurons gate hippocampal output to entorhinal cortex via oriens lacunosum moleculare interneurons. *Proceedings of the National Academy of Sciences of the United States of America*, *115*(8), E1886–E1895. https://doi.org/10.1073/pnas.1712538115

Haas, K. F., & Macdonald, R. L. (1999). GABAA receptor subunit gamma2 and delta subtypes confer unique kinetic properties on recombinant GABAA receptor currents in mouse fibroblasts. *The Journal of Physiology*, *514 (Pt 1*(Pt 1), 27–45. https://doi.org/10.1111/j.1469-7793.1999.027af.x

Haas, K. Z., Sperber, E. F., Opanashuk, L. A., Stanton, P. K., & Moshé, S. L. (2001). Resistance of immature hippocampus to morphologic and physiologic alterations following status epilepticus or kindling. *Hippocampus*, *11*(6), 615–625. https://doi.org/10.1002/hipo.1076

Hage, T. A., & Salkoff, L. (2012). *to Persistent Sodium Currents*. *32*(8), 2714–2721. https://doi.org/10.1523/JNEUROSCI.5088-11.2012.Sodium-Activated

Hamilton, S. E., Loose, M. D., Qi, M., Levey, A. I., Hille, B., McKnight, G. S., Idzerda, R. L., & Nathanson, N. M. (1997). Disruption of the m1 receptor gene ablates muscarinic receptor-dependent M current regulation and seizure activity in mice. *Proceedings of the National Academy of Sciences of the United States of America*, *94*(24), 13311–13316. https://doi.org/10.1073/pnas.94.24.13311

Hansen, K. B., Wollmuth, L. P., Bowie, D., Furukawa, H., Menniti, F. S., Sobolevsky, A. I., Swanson, G. T., Swanger, S. A., Greger, I. H., Nakagawa, T., McBain, C. J., Jayaraman, V., Low, C.-M., Dell'Acqua, M. L., Diamond, J. S., Camp, C. R., Perszyk, R. E., Yuan, H., & Traynelis, S. F. (2021). Structure, Function, and Pharmacology of Glutamate Receptor Ion Channels. *Pharmacological Reviews*, *73*(4), 298–487. https://doi.org/10.1124/pharmrev.120.000131

Hansen, N., Widman, G., Hattingen, E., Elger, C. E., & Kunz, W. S. (2017). Mesial temporal lobe epilepsy associated with KCNT1 mutation. *Seizure*, *45*, 181–183. https://doi.org/10.1016/j.seizure.2016.12.018

Happ, D. F., & Tasker, R. A. (2016). A method for objectively quantifying propidium iodide exclusion in organotypic hippocampal slice cultures. *Journal of Neuroscience Methods*, *269*, 1–5. https://doi.org/10.1016/j.jneumeth.2016.05.006

Hasham, M. I., Pelech, S. L., & Krieger, C. (1997). Glutamate-mediated activation of protein kinase C in hippocampal neurons. *Neuroscience Letters*, *228*(2), 115–118. https://doi.org/10.1016/s0304-3940(97)00382-0

Hauser, W. A., Annegers, J. F., & Kurland, L. T. (1993). Incidence of Epilepsy and Unprovoked Seizures in Rochester, Minnesota: 1935–1984. *Epilepsia*, *34*(3), 453–458. https://doi.org/10.1111/j.1528-1157.1993.tb02586.x

Heginbotham, L., Abramson, T., & MacKinnon, R. (1992). A functional connection between the pores of distantly related ion channels as revealed by mutant K+ channels. *Science (New York, N.Y.)*, *258*(5085), 1152–1155. https://doi.org/10.1126/science.1279807

Henley, J. M., & Wilkinson, K. A. (2013). AMPA receptor trafficking and the mechanisms underlying synaptic plasticity and cognitive aging. *Dialogues in Clinical Neuroscience*, *15*(1), 11–27. https://doi.org/10.31887/DCNS.2013.15.1/jhenley

Heron, S. E., Scheffer, I. E., Berkovic, S. F., Dibbens, L. M., & Mulley, J. C. (2007). Channelopathies in Idiopathic Epilepsy. *Neurotherapeutics*, *4*(2), 295–304. https://doi.org/10.1016/j.nurt.2007.01.009

Heron, S. E., Smith, K. R., Bahlo, M., Nobili, L., Kahana, E., Licchetta, L., Oliver, K. L., Mazarib, A., Afawi, Z., Korczyn, A., Plazzi, G., Petrou, S., Berkovic, S. F., Scheffer, I. E., & Dibbens, L. M. (2012). Missense mutations in the sodium-gated potassium channel gene KCNT1 cause severe autosomal dominant nocturnal frontal lobe epilepsy. *Nature Genetics*, *44*(11), 1188–1190. https://doi.org/10.1038/ng.2440

Ho, S. S., Kuzniecky, R. I., Gilliam, F., Faught, E., & Morawetz, R. (1998). Temporal lobe developmental malformations and epilepsy: Dual pathology and bilateral hippocampal abnormalities. *Neurology*, *50*(3), 748–754. https://doi.org/10.1212/WNL.50.3.748

Hollmann, M., & Heinemann, S. (1994). Cloned glutamate receptors. *Annual Review of Neuroscience*, *17*, 31–108. https://doi.org/10.1146/annurev.ne.17.030194.000335

Holmes, G. L. (1995). *Role of Glutamate and GABA in the Pathophysiology of Epilpsy*. *9*(7 995), 208–219. *Mental Retardation and Developmental Disabilities*. https://doi.org/10.1002/mrdd.1410010309

Holopainen, I. E. (2005). Organotypic hippocampal slice cultures: A model system to study basic cellular and molecular mechanisms of neuronal cell death, neuroprotection, and synaptic plasticity. *Neurochemical Research*, *30*(12), 1521–1528. https://doi.org/10.1007/s11064-005-8829-5

Hu, R. Q., Koh, S., Torgerson, T., & Cole, A. J. (1998). Neuronal stress and injury in C57/BL mice after systemic kainic acid administration. *Brain Research*, *810*(1–2), 229–240. https://doi.org/10.1016/s0006-8993(98)00863-4

Hu, W., Tian, C., Li, T., Yang, M., Hou, H., & Shu, Y. (2009). Distinct contributions of Na(v)1.6 and Na(v)1.2 in action potential initiation and backpropagation. *Nature Neuroscience*, *12*(8), 996–1002. https://doi.org/10.1038/nn.2359

Huettner, J. E. (2003). Kainate receptors and synaptic transmission. *Progress in Neurobiology*, *70*(5), 387–407. https://doi.org/10.1016/s0301-0082(03)00122-9

Humpel, C. (2015). Neuroscience forefront review organotypic brain slice cultures: A review. *Neuroscience*, *305*, 86–98. https://doi.org/10.1016/j.neuroscience.2015.07.086

Igelström, K. M. (2013). Is slack an intrinsic seizure terminator? *Neuroscientist*, *19*(3), 248–254. https://doi.org/10.1177/1073858412446311

Ishii, A., Shioda, M., Okumura, A., Kidokoro, H., Sakauchi, M., Shimada, S., Shimizu, T., Osawa, M., Hirose, S., & Yamamoto, T. (2013). A recurrent KCNT1 mutation in two sporadic cases with malignant migrating partial seizures in infancy. *Gene*, *531*(2), 467–471. https://doi.org/10.1016/j.gene.2013.08.096

Jan, L. Y., & Jan, Y. N. (2012). Voltage-gated potassium channels and the diversity of electrical signalling. *The Journal of Physiology*, *590*(11), 2591–2599. https://doi.org/10.1113/jphysiol.2011.224212

Jefferys, J. G. R., Menendez de la Prida, L., Wendling, F., Bragin, A., Avoli, M., Timofeev, I., & Lopes da Silva, F. H. (2012). Mechanisms of physiological and epileptic HFO generation. *Progress in Neurobiology*, *98*(3), 250–264. https://doi.org/10.1016/j.pneurobio.2012.02.005

Jiajia, L., Shinghung, M., Jiacheng, Z., Jialing, W., Dilin, X., Shengquan, H., Zaijun, Z., Qinwen, W., Yifan, H., & Wei, C. (2017). Assessment of neuronal viability using fluorescein diacetate-propidium iodide double staining in cerebellar granule neuron culture. *Journal of Visualized Experiments*, *2017*(123), 1–7. https://doi.org/10.3791/55442

Jiang, Y., Pico, A., Cadene, M., Chait, B. T., & MacKinnon, R. (2001). Structure of the RCK domain from the E. coli K+channel and demonstration of its presence in the human BK channel. *Neuron*, *29*(3), 593–601. https://doi.org/10.1016/S0896-6273(01)00236-7

Johnston, J., Forsythe, I. D., & Kopp-Scheinpflug, C. (2010). Going native: Voltage-gated potassium channels controlling neuronal excitability. *Journal of Physiology*, *588*(17), 3187–3200. https://doi.org/10.1113/jphysiol.2010.191973

Johnston, J., Griffin, S. J., Baker, C., Skrzypiec, A., Chernova, T., & Forsythe, I. D. (2008). Initial segment Kv2.2 channels mediate a slow delayed rectifier and maintain high frequency action potential firing in medial nucleus of the trapezoid body neurons. *The Journal of Physiology*, *586*(14), 3493–3509. https://doi.org/10.1113/jphysiol.2008.153734

Joiner, W. J., Tang, M. D., Wang, L. Y., Dworetzky, S. I., Boissard, C. G., Gan, L., Gribkoff, V. K., & Kaczmarek, L. K. (1998). Formation of intermediate-conductance calcium-activated potassium channels by interaction of Slack and Slo subunits. *Nature Neuroscience*, *1*(6), 462–469. https://doi.org/10.1038/2176

Jonas, P., Racca, C., Sakmann, B., Seeburg, P. H., & Monyer, H. (1994). Differences in Ca2+ permeability of AMPA-type glutamate receptor channels in neocortical neurons caused by differential GluR-B subunit expression. *Neuron*, *12*(6), 1281–1289. https://doi.org/10.1016/0896-6273(94)90444-8

Ju, Y., & Tam, K. Y. (2022). Pathological mechanisms and therapeutic strategies for Alzheimer's disease. *Neural Regeneration Research*, *17*(3), 543–549. https://doi.org/10.4103/1673-5374.320970

Kaczmarek, L. K. (2013). *Slack, Slick and Sodium-Activated Potassium Channels*. ISRN Neuroscience, 2013(2013). https://doi.org/10.1155/2013/354262

Kaczmarek, L. K., Aldrich, R. W., Chandy, K. G., Grissmer, S., Wei, A. D., & Wulff, H. (2017). International union of basic and clinical pharmacology. C. Nomenclature and properties of calcium-activated and sodium-activated potassium channels. *Pharmacological Reviews*, *69*(1), 1–11. https://doi.org/10.1124/pr.116.012864

Kameyama, M., Kakei, M., Sato, R., Shibasaki, T., Matsuda, H., & Irisawa, H. (1984). Intracellular Na+ activates a K+ channel in mammalian cardiac cells. *Nature*, *309*(5966), 354–356. https://doi.org/10.1038/309354a0

Kang, D. H., Heo, R. W., Yi, C., Kim, H., Choi, C. H., & Roh, G. S. (2015). High-fat diet-induced obesity exacerbates kainic acid-induced hippocampal cell death. *BMC Neuroscience*, *16*(1), 72. https://doi.org/10.1186/s12868-015-0202-2

Kaplan, D. I., Isom, L. L., & Petrou, S. (2016). Role of sodium channels in epilepsy. *Cold Spring Harbor Perspectives in Medicine*, *6*(6), 1–17. https://doi.org/10.1101/cshperspect.a022814

Kearney, J. A., Plummer, N. W., Smith, M. R., Kapur, J., Cummins, T. R., Waxman, S. G., Goldin, A. L., & Meisler, M. H. (2001). A gain-of-function mutation in the sodium channel gene Scn2a results in seizures and behavioral abnormalities. *Neuroscience*, *102*(2), 307–317. https://doi.org/10.1016/s0306-4522(00)00479-6

Keiser, J., & Utzinger, J. (2010). Chapter 8 - The Drugs We Have and the Drugs We Need Against Major Helminth Infections. In X.-N. Zhou, R. Bergquist, R. Olveda, & J. B. T.-A. in P. Utzinger (Eds.), *Important Helminth Infections in Southeast Asia: Diversity and Potential for Control and Elimination, Part B* (Vol. 73, pp. 197–230). Academic Press. https://doi.org/https://doi.org/10.1016/S0065-308X(10)73008-6

Kim, G. E., & Kaczmarek, L. K. (2014). Emerging role of the KCNT1 Slack channel in intellectual disability. *Frontiers in Cellular Neuroscience*, *8*(July), 1–12. https://doi.org/10.3389/fncel.2014.00209

Kim, U., & McCormick, D. a. (1998). Functional and ionic properties of a slow afterhyperpolarization in ferret perigeniculate neurons in vitro. *J Neurophysiol*, *80*(3), 1222–1235. https://doi.org/10.1152/jn.1998.80.3.1222

Knierim, J. J. (2015). The hippocampus. *Current Biology*, *25*(23), R1116–R1121. https://doi.org/10.1016/j.cub.2015.10.049

Köhling, R. (2002). Voltage-gated sodium channels in epilepsy. *Epilepsia*, *43*(11), 1278–1295. https://doi.org/10.1046/j.1528-1157.2002.40501.x

Kress, G. J., & Mennerick, S. (2009). Action potential initiation and propagation: upstream influences on neurotransmission. *Neuroscience*, *158*(1), 211–222. https://doi.org/10.1016/j.neuroscience.2008.03.021

Krogsgaard-Larsen, P., Honoré, T., Hansen, J. J., Curtis, D. R., & Lodge, D. (1980). New class of glutamate agonist structurally related to ibotenic acid. *Nature*, *284*(5751), 64–66. https://doi.org/10.1038/284064a0

Krüger, J., Schubert, J., Kegele, J., Labalme, A., Mao, M., Heighway, J., Seebohm, G., Yan, P., Koko, M., Aslan-Kara, K., Caglayan, H., Steinhoff, B. J., Weber, Y. G., Keo-Kosal, P., Berkovic, S. F., Hildebrand, M. S., Petrou, S., Krause, R., May, P., … Lerche, H. (2022). Loss-of-function variants in the KCNQ5 gene are implicated in genetic generalized epilepsies. *EBioMedicine*, *84*, 104244. https://doi.org/10.1016/j.ebiom.2022.104244

Kuang, Q., Purhonen, P., & Hebert, H. (2015). Structure of potassium channels. *Cellular and Molecular Life Sciences*, *72*(19), 3677–3693. https://doi.org/10.1007/s00018-015-1948-5

Kubota, M., & Saito, N. (1991). Sodium- and calcium-dependent conductances of neurones in the zebra finch hyperstriatum ventrale pars caudale in vitro. *The Journal of Physiology*, *440*, 131–142. https://doi.org/10.1113/jphysiol.1991.sp018700

Lallement, G., Carpentier, P., Collet, A., Pernot-Marino, I., Baubichon, D., & Blanchet, G. (1991). Effects of soman-induced seizures on different extracellular amino acid levels and on glutamate uptake in rat hippocampus. *Brain Research*, *563*(1–2), 234–240. https://doi.org/10.1016/0006-8993(91)91539-d

Lavoie, A. M., Tingey, J. J., Harrison, N. L., Pritchett, D. B., & Twyman, R. E. (1997). Activation and deactivation rates of recombinant GABA(A) receptor channels are dependent on alpha-subunit isoform. *Biophysical Journal*, *73*(5), 2518–2526. https://doi.org/10.1016/S0006-3495(97)78280-8

Lehericy, S., Dormont, D., Semah, F., Clemenceau, S., Granat, O., Marsault, C., & Baulac, M. (1995). Developmental abnormalities of the medial temporal lobe in patients with temporal lobe epilepsy. *American Journal of Neuroradiology*, *16*(4), 617–626.

Lehman, A., Thouta, S., Mancini, G. M. S., Naidu, S., van Slegtenhorst, M., McWalter, K., Person, R., Mwenifumbo, J., Salvarinova, R., Guella, I., McKenzie, M. B., Datta, A., Connolly, M. B., Kalkhoran, S. M., Poburko, D., Friedman, J. M., Farrer, M. J., Demos, M., Desai, S., & Claydon, T. (2017). Loss-of-Function and Gain-of-Function Mutations in KCNQ5 Cause Intellectual Disability or Epileptic Encephalopathy. *American Journal of Human Genetics*, *101*(1), 65–74. https://doi.org/10.1016/j.ajhg.2017.05.016

Lerma, J., & Marques, J. M. (2013). Kainate receptors in health and disease. *Neuron*, *80*(2), 292–311. https://doi.org/10.1016/j.neuron.2013.09.045

Lévesque, M., & Avoli, M. (2013). The kainic acid model of temporal lobe epilepsy. *Neuroscience and Biobehavioral Reviews*, *37*(10), 2887–2899. https://doi.org/10.1016/j.neubiorev.2013.10.011

Lévesque, M., Biagini, G., de Curtis, M., Gnatkovsky, V., Pitsch, J., Wang, S., & Avoli, M. (2021). The pilocarpine model of mesial temporal lobe epilepsy: Over one decade later, with more rodent species and new investigative approaches. *Neuroscience and Biobehavioral Reviews*, *130*(August), 274–291. https://doi.org/10.1016/j.neubiorev.2021.08.020

Lévesque, M., Langlois, J. M. P., Lema, P., Courtemanche, R., Bilodeau, G.-A., & Carmant, L. (2009). Synchronized gamma oscillations (30–50 Hz) in the amygdalo-hippocampal network in relation with seizure propagation and severity. *Neurobiology of Disease*, *35*(2), 209–218. https://doi.org/https://doi.org/10.1016/j.nbd.2009.04.011

Li, J.-M., Zeng, Y.-J., Peng, F., Li, L., Yang, T.-H., Hong, Z., Lei, D., Chen, Z., & Zhou, D. (2010). Aberrant glutamate receptor 5 expression in temporal lobe epilepsy lesions. *Brain Research*, *1311*, 166–174. https://doi.org/https://doi.org/10.1016/j.brainres.2009.11.024

Lim, C. X., Ricos, M. G., Dibbens, L. M., & Heron, S. E. (2016). KCNT1 mutations in seizure disorders: The phenotypic spectrum and functional effects. *Journal of Medical Genetics*, *53*(4), 217–225. https://doi.org/10.1136/jmedgenet-2015-103508

Lin, W.-C., Tsai, M.-C., Davenport, C. M., Smith, C. M., Veit, J., Wilson, N. M., Adesnik, H., & Kramer, R. H. (2015). A Comprehensive Optogenetic Pharmacology Toolkit for In Vivo Control of GABA(A) Receptors and Synaptic Inhibition. *Neuron*, *88*(5), 879–891. https://doi.org/10.1016/j.neuron.2015.10.026

Lipton, S. A., & Rosenberg, P. A. (1994). Excitatory amino acids as a final common pathway for neurologic disorders. *The New England Journal of Medicine*, *330*(9), 613–622. https://doi.org/10.1056/NEJM199403033300907

Lopez-Santiago, L. F., Yuan, Y., Wagnon, J. L., Hull, J. M., Frasier, C. R., O'Malley, H. A., Meisler, M. H., & Isom, L. L. (2017). Neuronal hyperexcitability in a mouse model of SCN8A epileptic encephalopathy. *Proceedings of the National Academy of Sciences of the United States of America*, *114*(9), 2383–2388. https://doi.org/10.1073/pnas.1616821114

Lothman, E. W., Collins, R. C., & Ferrendelli, J. A. (1981). Kainic acid-induced limbic seizures: electrophysiologic studies. *Neurology*, *31*(7), 806–812. https://doi.org/10.1212/wnl.31.7.806

Lowry, E. R., Kruyer, A., Norris, E. H., Cederroth, C. R., & Strickland, S. (2013). The GluK4 kainate receptor subunit regulates memory, mood, and excitotoxic neurodegeneration. *Neuroscience*, *235*, 215–225. https://doi.org/10.1016/j.neuroscience.2013.01.029

Lu, R., Bausch, A. E., Kallenborn-Gerhardt, W., Stoetzer, C., Debruin, N., Ruth, P., Geisslinger, G., Leffler, A., Lukowski, R., & Schmidtko, A. (2015a). Slack channels expressed in sensory neurons control neuropathic pain in mice. *Journal of Neuroscience*, *35*(3), 1125–1135. https://doi.org/10.1523/JNEUROSCI.2423-14.2015

Lu, R., Bausch, A. E., Kallenborn-Gerhardt, W., Stoetzer, C., Debruin, N., Ruth, P., Geisslinger, G., Leffler, A., Lukowski, R., & Schmidtko, A. (2015b). Slack Channels Expressed in Sensory Neurons Control Neuropathic Pain in Mice. *Journal of Neuroscience*, *35*(3), 1125–1135. https://doi.org/10.1523/JNEUROSCI.2423-14.2015

Lu, R., Metzner, K., Zhou, F., Flauaus, C., Balzulat, A., Engel, P., Petersen, J., Ehinger, R., Bausch, A., Ruth, P., Lukowski, R., & Schmidtko, A. (2021). Functional Coupling of Slack Channels and P2X3 Receptors Contributes to Neuropathic Pain Processing. *International Journal of Molecular Sciences*, *22*(1). https://doi.org/10.3390/ijms22010405

Lu, S., Das, P., Fadool, D. A., & Kaczmarek, L. K. (2010). The slack sodium-activated potassium channel provides a major outward current in olfactory neurons of Kv1.3-/- super-smeller mice. *Journal of Neurophysiology*, *103*(6), 3311–3319. https://doi.org/10.1152/jn.00607.2009

Lukas, R. J., Changeux, J. P., Le Novère, N., Albuquerque, E. X., Balfour, D. J. K., Berg, D. K., Bertrand, D., Chiappinelli, V. A., Clarke, P. B. S., Collins, A. C., Dani, J. A., Grady, S. R., Kellar, K. J., Lindstrom, J. M., Marks, M. J., Quik, M., Taylor, P. W., & Wonnacott, S. (1999). International union of pharmacology. XX. Current status of the nomenclature for nicotinic acetylcholine receptors and their subunits. *Pharmacological Reviews*, *51*(2), 397–401.

Madry, C., Mesic, I., Bartholomäus, I., Nicke, A., Betz, H., & Laube, B. (2007). Principal role of NR3 subunits in NR1/NR3 excitatory glycine receptor function. *Biochemical and Biophysical Research Communications*, *354*(1), 102–108. https://doi.org/10.1016/j.bbrc.2006.12.153

Makinson, C. D., Tanaka, B. S., Sorokin, J. M., Wong, J. C., Christian, C. A., Goldin, A. L., Escayg, A., & Huguenard, J. R. (2017). Regulation of Thalamic and Cortical Network Synchrony by Scn8a. *Neuron*, *93*(5), 1165-1179.e6. https://doi.org/10.1016/j.neuron.2017.01.031

Maljevic, S., & Lerche, H. (2013). Potassium channels: a review of broadening therapeutic possibilities for neurological diseases. *Journal of Neurology*, *260*(9), 2201–2211. https://doi.org/10.1007/s00415-012-6727-8

Martin, H. C., Kim, G. E., Pagnamenta, A. T., Murakami, Y., Carvill, G. L., Meyer, E., Copley, R. R., Rimmer, A., Barcia, G., Fleming, M. R., Kronengold, J., Brown, M. R., Hudspith, K. A., Broxholme, J., Kanapin, A., Cazier, J. B., Kinoshita, T., Nabbout, R., Bentley, D., … Taylor, J. C. (2014). Clinical whole-genome sequencing in severe early-onset epilepsy reveals new genes and improves molecular diagnosis. *Human Molecular Genetics*, *23*(12), 3200–3211. https://doi.org/10.1093/hmg/ddu030

Martinez-Espinosa, P. L., Wu, J., Yang, C., Gonzalez-Perez, V., Zhou, H., Liang, H., Xia, X. M., & Lingle, C. J. (2015). Knockout of Slo2.2 enhances itch, abolishes KNa current, and increases action potential firing frequency in DRG neurons. *ELife*, *4*(November 2015), 1–27. https://doi.org/10.7554/eLife.10013

Mathern, G. W., Pretorius, J. K., Kornblum, H. I., Mendoza, D., Lozada, A., Leite, J. P., Chimelli, L., Born, D. E., Fried, I., Sakamoto, A. C., Assirati, J. A., Peacock, W. J., Ojemann, G. A., & Adelson, P. D. (1998). Altered Hippocampal Kainate-Receptor mRNA Levels in Temporal Lobe Epilepsy Patients. *Neurobiology of Disease*, *5*(3), 151–176. https://doi.org/https://doi.org/10.1006/nbdi.1998.0200

Matt, L., Pham, T., Skrabak, D., Hoffmann, F., Eckert, P., Yin, J., Gisevius, M., Ehinger, R., Bausch, A., Ueffing, M., Boldt, K., Ruth, P., & Lukowski, R. (2021). The Na+-activated K+ channel Slack contributes to synaptic development and plasticity. *Cellular and Molecular Life Sciences*, *78*(23), 7569–7587. https://doi.org/10.1007/s00018-021-03953-0

McKhann, G. M. 2nd, Wenzel, H. J., Robbins, C. A., Sosunov, A. A., & Schwartzkroin, P. A. (2003). Mouse strain differences in kainic acid sensitivity, seizure behavior, mortality, and hippocampal pathology. *Neuroscience*, *122*(2), 551–561. https://doi.org/10.1016/s0306-4522(03)00562-1

McTague, A., Nair, U., Malhotra, S., Meyer, E., Trump, N., Gazina, E. V., Papandreou, A., Ngoh, A., Ackermann, S., Ambegaonkar, G., Appleton, R., Desurkar, A., Eltze, C., Kneen, R., Kumar, A. V., Lascelles, K., Montgomery, T., Ramesh, V., Samanta, R., Kurian, M. A. (2018). Clinical and molecular characterization of KCNT1-related severe early-onset epilepsy. *Neurology*, *90*(1), E55–E66. https://doi.org/10.1212/WNL.0000000000004762

Medvedev, A., Mackenzie, L., Hiscock, J. J., & Willoughby, J. O. (2000). Kainic acid induces distinct types of epileptiform discharge with differential involvement of hippocampus and neocortex. *Brain Research Bulletin*, *52*(2), 89–98. https://doi.org/https://doi.org/10.1016/S0361-9230(00)00239-2

Meera, P., Wallner, M., Song, M., & Toro, L. (1997). Large conductance voltage- and calcium-dependent K+ channel, a distinct member of voltage-dependent ion channels with seven N-terminal transmembrane segments (S0-S6), an extracellular N terminus, and an intracellular (S9-S10) C terminus. *Proceedings of the National Academy of Sciences of the United States of America*, *94*(25), 14066–14071. https://doi.org/10.1073/pnas.94.25.14066

Melyan, Z., Wheal, H. V, & Lancaster, B. (2002). Metabotropic-mediated kainate receptor regulation of IsAHP and excitability in pyramidal cells. *Neuron*, *34*(1), 107–114. https://doi.org/10.1016/s0896-6273(02)00624-4

Miguel Sanz, C., Martinez Navarro, M., Caballero Diaz, D., Sanchez-Elexpuru, G., & Di Donato, V. (2023). Toward the use of novel alternative methods in epilepsy modeling and drug discovery. *Frontiers in Neurology*, *14*(August). https://doi.org/10.3389/fneur.2023.1213969

Mikati, M. A., Jiang, Y. H., Carboni, M., Shashi, V., Petrovski, S., Spillmann, R., Milligan, C. J., Li, M., Grefe, A., McConkie, A., Berkovic, S., Scheffer, I., Mullen, S., Bonner, M., Petrou, S., & Goldstein, D. (2015). Quinidine in the treatment of KCNT1-positive epilepsies. *Annals of Neurology*, *78*(6), 995–999. https://doi.org/10.1002/ana.24520

Mikati, M. A., Werner, S., Shehab, L., Shamseddine, A., Simaan, E., Liu, Z., Tarif, S., Stafstrom, C., & Holmes, G. (2003). Stages of status epilepticus in the developing brain. *Epilepsy Research*, *55*(1–2), 9–19. https://doi.org/10.1016/S0920-1211(03)00089-5

Milh, M., Falace, A., Villeneuve, N., Vanni, N., Cacciagli, P., Assereto, S., Nabbout, R., Benfenati, F., Zara, F., Chabrol, B., Villard, L., & Fassio, A. (2013). Novel Compound Heterozygous Mutations in TBC1D24 Cause Familial Malignant Migrating Partial Seizures of Infancy. *Human Mutation*, *34*(6), 869–872. https://doi.org/10.1002/humu.22318

Millan, M. H., Chapman, A. G., & Meldrum, B. S. (1993). Extracellular amino acid levels in hippocampus during pilocarpine-induced seizures. *Epilepsy Research*, *14*(2), 139–148. https://doi.org/10.1016/0920-1211(93)90018-3

Milligan, C. J., Li, M., Gazina, E. V., Heron, S. E., Nair, U., Trager, C., Reid, C. A., Venkat, A., Younkin, D. P., Dlugos, D. J., Petrovski, S., Goldstein, D. B., Dibbens, L. M., Scheffer, I. E., Berkovic, S. F., & Petrou, S. (2014). KCNT1 gain of function in 2 epilepsy phenotypes is reversed by quinidine. *Annals of Neurology*, *75*(4), 581–590. https://doi.org/10.1002/ana.24128

Minghui, R., Kestel, D., Wiebe, S., & Brodie, M. (2014). *A public health imperative*. 8. WHO Reference Number: WHO/MSD/MER/19.2. ISBN: 978-92-4-151593-1.

Mody, I., & Pearce, R. A. (2004). Diversity of inhibitory neurotransmission through GABA(A) receptors. *Trends in Neurosciences*, *27*(9), 569–575. https://doi.org/10.1016/j.tins.2004.07.002

Møller, R. S., Heron, S. E., Larsen, L. H. G., Lim, C. X., Ricos, M. G., Bayly, M. A., Van Kempen, M. J. A., Klinkenberg, S., Andrews, I., Kelley, K., Ronen, G. M., Callen, D., McMahon, J. M., Yendle, S. C., Carvill, G. L., Mefford, H. C., Nabbout, R., Poduri, A., Striano, P., Dibbens, L. M. (2015). Mutations in KCNT1 cause a spectrum of focal epilepsies. *Epilepsia*, *56*(9), e114–e120. https://doi.org/10.1111/epi.13071

Mosbacher, J., Schoepfer, R., Monyer, H., Burnashev, N., Seeburg, P. H., & Ruppersberg, J. P. (1994). A molecular determinant for submillisecond desensitization in glutamate receptors. *Science (New York, N.Y.)*, *266*(5187), 1059–1062. https://doi.org/10.1126/science.7973663

Moser, M. B., & Moser, E. I. (1998). Functional differentiation in the hippocampus. *Hippocampus*, *8*(6), 608–619. https://doi.org/10.1002/(SICI)1098-1063(1998)8:6<608::AID-HIPO3>3.0.CO;2-7

Mott, D. D., Rojas, A., Fisher, J. L., Dingledine, R. J., & Benveniste, M. (2010). Subunit-specific desensitization of heteromeric kainate receptors. *The Journal of Physiology*, *588*(Pt 4), 683–700. https://doi.org/10.1113/jphysiol.2009.185207

Mouri, G., Jimenez-Mateos, E., Engel, T., Dunleavy, M., Hatazaki, S., Paucard, A., Matsushima, S., Taki, W., & Henshall, D. C. (2008). Unilateral hippocampal CA3-predominant damage and short latency epileptogenesis after intra-amygdala microinjection of kainic acid in mice. *Brain Research*, *1213*, 140–151. https://doi.org/10.1016/j.brainres.2008.03.061

Müller-Gärtner, H. W., Mayberg, H. S., Fisher, R. S., Lesser, R. P., Wilson, A. A., Ravert, H. T., Dannals, R. F., Wagner, H. N. J., Uematsu, S., & Frost, J. J. (1993). Decreased hippocampal muscarinic cholinergic receptor binding measured by 123I-iododexetimide and single-photon emission computed tomography in epilepsy. *Annals of Neurology*, *34*(2), 235–238. https://doi.org/10.1002/ana.410340221

Müller, C. J., Gröticke, I., Hoffmann, K., Schughart, K., & Löscher, W. (2009). Differences in sensitivity to the convulsant pilocarpine in substrains and sublines of C57BL/6 mice. *Genes, Brain and Behavior*, *8*(5), 481–492. https://doi.org/10.1111/j.1601-183X.2009.00490.x

Murley, A. G., & Rowe, J. B. (2018). Neurotransmitter deficits from frontotemporal lobar degeneration. *Brain : A Journal of Neurology*, *141*(5), 1263–1285. https://doi.org/10.1093/brain/awx327

Nagao, T., Alonso, A., & Avoli, M. (1996). Epileptiform activity induced by pilocarpine in the rat hippocampal-entorhinal slice preparation. *Neuroscience*, *72*(2), 399–408. https://doi.org/10.1016/0306-4522(95)00534-x

Nakanishi, S., & Masu, M. (1994). Molecular diversity and functions of glutamate receptors. *Annual Review of Biophysics and Biomolecular Structure*, *23*, 319–348. https://doi.org/10.1146/annurev.bb.23.060194.001535

Nanou, E., Kyriakatos, A., Bhattacharjee, A., Kaczmarek, L. K., Paratcha, G., & El Manira, A. (2008). Na+-mediated coupling between AMPA receptors and KNa channels shapes synaptic transmission. *Proceedings of the National Academy of Sciences of the United States of America*, *105*(52), 20941–20946. https://doi.org/10.1073/pnas.0806403106

Nasrallah, K., Agustina Frechou, M., Yoon, Y. J., Persaud, S., Tiago Goncalves, J., & Castillo, P. E. (2022). Seizure-induced strengthening of a recurrent excitatory circuit in the dentate gyrus is proconvulsant. *Proceedings of the National Academy of Sciences of the United States of America*, *119*(32), 1–11. https://doi.org/10.1073/pnas.2201151119

Neligan, A., Hauser, W. A., & Sander, J. W. (2012). The epidemiology of the epilepsies. In *Handbook of Clinical Neurology* (1st ed., Vol. 107). Elsevier B.V. https://doi.org/10.1016/B978-0-444-52898-8.00006-9

Niday, Z., & Tzingounis, A. V. (2018). Potassium Channel Gain of Function in Epilepsy: An Unresolved Paradox. *The Neuroscientist : A Review Journal Bringing Neurobiology, Neurology and Psychiatry*, *24*(4), 368–380. https://doi.org/10.1177/1073858418763752

Noraberg, J., Kristensen, B. W., & Zimmer, J. (1999). Markers for neuronal degeneration in organotypic slice cultures. *Brain Research. Brain Research Protocols*, *3*(3), 278–290. https://doi.org/10.1016/S1385-299X(98)00050-6

Nuñez, A., & Buño, W. (2021). The Theta Rhythm of the Hippocampus: From Neuronal and Circuit Mechanisms to Behavior. *Frontiers in Cellular Neuroscience*, *15*, 649262. https://doi.org/10.3389/fncel.2021.649262

Nuwer, M. O., Picchione, K. E., & Bhattacharjee, A. (2010). PKA-Induced Internalization of Slack KNa Channels Produces Dorsal Root Ganglion Neuron Hyperexcitability. *Journal of Neuroscience*, *30*(42), 14165–14172. https://doi.org/10.1523/JNEUROSCI.3150-10.2010

Oliva, M., Berkovic, S. F., & Petrou, S. (2012). Sodium channels and the neurobiology of epilepsy. *Epilepsia*, *53*(11), 1849–1859. https://doi.org/10.1111/j.1528-1167.2012.03631.x

Oliver, K. L., Franceschetti, S., Milligan, C. J., Muona, M., Mandelstam, S. A., Canafoglia, L., Boguszewska-Chachulska, A. M., Korczyn, A. D., Bisulli, F., Di Bonaventura, C., Ragona, F., Michelucci, R., Ben-Zeev, B., Straussberg, R., Panzica, F., Massano, J., Friedman, D., Crespel, A., Engelsen, B. A., … Berkovic, S. F. (2017). Myoclonus epilepsy and ataxia due to KCNC1 mutation: Analysis of 20 cases and K(+) channel properties. *Annals of Neurology*, *81*(5), 677–689. https://doi.org/10.1002/ana.24929

Olney, J. W. (1989). Glutamate, a neurotoxic transmitter. *Journal of Child Neurology*, *4*(3), 218–226. https://doi.org/10.1177/088307388900400315

Olsen, R. W., & Sieghart, W. (2008). International Union of Pharmacology. LXX. Subtypes of gamma-aminobutyric acid(A) receptors: classification on the basis of subunit composition, pharmacology, and function. Update. *Pharmacological Reviews*, *60*(3), 243–260. https://doi.org/10.1124/pr.108.00505

Ottman, R. (2005). Analysis of genetically complex epilepsies. *Epilepsia*, *46*(SUPPL. 10), 7–14. https://doi.org/10.1111/j.1528-1167.2005.00350.x

Owens, D. F., & Kriegstein, A. R. (2002). Is there more to GABA than synaptic inhibition? *Nature Reviews Neuroscience*, *3*(9), 715–727. https://doi.org/10.1038/nrn919

Oyrer, J., Maljevic, S., Scheffer, I. E., Berkovic, S. F., Petrou, S., & Reid, C. A. (2018). Ion channels in genetic epilepsy: From genes and mechanisms to disease-targeted therapies. *Pharmacological Reviews*, *70*(1), 142–173. https://doi.org/10.1124/pr.117.014456

Palomero-Gallagher, N., Schleicher, A., Bidmon, H.-J., Pannek, H.-W., Hans, V., Gorji, A., Speckmann, E.-J., & Zilles, K. (2012). Multireceptor analysis in human neocortex reveals complex alterations of receptor ligand binding in focal epilepsies. *Epilepsia*, *53*(11), 1987–1997. https://doi.org/10.1111/j.1528-1167.2012.03634.x

Partin, K. M., Patneau, D. K., & Mayer, M. L. (1994). Cyclothiazide differentially modulates desensitization of alpha-amino-3-hydroxy-5-methyl-4-isoxazolepropionic acid receptor splice variants. *Molecular Pharmacology*, *46*(1), 129–138.

Paternain, A. V, Herrera, M. T., Nieto, M. A., & Lerma, J. (2000). GluR5 and GluR6 kainate receptor subunits coexist in hippocampal neurons and coassemble to form functional receptors. *The Journal of Neuroscience : The Official Journal of the Society for Neuroscience*, *20*(1), 196–205. https://doi.org/10.1523/JNEUROSCI.20-01-00196.2000

Pellegrini-Giampietro, D. E., Gorter, J. A., Bennett, M. V. L., & Zukin, R. S. (1997). The GluR2 (GluR-B) hypothesis: Ca2+-permeable AMPA receptors in neurological disorders. *Trends in Neurosciences*, *20*(10), 464–470. https://doi.org/10.1016/S0166-2236(97)01100-4

Perucca, P., Dubeau, F., & Gotman, J. (2014). Intracranial electroencephalographic seizure-onset patterns: effect of underlying pathology. *Brain : A Journal of Neurology*, *137*(Pt 1), 183–196. https://doi.org/10.1093/brain/awt299

Peters, H. C., Hu, H., Pongs, O., Storm, J. F., & Isbrandt, D. (2005). Conditional transgenic suppression of M channels in mouse brain reveals functions in neuronal excitability, resonance and behavior. *Nature Neuroscience*, *8*(1), 51–60. https://doi.org/10.1038/nn1375

Pham, T., Hussein, T., Calis, D., Bischof, H., Skrabak, D., Cruz Santos, M., Maier, S., Spähn, D., Kalina, D., Simonsig, S., Ehinger, R., Groschup, B., Knipper, M., Plesnila, N., Ruth, P., Lukowski, R., & Matt, L. (2023). BK channels sustain neuronal Ca(2+) oscillations to support hippocampal long-term potentiation and memory formation. *Cellular and Molecular Life Sciences : CMLS*, *80*(12), 369. https://doi.org/10.1007/s00018-023-05016-y

Picard, F., Bruel, D., Servent, D., Saba, W., Fruchart-Gaillard, C., Schöllhorn-Peyronneau, M.-A., Roumenov, D., Brodtkorb, E., Zuberi, S., Gambardella, A., Steinborn, B., Hufnagel, A., Valette, H., & Bottlaender, M. (2006). Alteration of the in vivo nicotinic receptor density in ADNFLE patients: a PET study. *Brain : A Journal of Neurology*, *129*(Pt 8), 2047–2060. https://doi.org/10.1093/brain/awl156

Pin, J. P., & Duvoisin, R. (1995). The metabotropic glutamate receptors: structure and functions. *Neuropharmacology*, *34*(1), 1–26. https://doi.org/10.1016/0028-3908(94)00129-g

Pirker, S., Schwarzer, C., Wieselthaler, A., Sieghart, W., & Sperk, G. (2000). GABA(A) receptors: immunocytochemical distribution of 13 subunits in the adult rat brain. *Neuroscience*, *101*(4), 815–850. https://doi.org/10.1016/s0306-4522(00)00442-5

Pitkänen, A., Lukasiuk, K., Dudek, F. E., & Staley, K. J. (2015). Epileptogenesis. *Cold Spring Harbor Perspectives in Medicine*, *5*(10). https://doi.org/10.1101/cshperspect.a022822

Popovic, D., Nuss, P., & Vieta, E. (2015). Revisiting loxapine: A systematic review. *Annals of General Psychiatry*, *14*(1), 10–17. https://doi.org/10.1186/s12991-015-0053-3

Poulsen, F. R., Jahnsen, H., Blaabjerg, M., & Zimmer, J. (2002). Pilocarpine-induced seizure-like activity with increased BNDF and neuropeptide Y expression in organotypic hippocampal slice cultures. *Brain Research*, *950*(1–2), 103–118. https://doi.org/10.1016/S0006-8993(02)03009-3

Puttachary, S., Sharma, S., Tse, K., Beamer, E., Sexton, A., Crutison, J., & Thippeswamy, T. (2015). Immediate epileptogenesis after kainate-induced status epilepticus in C57BL/6J mice: Evidence from long term continuous video-EEG telemetry. *PLoS ONE*, *10*(7), 1–21. https://doi.org/10.1371/journal.pone.0131705

Quraishi, I. H., Mercier, M. R., McClure, H., Couture, R. L., Schwartz, M. L., Lukowski, R., Ruth, P., & Kaczmarek, L. K. (2020). Impaired motor skill learning and altered seizure susceptibility in mice with loss or gain of function of the Kcnt1 gene encoding Slack (KNa1.1) Na+-activated K+ channels. *Scientific Reports*, *10*(1), 3213. https://doi.org/10.1038/s41598-020-60028-z

Quraishi, I. H., Stern, S., Mangan, K. P., Zhang, Y., Ali, S. R., Mercier, M. R., Marchetto, M. C., McLachlan, M. J., Jones, E. M., Gage, F. H., & Kaczmarek, L. K. (2019). An epilepsy-associated KCNT1 mutation enhances excitability of human iPSC-derived neurons by increasing slack KNa currents. *Journal of Neuroscience*, *39*(37), 7438–7449. https://doi.org/10.1523/JNEUROSCI.1628-18.2019

Racine, R., Okujava, V., & Chipashvili, S. (1972). Modification of seizure activity by electrical stimulation. 3. Mechanisms. *Electroencephalography and Clinical Neurophysiology*, *32*, 295–299. https://doi.org/Doi 10.1016/0013-4694(72)90178-2

Raedt, R., Van Dycke, A., Van Melkebeke, D., De Smedt, T., Claeys, P., Wyckhuys, T., Vonck, K., Wadman, W., & Boon, P. (2009). Seizures in the intrahippocampal kainic acid epilepsy model: characterization using long-term video-EEG monitoring in the rat. *Acta Neurologica Scandinavica*, *119*(5), 293–303. https://doi.org/10.1111/j.1600-0404.2008.01108.x

Represa, A., Le Gall La Salle, G., & Ben-Ari, Y. (1989). Hippocampal plasticity in the kindling model of epilepsy in rats. *Neuroscience Letters*, *99*(3), 345–350. https://doi.org/10.1016/0304-3940(89)90471-0

Rizzi, S., Knaus, H. G., & Schwarzer, C. (2016). Differential distribution of the sodium-activated potassium channels slick and slack in mouse brain. *Journal of Comparative Neurology*, *524*(10), 2093–2116. https://doi.org/10.1002/cne.23934

Rodríguez-Moreno, A., & Lerma, J. (1998). Kainate receptor modulation of GABA release involves a metabotropic function. *Neuron*, *20*(6), 1211–1218. https://doi.org/10.1016/s0896-6273(00)80501-2

Ronne-Engström, E., Hillered, L., Flink, R., Spännare, B., Ungerstedt, U., & Carlson, H. (1992). Intracerebral microdialysis of extracellular amino acids in the human epileptic focus. *Journal of Cerebral Blood Flow and Metabolism : Official Journal of the International Society of Cerebral Blood Flow and Metabolism*, *12*(5), 873–876. https://doi.org/10.1038/jcbfm.1992.119

Rose, C. R. (2002). Book Review: Na+ Signals at Central Synapses. *The Neuroscientist*, *8*(6), 532–539. https://doi.org/10.1177/1073858402238512

Rose, C. R., & Konnerth, A. (2001). NMDA receptor-mediated Na+ signals in spines and dendrites. *The Journal of Neuroscience : The Official Journal of the Society for Neuroscience*, *21*(12), 4207–4214. https://doi.org/10.1523/JNEUROSCI.21-12-04207.2001

Rozas, J. L., Paternain, A. V., & Lerma, J. (2003). Noncanonical signaling by ionotropic kainate receptors. *Neuron*, *39*(3), 543–553. https://doi.org/10.1016/S0896-6273(03)00436-7

Rusina, E., Bernard, C., & Williamson, A. (2021). The kainic acid models of temporal lobe epilepsy. *ENeuro*, *8*(2). https://doi.org/10.1523/ENEURO.0337-20.2021

Rutkowska-Wlodarczyk, I., Aller, M. I., Valbuena, S., Bologna, J.-C., Prézeau, L., & Lerma, J. (2015). A proteomic analysis reveals the interaction of GluK1 ionotropic kainate receptor subunits with Go proteins. *The Journal of Neuroscience : The Official Journal of the Society for Neuroscience*, *35*(13), 5171–5179. https://doi.org/10.1523/JNEUROSCI.5059-14.2015

Safronov, B. V, & Vogel, W. (1996). Properties and functions of Na(+)-activated K+ channels in the soma of rat motoneurones. *The Journal of Physiology*, *497 (Pt 3*(Pt 3), 727–734. https://doi.org/10.1113/jphysiol.1996.sp021803

Salami, P., Lévesque, M., Benini, R., Behr, C., Gotman, J., & Avoli, M. (2014). Dynamics of interictal spikes and high-frequency oscillations during epileptogenesis in temporal lobe epilepsy. *Neurobiology of Disease*, *67*, 97–106. https://doi.org/10.1016/j.nbd.2014.03.012

Salkoff, L., Butler, A., Ferreira, G., Santi, C., & Wei, A. (2006). High-conductance potassium channels of the SLO family. *Nature Reviews Neuroscience*, *7*(12), 921–931. https://doi.org/10.1038/nrn1992

Sanchez-Vives, M. V, Nowak, L. G., & McCormick, D. A. (2000). Cellular mechanisms of long-lasting adaptation in visual cortical neurons in vitro. *The Journal of Neuroscience : The Official Journal of the Society for Neuroscience*, *20*(11), 4286–4299. https://doi.org/10.1523/JNEUROSCI.20-11-04286.2000

Sandler, V. M., Puil, E., & Schwarz, D. W. (1998). Intrinsic response properties of bursting neurons in the nucleus principalis trigemini of the gerbil. *Neuroscience*, *83*(3), 891–904. https://doi.org/10.1016/s0306-4522(97)00415-6

Santi, C. M. (2006). Opposite Regulation of Slick and Slack K+ Channels by Neuromodulators. *Journal of Neuroscience*, *26*(19), 5059–5068. https://doi.org/10.1523/JNEUROSCI.3372-05.2006

Scharfman, H. E. (2007). The neurobiology of epilepsy. *Current Neurology and Neuroscience Reports*, *7*(4), 348–354. https://doi.org/10.1007/s11910-007-0053-z

Schattling, B., Fazeli, W., Engeland, B., Liu, Y., Lerche, H., Isbrandt, D., & Friese, M. A. (2016). Activity of Na(V)1.2 promotes neurodegeneration in an animal model of multiple sclerosis. *JCI Insight*, *1*(19), e89810. https://doi.org/10.1172/jci.insight.89810

Scheffer, I. E., Berkovic, S., Capovilla, G., Connolly, M. B., French, J., Guilhoto, L., Hirsch, E., Jain, S., Mathern, G. W., Moshé, S. L., Nordli, D. R., Perucca, E., Tomson, T., Wiebe, S., Zhang, Y. H., & Zuberi, S. M. (2017). ILAE classification of the epilepsies: Position paper of the ILAE Commission for Classification and Terminology. *Epilepsia*, *58*(4), 512–521. https://doi.org/10.1111/epi.13709

Schindelin, J., Arganda-Carreras, I., Frise, E., Kaynig, V., Longair, M., Pietzsch, T., Preibisch, S., Rueden, C., Saalfeld, S., Schmid, B., Tinevez, J.-Y., White, D. J., Hartenstein, V., Eliceiri, K., Tomancak, P., & Cardona, A. (2012). Fiji: an open-source platform for biological-image analysis. *Nature Methods*, *9*(7), 676–682. https://doi.org/10.1038/nmeth.2019

Schoepp, D. D. (2001). Unveiling the functions of presynaptic metabotropic glutamate receptors in the central nervous system. *The Journal of Pharmacology and Experimental Therapeutics*, *299*(1), 12–20. PMID: 11561058

Schreiber, M., Wei, A., Yuan, A., Gaut, J., Saito, M., & Salkoff, L. (1998). Slo3, a novel pH-sensitive K+ channel from mammalian spermatocytes. *Journal of Biological Chemistry*, *273*(6), 3509–3516. https://doi.org/10.1074/jbc.273.6.3509

Schulz, J. M., Knoflach, F., Hernandez, M.-C., & Bischofberger, J. (2018). Dendrite-targeting interneurons control synaptic NMDA-receptor activation via nonlinear α5-GABAA receptors. *Nature Communications*, *9*(1), 3576. https://doi.org/10.1038/s41467-018-06004-8

Schwarz, J. R., Glassmeier, G., Cooper, E. C., Kao, T.-C., Nodera, H., Tabuena, D., Kaji, R., & Bostock, H. (2006). KCNQ channels mediate IKs, a slow K+ current regulating excitability in the rat node of Ranvier. *The Journal of Physiology*, *573*(Pt 1), 17–34. https://doi.org/10.1113/jphysiol.2006.106815

Schwindt, P. C., Spain, W. J., & Crill, W. E. (1989). Long-lasting reduction of excitability by a sodium-dependent potassium current in cat neocortical neurons. *J. Neurophysiol.*, *61*(2), 233–244. https://doi.org/022-3077/89

Seeburg, P. H. (1996). The role of RNA editing in controlling glutamate receptor channel properties. *Journal of Neurochemistry*, *66*(1), 1–5. https://doi.org/10.1046/j.1471-4159.1996.66010001.x

Sendrowski, K., & Sobaniec, W. (2013). Hippocampus, hippocampal sclerosis and epilepsy. *Pharmacological Reports*, *65*(3), 555–565. https://doi.org/10.1016/S1734-1140(13)71033-8

Seo, J., Jung, S., Lee, S. Y., Yang, H., Kim, B. S., Choi, J., Bang, M., Shin, H. S., & Jeon, D. (2013). Early deficits in social behavior and cortical rhythms in pilocarpine-induced mouse model of temporal lobe epilepsy. *Experimental Neurology*, *241*(1), 38–44. https://doi.org/10.1016/j.expneurol.2012.11.024

Sheardown, M. J., Suzdak, P. D., & Nordholm, L. (1993). AMPA, but not NMDA, receptor antagonism is neuroprotective in gerbil global ischaemia, even when delayed 24 h. *European Journal of Pharmacology*, *236*(3), 347–353. https://doi.org/10.1016/0014-2999(93)90470-3

Shinozaki, H., & Konishi, S. (1970). Actions of several anthelmintics and insecticides on rat cortical neurones. *Brain Research*, *24*(2), 368–371. https://doi.org/10.1016/0006-8993(70)90122-8

Shore, A. N., Colombo, S., Tobin, W. F., Petri, S., Cullen, E. R., Dominguez, S., Bostick, C. D., Beaumont, M. A., Williams, D., Khodagholy, D., Yang, M., Lutz, C. M., Peng, Y., Gelinas, J. N., Goldstein, D. B., Boland, M. J., Frankel, W. N., & Weston, M. C. (2020). Reduced GABAergic Neuron Excitability, Altered Synaptic Connectivity, and Seizures in a KCNT1 Gain-of-Function Mouse Model of Childhood Epilepsy. *Cell Reports*, *33*(4), 108303. https://doi.org/10.1016/j.celrep.2020.108303

Sigel, E., & Steinmann, M. E. (2012). Structure, function, and modulation of GABA(A) receptors. *The Journal of Biological Chemistry*, *287*(48), 40224–40231. https://doi.org/10.1074/jbc.R112.386664

Simms, B. A., & Zamponi, G. W. (2014). Neuronal voltage-gated calcium channels: Structure, function, and dysfunction. *Neuron*, *82*(1), 24–45. https://doi.org/10.1016/j.neuron.2014.03.016

Skrabak, D., Bischof, H., Pham, T., Ruth, P., Ehinger, R., Matt, L., & Lukowski, R. (2023). Slack K+ channels limit kainic acid-induced seizure severity in mice by modulating neuronal excitability and firing. *Communications Biology*, *6*(1), 1–12. https://doi.org/10.1038/s42003-023-05387-9

Smolders, I., Khan, G. M., Manil, J., Ebinger, G., & Michotte, Y. (1997). NMDA receptor-mediated pilocarpine-induced seizures: characterization in freely moving rats by microdialysis. *British Journal of Pharmacology*, *121*(6), 1171–1179. https://doi.org/10.1038/sj.bjp.0701231

Son, J.-H., & Winzer-Serhan, U. H. (2006). Postnatal expression of alpha2 nicotinic acetylcholine receptor subunit mRNA in developing cortex and hippocampus. *Journal of Chemical Neuroanatomy*, *32*(2–4), 179–190. https://doi.org/10.1016/j.jchemneu.2006.09.001

Sontheimer, H. (2015). Diseases of the Nervous System. In *Diseases of the Nervous System* (pp. 61–94). Elsevier Inc. https://doi.org/http://dx.doi.org/10.1016/B978-0-12-800244-5.00003-3

Spitznagel, B. D., Mishra, N. M., Qunies, A. M., Prael, F. J., Du, Y., Kozek, K. A., Lazarenko, R. M., Denton, J. S., Emmitte, K. A., & Weaver, C. D. (2020). VU0606170, a Selective Slack Channels Inhibitor, Decreases Calcium Oscillations in Cultured Cortical Neurons. *ACS Chemical Neuroscience*, *11*(21), 3658–3671. https://doi.org/10.1021/acschemneuro.0c00583

Stafstrom, C. E. (2007). Persistent Sodium Current and Its Role in Epilepsy. *Epilepsy Currents*, *7*(1), 15–22. https://doi.org/10.1111/j.1535-7511.2007.00156.x

Stern-Bach, Y., Bettler, B., Hartley, M., Sheppard, P. O., O'Hara, P. J., & Heinemann, S. F. (1994). Agonist selectivity of glutamate receptors is specified by two domains structurally related to bacterial amino acid-binding proteins. *Neuron*, *13*(6), 1345–1357. https://doi.org/10.1016/0896-6273(94)90420-0

Sun, Y., Olson, R., Horning, M., Armstrong, N., Mayer, M., & Gouaux, E. (2002). Mechanism of glutamate receptor desensitization. *Nature*, *417*(6886), 245–253. https://doi.org/10.1038/417245a

Tamsett, T. J., Picchione, K. E., & Bhattacharjee, A. (2009). NAD+ Activates KNa Channels in Dorsal Root Ganglion Neurons. *Journal of Neuroscience*, *29*(16), 5127–5134. https://doi.org/10.1523/JNEUROSCI.0859-09.2009

Tang, Q. Y., Zhang, F. F., Xu, J., Wang, R., Chen, J., Logothetis, D. E., & Zhang, Z. (2016). Epilepsy-Related Slack Channel Mutants Lead to Channel Over-Activity by Two Different Mechanisms. *Cell Reports*, *14*(1), 129–139. https://doi.org/10.1016/j.celrep.2015.12.019

Teles-Grilo Ruivo, L. M., & Mellor, J. R. (2013). Cholinergic modulation of hippocampal network function. *Frontiers in Synaptic Neuroscience*, *5*(JUL), 1–15. https://doi.org/10.3389/fnsyn.2013.00002

Thiffault, I., Speca, D. J., Austin, D. C., Cobb, M. M., Eum, K. S., Safina, N. P., Grote, L., Farrow, E. G., Miller, N., Soden, S., Kingsmore, S. F., Trimmer, J. S., Saunders, C. J., & Sack, J. T. (2015). A novel epileptic encephalopathy mutation in KCNB1 disrupts Kv2.1 ion selectivity, expression, and localization. *The Journal of General Physiology*, *146*(5), 399–410. https://doi.org/10.1085/jgp.201511444

Thompson, S. M., Fortunato, C., McKinney, R. A., Müller, M., & Gähwiler, B. H. (1996). Mechanisms underlying the neuropathological consequences of epileptic activity in the rat hippocampus in vitro. *The Journal of Comparative Neurology*, *372*(4), 515–528. https://doi.org/10.1002/(SICI)1096-9861(19960902)372:4<515::AID-CNE2>3.0.CO;2-7

Thomson, S. J., Hansen, A., & Sanguinetti, M. C. (2015). Identification of the Intracellular Na $^{+}$ Sensor in Slo2.1 Potassium Channels. *Journal of Biological Chemistry*, *290*(23), 14528–14535. https://doi.org/10.1074/jbc.M115.653089

Tomasello, D. L., Gancarz-Kausch, A. M., Dietz, D. M., & Bhattacharjee, A. (2015). Transcriptional Regulation of the Sodium-activated Potassium Channel SLICK (KCNT2) Promoter by Nuclear Factor-κB. *The Journal of Biological Chemistry*, *290*(30), 18575–18583. https://doi.org/10.1074/jbc.M115.643536

Toyoda, I., Fujita, S., Thamattoor, A. K., & Buckmaster, P. S. (2015). Unit Activity of Hippocampal Interneurons before Spontaneous Seizures in an Animal Model of Temporal Lobe Epilepsy. *The Journal of Neuroscience : The Official Journal of the Society for Neuroscience*, *35*(16), 6600–6618. https://doi.org/10.1523/JNEUROSCI.4786-14.2015

Traynelis, S. F., Wollmuth, L. P., McBain, C. J., Menniti, F. S., Vance, K. M., Ogden, K. K., Hansen, K. B., Yuan, H., Myers, S. J., & Dingledine, R. (2010). Glutamate receptor ion channels: structure, regulation, and function. *Pharmacological Reviews*, *62*(3), 405–496. https://doi.org/10.1124/pr.109.002451

Trepel, M. (2015). *Neuroanatomie Struktur und Funtion* (6th ed.). Urban & Fischer in Elsevier. (ISBN)978-3-437-41287-5

Trimmer, J. S. (2015). Subcellular localization of K+ channels in mammalian brain neurons: remarkable precision in the midst of extraordinary complexity. *Neuron*, *85*(2), 238–256. https://doi.org/10.1016/j.neuron.2014.12.042

Turski, W. A., Cavalheiro, E. A., Turski, L., & Kleinrok, Z. (1983). Intrahippocampal bethanechol in rats: behavioural, electroencephalographic and neuropathological correlates. *Behavioural Brain Research*, *7*(3), 361–370. https://doi.org/10.1016/0166-4328(83)90026-8

Tzingounis, A. V, Heidenreich, M., Kharkovets, T., Spitzmaul, G., Jensen, H. S., Nicoll, R. A., & Jentsch, T. J. (2010). The KCNQ5 potassium channel mediates a component of the afterhyperpolarization current in mouse hippocampus. *Proceedings of the National Academy of Sciences of the United States of America*, *107*(22), 10232–10237. https://doi.org/10.1073/pnas.1004644107

Uchino, S., Wada, H., Honda, S., Hirasawa, T., Yanai, S., Nakamura, Y., Ondo, Y., & Kohsaka, S. (2003). Slo2 sodium-activated K+channels bind to the PDZ domain of PSD-95. *Biochemical and Biophysical Research Communications*, *310*(4), 1140–1147. https://doi.org/10.1016/j.bbrc.2003.09.133

Urban-Ciecko, J., & Barth, A. L. (2016). Somatostatin-expressing neurons in cortical networks. *Nature Reviews. Neuroscience*, *17*(7), 401–409. https://doi.org/10.1038/nrn.2016.53

van Velzen, M., Dahan, A., & Niesters, M. (2020). Neuropathic Pain: Challenges and Opportunities. In *Frontiers in pain research (Lausanne, Switzerland)* (Vol. 1, p. 1). https://doi.org/10.3389/fpain.2020.00001

Vandecasteele, M., Varga, V., Berényi, A., Papp, E., Barthó, P., Venance, L., Freund, T. F., & Buzsáki, G. (2014). Optogenetic activation of septal cholinergic neurons suppresses sharp wave ripples and enhances theta oscillations in the hippocampus. *Proceedings of the National Academy of Sciences of the United States of America*, *111*(37), 13535–13540. https://doi.org/10.1073/pnas.1411233111

Vanderver, A., Simons, C., Schmidt, J. L., Pearl, P. L., Bloom, M., Lavenstein, B., Miller, D., Grimmond, S. M., & Taft, R. J. (2014). Identification of a novel de novo p.Phe932Ile KCNT1 mutation in a patient with leukoencephalopathy and severe epilepsy. *Pediatric Neurology*, *50*(1), 112–114. https://doi.org/10.1016/j.pediatrneurol.2013.06.024

Vargas-Sánchez, K., Mogilevskaya, M., Rodríguez-Pérez, J., Rubiano, M. G., Javela, J. J., & González-Reyes, R. E. (2018). Astroglial role in the pathophysiology of status epilepticus: An overview. *Oncotarget*, *9*(42), 26954–26976. https://doi.org/10.18632/oncotarget.25485

Voipio, J., & Kaila, K. (2000). GABAergic excitation and K(+)-mediated volume transmission in the hippocampus. *Progress in Brain Research*, *125*, 329–338. https://doi.org/10.1016/S0079-6123(00)25022-X

Vyklicky, V., Korinek, M., Smejkalova, T., Balik, A., Krausova, B., Kaniakova, M., Lichnerova, K., Cerny, J., Krusek, J., Dittert, I., Horak, M., & Vyklicky, L. (2014). Structure, function, and pharmacology of NMDA receptor channels. *Physiological Research*, *63*(Suppl 1), S191-203. https://doi.org/10.33549/physiolres.932678

Wang, L.-S., Wang, L., Wang, L., Wang, G., Li, Z.-H., & Wang, J.-J. (2009). Effect of 1-butyl-3-methylimidazolium tetrafluoroborate on the wheat (Triticum aestivum L.) seedlings. *Environmental Toxicology*, *24*(3), 296–303. https://doi.org/10.1002/tox

Wang, Y., Tan, B., Wang, Y., & Chen, Z. (2021). Cholinergic signaling, neural excitability, and epilepsy. *Molecules*, *26*(8), 1–14. https://doi.org/10.3390/molecules26082258

Wang, Z., Chen, Y., Lü, Y., Chen, X., Cheng, L., Mi, X., Xu, X., Deng, W., Zhang, Y., Wang, N., Li, J., Li, Y., & Wang, X. (2015). Effects of JIP3 on epileptic seizures: Evidence from temporal lobe epilepsy patients, kainic-induced acute seizures and pentylenetetrazole-induced kindled seizures. *Neuroscience*, *300*, 314–324. https://doi.org/10.1016/j.neuroscience.2015.05.008

Watkins, J. C. (1962). The Synthesis of some Acidic Amino Acids Possessing Neuropharmacological Activity. *Journal of Medicinal and Pharmaceutical Chemistry*, *5*, 1187–1199. https://doi.org/10.1021/jm01241a010

Waxman, S. G., & Zamponi, G. W. (2014). Regulating excitability of peripheral afferents: emerging ion channel targets. *Nature Neuroscience*, *17*(2), 153–163. https://doi.org/10.1038/nn.3602

Weinstein, S. (2016). Seizures and epilepsy: An overview. *Epilepsy: The Intersection of Neurosciences, Biology, Mathematics, Engineering, and Physics*, 65–77. https://doi.org/10.1201/b10866-10

Weiss, S. A., Alvarado-Rojas, C., Bragin, A., Behnke, E., Fields, T., Fried, I., Engel, J. J., & Staba, R. (2016). Ictal onset patterns of local field potentials, high frequency oscillations, and unit activity in human mesial temporal lobe epilepsy. *Epilepsia*, *57*(1), 111–121. https://doi.org/10.1111/epi.13251

Wisedchaisri, G., Tonggu, L., McCord, E., Gamal El-Din, T. M., Wang, L., Zheng, N., & Catterall, W. A. (2019). Resting-State Structure and Gating Mechanism of a Voltage-Gated Sodium Channel. *Cell*, *178*(4), 993-1003.e12. https://doi.org/10.1016/j.cell.2019.06.031

Witter, M. P., Kleven, H., & Kobro Flatmoen, A. (2017). Comparative Contemplations on the Hippocampus. *Brain, Behavior and Evolution*, *90*(1), 15–24. https://doi.org/10.1159/000475703

Wollmuth, L. P., Kuner, T., & Sakmann, B. (1998). Intracellular Mg2+ interacts with structural determinants of the narrow constriction contributed by the NR1-subunit in the NMDA receptor channel. *The Journal of Physiology*, *506 (Pt 1*(Pt 1), 33–52. https://doi.org/10.1111/j.1469-7793.1998.00033.x

Wright, A., & Vissel, B. (2012). The essential role of AMPA receptor GluR2 subunit RNA editing in the normal and diseased brain. *Frontiers in Molecular Neuroscience*, *5*, 34. https://doi.org/10.3389/fnmol.2012.00034

Wu, G., Lu, Z. H., Wang, J., Wang, Y., Xie, X., Meyenhofer, M. F., & Ledeen, R. W. (2005). Enhanced susceptibility to kainate-induced seizures, neuronal apoptosis, and death in mice lacking gangliotetraose gangliosides: Protection with LIGA 20, a membrane-permeant analog of GM1. *Journal of Neuroscience*, *25*(47), 11014–11022. https://doi.org/10.1523/JNEUROSCI.3635-05.2005

Wu, J., Quraishi, I. H., Zhang, Y., Bromwich, M., & Kaczmarek, L. K. (2023). Disease-causing Slack potassium channel mutations produce opposite effects on excitability of excitatory and inhibitory neurons. *BioRxiv : The Preprint Server for Biology*. https://pubmed.ncbi.nlm.nih.gov/36824888/%0Ahttp://www.pubmedcentral.nih.gov/articlerender.fcgi?artid=PMC9948954

Xu, D., Chen, S., Yang, J., Wang, X., Fang, Z., & Li, M. (2022). Precision therapy with quinidine of KCNT1-related epileptic disorders: A systematic review. *British Journal of Clinical Pharmacology*, *88*(12), 5096–5112. https://doi.org/10.1111/bcp.15479

Yaari, Y., & Beck, H. (2002). “Epileptic neurons” in temporal lobe epilepsy. *Brain Pathology*, *12*(2), 234–239. doi: 10.1111/j.1750-3639.2002.tb00438.x

Yakel, J. L. (2013). Cholinergic receptors: Functional role of nicotinic ACh receptors in brain circuits and disease. *Pflugers Archiv European Journal of Physiology*, *465*(4), 441–450. https://doi.org/10.1007/s00424-012-1200-1

Yang, B., Desai, R., & Kaczmarek, L. K. (2007). Slack and slick KNa channels regulate the accuracy of timing of auditory neurons. *Journal of Neuroscience*, *27*(10), 2617–2627. https://doi.org/10.1523/JNEUROSCI.5308-06.2007

Yang, B., Gribkoff, V. K., Pan, J., Damagnez, V., Dworetzky, S. I., Boissard, C. G., Bhattacharjee, A., Yan, Y., Sigworth, F. J., & Kaczmarek, L. K. (2006). Pharmacological activation and inhibition of Slack (Slo2.2) channels. *Neuropharmacology*, *51*(4), 896–906. https://doi.org/10.1016/j.neuropharm.2006.06.003

Yang, F., Hanon, S., Lam, P., & Schweitzer, P. (2009). Quinidine Revisited. *American Journal of Medicine*, *122*(4), 317–321. https://doi.org/10.1016/j.amjmed.2008.11.019

Yao, Y., & Mayer, M. L. (2006). Characterization of a soluble ligand binding domain of the NMDA receptor regulatory subunit NR3A. *The Journal of Neuroscience : The Official Journal of the Society for Neuroscience*, *26*(17), 4559–4566. https://doi.org/10.1523/JNEUROSCI.0560-06.2006

Yu, F. H., & Catterall, W. A. (2003). Overview of the voltage-gated sodium channel family. Genome Biology, 4(3), 207. https://doi.org/10.1186/gb-2003-4-3-207

Yu, F. H., Mantegazza, M., Westenbroek, R. E., Robbins, C. A., Kalume, F., Burton, K. A., Spain, W. J., McKnight, G. S., Scheuer, T., & Catterall, W. A. (2006). Reduced sodium current in GABAergic interneurons in a mouse model of severe myoclonic epilepsy in infancy. *Nature Neuroscience*, *9*(9), 1142–1149. https://doi.org/10.1038/nn1754

Yuan, A., Dourado, M., Butler, A., Walton, N., Wei, A., & Salkoff, L. (2000). SLO-2, a K+ channel with an unusual Cl- dependence. *Nature Neuroscience*, *3*(8), 771–779. https://doi.org/10.1038/77670

Yuan, A., Santi, C. M., Wei, A., Wang, Z. W., Pollak, K., Nonet, M., Kaczmarek, L., Crowder, C. M., & Salkoff, L. (2003). The sodium-activated potassium channel is encoded by a member of the Slo gene family. *Neuron*, *37*(5), 765–773. https://doi.org/10.1016/S0896-6273(03)00096-5

Yuan, T., Wang, Y., Jin, Y., Xu, S., Zhang, H., Chen, Q., Li, N., Ma, X., Song, H., Peng, C., Yang, H., Geng, Z., Dong, J., Duan, G., Sun, Q., Yang, Y., Yang, F., & Huang, Z. (2023). *Coupling of Slack and {NaV}1.6 sensitizes Slack to quinidine blockade and guides anti-seizure strategy development*. https://doi.org/10.7554/elife.87559.1

Zhang, J., Liu, S., Fan, J., Yan, R., Huang, B., Zhou, F., Yuan, T., Gong, J., Huang, Z., & Jiang, D. (2023). Structural basis of human Slo2.2 channel gating and modulation. *Cell Reports*, *42*(8), 112858. https://doi.org/10.1016/j.celrep.2023.112858

Zhang, Q., Gao, S. H., Shen, Z. S., Wang, Y., Hu, S. W., Duan, G. B., Liu, Y., Zhong, D. Y., Liu, J., Sun, M. H., Zhang, X., Cao, T. Y., Cao, J. L., Tang, Q. Y., & Zhang, Z. (2022). The Slack Channel Regulates Anxiety-Like Behaviors via Basolateral Amygdala Glutamatergic Projections to Ventral Hippocampus. *Journal of Neuroscience*, *42*(14), 3049–3064. https://doi.org/10.1523/JNEUROSCI.2027-21.2022

Zhang, Y., Cao, S. X., Sun, P., He, H. Y., Yang, C. H., Chen, X. J., Shen, C. J., Wang, X. D., Chen, Z., Berg, D. K., Duan, S., & Li, X. M. (2016). Loss of MeCP2 in cholinergic neurons causes part of RTT-like phenotypes via α7 receptor in hippocampus. *Cell Research*, *26*(6), 728–742. https://doi.org/10.1038/cr.2016.48

Zhang, Z., Rosenhouse-Dantsker, A., Tang, Q.-Y., Noskov, S., & Logothetis, D. E. (2010). The RCK2 domain uses a coordination site present in Kir channels to confer sodium sensitivity to Slo2.2 channels. *The Journal of Neuroscience : The Official Journal of the Society for Neuroscience*, *30*(22), 7554–7562. https://doi.org/10.1523/JNEUROSCI.0525-10.2010

Zhou, F., Metzner, K., Engel, P., Balzulat, A., Sisignano, M., Ruth, P., Lukowski, R., Schmidtko, A., & Lu, R. (2022). Slack Potassium Channels Modulate TRPA1-Mediated Nociception in Sensory Neurons. *Cells*, *11*(10). https://doi.org/10.3390/cells11101693

10. Publications and congresses

10.1. Publications

Matt, L., Pham, T., **Skrabak, D.**, Hoffmann, F., Eckert, P., Yin, J., Gisevius, M., Ehinger, R., Bausch, A., Ueffing, M., Boldt, K., Ruth, P., & Lukowski, R. (2021). The Na+-activated K+ channel Slack contributes to synaptic development and plasticity. *Cellular and Molecular Life Sciences*, *78*(23), 7569–7587. https://doi.org/10.1007/s00018-021-03953-0

Burgstaller, S., Wagner, T. R., Bischof, H., Bueckle, S., Padamsey, A., Frecot, D., Kaiser, P. D., **Skrabak, D.**, Malli, R., Lukowski, R., & Rothbauer, U. (2022). Monitoring extracellular ion and metabolite dynamics with recombinant nanobody-fused biosensors. *IScience*, *25*(9), 104907. https://doi.org/10.1016/j.isci.2022.104907

Skrabak, D., Bischof, H., Pham, T., Ruth, P., Ehinger, R., Matt, L., & Lukowski, R. (2023). Slack K+ channels limit kainic acid-induced seizure severity in mice by modulating neuronal excitability and firing. *Communications Biology*, *6*(1), 1–12. https://doi.org/10.1038/s42003-023-05387-9

Pham, T., Hussein, T., Calis, D., Bischof, H., **Skrabak, D.**, Cruz Santos, M., Maier, S., Spähn, D., Kalina, D., Simonsig, S., Ehinger, R., Groschup, B., Knipper, M., Plesnila, N., Ruth, P., Lukowski, R., & Matt, L. (2023). BK channels sustain neuronal Ca(2+) oscillations to support hippocampal long-term potentiation and memory formation. *Cellular and Molecular Life Sciences : CMLS*, *80*(12), 369. https://doi.org/10.1007/s00018-023-05016-y

10.2. Congress contributions

David Skrabak, Rebekka Ehinger, Peter Ruth, Helmut Bischof, Lucas Matt, Robert Lukowski. “The role of the sodium-activated potassium channel Slack

in kainic acid and pilocarpine induced epilepsy models”. The first conference of the GRK 2381 doctoral researchers: CanCaN 2021 “Cancer, Cardiovascular Diseases & Neurological Disorders”. Tübingen, November 17 - 19, 2021. **Poster.**

David Skrabak, Helmut Bischof, Rebekka Ehinger, Peter Ruth, Lucas Matt, Robert Lukowski. “The role of the sodium-activated potassium channel Slack in kainic acid and pilocarpine induced epilepsy models”. Annual Meeting of the German Pharmaceutical Society – DPhG. From Behring to Biotechnology – moving Pharmaceutical Sciences towards One Health. Marburg, September 13 – 16, 2022. **Poster.**

“Lesmüller”-poster award, category Pharmacology.

David Skrabak, Helmut Bischof, Thomas Pham, Peter Ruth, Rebekka Ehinger, Lucas Matt, Robert Lukowski. ”Slack K^+ channels limit kainic acid-induced seizure severity by modulating neuronal excitability and firing”. Annual Meeting of the German Pharmaceutical Society – DPhG. Translational Pharmacy – Practice & Perspective. Tübingen, October 7 – 10, 2023. **Poster.**

“Lesmüller”-poster award, category Pharmacology.

11. Danksagung

Mein besonderer Dank geht an Prof. Dr. Robert Lukowski für die hervorragende wissenschaftliche Betreuung, interessante und voranbringende Diskussionen, kritische Korrekturen und anspruchsvolle Haltung, die mich sehr geschult und weitergebracht hat. Zudem möchte ich mich für das breite Methoden-Spektrum bedanken, das es mir ermöglichte, vielseitig und mit viel Freiraum wissentlichen Fragestellungen nachzugehen.

Prof. Dr. Peter Ruth danke ich sehr für die guten wissenschaftlichen Ideen, das entgegengebrachte Vertrauen und die Bereitstellung von Möglichkeiten.

Prof. Dr. Dr. Achim Schmidtko möchte ich herzlich für den interessanten wissenschaftlichen Austausch, Begutachtung meiner Dissertation und der nachfolgenden Disputation danken.

Dr. Lucas Matt möchte ich herzlich für einen immer sehr offenen und freundschaftlichen Austausch und Umgang, sowie großer Hilfe bei TVA, TVanz, Manuskript usw. bedanken. Technische Hilfe und offene Ansprache waren für mich wissenschaftlich und persönlich sehr wertvoll.

Dr. Helmut Bischof möchte ich für seine umfangreichen wissenschaftlichen und methodischen Ideen, Unterstützungen, Problemlösungen und Diskussionen danke. Zusammen mit einer mentalen und vor allem freundschaftlichen Unterstützung, auch von Sandra Burgstaller, waren viele Hürden überwindbar. Diese Kollegschaft und vor allem Freundschaft möchte ich nicht missen!

Ein besonderer Dank geht natürlich an Rebekka und auch Anna für die Betreuungen zu Beginn. Zudem bedanke ich mich bei meinen Kollegen, David, Thomas, Selina, Melanie, Tamara, Lena, Jiaqi, Ying, Loni, und dem gesamten Arbeitskreis. Danke für eure Unterstützung, die sehr witzigen Mittagspausen und Bierrunden und all den Spaß in- und außerhalb der Arbeit.

Außerdem bedanke ich mich herzlich bei Clement und Michael für die technische Hilfe und vor allem unterhaltsamen Pausen, Gesprächen und Witzeleien.

Zuletzt möchte ich meiner Familie für Geduld und Unterstützung bedanken die private Entscheidungen und Herausforderungen parallel zur Promotion gestürzt haben. Was insbesondere von meiner Frau gehört, und mit viel Geduld mitgetragen wurde. Mit Ihr und Jakob gelang ein sehr anspruchsvolles, aber sinnstiftendes und wunderbares Gegengewicht zur Zeit am Institut, von dem ich heute weiß, dass es mich maßgeblich weitergebracht hat und einen enorm wichtigen und wertvollen Fixpunkt geschaffen hat.